TITLE PAGE

A Study of the Nature, Timing, and Processes in the Mount Isa Lead-Zinc Orebodies; their Relationship to Adjacent Copper Orebodies and the Lead-Zinc Systems at McArthur River, Hilton, and Mount Novit.

VOLUME I

Thesis submitted by

William George PERKINS BSc.*U.N.E.* B. Econ.*U of Q'ld* MSc. *JCUNQ.*

in June 1996

for the degree of Doctor of Philosophy

in the Department of Earth Sciences

James Cook University of North Queensland

STATEMENT OF ACCESS

I, the undersigned, the author of this thesis, understand that James Cook Univesity of North Queensland will make it available for use within the University Library and, by microfilm or other means, allow access to users in other approved libraries. All users consulting this thesis will have to sign the following statement:

> In consulting this thesis I agree not to copy or closely paraphrase it in whole or in part without the written consent of the author; and to make proper written acknowledgement for any assistance which I have obtained from it.

Beyond this, I do not wish to place any restriction on access to this thesis.

William G. Perkins 11 June 1996

ACKNOWLEDGMENTS

Many colleagues have been involved in the preparation of this thesis. A base of detailed mine mapping, reports, and discussions with past and present mine geologists and outside researchers has been invaluable. In particular, assistance has been provided by John Knights, Mike Hawkins, Dave Hutton, Dale Sims, Sue Noviello, Dave Morris, Steve Bartrop, Colin Brodie, Bill Sheppard, Ross Logan, Bill Croxford, Dave Finn and Jim Whitelock. Support for undertaking the project has been given by Ken Dredge, Peter Forrestal, Barry Sullivan, Brice Mutton, Don Zimmerman, Peter Stoker, Ross Fardon, and Ian Willis.

For specific parts of the thesis I have discussed the work with many colleagues, and thank Keith Hannan for assistance with the Part B sulphur isotope interpretation, and for criticism of an earlier draft of Part A. Eoin Rothery has helped at a critical stage by transferring the geochemical data in part D into Micromine diagrams.

I am grateful to my employer, MIM Holdings Limited, for both generous financial support and for permission to publish Parts A and B of this report. The work of Shirley Schultz, Helen Richmond, Margaret Cleary and her staff in drafting the diagrams is greatly appreciated, as is assistance with photography provided by Brian Pump of JCUNQ.

An earlier version of Part A of this thesis was thoroughly read by three Economic Geology reviewers, who suggested many modifications, most of which I have adopted. In particular, I have attempted to further separate the observations from the interpretations, but have maintained the overall interpretation, for which I accept responsibility. Two subsequent reviewers of Parts A and B have also located presentation errors as a result of detailed proof reading. I thank the two reviewers for Ore Geology Reviews for their comments, and, in particular, I have attempted to address the reasons for the difference between this interpretation and that of McClay (1979). Gordon Lister has been invaluable as a source of encouragement and reasoning for the revision of this part.

I would like to especially thank Stewart Eldridge from ANU Research School of Earth Sciences for doing the SHRIMP sulphur isotope work on my samples, and for discussing the results of this, and earlier work, so extensively with me.

I thank the staff, especially Bob Carter, and students of James Cook University for their assistance, and, in particular, I am indebted to my supervisor, Tim Bell, for his exceptional enthusiasm and instruction.

Frank Walsh has provided clear thinking when it was most needed. Most importantly, my wife, Di, has been of exceptional value in support and encouragement, and without her I would not have persisted.

SUMMARY

This thesis is written in four parts, the first three of which either have been, or are intended to be submitted to journals for publication and hence have their own individual abstracts. Part A presents the results of work on the Mount Isa lead-zinc orebodies themselves. Part B addresses the formation of the major development of fine-grained pyrite bodies at Mount Isa, incorporating some of the evidence and argument from the HYC deposit at McArthur River. Part C combines investigations of similar aspects of the mineralisation at the HYC deposit, Hilton deposit, and the non-commercial Mount Novit prospect, and attempts to draw comparisons between these systems and Mount Isa. Part D presents geochemical data for Mount Isa and Hilton deposits and discusses some of the constraints on processes of ore formation.

The central thesis is that the Mount Isa lead-zinc lodes have not formed by synsedimentary processes, as almost universally believed, but are the result of shear-controlled replacement along bedding, following lithification, peak metamorphism, and the bulk of the ductile deformation. Fine-grained stratiform pyrite forms a major part of many sediment-hosted lead-zinc systems, and is universally regarded as forming in early diagenesis, as a result of biogenic sulfate reduction. Stratiform pyrite at Mount Isa has characteristics suggesting it did not form early in diagenesis, but was deposited probably by abiogenic sulfate reduction, after development of both a bedding-parallel and a cross-cutting cleavage. This proposed late origin of the Mount Isa fine-grained pyrite is consistent with reinterpretation of existing sulphur isotopic data that suggests that the two generations of fine-grained pyrite at HYC are hydrothermal rather than biogenic.

Timing relationships for HYC, Hilton and Mount Novit are not as diagnostic as those at Mount Isa. However, Hilton and Mount Novit appear very similar to Mount Isa in terms of timing and ore controls. HYC sulphide relationships are significantly different in that the bulk of the sulphides appear to have replaced bituminous material, rather than metasomatic carbonates and silicates as at the other three deposits. Many features suggest that the HYC sulphides are post-compaction, are younger than ubiquitous microthrust structures, and form at some stage during a post-McArthur Group compressive deformation.

TABLE OF CONTENTS

These four parts have an individual Table of Contents at the beginning of each.

STATEMENT ON SOURCES

DECLARATION

I declare that this thesis is my own work and has not been submitted in any form for another degree at any university or other institution of tertiary education. Information derived from the published or unpublished work of others has been acknowledged in the text and a list of references is given.

William G. Perkins 11 June 1996

PART A.

Mount Isa Lead - Zinc Orebodies: Replacement Lodes in a Zoned Syndeformational Copper - Lead - Zinc System?

PART A.

ABSTRACT

Examination of the microstructural and textural development of the lead-zinc mineralization at Mount Isa reveals that it formed cogenetically with the large-scale Cu orebodies by late syndeformational replacement. The constraints on mineralization provided by the sedimentological framework (Neudert,1984) and timing criteria place the lead-zinc and its associated pyrrhotite and layer-parallel pyrite as forming late in the last major phase of deformation affecting the Mine area. This is the same event as that which formed the copper ore (Perkins, 1984; Swager, 1985a) and indicates copper-lead-zinc to be a zoned late-stage epigenetic system.

A succession of stratigraphically-constrained samples traced into the orebody reveals the progressive development of an alteration system that formed from well-laminated carbonaceous siltstones and mudstones. At the periphery, alteration consists of bleaching by destruction of carbonaceous seams and enhanced growth of dolomite. Progressively further inwards, it changes to mica and albite-bearing "buff alteration", commonly into siderite, magnetite and stilpnomelane, through a chloritic zone, to ultimately massive "silica-dolomite" alteration. Paralleling this alteration was the formation of abrupt pyrite-pyrrhotite transitions, and a zonation from sphalerite to galena to chalcopyrite.

The characteristic folded and breccia ores were not the result of ductile or fluid-assisted deformation of pre-existing sulphide-siltstone interlayers, but instead formed by shear-controlled carbonate alteration that was ultimately replaced by sulphides. Layer-parallel mineralization commonly terminates abruptly on or near extensional dolomite veins that formed progressively through the last major deformation event in the mine. Layer-parallel mineralization formed at the same time as ore in folded and brecciated zones.

Evidence cited in previous studies for large-scale remobilization and recrystallization during deformation, which is a logical consequence if mineralization had been an integral part of the sedimentary succession, can be more consistently interpreted as resulting from a single cycle of sulphide deposition. Both bedding-parallel and cross-cutting structures that control the localization of mineralization existed prior to the precipitation of sulphides. Dissolution of sulphides only occurs where there is a paragenetic sequence of sulphides, with fine-grained pyrite locally overprinted by all other economic sulphides (Grondijis and Schouten, 1937). Sphalerite is overprinted by galena, and both are overprinted by chalcopyrite, which everywhere is paragenetically the youngest sulphide.

Copper-lead-zinc formed from hydrothermal solutions entering the region of the ramp of the Paroo Fault and then migrating outwards to form an evolving alteration system during the formation of both the layer-parallel and cross-cutting steep cleavages. This was overprinted by a relatively short-lived mineralization event to form the zoned copper-lead-zinc system.

Implications of this interpretation for other similar deposits around the world are profound. It indicates a necessity to re-examine many other deposits using techniques that relate ore textures to associated structures at all scales. A completely different ore genesis paradigm may result and exploration concepts may need to be substantially modified.

INTRODUCTION

The Mount Isa copper-lead-zinc system is one of the world's largest and best-known sediment-hosted base metal sulphide deposits. It is unique in that it contains major copper orebodies close to a series of lead-zinc lodes. Copper and lead-zinc stoping blocks can lie within tens of metres of each other, but there are limited areas of the lead-zinc part of the system that contain any significant copper, and very restricted copper ores with lead-zinc contamination. Mathias and Clark (1975) provided the most complete description of the ore system, with copper contained within a silica-dolomite body, and lead-zinc lodes arranged in an *en echelon* pattern around it.

Interpretations of the origin of the lead-zinc lodes were first published in 1942 (Blanchard and Hall, 1942). The bedding-plane shear-controlled epigenetic origin proposed then, was continued in further publications, until, influenced by ideas such as those of Knight (1957), a syngenetic origin was advanced (Murray, 1961). The limited copper that had been discovered at the time of the earlier work was also regarded as being of replacement origin and related to a phase of overthrusting from the south-west. By the early 1960's both the copper and lead-zinc orebodies were commonly regarded as being formed during deposition of the Urquhart Shale host (Stanton, 1962, 1963), although there were exceptions to this view with respect to copper (Murray, 1961; Smith and Walker, 1972). Structural and microstructural studies (Perkins, 1981,1984; Swager, 1985a) proposed a syndeformational replacement model for copper ore formation. These studies did not investigate the lead-zinc ores, but no reason was seen at that time to question the assumption that they were essentially syngenetic.

A major sedimentological study of the upper formations of the Mount Isa Group constrained the depositional environment of the sediments hosting the mineralization (Neudert and Russell, 1981, Neudert,1983, 1984) to the shallow water slope to basin facies of a playa lake environment. This meant that exhalative processes were largely ruled out because of temperature constraints on boiling. Furthermore, the interpretation by this author that the stratiform sulphides were not in the pelagic parts of the sedimentary cycle, but in the current deposits, indicated that they had to be introduced at some time after deposition. Neudert(1983) proposed that the sedimentary environment was sulphate-rich and that this sulphate remained essentially in situ and was used as the source of sulphur for the deposition of all sulphides. He envisaged a sequence of deposition beginning with early diagenetic fine-grained pyrite and sphalerite, passing through sphalerite and galena of later diagenetic origin, and finishing with galena, pyrrhotite and chalcopyrite during deformation.

The close spatial relationship between the two ore types, and the consequent element of coincidence if they had formed at different times, remained difficult to explain. Waring (1990,1991) interpreted iron-rich mineral distribution patterns to represent an early diagenetic lead-zinc system that has subsequently been metamorphosed and controls the margins of later copper-associated alteration. Although McGoldrick (1989) accepted that the 'silica- dolomite' was a late alteration system, he used mostly geochemical evidence to argue for a cogenetic formation of both ore types during early diagenesis. The notion that the lead-zinc and copper orebodies are temporally related has powerful appeal. The coincidence problem that arises of two large orebodies in the one location if they are not cogenetic, and the work of Neudert (1983,1984), prompted the study described here.

In the history of investigations of Mount Isa lead-zinc the most remarkable feature to be explained has been the exceptionally stratiform nature of the sulphides comprising these lodes. Earlier workers advocated *lit-par-lit* replacement, but detailed observational evidence cited for this was fairly quickly surpassed by the new syngenetic paradigm, which seemed eminently more reasonable. Textural observation was superseded by geochemical approaches to deposit modelling. This led to the universal acceptance that the sulphides were an integral part of the sedimentary succession, and debate has centred on whether they are strictly syngenetic or formed during diagenesis. Cross-cutting relationships of various types were then explained by "remobilization" and/or "recrystallization", leaving the emphasis on the overall bedding-parallel nature as the principal evidence that the lead-zinc sulphides were formed with the sediments. Marker horizons show that the ore boundaries changed their stratigraphic positions only gradually, and this could be accounted for by facies changes.

In order to re-examine the timing of lead-zinc, this study addresses all styles of mineralization, but concentrates on an interpretation of the most finely lamina-parallel mineralization, of the style whose stratiform nature resulted in the model that these sulphides formed with the host sediments. In order to establish criteria that could indicate the timing of this style of economic sulphide, samples had to be selected where relationships to the structural elements could be seen. Only in this sense was there any bias in site selection.

Structural and microstructural techniques applied to both underground exposure and drill core have been the main investigation method employed in the present study. Some selected whole-rock geochemistry and X-ray diffractometry have also been used, as has ion microprobe determination of sulphur isotopes. The results of this work are not reported here but are presented in Perkins (1996a).

GEOLOGICAL SETTING

A well-laminated sequence of current-deposited siltstones and mudstones characterize the mid-Proterozoic Urquhart Shale (Neudert, 1983, 1988), which hosts both the lead-zinc and copper orebodies at Mount Isa Mine (Fig. 1). Neudert (1983) recognized two facies within the

upper Urquhart Shale. Facies I and variant Ia are dominated by mudstones and thinly laminated carbonaceous siltstones. Facies II contains significant amounts of massive and cross-laminated siltstone, and generally lacks mudstone and finely laminated siltstone. These two facies could not be clearly distinguished in the lower Urquhart Shale, which Neudert (1983) grouped into a non-channelled and a nodular facies. The sequence dips west at 60%-65% and is overlain by a thicker-bedded sequence of dolomitic siltstones and sandstones, followed by a shaley unit, which is truncated to the west by the Paroo Fault (Fig. 1). Between the Paroo Fault and the Mount Isa Fault, is a narrow sequence of basaltic metavolcanics. Further west is the "Judenan Fold Belt" and a locally overturned amphibolite-grade belt of Eastern Creek Volcanics (Fig. 1). In the mine, the Paroo Fault has a complex shape, and changes dip from steep west to shallow east, where it ramps across bedding and becomes known as the "greenstone basement fault" The cross-sections of Mathias and Clark (1975), and Perkins (1984) show this relationship, and also that of the economic limits of the lead-zinc and copper orebodies. Lead-zinc mineralization spans a stratigraphic thickness of 950 metres.

Mathias and Clark (1975) and Perkins (1984) have described in detail the geometric features of the silica-dolomite host to copper mineralization, which is a readily mappable body characterised by coarse-grained dolomite or its silicified equivalent. This body contains all the copper ore as chalcopyrite. Chalcopyrite can occur elsewhere in various types of dolomite veins, or in extensional sites within the lead- zinc orebodies but is much less common.

GEOMETRY OF LEAD-ZINC ORE DISTRIBUTION

Lead-zinc orebodies are located around, and extend outwards between stratabound marginal lobes of the silica dolomite. Although ore boundaries are economic limits and enclose packages of both sulphides and barren rock they generally have relatively abrupt hangingwalls and footwalls and form natural tabular plates of sulphide-rich stratigraphy. They make a distinctive *en echelon* pattern in both cross-section and level plan (Fig. 2) with the more westerly orebodies (Black Star Numbers 1 to 5) occurring at higher levels and in more northerly positions, and the narrower Racecourse orebodies (5/60 to 14/30) occupying progressively deeper and more southerly positions. Figure 2 highlights the transgressive nature of the enveloping surfaces of the lead-zinc orebodies. This trends at 345% across the stratigraphy, parallel with the fold hinges and the limits of silica-dolomite. The less well-developed Rio Grande orebodies, towards the southern end of the mine, have more of a "halo" pattern around the silica-dolomite and the major 1100 copper orebody which it contains (see Perkins, 1984, fig. 4).

Within their defined stratigraphy, the orebodies have approximately an elliptical shape, with their long axes plunging north at 55%-60%, as shown by No. 7 orebody (Fig. 2b). This longitudinal section highlights the relationship of ore to the projected position of the "greenschist

basement" and the anticlinal hinge of the Mount Isa Fold. Most observations reported in this paper are taken from within this orebody and can be spatially related to this section.

MESOSCOPIC FEATURES OF LEAD-ZINC OREBODIES

Sulphide occurrences consist of a number of styles. In order of decreasing stratiform nature these are; finely laminated pyritic layers; generally sphaleritic layers with variable amounts of galena, pyrrhotite and pyrite; galena-rich folded zones and breccias sub-parallel to bedding; and distinctly cross-cutting sulphides of all types. Much of the galena occurs in near-bedding parallel breccia veins that contain a variable amount of sphalerite. Silver, occurring as freibergite, is closely associated with galena, and not identifiable except in polished section. An illustration of the range of mineralization styles is shown in Fig. 3.

The 7 orebody sedimentary sequence in the unmineralized section (apart from minor pyrite), three km to the north of the mine (41,000N), consists of alternating laminated coarse siltstones (88%), non-laminated fine siltstones and mudstones thicker than 1 cm (7%) and feldspathic cherts (1%). The remainder of the sequence at this locality consists of blue-grey calcitic alteration with calcite veins. Using the stratigraphic framework of Neudert (1983), the same sequence towards the top of 7 orebody (B sequence) also contains these sedimentary units. Finely laminated siltstones, which equate with the stratiform lead-zinc in the 7 orebody sequence, exhibit lamina-for-lamina correlation over distances up to five km (Fig. 4). This shows that, notwithstanding accentuation of laminae by subsequent shortening and shear, individual sub-millimetre dolomite-rich bands are depositional units and not the result of stylolamination of thick current deposits. This level of correlation indicates that they may be the product of basin-wide events. R. Myers (pers. comm, 1994) has interpreted sequences similar to these at the Hilton deposit as sulphate evaporites.

Figure 5 shows profiles across the No. 7 lead-zinc orebody for two separate locations that show the change in mineralization position with respect to stratigraphic markers, together with the changes in style of mineralization with respect to its grade. The stratigraphic markers used in the lead-zinc orebodies are known as "tuffaceous marker beds" (from now on called TMBs). These consist in the mine vicinity of a very fine-grained assemblage of microcline, quartz and dolomite (Croxford, 1964). Four of these markers have been used in 7 Orebody (Perkins, 1984) for establishing the alteration and mineralization changes with respect to stratigraphy. The thickest is the marker at the footwall extremity of the section (Fig. 5), and it is this layer in which Croxford (1964) has elsewhere recognized shard textures. Correlation of laminae above and below these markers verifies that they are chronostratigraphic units (Fig. 4). The mineralized sequences consist of intercalations of variable thicknesses of sulphide-rich and sulphide-poor layers. The profiles in Fig. 5 also show the locations of folds and shear zones within the orebody interval. Marked changes occur in the content of sphalerite and fine-grained

pyrite, and the position of these sulphides with respect to stratigraphy. Another illustration of the transgressive nature of mineralization in 12 orebody is shown in the fence profile of Fig. 6.

STRUCTURAL FEATURES OF LEAD-ZINC OREBODIES

The folding events and faults that have affected the mine sequence are described successively from oldest to youngest. To aid the reader a summary of the deformation history is provided in Table 1 and the larger structures are shown in plan view on Fig. 2. Cleavage microstructures, fractures and veins are related chronologically to the folds and shear zones.

Fold structures in the lead-zinc orebodies

Fold shapes and styles within lead-zinc orebodies are well illustrated by previous studies (e.g. Hewett and Solomon, 1967, McClay, 1979). Orientation data for mesoscopic folds and axial plane cleavage in both lead-zinc and copper areas of the mine are summarized in Perkins (1984). There are four main styles and orientations of folds:

1. Limited numbers of folds with axial planes parallel to bedding and verging west;
2. Folds with axial planes parallel to bedding and verging east;
3. Folds with axial planes at a high angle to bedding;
4. The "normal" asymmetric folds with steep axial planes and verging east.

The first set (D_1) have wavelengths of 1mm to 200mm and verge west in a consistently west younging sequence (Fig. 7). The second set (D_2; Fig. 8) verge east within the same consistently west younging sequence. The third set ($D_{2.5}$; e.g., Bell & Hickey, 1996), which appear to have some association with mineralization, are developed with sub-horizontal axial planes and rotate bedding and the axial planes of D_2 folds top to the east (Fig. 8). These folds may either die out along their axial planes into mineralized layers, or have axial planes that curve into S_3 (Fig. 8, location A). The fourth "normal" set (D_3; Fig. 8), have different styles depending on whether they cross mineralized horizons. In contrast to generally simple anticline-syncline pairs in unmineralized siltstones, the same fold zones in mineralized horizons show complex shapes, overprint intrafolial D_2 folds (Fig. 8), and locally show an axial plane slaty cleavage oblique to bedding. These folds are asymmetric and have a consistent sense of vergence indicating anticline east. In the northern areas of the mine most folds are north plunging. In southern parts of the mine most plunge to the south (Perkins, 1984). Thus, the better developed lead-zinc orebodies are associated with north-plunging folds.

Mount Isa Fold

The Mount Isa Fold, which formed during D_3 (Perkins, 1984; Bell et al., 1988) is the largest fold in the mine, with a wavelength of 200 to 400 metres and an amplitude of 130 metres

(Figs 2, 12a). It plunges to the north at 45%-60% and has a near vertical axial plane and short limb. The Racecourse Shear runs close to the anticlinal hinge of the Mount Isa Fold in Fig. 2 but in the north of the mine cuts to the west of this hinge and gives an apparent east block upwards movement in cross-section.

Foliations and lineations

Foliation and lineation measurements related to mesoscopic folds are shown in Perkins (1984). Cleavage microstructures are described more fully in Swager (1985a). Locally, a cleavage can be seen axial plane to D1 folds (Fig. 7a) that is also folded around D3 folds (Fig. 7b). However, apart from locally developed cleavages associated with folds towards the Paroo Fault, there are only two distinctive cleavages throughout the mine. The most obvious cleavage in the lead-zinc areas is parallel or sub-parallel to bedding. This cleavage, called S_2 by Swager (1985a), is defined by carbonaceous seams at a very low angle or parallel to bedding and is overprinted by cleavage that is always oblique to bedding, S_3 (Perkins,1984; Swager,1985a). This cleavage is generally not visible mesoscopically at higher levels in the lead-zinc areas, but is apparent in thin section (Fig. 7a). The modal orientation for S_3 in the mine is 80%-->258%.

Lineations on bedding surfaces are more obvious than their associated foliations, and are generally parallel to D_3 fold hinges. In some locations two sets of lineations can be seen on partings parallel to bedding. The later, stronger set parallel D_3 hinges and overprint the earlier set which can be a product of D_2 or $D_{2.5}$.

Cross-cutting fractures and veins

Figure 9 shows an array of cross-cutting fractures and veins in a lead-zinc orebody, and Fig. 5 illustrates their change in density between exposures. They have a range of orientations to bedding, but generally dip east, with the most deformed and dissolved (Swager, 1985a) veins having the steepest dip to the east. The majority of the veins show offset with a reverse component, indicating extension in the plane of bedding as described at Hilton mine by Valenta (1988,1989,1994a), although some, particularly those more continuous veins associated with flexural folds, have the opposite displacement. The former are referred to as D_2 veins by Swager (1985a) and Bell et. al. (1988). Where slickensides can be measured on carbonaceous shears on which the veins have nucleated they pitch at 90%. These veins are closely associated with zones of shear on bedding. They are thrust upwards to the east on these shears. An interplay of east-dipping veins is common, such that earlier-formed veins are displaced by shears, which are cut by younger more bedding perpendicular veins, which are in turn displaced by shears. Although east-dipping veins have a radial disposition around folds (Fig. 5b) and show extension in the plane of bedding on both limbs, they are not bc fractures relative to those folds. That is, they are neither perpendicular to bedding nor contain the fold axis. Typical veins dip 60%-65% towards

080% on the long limb of the Mount Isa Fold and 55% towards 185% on the short limb. Healed thrust faults, with vertical displacements generally of 20-50cm, are cut by most east-dipping veins (Perkins, 1984, fig. 34). The largest thrust fault observed has 100 metres displacement. A healed fault of similar appearance on the short limb of the Mount Isa Fold, maintains the same vergence relationship to bedding and dips more shallowly east suggesting that such thrusts formed earlier than the folds.

ALTERATION AND MINERALIZATION

Lithological changes in and around lead-zinc orebodies have been addressed by Neudert (1983) and Waring (1990,1991). They ascribed some variations to primary depositional processes, and others to what seemed to be a later overprint. Neudert (1983) interpreted some changes as being due to diagenesis, and others, particularly calcitization, as being post-diagenetic. Waring (1990), using Neudert's (1983) sedimentological framework, chartered a mineralogical (mainly phyllosilicate), and geochemical history in some samples that he regarded as being associated with early diagenetic lead-zinc mineralization, subsequently metamorphosed and overprinted by silica-dolomite alteration. Features which Waring (1990, 1991) interpreted as being of metamorphic origin were; a biotite/stilpnomelane/magnetite assemblage, some recrystallization of sulphides, and a calcitic banding recorded beyond the mine area, which was interpreted to form from a reaction between calcite and potash feldspar.

Potassic alteration

Croxford (1962, 1964) and Waring (1989) interpreted spatial and genetic relationships between sulphides and potassium feldspar. Croxford considered that although potassium feldspar was an authigenic component, it was a proxy for the amount of volcanic material in the sequence, given that it was most concentrated in the TMBs, which he had identified as containing shard textures. Waring (1989) noted a strong association between sulphides, particularly zinc, and potassium. Potassic enrichment consists of fine-grained Kfeldspar, muscovite, and biotite.

The distribution along strike of these minerals has been examined in two TMB horizons to determine why these horizons are not readily recognizable to the north of the mine. The first of these, the 14/30 TMB, on the 8150N cross-section at depth is a distinctive sequence consisting of a light grey non-laminated fine-grained K-feldspar-rich base of 110 mm, with a 105 mm highly feldspathic flecked and banded sequence above. C. Brodie and S. Bartrop (pers. comm. 1991) have correlated the same horizon to a level 800 metres higher in the same 8150N cross-section based on a detailed comparison of alternating sequences of laminated and non-laminated layers. Here it consists of a 48mm grey non-laminated layer with a 25mm darker banded top. Five hundred metres further north (8650N) the same horizon has a 75mm non-

laminated base, with a banded top of at least 15mm. These beds have only a very minor development of fine-grained K-feldspar, and are composed mostly of quartz, muscovite and biotite.

The second TMB examined, which occurs at the base of 7 orebody (refer Fig. 3), shows even more marked changes. This TMB is normally 50mm in width, and contains extensive cross-cutting veins. On 9A sublevel, beginning at 7005N, this marker bed changes abruptly along strike, over approximately 6 metres, from 50mm of fine-grained feldspathic rock to 30mm of greenish-grey highly biotitic siltstone with bands of sphalerite. Another 8 metres further north, it again becomes a 50mm grey fine-grained feldspathic layer. The same horizon at 41000N (i.e., another four kilometres north) is no longer recognizable as a TMB but was identified by correlating the laminite sequence above and below (Fig. 4). It is a weakly potassic, vaguely laminated, dark grey layer with no cross-fractures. In thin section it shows a basal 3mm well-preserved zone of glass shards in a carbonaceous matrix. Above this is an increasing density of interlocking felted mass of sericite in which the shard shapes become progressively less distinct. Thus the Mount Isa marker beds, although quite consistent within the mine, lose their diagnostic character within three kilometres north of it, and their highly feldspathic nature is better explained as part of a potassic alteration halo, preferentially affecting particular mica-rich layers, rather than potash added from the coeval lake waters during diagenesis (Croxford, 1962, Neudert, 1984).

Cross-fractures and their associated veins, which are ubiquitous in the feldspar-rich TMBs, indicate that the beds have behaved as rigid bodies during ductile deformation of adjacent laminated sequences. Individual blocks of feldspathised layers, separated by fractures, commonly exhibit extensional relationships, with underlying laminated sequences folded to accommodate the movement on the cross-fractures. The transition to micaceous alteration is associated with a thickness decrease of about 40%, indicating that shortening strain was accommodated by fracture formation in the feldspathic zones and ductile deformation in the micaceous zones. The overall relationships suggest an early D_2 origin for the fine-grained feldspar alteration.

Alteration in the 7 orebody hangingwall sequence

In order to minimize the effect of sedimentological variation, one of the approaches of this study has been to document the changes in composition and texture of a sequence correlated and bounded by two TMBs. These units are in the hangingwall of 7 Orebody and are referred to as the "B" sequence. The sequence immediately above it, which lies beneath the next higher TMB in the stratigraphic succession, is referred to below as the "A" sequence. Additional observations and analyses (Fig. 10) have been added since that illustrated in Perkins (1984). Data points are shown in Fig. 10a along with the stratigraphic thickness changes. These markers have been correlated over a distance of seven km.

A series of representative samples from the B sequence is shown in Figure 11. These samples represent the typical alteration sequence inwards from the least altered laminite. Separation between the twin markers ranges from 35mm to 400mm in the mine vicinity and up to 380mm in DDH F968 (2.6km north of the orebody). Typically, the intervening sequence consists of alternations of three laminated zones (e.g. layer 1 in Fig. 11) and two non-laminated zones (e.g. layer 2 in Fig. 11). Where the sequence is unaffected by obvious alteration, a lamina-by-lamina correlation can be achieved, and matches can be made between mineralized and unmineralized zones along strike. The main cause of variation in stratigraphic thickness occurs in two layers (layer 2 and the similar unlaminated layer above the lower TMB in Fig. 11) which vary from unlaminated fine siltstone and mudstone to the thick (150mm) discontinuously laminated 'flecked' potassic bands, most commonly seen as the 'flecked tops' of TMBs. Although these non-laminated layers are in places weakly mineralized, particularly by sphalerite, it is mostly the carbonaceous well-laminated zones that become mineralized along strike. Distally, they are mineralized by fine-grained pyrite (Fig. 11a). They pass through a zone of "nodular dolomite" (Fig. 11b), which displaces, disrupts and overprints the laminae, and is associated with a thickness increase of 35% relative to the unaffected laminite. These disrupted laminae still contain abundant fine-grained pyrite. The nodular dolomite layers, generally about 1mm in thickness but ranging up to 3mm, are then progressively associated with sulphide (Fig. 11b), initially consisting of sphalerite and ultimately of sphalerite plus galena. Pyrrhotite and euhedral pyrite may accompany these sulphides.

"Buff alteration", where the most obvious change is bleaching, by oxidation, of carbonaceous stylolaminae, and the parallel development of illite or albite, phlogopite, and biotite, also appears abruptly towards the south. On 11 level in the mine, this zone is carbonaceous at 7180N, and has become extensively buff altered 20 metres south at 7160N. Where buff alteration overprints finely laminated sequences, the rocks appear in hand specimen to be massive, but laminae are subtly revealed in thin section. On 11 level, 7058N (Fig. 11c), the buff altered zone in the unlaminated part of the B sequence (layer 2) consists of the following mineralogy in decreasing order of abundance; quartz, dolomite, muscovite, K feldspar, albite, siderite, phlogopite.

A zone of greenish-grey vaguely laminated siltstone (Fig. 11e), characterised by Fe-rich chlorite altered from brown and green biotite, occurs on the margins of the silica-dolomite. The marker beds are quite indistinct and narrow at this level, and correlation of the sequence becomes difficult. Below this the correlatable sequence is lost in a continuous zone of coarsely crystalline dolomite. The alteration and mineralization profiles of the B sequence are shown in Fig. 10.

Mineralization in the 7 orebody hangingwall sequence.

In the ensuing description the distribution of sulphides refers to those apparent in hand specimen. Lamina-parallel fine-grained pyrite extends outwards to 39,680N within the B

sequence, but is not present at 41,000N. The southern fine-grained pyrite boundary is shown on Fig. 10c. It pitches steeply northwards, sub-parallel to the anticlinal hinge of the Mount Isa Fold and about 200m south of it. There is a narrow zone of overlap of pyrite and pyrrhotite, with pyrrhotite extending inwards towards the silica-dolomite front. In these zones some layers are carbonaceous and pyritic, and others are bleached and contain pyrrhotite. The outer margin of pyrrhotite is closely related to bleaching and buff alteration. The maximum concentration of pyrrhotite is within the highly chloritic zone. Coarse-grained pyrite has a wider distribution than both pyrrhotite and fine-grained laminated pyrite.

Towards the orebody, sphalerite first appears as disseminations within the marker beds themselves, and then subsequently is associated with the nodular dolomite layers. It reaches its maximum development as almost monomineralic layers associated with approximately bedding-parallel margins rich in chlorite and muscovite. Sphalerite is distributed in a zone lying immediately south of the Mount Isa Fold and north of silica-dolomite. Galena has a restricted distribution and only constitutes more than 1% of the sequence immediately north of the silica-dolomite. Here it forms part of a breccia texture, consisting of veins between partially rotated laminated fragments, and minor bedding-parallel strands. Chalcopyrite occupies the deepest position and also undoubtedly occurs within completely dolomitized areas closer towards the greenstone contact. Distribution of all the sulphides within the B sequence is shown in Figs 10c and d.

The 7 Orebody hanging wall sequence reveals a progression of alteration and mineralization downwards towards silica-dolomite consisting of bleaching and carbonate grain coarsening plus sphalerite plus galena, to "buff-bed" alteration with pyrrhotite, to appearance of biotite, to chlorite-pyrrhotite. Sequences with well developed 'buff-bed' alteration have an antithetic relationship with fine-grained pyrite. That is, fine-grained pyrite ceases and pyrrhotite dominates where buff bed alteration commences in the same sequence from north to south.

Alteration profile

A cross-section showing the alteration profile across the entire mineralized system and its relationship to orebodies is shown in Fig. 12. The zones of bleaching and buff alteration can only be portrayed diagrammatically, as they are commonly limited to stratigraphic sections a few metres in width, separated by narrow zones of less altered siltstones. This combined pattern may persist down dip for more than a hundred metres. Only five holes were relogged on this section, with the bulk of data obtained from previous logging of about 80 holes and thirty development intersections spanning many years.

Phyllosilicate alteration

Timing of phyllosilicate alteration and its relationships were discussed by Swager et al. (1987). Phengite II, phlogopitic biotite, stilpnomelane and Fe-rich chlorite, were interpreted to form replacively and subsequent to the D_2 veins. Phengite II is locally a component of the buff alteration of this study, but is not ubiquitous, and requires thin section identification. The biotite in the B sequence is altered to chlorite and subsequently overprinted by pyrrhotite. Biotite and white mica fronts are locally formed around small-scale folds associated with east-dipping dolomite veins. Biotite above the 3500 Orebody silica-dolomite is replaced by sphalerite, both along bedding and around cross-cutting fractures. There are no examples of sulphides that have grown before associated phyllosilicates.

Siderite zones

Only one drill hole (I702 Vert.) with significant siderite in the vicinity of the 6999N section has been examined (Fig. 12b). Other sections indicate that there ought to be substantial siderite around the upper part of the silica-dolomite above the 3500 orebody, but this area has not been re-examined. The interval containing light brown siderite in I702 covers a vertical depth of 84 metres, and locally constitutes about 70% of the rock. Although graphite is not present and white dolomite veins are common, bedding laminations are generally visible. Siderite is not only discontinuous along bedding, but also forms laminated selvages along vein systems showing that it is an alteration product. It is strongly associated with magnetite, which varies from fine concentrated dustings to isolated grains up to 3mm. Stilpnomelane is common in the sideritic zone and occurs as fine needles 0.5 to 2mm, commonly aggregated into sinuous green veins at a high angle to bedding. Siderite, magnetite and stilpnomelane all appear to be overprinted by pyrite, pyrrhotite and chalcopyrite.

Sulphate evaporites?

A number of mineral aggregate shapes in the Mount Isa sequence have been interpreted to be due to original sulphate evaporites (McClay and Carlile, 1978; Neudert, 1984) and this has been incorporated into models for sulphur sources for mineralization, (e.g. Neudert, 1984; Andrew et. al., 1989). These features have been re-examined to see if they represent evaporitic sulphates; what was their original mineralogy, and what is their relationship to mineralization? Three broad groups of shapes have been interpreted to have originally been sulphates: i) well-terminated acicular columns now composed of dolomite and quartz; ii) vaguely terminated or ragged laths; and iii) irregular growths of carbonate referred to above as nodular dolomite.

The well-terminated columns have only been described in the silica-dolomite and have been extensively examined by J. Knights (pers. comm., 1984). Comparison of cross-sectional shapes with both published examples and unreplaced barites at the Hilton mine, led this investigator to the conclusion that the shapes are pseudomorphs after barite. Their random

discordant habit with respect to bedding also suggests that shortening normal to bedding was complete before they formed. This also indicates that they grew at the late stages of deformation, are not evaporitic in origin, and may be part of the alteration system.

An example of the more ragged lath shapes is shown in Fig. 13. In this case they are irregularly replaced by quartz, feldspar, and pyrrhotite. Where these shapes are not entirely replaced by pyrrhotite, the remainder of their form is occupied by a coarser-grained version of the surrounding rock constituents. This is generally dolomite, quartz, or K-feldspar. The most reasonable interpretation seems to be that they were sulphates, but were replaced by other phases before the sulphides. Again, it is noted that they do not occur in the least altered rock, suggesting that they were formed during the alteration process.

By far the most common texture ascribed to evaporitic processes, is that often referred to as nodular dolomite. There is a range of textural types. Neudert(1983) lists the following criteria for the interpretation of carbonate nodules (his NODC) : i) their "nodular fabric"; ii) their displacive growth in laminated dolomitic siltstone (L), and fine-grained pyrite-bearing laminated siltstone (PYL); and, iii) their association with pseudomorphs after sulphate evaporites. These were interpreted as suggesting that they were former sabkha-type evaporite-sulphate nodules. Neudert (1983) also recognized a range of styles of replacive metasomatic carbonate along bedding, and realized the difficulty of discriminating between these and his "evaporite nodules".

Nodular dolomite was regarded as being after evaporitic sulphate only in the lower Urquhart Shale (Neudert, 1984). The problem is best illustrated with respect to the B sequence, where the continuity of the textures can be examined in a time-stratigraphic horizon. Figure 14 is a sequence of sparry dolomite layers with thicknesses of between 0.5 and 3 mm, separated by discontinuous wavy bands of fine-grained pyrite. This same sequence, both to the north and south, becomes a finely laminated carbonaceous siltstone with individual laminae being correlatable over at least one kilometre. The lenticular shapes are composed of three generations of dolomite. The first is fine-grained and inclusion-rich, the second is up to 100 microns, more euhedral but still inclusion-rich, and the third is cleaner sparry dolomite associated with sphalerite aggregates. The overall distribution of the nodular zone can be directly related to the alteration patterns (Figs 10b and 12b) and is evidence against it being an early diagenetic sulphate texture.

Relationship with silica-dolomite alteration

Perkins (1984) demonstrated that silica-dolomite overprinted sequences containing the lead-zinc orebodies. Because it was assumed at that time that lead-zinc sulphides were an integral part of the sediment, the conclusion was reached that the silica-dolomite also overprinted the lead-zinc ore. Re-examination of the boundary zones between lead-zinc lodes and silica-dolomite, has revealed that this is not the case. Layers of coarse-grained dolomite, with a range of preservation of bedding trails, persist for large distances from mapped silica-dolomite

boundaries into sequences containing lead-zinc ore. In the 7 orebody, for example, on 13 Level 6570N, the orebody sequence consists of 15% coarsely crystalline dolomite, and yet this location lies 80 metres north of the mapped silica-dolomite boundary. The tendency has been to show silica-dolomite and lead-zinc ore as being mutually exclusive on published diagrams, whereas when a strict rock type definition is used there are substantial areas of overlap. Although it is associated with less laminae disruption and is coarser-grained, the bedding-controlled porphyroblastic dolomite forming the "recrystallized shales" of the silica-dolomite (Perkins, 1984; Swager, 1985a) constitutes a textural continuum to the nodular dolomite of the lead-zinc zones. The silica-dolomite overprint on the B sequence shows a complex pattern (Fig. 10 and Perkins, 1984).

Distribution of sulphides

Patterns of fine-grained pyrite and pyrrhotite distribution were produced at 1:2500 scale from 77 drill holes and 12 development headings on the section. They were then generalised to 1:1000 from 15 longer holes using average values with a minimal width of 10 metres (Fig. 12c). Lead and zinc grades (Fig. 12d) have been generalised from detailed cross-sections at 1:500 produced by D. Hutton. Sequences that contain both pyrite and pyrrhotite are shown as areas of overlap. Features of importance in Fig. 12 are: i) the wide expanse across dip of fine-grained pyrite, ii) the grossly antipathetic relationship of pyrite and pyrrhotite, iii) the formation of two distinct centres of mineralization other than pyrite either side of the short limb of the Mount Isa Fold, and iv) the abrupt diminution to low levels of lead and zinc close to the anticlinal hinge of the Mount Isa Fold.

In longitudinal section, the southern ends of the orebodies close to the silica-dolomite are enriched in galena relative to sphalerite, and also the ratio of silver-bearing tetrahedrite to galena increases markedly. These trends are shown in fig. 13 of Mathias and Clark (1975), which charts the silver, lead, and zinc grades in the lowermost three metres of 7 orebody.

Within a stratigraphic horizon, the zonation outwards is from copper ore to a low-grade copper zone, then abruptly into silver-rich galena ore, outwards into more sphaleritic mineralization and ultimately to fine-grained pyrite. This corresponds to the same zonal pattern on cross-sections, and is supportive evidence of Cu-Pb-Zn being a single zoned system.

Sulphide textures

Sulphide textures have been described by Grondijis and Schouten (1937), and Croxford (1962). However, most of this earlier work was done using polished blocks, without concurrent transmitted light observation. The descriptions below were compiled using polished thin sections.

Pyrrhotite: Pyrrhotite occurs commonly as either disseminated lath-like, or bladed aggregates, irregularly arranged along bedding and randomly oriented to it, or more or less continuous bands along bedding. Many of the bladed aggregates have relict fringes of other minerals pseudomorphing even earlier precursors. Examples of the range of pyrrhotite types are illustrated in Figs 11 and 13. Pyrrhotite has characteristic ellipsoidal and globular shapes when surrounded by other sulphides.

Galena: Most galena occurs as either subhedral aggregates where associated with coarse-grained gangue minerals, or as connected wisps and lenses where associated with finer-grained dolomitic siltstones. Cross-cutting styles (Fig. 5a) are generally coarser-grained.

Sphalerite: Much more sphalerite than galena occurs as finer-grained aggregates in minimally altered feldspathic siltstone. Where associated with coarse-grained gangue minerals it occurs as almost continuous aggregates, and invariably with galena.

Pyrite: A range of forms of pyrite may occur, either together or in isolation. Typically, the finest-grained pyrite (commonly called Pyrite I) consists of composite grains in the 10 to 20 micron range, with a range of cleaner core shapes and more inclusion-rich spongy outer zones. Up to seven growth zones have been identified by SEM examination (Perkins, 1986a). Where these individual zoned crystals become sufficiently close-packed, a range of impingement structures have developed. Continued development of more euhedral overgrowths can have resulted in almost massive pyritization of the host carbonaceous siltstone. Much bedding-parallel pyrite, sometimes referred to as "brassy pyrite", is discontinuous along bedding in contrast to the zoned fine-grained pyrite described above, with which it is commonly associated. It is more euhedral and coarser grained, and commonly terminates abruptly on fractures at a high angle to bedding (Neudert, 1988; Waring,1990). The other main form of pyrite (Pyrite II) occurs as coarse-grained single crystals or clusters, which may be strung out along more coarsely-grained dolomitic layers, or randomly located within more massive siltstones or cross-cutting veins. These pyrite grains do not have internal rounded zoned cores. In the B sequence nearly all stratiform pyrite is of the fine-grained type, and no brassy pyrite is present in Fig. 10c.

As thoroughly described by Grondijis and Schouten (1937) and Croxford (1962), locally all the sulphides, (i.e. chalcopyrite, pyrrhotite, galena, and sphalerite) show various replacement textures with zoned fine-grained pyrite. All evidence indicates that it was the earliest sulphide to form.

Sulphide relationship to quartz and dolomite

Interpretation of the boundaries between sulphides and adjacent gangue minerals, particularly quartz and dolomite, is critical to understanding the timing of sulphide formation. Typical features of these relationships at microscope scale are presented in Fig. 15. Sulphide boundaries are shown relative to these gangue minerals at a range of grain sizes, both along bedding and cross-cutting veins. Similar boundary relationships occur where the adjacent quartz

or dolomite shows deformation or partial recrystallization textures. An interpretation of these boundaries is discussed below.

Sulphide-sulphide textures

Some of the sulphide/sulphide relationships have been extensively documented and analyzed. In particular, the diagnostic zoned structure of fine-grained pyrite is readily recognized when partly or largely pseudomorphed by all subsequent sulphides, (Grondijis and Schouten, 1937; Croxford, 1962). One of the most important relationships is that between sphalerite and galena. Their normal distributional relationships are shown in Fig. 16 and fig. 38 of Grondijis and Schouten (1937). However, the nature of the boundaries between these sulphides in contact changes according to the volumetric proportion of galena. Where galena is less than 20% of the total sulphide volume, such as the right half of Fig. 16b, it occurs as strings of fine blebs between sphalerite bodies, or as cusp-shaped forms within them. With increasing proportion of galena, the sphalerite becomes more rounded. At high proportions of galena (Fig. 16a), sphalerite appears as subrounded inclusions or lenses.

Distribution of styles of mineralization

Fine-grained galena along laminations is best developed deep within individual orebodies, where lead grades are high, sphalerite is generally much diminished, and chalcopyrite is ubiquitous. This textural style is commonly close to silica-dolomite boundaries, such as 5 orebody 11 level 6540N, and is everywhere associated with close-spaced veinlets rich in galena. Further outwards, galena occurs more commonly in breccia veins and folded zones. At the periphery of the lead-zinc system, galena is more likely to occur with coarse-grained dolomite either sub-parallel with bedding or as cross-cutting veins. Sphalerite is well developed along bedding to quite distal zones with increasing outwards concentration along small-scale veinlets. The most distal sites are disseminations in TMBs and are associated with coarser-grained carbonate aggregates.

STRUCTURAL RELATIONSHIPS OF ALTERATION AND MINERALIZATION

"Bleaching" and "buff alteration"

In the interpretation of Neudert (1984), much of what was included in his "facies II", appears to coincide with the areas of bleaching. Facies II represents thicker bedded and early cemented siltstones (Neudert, 1984). Where thicker beds form a high proportion of the sequence, such as between the 7/20 and 8 orebodies, the author has no problem with this interpretation.

The difficulty arises with thick sequences of very light coloured laminated and non-laminated units that can be correlated with dark grey and carbonaceous laminites in adjacent drill holes higher up dip. Zones of transition between them have lighter coloured layers that show abrupt fronts with finely laminated carbonaceous siltstones. Figure 17 shows three layers of dolomitic aggregate that from top to bottom are massive, abruptly discontinuous and fragmented. The fragmented layer is typical of the nodular dolomite. The central layer is typical of what was regarded as a concretion. The massive layer, which is continuous for hundreds of metres, is typical of what has been regarded as primary thick siltstone (Neudert, 1983). However, Fig. 17 shows that all three layers can have formed from the same primary lithology, that is, the carbonaceous laminite from which the central layer has developed. The 60% thickness change in the central layer is associated with an accentuated lamina-parallel foliation in the carbonaceous laminite, which flattens and folds earlier microveinlets. Cross-cutting replacive vein structures, with the same crystallinity as the lighter bleached lenses are also folded with axial planes and overprinting carbonaceous cleavage parallel to bedding. Thus thick sequences of bleached and buff-altered siltstones have an origin that is the same as local concretionary fronts and that they are an early effect of a zoned alteration system.

Breccia veins and ores in folded zones

Galena-rich breccia veins generally overprint extensional fault-veins on at least one margin (Figs 3a and 18). This overprinting has the effect of removing correlatable stratigraphy and smoothing out fault irregularities. Breccia textures show a continuum from almost intact intrafolial folds (e.g. Fig. 8) to microbreccia (e.g. Fig. 3a). The breccia texture apparently results from variable replacement of intrafolial folds preserving various portions of the original folded structure (Fig. 18a). Where sulphides constitute less than about 50% of the non-bedded part of the rock, the formation of discrete breccia fragments appears to result from fracture-controlled coarse-grained dolomite replacement, similar to that for breccia veins in copper ore (Perkins, 1984; Fig. 17). This dolomite may subsequently be locally replaced by quartz, with both phases variably replaced by sulphides (Fig. 15b). Many individual breccia fragments are rounded, and bedding may show greater rotation between closely adjacent fragments than can be accounted for by folding and subsequent dolomitization alone.

Transgression of fold hinges and limbs and overprinting of S_3 axial plane cleavage by sulphide-gangue assemblages apparently occurs via an initial replacement of laminations by metasomatic dolomite, followed by progressive replacement of that dolomite by sulphides (Fig. 19). This example reveals a less advanced stage of alteration of a folded sequence and can be interpreted as leading to the formation of relict portions of folds as illustrated in Fig. 18a.

There is a complex relationship between extension on fractures at an angle to bedding, subsequent dextral shear along these fractures, shortening and cleavage formation, and alteration and mineralization (Fig. 20). In this example from 5 orebody, there is a well developed set of

extensional fractures in the unmineralized layers whose traces abruptly rotate dextrally into the altered layers and turn sub-parallel to bedding. Relict shear traces, commonly located by chlorite zones, can be tracked, by laminae matching on either side, to where they intersect the next unmineralized band. Traces of these shears have irregular folded shapes as they weave between displaced laminae. The folding of juxtaposed layers and shear traces indicates a phase of shortening that has produced buckles in thicker layers and tight folds in thin layers surrounded by gangue alteration and sulphides subsequent to extensional shearing and dextral rotation.

Laminated mineralization

For the purpose of examining timing relationships in laminated sulphide-bearing sequences, a division has been made into those sequences associated with coarse-grained carbonate and those which are not. In reality, there is a continuous gradation between the two types.

Coarse-grained carbonate associated: Layer-parallel sphalerite and galena associated with coarse grained carbonate are commonly extremely discontinuous along strike, particularly towards the northern extremities of the orebodies. Sequences up to 0.5 metres in width may contain 12% combined lead-zinc, with the same interval in a drill hole 20m away containing virtually no lead-zinc mineralization. Narrower intervals of mineralization may die out between the floor and back of the 2.8 metre high development walls. Structural relationships for this style can be determined from mineralization fronts that are spatially related to flexures around east-dipping veins (Fig. 21). Although axial plane cleavage is only weakly developed in the folds examined, flexures are commonly associated with more normal upright east-verging D_3 folds, indicating that they belong to that event. Dilation on bedding may terminate in the vicinity of the flexure and be related to it as shown in Fig. 22. In this example, dilation and replacement of the finer-grained mudstone layer is associated with the development of a fold with an axial plane cleavage (S_3). The sphalerite replacement front, both within the zone of coarse dolomite replacement and within the laminations, coincides with this flexural limb.

Non-carbonate associated: This style of mineralization, most commonly pyrite and sphalerite, but rarely galena and pyrrhotite, contains the smallest aggregates of sulphide grains developed in the Mount Isa system. Individual sphalerite aggregates may range from 5 to 50 microns. Examples of abruptly discontinuous finely laminated sphalerite showing timing relationships, and a front of galena-rich mineralization are shown in Fig. 23.

A series of east-dipping veins is associated with abrupt cessation of fine-grained sphalerite in laminated potassic siltstone (Fig. 23a,b) in 7 orebody, 7060mN, 11 Level. Sequences can be correlated across veins where they continue with essentially no sphalerite, but become abruptly mineralized again across another vein. The non-mineralized gap in Fig. 23 is 370mm measured down dip. The two veins controlling mineralization have orientations of 56%

-> 122% and 57% -> 124% where bedding is 72%-> 268% (dip and dip direction) and the intersection lineation on bedding plunges 62% -> 322%.

In a vertical east-west plane, the bedding is consistently displaced across veins with an upper block west motion but this is generally of the order of a few millimetres. The fractures thus result in extension in the plane of bedding. Many of the veins terminate in slight flexures of bedding, showing that large displacements along the bedding/vein intersection are not possible. The transgressive front of sphalerite mineralization, although spatially associated with the east-dipping veins, does not always coincide with them. Where it does not, it generally coincides with a very slight flattening of bedding. Where sphalerite does terminate on the veins, the veins themselves are also partially replaced by sphalerite in conjunction with pyrite and pyrrhotite (Fig. 23c). This is interpreted to indicate that the sphalerite precipitated in the veins during the same event in which it precipitated in the laminae. Similarly, veins located within the sphalerite-mineralized zone are themselves replaced by sphalerite, whereas those outside are not.

The sequence at the locality of Fig. 23 also contains pyrite and pyrrhotite. Most of the pyrite is fine-grained, occurring as almost continuous wavy laminations with a spacing of approximately 0.5mm. There is no obvious change in pyrite concentration or distribution across the east-dipping fractures. Pyrrhotite occurs in distinct bands, but is more or less disseminated along them. Coarser concentrations of pyrrhotite are up to 2mm wide and may be almost continuous along bedding. Much of the pyrrhotite occurs as ragged lenses, with lengths about 3-5mm and widths of 0.7mm. The pyrrhotite aggregates are slightly oblique to the average bedding and in vertical section are steeper, more parallel with S_3 cleavage. Where laminae are wavy, pyrrhotite aggregates are not only better developed, but distinctly replace that part of the laminae which is more parallel to S_3. In the plane of bedding, pyrrhotite aggregates have ragged lath-shapes, with no preferred orientation. Both east-dipping and north-west dipping veins show extensive development of replacive pyrrhotite, with protrusion of pyrrhotite aggregates outwards into the laminae on either side of the vein. As with pyrite, there is no obvious change in pyrrhotite concentration across the east dipping veins.

Mineralized zones diminishing to background levels over distances of a few metres are quite common, particularly in the northern extremities of the orebodies. Many localities showing abruptly terminating mineralization on, or in the immediate vicinity of, cross-cutting structures, have now been located. Some other examples are: 7 orebody 7060N 7 Level; 7 orebody 9C sublevel 7030N, 8 orebody 7340N (Drill hole K734 East decline at 96.7m.). The orientations of the measured fractures and veins that control these sulphide fronts are shown in Fig. 24. They mostly belong to the east-dipping set (D_2 veins of Swager, 1985a), but some strike more east-west and have steep dips.

Fine-grained pyrite: A complete discussion of fine-grained pyrite and its timing relationships is presented by Perkins (1996b). Although fine-grained pyrite always seems to be paragenetically earlier than all other sulphides, it also shows microstructural evidence of late replacive precipitation, overprinting both the S_2 cleavage parallel to bedding and the cross-

cutting S_3 cleavage, although it is continuous across the same structures that terminate the sphalerite. Its spatial association also indicates that it belongs to the same system as the lead-zinc mineralization.

Gross structural features

Lead-zinc orebodies are spatially related to two major structures; the Paroo-Basement fault ramp system and the Mount Isa Fold. They form around the silica-dolomite, which is in turn controlled largely by the Paroo-basement ramp (Perkins, 1984). The upper and lower bounding surfaces of lead-zinc ore are sub-parallel with this structure (Fig. 12). Alteration associated with lead-zinc orebodies is argued above to be contiguous with the silica-dolomite. The eastern termination of the lead-zinc lodes, constituting part of the *en echelon* pattern described earlier, is closely related to the Mount Isa Fold (Figs 2a and 12e). For example, 7 orebody ore grades on the western long limb of the fold diminish abruptly as the anticlinal hinge of the Mount Isa Fold is approached on 11 level. Grades drop from 7.0 m at 3.7% Pb and 8.2% Zn at 7270N, to 500ppm Pb and 2400ppm Zn in the hinge only 45 m north. Layer-parallel pyrite, in contrast, continues around the hinge with no obvious change in abundance. Mineralization on the sub-vertical short limb of the Mount Isa Fold only reaches mineable ore grade in 14-10/30 orebody (Fig 12). In plan, this lens rapidly diminishes in grade within about 30 m of both the anticlinal and synclinal hinges (N. Davies, pers. comm., 1989). Ore in a stope face in this short limb showed no obvious differences from that in the long limb, although there were no associated extensional veins or development of near-bedding parallel breccias at that locality.

DISCUSSION

Timing criteria

Two important principles are relevant to the application of timing criteria for alteration and mineralization. Firstly, there is the uniqueness of an interpretation in a given sample, and this is further discussed below. Secondly, there is the interpretation applied to samples that do not contain suitable microstructures for timing constraints. The principle followed herein is that, where sulphide textural relationships in such samples are the same as those where timing criteria are available, then it is reasonable to assign the same timing to them.

Evidence for sulphides being syngenetic, diagenetic or epigenetic (Tourtelot and Vine, 1976) must also be addressed. Neudert (1984) presented a detailed argument against syngenetic accumulation of sulphides, and argued that metals must have been introduced into the sediment pile. Some evidence for diagenetic timing was cited, and recognition was given to coarser-grained bedding-parallel pyrite being controlled by fractures, although the age of these fractures

was unknown. An early diagenetic timing for at least the initial Zn-rich stage of sulphide formation was suggested by the interpretation of sulphate as an integral component of the sediment, and some evidence of burial compaction subsequent to sulphide growth. The evidence against sedimentary deposition of sulphides is supported by the observation that the sulphides examined have replacement relationships with their host gangue minerals (e.g. Figs 15, 18, 19, 22 and 23).

A finely stratiform sulphide habit, in deposits such as Mount Isa, is frequently cited as the main evidence for either a syngenetic or early diagenetic origin (Stanton, 1962; Gustafson and Williams, 1981). Fine aggregation of sulphides in different concentrations along adjacent beds, of itself, is not indicative of either a sedimentary or a diagenetic origin. This depends on whether there is alternative evidence that such a bedding-controlled distribution could be post-sedimentary. Discordant fronts of sulphides, such as those illustrated in Figs 21, 22 and 23, show that a stratiform distribution of sulphides along bedding has been superimposed subsequent to compaction of the sediment, and also subsequent to extensional fractures and veins.

Additional evidence for a diagenetic origin for much of the Mount Isa sulphides has mostly come from discussion of the fine-grained pyrite, and the availability of evaporite sulphate interpreted to be contained in the compacting sediments (Neudert, 1983). Arguments against the availability of sulphate at the diagenetic stage appear below, and the interpretation of fine-grained pyrite is discussed in detail by Perkins (1996b).

Timing of sulphide formation

Interpretation of the timing of precipitation of the stratiform sulphides is intimately related to the question of replacement relationships. If the evidence of replacement is accepted, then the textures and structures replaced designate the stage of evolution of the host prior to replacement. Distinctive structures illustrated herein and their relationship to sulphides include; the extensional fractures, flexures, and veins which terminate mineralization fronts; near bedding-parallel breccias which host the bulk of the galena-rich ore; and folds showing digestion by carbonates, quartz and sulphides.

Veins around which sulphide fronts occur are radially disposed on larger D_3 folds, and are not deformed by any foliation parallel to bedding. They have slightly dissolved boundaries where they are affected by S_3 cleavage, and textural characteristics that are the same as the D_2 veins of Swager (1985a). Sulphide fronts, such as those of Figs 21, 22 and 23, are interpreted to indicate that the sulphides are post-D_2 in origin.

Relationships to structures formed during the D_3 stage are illustrated in Figs 18,19 and 22. In these examples, D_3 folds appear to have been variably overprinted by dolomite and quartz and subsequently sulphides. The bedding-parallel fold zones and breccias, by analysis of the structures shown in Figs 18 and 20, indicate post-D_2 shearing on bedding-parallel zones that form dilational structures and nucleate neomorphic dolomite, quartz, and phyllosilicates. These

shear zones (Fig. 20) are apparently subsequently shortened to produce intrafolial D_3 folds, which continue (Fig. 18) to be overprinted by alteration minerals. Any stage of this alteration sequence appears to be overprinted by variable sulphide replacement of the alteration assemblage. Although alteration minerals show evidence of deformation and later overprinting by strain-free gangue assemblages, all generations can be replaced by sulphides.

Constraints on the timing of alteration and mineralization indicate that some growth of dolomite and veining began early in the formation of the bedding-parallel cleavage, and continued through it. Carbonate and quartz deposition continued during the cross-cutting D_3 folding, and sulphides were deposited late in the formation of the S_3 cleavage.

Remobilization, deformation and recrystallization versus dissolution, solution transfer and crystallization

In order to evaluate the evidence for a syndeformational origin for mineralization, it is necessary to discuss the concepts of remobilization and recrystallization, as applied to stratiform deposits. Using the definitions of Marshall and Gilligan (1987), remobilization involves the transfer of sulphides from their initial site of deposition to another local site. It generally refers to plastic behaviour during deformation resulting in bedding-parallel or cross-cutting vein structures, but can refer to dissolution and reprecipitation. Implicit in the definition is that the sulphide was present in the immediate environment in an earlier form.

The most comprehensive study to document remobilization at Mount Isa was that by McDonald (1970), who sampled a series of intercepts of a galena-rich layer through a fold zone. Using trace element variations and textural relationships, he concluded that galena was enriched in the fold hinges relative to the limbs, but that this enrichment was not associated with depletion in the limbs. The galena concentration in the southern long limb between 15 and 40 m south of the anticlinal hinge, was regarded as the base level. Thus the study did not document remobilization, but could be equally compatible with a total introduction of galena from outside the system. That is, it does not rule out "mobilization" as defined by Marshall and Gilligan (1987). It relied on an assumption by McDonald (1970) that the galena and sphalerite were present as an integral part of the sedimentary succession prior to the deformation.

Other reports on the deformation and remobilization of Mount Isa ores have been made by Hewett and Solomon (1964) and McClay (1979, 1983b). Hewett and Solomon described structures associated with lead-zinc ore, which included throughgoing and intrafolial folds, boudins, tension gash fillings, sulphide-matrix breccias, and a range of sulphide-bearing veins. They then related these structures to deformation of lead-zinc ore, having assumed that the sulphides were already present in the immediate environment, as alternating bands with shaley layers, prior to plastic deformation.

One of the arguments to show that sulphides have been consistently deformed was used by McClay (1979). He presented observational data of Mount Isa fold profiles and classified

them according to dip isogons. He then correlated fold morphology and fold development with the rheology of sulphides, concluding that there was a hierarchy of competencies from massive galena through to carbonaceous siltstones, which was also consistent with experimental data. From routine observation of underground development, the relationships described by McClay (1979) appear to be compelling, even obvious, and have been the accepted interpretation of the fold relationships, even by this author, for many years.

There are two fundamental concerns with McClay's (1979) reasoning. Firstly, although he illustrated examples showing a hierarchy of competencies, this does not accord with my observations in the mine. Only in very rare instances do individual sulphidic layers consist of one sulphide alone, and gangue minerals undoubtedly constitute a significant proportion of McClay's (1979) samples. Certainly, class 2 and 3 folds in the mine are commonly filled with semi-massive galena, but other similar folds may be highly pyrrhotitic or even sphaleritic (e.g. Figs 8 and 19). Commonly, galena-rich zones are associated with only gentle flexuring and yet this is a highly incompetent mineral (e.g., fig. 5e in McClay, 1979). Alternatively, the extended hinges shown in his fig. 5f are filled with gangue minerals, rather than the galena required by his model. Apart from this, asymmetric folds, identical to those commonly containing galena but instead consisting of mostly dolomite and only minor galena in the hinges, occur in 8 orebody, 13B sublevel.

The second major problem is that McClay (1979) did not recognize sulphide replacement spatially associated with folding. There are actually two types of replacement to consider. The first is the overprinting of folded layers by gangue minerals (Figs 3a,8, 18a,b, 19). The second is the replacement of the gangue minerals by sulphides (Figs 15a,b,c, 18a,b, and 19). Indeed, McClay's (1979) fig. 5c illustrates a spectacular example of dolomitic folds variably overprinted by a "galena matrix" The fold shapes in his fig. 5d also appear to be partly ingested by "fine-grained galena" The identical replacement textures of gangue minerals by sulphides, both in ores exhibiting folds, where according to McClay (1979) sulphides have migrated, and in non-folded parallel-layered ores, as documented in this study, are not discussed in McClay's work.

The relationships illustrated by McClay (1979) are explained here as the result of progressive syndeformational replacement of intervening finely laminated layers by gangue minerals, followed by the overprinting of these variably replaced layers by sulphides. An increase in the intensity of dolomite replacement towards the main mass of silica-dolomite, is paralleled by an increase in galena relative to sphalerite. Folds containing mainly fine-grained pyrite layers are more similar in style and less tight, because pyrite replaces the carbonaceous laminae, and there is much less gangue alteration. In contrast to McClay's (1979) interpretation, fold styles are explained by the primary combination of laminated and unlaminated layers, and the extent and nature of syndeformational alteration.

Previously, researchers have illustrated apparent deformation textures affecting sulphides at Mount Isa with photographs of mesoscopic folds rather microstructures showing deformation of sulphides. However, McDonald (1970) showed elongate shape fabrics in galena which

defined a foliation deflected around a pyrite megacryst (his fig. 5B), twinned sphalerite fragmented and infilled by galena and non-sulphides (his fig. 5C.) and elongated galena, sphalerite and pyrrhotite grains (his fig. 8D). His study also referred to sulphide schists constituting the galena-rich layer, and the penetration of galena into intergranular boundaries in other assemblages, which "fragmented them" (p.296). Although, foliation development in galena is clearly indicative of deformation, he provided insufficient information on the relationship between sulphides, dolomite and silicates to assess the significance of replacement, which he did not consider as a possible textural explanation. Such structures can form by a combination of the deformation effects of D_3 and younger events plus replacement. Transgression of the galena-rich layer across the shale layer, and splitting of the galena-rich layer (his fig. 4), are also features indicative of replacive relationships.

McClay and Ellis (1983) and McClay (1983b) also described textures they ascribe to deformation of Mount Isa sulphides. These consist of both shape elongation fabrics in galena and fine-grained coalescing pyrite, and a moderately developed crystallographic orientation of (110) poles in galena at a high angle to the foliation plane. Documentation of some sulphide deformation features is not conclusive evidence that all sulphides were present in the sequence prior to the onset of deformation. Apart from this, this study has documented mineralization occuring during D_3 and hence it could have been overprinted late in D3 or the localized younger deformations that overprinted these rocks (Perkins, 1984; Bell & Hickey, 1996). In the examples shown in McClay (1983b; his figs 7A and 7B), the deformed galena is from a flattened fold and the galena with equant grain texture is from a fold limb. The equant galena is referred to as "deformed" even though there is no foliation present. Presumably he claimed this because this sample comes from a galena breccia band. The textures could equally be impingement textures as a result of grain growth. Studies prior to McClay and Ellis (1983) and McClay (1989) did not consider a fluid phase was involved in the transport and deposition of sulphides. The recognition of the involvement of fluids requires that, for "remobilization" to be a viable explanation, there should be evidence of partial (or complete) dissolution of sulphides at some sites to account for deposition at sites formed late in the deformation history.

Recrystallization takes place by the migration of high angle grain boundaries. Discussions of recrystallization of sulphide aggregates by Stanton (1964) and Atkinson (1976) refer to the formation of lowest free energy states as a result of annealing. Deformation and metamorphism of sulphide ores have been addressed both by textural observation and heating/cooling of natural aggregates. Most of these studies assume that sulphides form aggregates consisting only of sulphides, at least to hand specimen scale, and experimental work has been concentrated on monomineralic sulphides, particularly galena. Textural relationships become much more readily understood if one looks at the range of sulphide/gangue assemblages, and examines the characteristics of the boundaries between sulphide and gangue. Even if there has been subsequent recrystallization, either of the gangue minerals or the sulphides, then some evidence of a pre-existing deformation history should still be recorded in the gross shapes of the

sulphide/gangue boundaries. For example, if a sulphide-gangue assemblage is deformed, ductility contrasts between sulphide and gangue should produce stretched sulphide aggregates, or at least some evidence of a foliation which is visible in the sulphide-gangue boundaries. The boundaries of these aggregates should still have stretched shapes even if the sulphides and/or the gangue are subsequently recrystallized. These differences in textures resulting from a previously deformed sulphide being recrystallized, and that resulting from a post- (or synchronous with late stages of) deformation replacement origin are illustrated in Fig. 25.

A related question is whether the evidence for sulphide-gangue replacement is consistent with later deformation of either the sulphide or the metasome. Where the range of textures indicates that sulphides have progressively replaced an undeformed dolomite, for example, the argument used above indicates that there cannot have been an earlier deformed precursor to this assemblage. The problem arises where deformed dolomite coexists with sulphides. An argument can be made that these associations represent an earlier dolomite/sulphide aggregate that has been deformed, and is a potential source of either or both dolomite or sulphide to be reprecipitated in an undeformed state. What is critical in this case, is whether the dolomite and sulphide have been deformed together or whether the sulphide has replaced the deformed dolomite. In the example illustrated (Fig. 15e), the preservation of optically continuous relict dolomite is indicative of the latter.

It is conceivable one could accept the evidence for late timing of all sulphides but still argue that they existed in the immediate vicinity in some undefined earlier form. However, this is inconsistent with the metal zoning pattern, which indicates a primary distribution. Complete local redistribution is difficult to disprove, as it derives from a conviction that the metals in such deposits must be an integral part of the sediment. There should, however, be no need to invoke a process for which there is no evidence. It seems extremely unlikely that processes can be so efficient that they can not only produce dissolution and reprecipitation in the same vicinity, but that no evidence should be preserved of partial dissolution.

Relationship with copper mineralization

Timing: The interpretation of lead-zinc as having the same microstructural timing as copper, changes many suppositions of the relationship between them. In most samples, chalcopyrite occupies both the paragenetically youngest and most extensional sites. Superficially, it commonly appears that chalcopyrite was deposited in veins that overprint well-laminated sphalerite and galena. Detailed examination shows, however, that such veins were in existence prior to deposition of, not only chalcopyrite, but also sphalerite and galena (e.g. Figs 21, 22, 23). Similarly, massive silica-dolomite alteration does not overprint the lower terminations of lead-zinc orebodies, but there is a very abrupt upwards increase in galena concentration replacing the dolomite.

Distribution: Plotting of lower concentrations of both lead-zinc and copper reveals a more continuous distribution (Fig. 12d), rather than highlighting the spatially separated orebodies. It also shows substantial lead and zinc up dip from the 3500 Cu orebody that is not indicated in orebody plots. In the plane of bedding, there is a variable zone of diminishing chalcopyrite concentration extending out to a relatively sharp front of galena followed by sphalerite. Chalcopyrite concentrations at +1000 ppm continue out into lead-zinc. From within the silica-dolomite, a consistent outwards zonation of Cu-->Pb-->Zn is always observed.

Alteration zonation: Previous work focused on the silica-dolomite and it was interpreted as an alteration system in Perkins (1984). Phyllosilicate patterns and textures around the silica-dolomite were examined by Swager (1983), and interpreted to result from alteration during the D_2 and D_3 events (Swager et. al. 1987). In contrast, Waring (1991), interpreted the biotite-stilpnomelane-magnetite assemblage as being the metamorphic product of Fe-carbonate-K-feldspar-rich portions of the Urquhart Shale. Local cross-cutting development, textural relationships, common abrupt fronts and the zoning pattern associated with ore formation, indicate that all of these features are better interpreted as the result of metasomatic alteration.

Other features of the mineral distribution also appear to be the result of alteration. The occurrence of calcite in drill hole F968, 2.7km north of the mine, and in the southern part of the mine, was interpreted by Neudert (1983) and Waring (1990) as an alteration product. The zonal pattern of fine-grained K-feldspar found in this study, both within distinctive TMBs and in the laminated sequence, suggests that this mineral is also of hydrothermal origin.

Mesoscopic structural controls

Bedding obviously plays the dominant role in fluid movement to form both the alteration and mineralization distribution. The well-laminated carbonaceous siltstones are the more effective fluid transfer zones, although less well laminated mudstones are ultimately mineralized where suitable structures exist to cause dilation within or adjacent to them. Shear along bedding can cause dilation through fold formation allowing dolomitization and partial to complete overprinting of layers (Figs 20, 22).

Metasomatic gangue minerals, mainly dolomite, are apparently controlled in a subsidiary fashion by a complex of cross-cutting fractures. Dominant among these are east-dipping fractures at a range of scales, resulting in mineralized veins that may be continuous for metres, down to closely-spaced tension fractures which give the "shattered" appearance to galena-rich ores (e.g., Fig. 23e). Microfracture between and within gangue minerals has allowed nucleation of sulphides that have then progressively replaced these earlier-formed minerals.

Controls on the sequence of alteration mineral growth are suggested by higher strains in the most altered parts of the rock (refer Figs. 18,19 and 20). It is inferred from other examples of finer-grained calcitic alteration that show extreme rotation of extensional veins into the altered zones, that metasomatic carbonate deposition continued during formation of the extensional

veins. Because the traces of extensional shears (e.g. Fig. 20) are commonly obliterated by growth of alteration minerals, it is further inferred that continued growth and precipitation of new dolomite took place during the shortening phase, particularly where layers pull apart from those adjacent. Chlorite sheaves (Fig. 20) are unfolded immediately adjacent to isoclinally folded layers, indicating late growth. Sulphides have apparently overgrown dolomite, quartz and chlorite, and again appear to be the last phases, essentially at the close of the deformation sequence.

Many sphalerite fronts, particularly where they do not terminate on distinct veins, are associated with flexures in bedding that may represent only slight changes in bedding dip (Figs 21,22 and 23d). The axial planes of these flexures dip at intermediate angles to the east (Fig. 21), and the sulphide fronts coincide in some cases (Fig. 22) with west block up shear on bedding which produces dilation in the vicinity of the flexures. This appears to be due to inhomogeneous deformation effects subsequent to the development of the east-dipping fractures on which the veins have nucleated. Many features of the ores can be explained by a combination of controls by bedding, shear and dilation on bedding, and cross-cutting D_2 veins. In particular, the gradually discordant nature of mineral abundance across bedding can be related to transfer upwards via the east-dipping fractures.

The bounding surface of the upper terminations of the lead-zinc orebodies on the western long limb of the Mount Isa Fold forms an approximate vertical plane sub-parallel to the axial surface of the fold. (Figs 12d,e). Only one orebody is known to have formed on the short limb of the fold (Fig. 12e) and, although there is substantial development of mainly zinc-rich sulphide on the eastern long limb, it only locally reaches ore grade. These sulphide zones cover a stratigraphic interval of about 700 m and extend about two km north-south. Preferential dilation on bedding on the western long limb of the Mount Isa Fold, locked between the Basement fault and the anticlinal hinge, may explain the better development of ore on that limb compared with the short limb and the eastern long limb. The geometry of the Mount Isa Fold apparently exerts a major influence on mineralization, playing a similar role on a large scale to the flexures which control mineralization fronts on the scale of exposures in the mine.

Significance of distribution of sulphide styles

The more stratiform distribution of sulphides, particularly galena, in lead-rich areas towards the silica-dolomite is consistent with more complete sulphide replacement of bedding at the core of the system, and extensional sites becoming more important further outwards. This is completely opposite to the relationships predicted by models of early lead-zinc overprinted by massive alteration, whereby the most pristine bedded mineralization should be preserved at the extremities of the system.

The association of fine-grained pyrite with the carbonaceous stylolaminae, and pyrrhotite with the buff-altered zones, can be interpreted in two ways. Either pyrite is removed during

oxidation or, more consistently with the microstructural timing evidence, where this carbonaceous matter is oxidized during alteration, pyrite does not precipitate in such zones.

Source of sulphur

Beginning with McClay and Carlile (1978), the sedimentary rocks hosting the ores have been interpreted as an evaporitic sequence, with the consequent potential to produce large quantities of sulphate as an integral part of the sediment. Neudert (1984), argued for the intrabasinal formation of sulphate during diagenetic modification of the current-deposited siltstones at shallow depths in the sediment. During compaction, this sulphate was interpreted to have reacted with introduced iron to produce diagenetic pyrite, by a process of biogenic sulphate reduction. Subsequently, the residual sulphate was used to precipitate galena, sphalerite and even the chalcopyrite of the copper ores.

Other ideas on sulphur sources for mineralization have come from application of work done at McArthur River. Trudinger and Williams (1982), and Muir (1983), have interpreted at least the fine-grained pyrite at Mount Isa to be deposited by biogenic sulphate reduction. The evidence for this is the association of pyrite with carbonaceous material and the distribution of sulphur isotopes.

The common association of fine-grained pyrite with carbonaceous seams, satisfies the requirement of a reductant in the immediate environment. The presence of sulphate at the time of sulphide deposition, however, is not supported by: i) wholesale replacement of the laminite by pyrite; ii) possible sulphate shapes already being replaced by other phases, and; iii) the degree of post-depositional shortening in the rock. Dissolution of early sulphate should have been accelerated during the formation of the bedding-parallel cleavage. It is concluded, therefore, that the sulphur for pyrite deposition was introduced in an oxidized form simultaneously with the iron, and reduced in the carbonaceous seams. Similarly, the range of metasomes for the other sulphides, that is, galena, sphalerite, and pyrrhotite, and their late timing, also indicate that sulphur was introduced with the metals. Examination of sulphur isotopes and their distribution is discussed in Perkins (1996b).

Source of metals

The approach demonstrated herein to understanding the mineralizing system does not provide answers to the question of the metal source. It does, however, suggest constraints on what source or sources of metals may be possible. It suggests that there may be a single source for lead, zinc and copper. The most commonly advocated source of metals for deposits of this type is from within the host sediment pile, with transport in evolved basinal brines (Renfro, 1974; Gustafson and Williams, 1981; Neudert, 1984; Sawkins, 1984; Bethke,1986). The post-lithification and syn-deformation timing of sulphide formation argues strongly against this being

a likely source. More recently, Solomon and Heinrich (1990), presented a case for North-west Queensland deposits having derived their lead and zinc from the sequence beneath the orebodies, with heat supplied by radioactive decay from adjacent granites. Although they were modelling deposits formed essentially syngenetically, such a granite-driven system is also possible for a post-metamorphic origin.

Fluid conditions interpreted from the copper orebodies (Heinrich et. al. 1989; Waring, 1990), indicate a moderately saline brine (20-25wt.% NaCl) depositing chalcopyrite at temperatures between 200%-250%C. Copper derivation via leaching of metabasalts beneath the mine has commonly been inferred (Smith and Walker,1972; Wilson et. al. 1985; Hannan, 1989), but is not supported by either lead isotope interpretation (Gulson et. al. 1983) or timing of chalcopyrite in the metabasalts. Much of the chalcopyrite in the metabasalts occurs as a replacement of metamorphic minerals in former amygdales or in veins, and is unlikely to be the source of copper in the orebodies (Swager, 1985b). Furthermore, the fluid associated with alteration of metabasalts beneath the Mine was found to be chemically similar to that associated with copper mineralization, but not to that associated with regional-scale alteration of the metabasalts (Hannan et. al., 1993).

Circumstantial evidence suggests that neither copper nor lead and zinc are locally derived and deposited from basinal brines, and a deep-seated metal source tapped by juvenile fluids is a distinct possibility. Further constraints on fluids and metal sources requires continuation of investigations done on the copper orebodies, and the development of a more geochemical model.

Hypothetical model of the Cu-Pb-Zn ore system

A possible updated ore formation model based on that interpreted for copper (Perkins, 1984; Swager, 1985a; Heinrich et. al. 1989; Waring, 1990) and incorporating the observations described herein, can be proposed. The major changes to the earlier model relate to the interpretation of fine-grained pyrite, galena and sphalerite and their timing relative to silica-dolomite processes. The model must allow for a relatively protracted development of the alteration system relative to the microstructural evolution, followed by a relatively short-lived mineralizing phase, in which chalcopyrite deposition is paragenetically youngest at any given location.

The model is interpreted to show the following sequence of development (Fig. 26). Initially, the Paroo Fault cut across the Mount Isa Group, probably forming as a thrust flat and ramp complex (Bell, 1983; Bell et. al., 1988), and placed Cromwell Metabasalt against Urquhart Shale. Some alteration, mainly restricted to hydrothermal clays along the fault, formed at this stage. Wholesale metasomatic alteration, consisting of chloritization of the underlying metabasalts (Swager, 1983), potash metasomatism, bleaching and replacive vein formation in the Urquhart Shales, began during continuing east-west shortening deformation that resulted in

the formation of a near-bedding-parallel cleavage (S_2), above the ramp. Phengitic mica alteration probably also developed largely during this phase (Swager et. al., 1987).

Layer-parallel carbonate alteration proceeded during the shortening deformation, which produced a cleavage (S_3) at a distinct angle to bedding. During this stage, biotite deposition along both bedding and cross-cutting fractures occurred. A zone of iron-rich alteration with siderite, Fe-rich chlorite, stilpnomelane, and magnetite formed at a variable distance from the Basement ramp. Introduction of sulphate, probably mostly barite, also occurred at this stage. An outward-growing silicification front overprinted weakly carbonate-coarsened siltstones and earlier-formed replacive dolomite along bedding and cross-fractures (Perkins, 1984; Swager, 1985a). Dolomite at the advancing front overprinted earlier iron-rich phyllosilicate alteration as well as being associated with its coarsening. Introduction of new dolomite advanced into more dilational sites along previously sheared horizons during a shortening phase, followed by some silicification.

At the close of this deformation and alteration event, the system changed to one of metal and sulphur introduction. Fine-grained pyrite was deposited as a result of inorganic sulphate reduction, mainly in carbonaceous zones. Pyrrhotite deposited in reduced and iron-rich altered zones, probably migrating outwards to overprint some pyrite. Chalcopyrite, galena and sphalerite may have deposited sequentially from a fluid that carried reduced sulphur, with a corresponding increase in the extent of bedding control in that order. The zoning pattern established was probably largely controlled by temperature. Migration outwards of the stability fields of sulphides, resulted in a zone refining pattern whereby earlier-deposited sulphides were progressively replaced by others, to result in chalcopyrite being paragenetically youngest. Alternatively, the sulphide system could have evolved with time such that all the sphalerite was deposited before all the galena, followed by all of the chalcopyrite.

Some deformation continued subsequent to ore formation. Strained and partly annealed galena resulted from deformation around conjugate extensional faults. At least the last stages of movement on the Buck Quartz Fault deformed some of the copper ore. Overall, however, there has been minimal structural modification of either the lead-zinc or the copper ore.

CONCLUSIONS

Examination of the textures of sulphide-gangue relationships has re-affirmed the dominance of replacement processes as the means of sulphide nucleation and growth. This means that all sulphides are clearly epigenetic.

Mineralization fronts with identical characteristics to the ubiquitous layer-parallel sulphides both overprint and terminate on veins and fractures that are post-lithification in origin.

Microstructural timing of the growth of gangue and sulphides indicates development of alteration minerals during both the S_2 and S_3 cleavage events, and sulphides late in the S_3 event. Rather than a complex history of bedded mineralization, followed by metamorphic

recrystallization and sulphide migration into late sites during deformation, all styles formed during a single event. Lead-zinc and copper (Perkins, 1984) are thus cogenetic and part of a single system.

Controls on the formation of the alteration and mineralization system are not sedimentary and diagenetic processes, but rather differential shear and cleavage formation in originally laminated dolomitic siltstones, and fracture propagation through interlayered less laminated siltstones and mudstones. As with the copper orebodies, the ramp structure of the Paroo Fault is the fundamental control on the zonal pattern of mineral distribution. The western long limb of the Mount Isa Fold is the other major structural control on ore formation.

This interpretation of Mount Isa mineralization removes the element of coincidence that exists with completely separate episodes of lead-zinc and copper. It removes the need to invoke the existence of major syndepositional faults controlling mineralization, for which little evidence exists, and it accommodates all observations of ore characteristics.

PART B.

Timing of Formation of Proterozoic Stratiform Fine-Grained Pyrite: Post-Diagenetic Cleavage Replacement?

TABLE OF CONTENTS

ABSTRACT

Stratiform fine-grained pyrite is regarded as an indicator of early diagenetic iron sulphide mineralisation in sediments. It is further regarded as having formed at this early stage where associated with many stratiform lead-zinc ore deposits throughout the world. Examination of the fine-grained stratiform pyrite at the Cu-Pb-Zn mine at Mount Isa, Queensland, however, indicates that at least at this locality, it formed at a much later stage.

A textural characteristic of the Mount Isa pyrite is that it normally overprints two generations of carbonaceous cleavage planes. The first of these (s_2) is sub-parallel to bedding and the second (s_3) is axial plane to the mesoscopic folds in the mine. The density of pyrite deposition is controlled by zones defined by these cleavages, commonly in association with neomorphic dolomite in adjacent laminae. In correlated finely laminated sequences, the pyrite appears to have overprinted the near-bedding parallel cleavage after complete compaction of the laminite. Most of the fine-grained pyrite is closely associated with other sulphides, sphalerite, galena and chalcopyrite, although it generally forms in layers adjacent to them. Where there is an overprinting relationship shown between the fine-grained pyrite and other sulphides, the pyrite is paragenetically earlier and either overgrown, or replaced, by the economic sulphides.

The overall distribution of fine-grained pyrite not only suggests a strong spatial association with the Cu-Pb-Zn system, but it continues outwards, both in the southerly and northerly direction, to form a halo to them. The gross distribution of fine grained pyrite strongly cross-cuts the stratigraphy, with its maximum development around the center of the mine and a progression of concentration to higher stratigraphic levels in the north. This is the same cross-cutting direction as the silica-dolomite boundary, the terminations of the lead-zinc orebodies, and the copper ore. In addition, a pyrite envelope occurs around the 3000/3500 copper orebodies in the northern footwall.

Distribution of sulphur isotopic ratios in fine-grained pyrite, on both the microscopic scale using the ion microprobe, and also on the scale of deposits using conventional methods, has been used as a major argument for early diagenetic deposition. In particular, the large spread of $\delta^{34}S$ values at the HYC deposit, McArthur River, is presumed to result from biogenic sulphate reduction, necessitating depositional processes operating during early diagenesis. This spread is not greatly different from that of the associated economic sulphides, which were interpreted as hydrothermal, suggesting that the fine-grained pyrite was itself hydrothermal. This alternative interpretation may also apply at Mount Isa, where a similar relationship is observed between the sulphur isotope systematics of pyrite and other sulphides.

Mount Isa fine-grained pyrite is therefore interpreted to have formed late in the main deformational event which produced mesoscopic structures in the mine sequence,

probably by abiogenic sulphate reduction. Thus pyrite formation was ultimately controlled by the same structures as those which controlled the Pb-Zn ores, which are the Paroo-Basement fault system, and shear along bedding in well-laminated carbonaceous siltstones, during formation of the s_3 cleavage.

INTRODUCTION

Stratiform fine-grained pyrite is not only a common accompaniment to sediment-hosted base metal deposits, but also forms in similar sedimentary sequences without other significant mineralisation. It constitutes a very substantial portion of the sulphide system at Mount Isa, Hilton, Lady Loretta, and McArthur River (HYC), and the relationship between this pyrite and the economic sulphides has been widely discussed (e.g. Grondijis and Schouten, 1937, Smith et. al. 1973, Williams, 1978a,b, Schieber,1990). Much of the analysis of the relationship of fine-grained pyrite to the ore-forming sulphides has been done at HYC, using both textural observation and sulphur isotope determinations. The HYC pyrite has been classified into pyrite 1(Py 1) and pyrite 2(Py 2), with the former commonly occurring as euhedral cores to the latter. Williams and Rye (1974) and Eldridge et. al.(1993) interpreted the Py 1 and Py 2 as having formed early in diagenesis by biogenic sulphate reduction, with the galena and sphalerite having a later diagenetic hydrothermal origin.

At Mount Isa, Grondijis and Schouten (1937), considered that the fine-grained pyrite could have formed syngenetically, in keeping with findings of European authors, but dismissed this because of the close association with the other sulphides which, according to them, must have had a late hydrothermal origin. This accorded with Blanchard and Hall (1942), who regarded the fine-grained pyrite as the paragenetically earliest of the epigenetic mineralisation. Other authors to consider the formation of fine-grained pyrite were Love and Zimmerman (1961), Croxford et. al. (1958), Croxford (1962), Neudert (1984), and McGoldrick (1986). Love and Zimmerman (1961), and Zimmerman (1963), maintained that microfossil forms were contained in the pyrite. They dissolved pyrite from clean pyrite concentrates using concentrated nitric acid, to reveal translucent bodies of organic material which they interpreted to be microfossil remains. These bodies were "generally rounded or slightly polygonal and they range in size from 1 to 12 microns" (Love and Zimmerman, 1961, p.885). In relating the morphological appearance of the organic bodies to that of the pyrite, the authors argued that the dark lines between the core spheres of their Py 1 and younger pyrite, or in some cases, between two zones of a central sphere, corresponded with their interpreted single or double-walled micro-organisms (p 887).

Neudert(1984) linked the formation of the earliest pyrite to indicators of sulphate in the sediments and interpreted it to form early in diagenesis by microbial reduction of residual sulphate. All subsequent pyrite and other sulphides were interpreted to obtain sulphur from either the earliest pyrite or residual sulphate. McGoldrick (1986), citing the observations of Muir (1983), concluded that the earliest generation spheroidal pyrite

formed soon after burial as a replacement of organic material and that much of the subsequent pyrite occurred as overgrowths during diagenesis.

The most comprehensive data base and interpretation of sulphur isotope analyses is that by Eldridge et. al.(1993) for the HYC deposit. The $\delta^{34}S$ values obtained using the ion microprobe for Py1 and Py2 varied from -13 to 15 and -5 to 45 per mil respectively, and illustrated a lack of homogeneity at the micron scale. A similar heterogeneity is shown by SHRIMP analysis of sulphur isotopic variation at Mount Isa (Eldridge et. al., 1985, S. Eldridge pers. comm. 1991).

The large spread of isotopic values for both Py1 and Py2 at HYC and for Py1 at Mount Isa was cited as the main evidence a biogenic origin for these both pyrite types. In addition, isotopic heterogeneity on the micron scale, extreme disequilibrium between both forms of pyrite and base metal sulphides, and the association between base metal sulphides and hydrothermal modification of the gangue, indicated to the authors a progression from biogenic to hydrothermal processes.

TEXTURAL VARIETIES OF PYRITE

Coarse-grained euhedral pyrite related to both copper and lead-zinc orebodies can occur as irregular disseminations and less commonly as bedding-parallel zones (Croxford,1962, Gulson et. al.,1983, Perkins,1984). This form has been widely interpreted as being more directly related to a hydrothermal copper-mineralising event. In contrast, bedding-parallel fine-grained pyrite is universally regarded as being of early diagenetic origin, and it is this form which is being examined here.

Bedding-parallel pyrite

Stratiform pyrite at Mount Isa is characterised by what appears to be a very regular and continuous distribution along the bedding, concentrating in bands of varying widths and separated by non-laminated carbonaceous siltstones (Fig. 1). Pyrite distributed along the bedding occurs in a number of forms, most recently described by Waring (1990). Many of these forms can occur together. One textural variant occurs as either single euhedral to subhedral crystals or aggregates, generally 20 to 200 μm across. Density of dissemination varies markedly along the bedding, from about 5 vol% to monomineralic pyrite bands This was termed "brassy pyrite" by Waring(1990), who showed examples terminating on fine fractures and veins (Fig. 2). Brassy pyrite constitutes a larger proportion in the "pyrite ribs" between lobes of copper orebodies, and the core of the main pyrite zones. The other main variety, which is generally referred to as fine-grained pyrite, consists of fine zoned crystals in the 2μm to 20μm range with a complex array of internal morphologies and outer shapes. It occurs as intimately bedding-parallel aggregates in densities ranging from approximately 0.1% to about 60%

of the bed. In hand specimen it is dark brown-yellow colored in contrast to the more reflective brassy pyrite. These two main styles are illustrated in Fig.2 with the brassy pyrite in this example being terminated by fractures, in contrast to the fine-grained pyrite. Aggregates of combinations of these types of pyrite can vary in form to include ovoid, worm-like, or interlocking lath-like shapes of brassy pyrite, varying from about 1 mm to 20 mm within continuous trains of fine-grained pyrite. The latter is characterised by wavy or anastomosing forms, described by Schieber (1990) as constituting "wavy-crinkly internal laminations of laminated pyrite beds" Where individual pyrite grains are closely packed, the wavy pattern encloses small augen of carbonaceous siltstone, with long axes commonly 0.3 to 3mm (Fig. 3)

Detailed morphology of fine-grained pyrite

A range of textural types of fine-grained pyrite generally occur in a single sample (Fig. 4). Pyrites resistant to etching tend to occur in bands, although zoned forms may also appear in the same bands. Most individual pyrites are zoned, with the degree of definition of the zones depending on the closeness of packing of the nucleii. In the past, reference has been made to two zones, but detailed examination has revealed up to seven zones. The central inclusion-free core, containing up to three zones, can vary from strongly euhedral to almost circular, with the subsequent spongier inclusion-rich zone (or zones), varying in annular thickness. A zonal stratigraphy can sometimes be seen between adjacent grains. The form of the zones indicates growth from the core to the rim, with progressive rounding where the cores are more euhedral. Preferential growth in four directions can lead to elongated star shapes, and these shapes are more likely to appear as sparse disseminations in layers on the edges of more highly concentrated pyrite. The myriad of different zonal combinations, and the development of euhedral shapes, indicate that the morphologies are not controlled by microfossil forms (c.f. Love and Zimmerman, 1961). The zoned shapes are interpreted to result from pulsed accretion, with variable incorporation of carbonaceous inclusion material, possibly as a result of the rapidity of deposition. The more euhedral "brassy pyrite" is not zoned, but may commonly overgrow the zoned shapes.

DISTRIBUTION OF FINE-GRAINED PYRITE

Gross distribution

The three-dimensional distribution of fine-grained pyrite can be portrayed on cross-sections, plans, and longitudinal projections. There is a large data base from mine logging and mapping which is difficult to summarize in a few illustrations. In older logging (pre-1977), pyrite was only logged as being 5-20% or >20%. Since then,

estimates of actual percentages have been recorded, and it is these newer data which have been used to compile the cross-section and plan shown in Fig. 5. Fine-grained pyrite in mine logging generally includes any close-packed pyrite along the bedding, and thus would include much of what in this study is called "brassy pyrite" or non-zoned fine euhedral pyrites, and thus overestimates the true concentration of fine-grained pyrite.

Characteristics of the distribution are a transgression of the richest part across stratigraphy, the very rapid diminution to the south and more gradual diminution to the north (Fig. 5), and the antithetic relationship to bedding-parallel pyrrhotite. The pyrrhotite relationship is shown in Part A, figs. 10c and 12c. The overall cross-cutting relationship to gross stratigraphy is related to two TMB marker units in Figure 5. The transgression across stratigraphy can also be related to the siliceous gossan on the surface. Although on aerial photographs the gossan appears to be a more or less continuous ridge traceable around the Mount Isa fold, its most upstanding part transgresses from the 14-23 orebody interval in the south (Rio Grande area), to 5/110 5/200 orebody interval at the northern end of the mine. This ridge appears to be a projection of the hangingwall part of the strongest concentration of bedding-parallel pyrite, and represents a transgression across stratigraphy of approximately 500 metres.

Although the fine-grained pyrite is controlled by bedding, this change in concentration along strike is in a NNW direction, which is parallel to the trend of the enveloping surfaces of the lead-zinc orebodies (relate Fig. 5b to 5c). This trend is also parallel to the gross margin of the footwall of the silica-dolomite (Fig. 5c) and to the trend of the high grade core of the 1100-500-650 copper orebody system (Perkins, 1984). As argued in Perkins (1984), as part of the evidence for late structural control of the copper orebody system, the NNW trend of the alteration and copper ore is parallel to the strike of the s_3 cleavage and the axial trace of the Mount Isa Fold. A control by this trend appears to also apply, not only for the lead-zinc lodes (Part A) but also for the fine-grained pyrite.

Distribution in the 7 orebody zone

A visual estimate of fine-grained pyrite in the 7 orebody sequence shows marked variations in overall concentration at various locations (Fig. 6). The maximum concentration is towards the silica-dolomite in the south and in the vicinity of the anticlinal hinge of the Mount Isa Fold. Concentration diminishes towards the north to about 4.5% at 38150N, 800 metres north of the fold (Fig. 6a). Another three km north at 41,000N the sequence contains only trace amounts of fine-grained pyrite, although total pyrite content is about 1%. Two and a half metres above the 7 orebody stratigraphy the 6 orebody sequence has approximately 1% fine-grained pyrite at this locality.

The B sequence in the hangingwall of 7 orebody has a similar distribution of fine-grained pyrite (Fig. 6b), and changes can be directly related to microfacies, with only minor pyrite in the non-laminated siltstone layers (Fig. 11, Part A). At 41,000N (Fig. 7, location A) there are only trace quantities of fine-grained pyrite, although two units containing coarser-grained euhedral pyrite exist. At 38,150N, (location B), the sequence again contains about 12% fine-grained pyrite. Even though the laminated sequences are continuous in strike for at least 13 kilometres, the zone containing fine-grained pyrite within that extends for only about 800 metres measured perpendicular to the shallow northerly plunge of the zone. At the inner boundary of the fine-grained pyrite, there is a narrow zone of overlap where the sequence contains both fine-grained pyrite and pyrrhotite (Part A, Fig. 10c).

STRUCTURAL AND MICROSTRUCTURAL RELATIONSHIPS

Changes in correlated zones

Changes in the textural characteristics of pyrite-bearing stratigraphy are observed in the B sequence. In Fig. 7, the upper barren laminite of the B sequence is approximately the same overall thickness as its pyritised equivalent, and the individual wavy laminations also have a similar spacing. In the sequence without pyrite, the dolomitic laminae are slightly more even in thickness and their boundaries are less sharply defined. This is consistent with the interpretation that the sequence was already shortened to this lamination spacing prior to the introduction of pyrite. Towards the sphalerite/mineralised zone, the same pyritic sequence becomes thicker, with the formation of neomorphic "nodular" dolomite taking the place of the finer carbonate laminae, (Part A., Fig. 14). The pyrite distribution is more irregular, concentrating in carbonaceous cleavage seams which anastomose around this dolomite. Total thickness of this layer reaches a maximum of 55mm where it is mineralised by pyrite, and 42mm where pyrrhotite is the only iron sulphide.

Relationship to folds and cleavage

In areas of mesoscopic folds, the axial plane cleavage (S_3) is commonly best represented by concentrated strands of fine-grained pyrite parallel to the cleavage (Fig. 1, and Perkins, 1984, Figs 21 and 33). These strands pinch in towards the non-laminated layers which do not contain pyrite. The simplest interpretation for these structures is that they represent concentration of pyrite following dissolution of the rock matrix during shortening, but this interpretation is challenged upon detailed examination.

Carbonaceous seams along bedding have a varying degree of parallelism or waviness, depending on the grain size of the carbonate in the layers between the seams.

The seams are most parallel where there is little neomorphic growth of carbonate in the intervening layers, and where there is substantial growth of new carbonate, as in the "nodular dolomites" (see Part A), the carbonaceous seams have an anastomosing pattern. These seams represent boundaries between correlated laminations, but, as demonstrated in Part A, they are enhanced by the formation of a bedding-parallel cleavage which is axial plane to isoclinal folds. This cleavage is referred to as s_2 in Perkins (1994) and Swager (1995).

Microscopic investigation of the relationship of fine-grained pyrite to cleavage development shows that the pyrite is all replacive with respect to its fine-grained host, with density controlled primarily by the variation in lamina composition. The close relationship between fine pyrite grains and either carbonaceous matter (presumably algal) and both bedding-parallel (s_2) and cross-cutting (s_3) carbonaceous cleavage seams (Fig.3 and Fig.11b, Fig.14 of Part A), also highlights the normal, although not exclusive, occurrence of this type of pyrite with the carbonaceous fraction of the rock.

Microstructures of pyrite concentrations along cleavage directions related to the hinge regions of folds are illustrated in Figs 8 and 9. Figure 8a shows a fold in laminae which contains large variations in concentration of fine-grained pyrite grains. It also has a well-developed axial plane s_3 carbonaceous cleavage. Obvious within the pyrite-rich laminae is a variation in concentration of pyrite that is controlled by lithons bounded by cleavage seams. This relationship cannot be explained by upgrading resulting from differential dissolution of the carbonate-rich rock, because, in the layers beneath the pyrite-rich layer, there is insufficient shortening and dissolution to account for the pyrite upgrading. This is shown by the continuity of bedding-parallel cleavage seams along the limb of the fold and the similar intensity of cleavage seam development beneath the more pyrite-rich area. Not only is the concentration of fine pyrite related to cleavage seam domains, examination of their relationships at high magnifications (Fig. 8b) shows that trains of pyrite are distributed along the individual seams and have an overprinting relationship with them. There is no tendency for the seams to deflect around the individual pyrite grains.

Lenticular concentrations of fine-grained pyrite along cleavage directions in an anticline (Fig. 9) are also indicative of precipitation subsequent to the formation of the fold. This is the same fold as that in Part A, (Fig. 7). Again, bedding-parallel seams around the tip of the pyrite aggregate demonstrate that pyrite concentration along the cleavage direction cannot be a superimposed effect caused by concentration of pre-existing pyrite during deformation. In this case, however, pyrite at one end of the aggregate (Fig. 9c) contains a zone where individual pyrites have a shape elongation

parallel to the cleavage direction and the long axis of the aggregate. This indicates that some dissolution has occurred along the cleavage direction subsequent to pyrite growth.

SULPHUR ISOTOPES

Data on sulphur isotopes in fine-grained pyrite at Mount Isa are available from a number of sources (Solomon,1965; Smith et. al., 1978; Andrew et. al., 1989; Eldridge, 1991, pers.comm.). Values of $\delta^{34}S$ range from 0 ‰ to 32 ‰ for all fine-grained pyrite irrespective of whether it occurs in the copper or lead-zinc orebodies. A major component of sulphur in the copper orebodies has been interpreted to be derived from pre-existing fine-grained pyrite (Andrew et. al., 1989). Extreme differences between sulphides in the same sample indicated that fine-grained pyrite did not provide the sulphur source for local chalcopyrite deposition, in agreement with the findings of Gulson et. al., 1983. Textural relationships showing that fine-grained pyrite is largely inert during chalcopyrite mineralisation, except for local pyrite replacement constituting a miniscule proportion of the mass of chalcopyrite, provide additional evidence against this proposition (Perkins, 1984)

The large spread of $\delta^{34}S$ values in fine-grained pyrite at Mount Isa has been interpreted to indicate an origin by biogenic sulphate reduction (Solomon, 1965, Smith et.al., 1978). The argument has been developed more thoroughly at HYC by Eldridge et. al., 1993, who found the distribution of $\delta^{34}S$ in fine-grained pyrite (Py 1) to range from -13‰ to 15 ‰, and for overgrowth pyrite (Py 2) from -5 ‰ to 45 ‰. In contrast, a hydrothermal origin involving exotic sulphur was invoked for associated galena and sphalerite, which ranged from -5 ‰ to 8 ‰. Mount Isa fine-grained pyrite, interpreted by the authors as biogenic, had $\delta^{34}S$ values which ranged from 0‰ to about 30 ‰, whereas other sulphides ranged from 11‰ to 27 ‰. The two types varied by as much as 25 per mil when spatially separated by only 100μm. No evidence was found for isotopic communication between sulphides even in very close proximity. In addition to the finely stratiform distribution, and the existence of iron monosulphides in present day environments, the sulphur isotope distributions have been used as a major argument for the fine-grained pyrite of large sediment-hosted ore deposits having formed during early diagenesis.

DISCUSSION

Introduction

The processes of formation of fine-grained pyrite in sediments are believed to be quite well understood (Berner, 1970), and this origin has been inferred for Proterozoic

sequences. Berner (1972, p. 347) summarised the formation of diagenetic pyrite thus -"In those sediments where organic matter accumulates faster than it can be destroyed, pore waters become anaerobic and the process of bacterial sulphate reduction begins. Hydrogen sulphide is formed and immediately some of it reacts with detrital Fe minerals in the sediments to form black Fe monosulphides, chiefly mackinawite, FeS, and greigite, Fe_3S_4. Some of the remaining H_2S is oxidized to elemental S by aerobic or anaerobic bacteria. A part of this elemental S then reacts with the Fe monosulphides, by way of solution precipitation reactions to form pyrite. The remaining elemental sulphur is oxidized bacteriologically to sulphate so it does not accumulate."

Formation of fine-grained pyrite during early diagenesis is favoured by the availability of concentration of readily available sulphate in the sediments. This is given support by interpretation of the Mount Isa and McArthur host sequences containing sulphate evaporites (McClay and Carlile, 1978; Neudert and Russell, 1981). This interpretation is investigated in Part A, where the alternative is put that the the textures represent either: 1)sulphate lath pseudomorphs precipitated as part of the syndeformational alteration system; or 2) formation as carbonate alteration rather than carbonate after sulphate evaporites in the case of the "nodular dolomites" Both these propositions do not support the availability of sulphate at the early diagenetic stage in sediments that host the high concentrations of fine-grained pyrite.

Sulphur isotopes

Sulphur isotope distributions from the scale of entire deposits to the micron scale have been a major, if not the major, influence on fine-grained pyrite being interpreted as an early diagenetic product. Biological activity requires that depositional processes take place within a restricted depth of sediment, and the amount of organic material limits the concentration of pyrite that can be produced. $\delta^{34}S$ values for early pyrites in Proterozoic North Australian deposits are heavier than those for other areas such as the Belt Supergroup. Strauss and Schieber(1990), while accepting that the pyrites in both cases are biogenic, suggest that this may result from a difference in paleoenvironmental conditions. Eldridge et. al.(1993), clearly demonstrate a lack of isotopic communication between pyrites and later sulphides, which negates the possible effect that later sulphides could have had on modification of isotopic signatures of earlier pyrites (Strauss and Schieber, 1990).

What criteria have been used to distinguish between $\delta^{34}S$ ranges indicating biogenic processes and those indicating hydrothermal processes? Eldridge et. al.(1993) interpret a range of 28‰ for Py1 and 50‰ for Py2 as biogenic and 19‰ for other sulphides as hydrothermal. Py1 varies in a single sample over a distance of millimetres by up to 10‰

whereas Py2 varies commonly by 10‰ and in one instance by 40‰. Data for other sulphides from single samples have maximum ranges for disparate sulphides (chalcopyrite and galena) of 13‰ and for the same sulphide (galena) of 10‰, showing that substantial variability exists for other sulphides over short distances. The Py1 population distribution is much more like that of galena than Py2. Combined galena-sphalerite-chalcopyrite distribution is intermediate between Py1 and Py2. An earlier reviewer stated that "a non-rigorous statistical test indicates that there is considerable overlap between Py1 and base metal sulphide populations whereas the Py2 and base metal populations are significantly different" All that can be said is that the variability for other sulphides is slightly less than that for Py1 and Py2. As Eldridge et. al. (1993) indicate, Py2 can be strongly zoned isotopically, with an increase of up to 11‰from core to rim. Without specific isotopic criteria, there appears to be no basis for separating base metal sulphides and pyrite into groups requiring completely different depositional mechanisms. If the base metals are hydrothermal, then can the pyrite be also, thus removing the main evidence for an early diagenetic origin for some of the sulphides? The morphology of individual pyrites showing a wide range of zoning shapes does not support any control by microfossils (Love and Zimmerman, 1961).

Recrystallisation.

Coarser-grained pyrite along bedding (referred to as "brassy pyrite") has been interpreted as resulting from metamorphic recrystallisation of early diagenetic pyrite (Hewett and Solomon, 1964). Fronts of more crystalline pyrite along carbonaceous beds which do not have fine-grained pyrite (Fig. 2), and the overgrowth relationship where fine-grained pyrite occurs in conjunction, indicate that this coarsely crystalline type of pyrite forms independently of, and subsequent to, the fine-grained form. This obviates the necessity of having to explain why metamorphic recrystallisation should affect some layers while adjacent layers remain fine-grained.

Relationship to pyrrhotite.

Part A discusses more fully the antipathetic relationship between fine-grained pyrite and pyrrhotite. This relationship has previously been discussed by Finlow-Bates et. al. (1977). They found, using linear correlation analysis and R-mode cluster analysis on quantitative mineral data, that pyrrhotite was preferentially associated with galena and sphalerite. Depletion of an already limited sulphur supply during sedimentation was postulated to result in precipitation of a primary FeS phase. What was not recognised, was that pyrrhotite abruptly gave way to fine-grained pyrite in the same layer, and not in separate layers (Part A. figs. 10,11). This change in iron sulphide species coincides with a rapid alteration transition from bleached, recrystallised, and buff-altered siltstones into

carbonaceous equivalents. In addition, there is some development of atoll replacement textures of pyrrhotite over fine-grained pyrite (Grondijis and Schouten, 1937; J. Knights, pers. comm., 1991). In general, however, there is limited overlap within the same narrow laminite sequences of pyrrhotite and fine-grained pyrite. Summarizing the discussion of Part A, it was interpreted that pyrrhotite deposited in the carbon-poor iron-enriched proximal part of the alteration system, and fine-grained pyrite deposited further out in the unoxidised laminites.

Timing of formation

Timing of pyrite deposition in laminations relative to sediment compaction is difficult to establish without examination of its relationship to both bedding-parallel and cross-cutting cleavage. Neudert(1983) argued that the pyrite in discontinuously laminated beds was concentrated as these horizons were compacted to become the laminated beds. McClay and Ellis(1983; figs. 4b,c and 5a) illustrated shape preferred orientation of zoned pyrites from Mount Isa, resulting from dissolution of outer zones on cleavage seams, and concluded that they existed prior to any deformation. In this study, even in zones where the pyrite has been intensely concentrated in the cleavage direction, this preferred orientation has only been observed locally within the aggregate. This suggests that dissolution of the rock during cleavage development is largely earlier than the pyrites. The B sequence correlations showed that the same lamination spacing existed three kilometres north of the sequence containing fine-grained pyrite. No noticeable difference existed apart from the dramatic increase in the density of pyrite in the mineralised section. Even within the finely laminated portions of the B sequence, the maximum concentration of fine-grained pyrite transgresses from the lower to the upper zone. Together with the textural evidence for a replacement origin for the pyrite, and the evidence for pyrite overprinting the s_3 cleavage, this is best interpreted as the pyrite being younger than the shortening normal to bedding.

CONCLUSIONS

Despite its fine-scale stratiform distribution, features of Mount Isa fine-grained pyrite at all scales combine to give some considerable support to a late epigenetic origin. These features include; 1 the halo pattern of pyrite in and around a copper-lead-zinc deposit which is interpreted to have formed replacively, late in the deformation history (Perkins, 1984; Part A.); 2 the NNW transgression of concentration of pyrite across stratigraphy, parallel to the axial trace of the folds and the s_3 cleavage; 3 the rapid diminution of pyrite abundances northwards and southwards; and 4 the overprinting of

pyrite on carbonaceous cleavage seams both parallel to bedding and axial plane to the major folds.

The main argument for an early diagenetic origin for the fine-grained pyrite is based on the sulphur isotope systematics of the comparable HYC deposit. Examination of these data shows that there is considerable overlap in $\delta^{34}S$ values for Py1 and Py2 with the accompanying galena and sphalerite, which is interpreted to have a hydrothermal origin. Extrapolating to the Mount Isa deposit, the sulphur isotope pattern also does not preclude the possibility of all sulphides, including the bedding-parallel fine-grained pyrite, being of hydrothermal origin.

Paragenetic relationships at Mount Isa and McArthur River indicate that zoned fine-grained pyrite is the first sulphide to deposit. However, rather than the Mount Isa deposit comprising at least two distinct mineralisation events, with the initial pyrite deposition being unrelated to at least the large copper orebody system, it appears to represent a single late-stage system, with fine-grained pyrite being paragenetically earliest. This may explain why large bodies of fine-grained pyrite do not appear to exist independently, and are generally intimately associated with stratiform and/or cross-cutting base metal deposits.

PART C.

Stratiform Replacement Lead-Zinc Deposits: A comparison between Mount Isa, Hilton, Mount Novit and McArthur River.

TABLE OF CONTENTS

TABLE OF CONTENTS

ABSTRACT

Comparison of four stratiform lead-zinc-silver deposits from Northern Australia, at Mount Isa, Hilton, McArthur River, and Mount Novit, reveals significant differences between them, but many critical features in common. As often suggested in the past, they appear to share a common origin.

This common origin, however, seems not to be that of the current paradigm as integral components of the sequences in which they occur. Instead, all are better interpreted as replacement deposits, formed during an east-west shortening event which is at least the second main deformational event that each sequence undergoes. The McArthur River deposit is distinctly different from the others, in that sphalerite and its included galena has directly replaced laminated bituminous bands. In contrast sphalerite and galena in the other three deposits has replaced either bedding-parallel or breccia-matrix metasomatic alteration minerals, mostly dolomite.

All deposits apparently occur adjacent to major reverse faults, rather than normal growth faults as commonly supposed. They are associated with major carbonate alteration systems, that are dolomitic in the immediate deposit environment. The degree of associated deformation is variable, with McArthur River being in the least deformed sequence, Mount Isa significantly more so, and Mount Novit and Hilton associated with quite deformed sequences but of different style.

The interpretation that these deposits share a similar origin, in spite of significant differences in many characteristics, again reinforces the necessity to re-examine other stratiform deposits around the world to see whether they are integral components of the sediment, or whether they may also be of late replacive origin.

INTRODUCTION

According to current publications, the three large stratiform lead-zinc-silver deposits of northern Australia; Mount Isa, Hilton and McArthur River (or H.Y.C.) formed as integral components of the sedimentary sequence in which they occur (e.g. Solomon et al., 1994). Using the definitions of Tourtelot and Vine (1976), discussion has centred on whether these deposits are syngenetic or diagenetic (e.g., Gustafson and Williams, 1981), or whether there may be different timing and processes between them. The possibility of them being strictly epigenetic and deposited after the host sequence, was not considered, even though the Mount Isa deposit had earlier been interpreted as epigenetic (e.g., Blanchard and Hall, 1942). Mount Isa and Hilton occur in the same stratigraphic interval and H.Y.C. lies in a similar lithological sequence with approximately the same age as determined by U-Pb in zircon dating (Page, 1981). They have many characteristics in common, especially the occurrence of sulphides in bands parallel to bedding, separated by bands of more or less barren siltstones. Their common features have led to the view that their origins are similar, and they are grouped as type examples of stratiform sediment-hosted lead-zinc deposits, often called "sedex" deposits (Solomon et al., 1994).

The Hilton deposit, with copper mineralisation but no orebodies, was studied by Valenta (1988, 1994a,b), and his thorough documentation of folding, shear zone and veining characteristics exists as a framework to refine timing relationships. Mount Novit, south of Mount Isa, is a small uneconomic lead-zinc deposit, also without significant copper, and is included because it shows indications of being in higher metamorphic grade rocks than Mount Isa and Hilton. It also lies in a different part of the stratigraphic sequence. The low metamorphic grade at H.Y.C. has been cited as an important reason to study this deposit, and it is often used as the type example of what these orebodies were like prior to metamorphism (Williams, 1979b).

Criteria indicating a late epigenetic replacement origin for Mount Isa lead-zinc are outlined in Part A. The main apparent difference between Mount Isa and the others is the presence of a major system of copper orebodies. Many have suggested that overprinting alteration associated with copper deposition was the cause of the peculiar textural relationships suggesting the lead-zinc had an apparent epigenetic origin. Consequently it became essential to compare Mount Isa with Hilton and H.Y.C.

In this paper, the four deposits are compared, particularly with respect to their structures, microstructures and timing criteria. The aim is to see what evidence exists that could establish whether there are fundamental differences between them, or whether they share a similar origin.

GEOLOGICAL SETTINGS

The locations of the deposits are shown in Figure 1, with H.Y.C. being 560 km NNW of the other group of three. Mount Isa is approximately equidistant from Mount Novit to the south and Hilton to the north, with the distance spanned being 40 kilometres. All deposits are in Middle Proterozoic sequences stratigraphically above a regional unconformity, which, in the Mount Isa area, separates cover sequence 2 from cover sequence 3 of Blake (1987).

Mount Isa

A description of the setting of the Mount Isa deposit is given in Part A. The total lead-zinc mineralised interval is a maximum of 1000 metres, with the ore-bearing zone spanning 650 metres (Fig. 2a). Important features include the location of tabular lead-zinc orebodies immediately outside the silica-dolomite alteration system, which in turn sits directly on the Paroo Fault, and the formation of almost all mineable lodes on the western long limb of the Mount Isa Fold.

Hilton

Hilton is in a similar structural position to Mount Isa and in the same stratigraphic sequence. The initial mining block lies 2km south of Hilton North, which is currently in the development phase. The deposit (Fig. 2b) lies in the Urquhart Shale, and consists of a series of tabular lodes, six of which are being mined. The maximum thickness of the mineralised interval is 370 metres. Hangingwall formations have been narrowed by faulting adjacent to both the initial mining block and Hilton North. The main parts of each deposit lie close to the Paroo Fault, which separates the Mount Isa Group from the westward-younging Eastern Creek Volcanics to the west. Valenta(1988) concluded that the sequence was considerably narrowed by strike faulting, rather than being an initially thinner sequence as a result of growth faulting (Smith, 1969).

H.Y.C.

Details of the setting of the H.Y.C. deposit are given in Cotton (1965) and Murray(1975) (Figs 2d, e). It occurs in the upper part of the Barney Creek Formation of the McArthur Group, where the mineralised interval averages 55 metres thick (Walker et al., 1977). The Barney Creek Formation appears to be thicker in a series of synclinal structures than in the surrounding highs, leading to the view that the synclines represent depositional sub-basins (Walker etal,1977). The formation comprises host carbonaceous siltstones, intercalated wedge-shaped polymict breccias, and a body of buff-cream dolomite breccia called the Cooley Dolomite.

Mount Novit

The Mount Novit prospect is a zone of weak to semi-massive sulphide forming an almost continuous belt which crops out as gossanous ridges over a strike of 6 km. It lies to the west of the Mount Isa Fault in an overturned sequence (Perkins and Poole, 1980), of strongly veined dolomitic siltstone that has been correlated with the Moondarra Siltstone (M. Neudert, pers. comm., 1982) (Fig. 2). To the west is a 150m sequence of micaceous schists and siltstones, 230m of highly strained cross-bedded quartzites and micaceous quartz sandstones. At the base of this section is a quartzite conglomerate up to 5m thick above an slight angular unconformity which correlates with that discovered by Proffett (1990), approximately 4km north. The maximum thickness of the mineralised zone on this section is 32m, with the higher grade intersection containing lead and zinc reaching 4.1 m.

OUTLINE OF INVESTIGATIONS

Mount Isa

The methods and areas studied are outlined in Part A. Briefly, the alteration patterns were identified along a stratigraphic horizon in 7 orebody (B sequence) and one cross-section (6999N) across the entire mineralised sequence, and most structural measurements for timing criteria are from northern areas close to the Mount Isa fold.

Hilton

Unlike Mount Isa, a comprehensive study has not been attempted at Hilton; rather, observations have been made of selected underground sites and drill core to obtain an overview of mineralisation styles. The well-documented structural framework established by Valenta (1988), with some modification, has been used to reassess the evidence for timing of mineralisation. Most initial mine block examination has been along a crosscut on 9C sublevel, around the altered dyke on 10 Level (Mathias et al., 1973), and at a series of sites in a non-producing lode to the hangingwall of 4 orebody called 4 pod. As well as routine examination of a series of drill holes in both the initial mining block and Hilton North, nine close-spaced holes in 4 pod on 11A sublevel have been logged in detail, and sampled for petrological examination and whole-rock analysis.

H.Y.C.

Again, fairly limited work was attempted at H.Y.C. Correlation constraints were used by R. Logan (pers. comm., 1991) to locate mineralised intersections in five drill holes that could be unequivocally matched. These intersections span a distance of 1100 metres, and belong to 8 orebody. Other intersections examined included the Cooley Dolomite and many polymict stratabound breccias, especially those with mineralised fragments. In addition, 24m of underground development has been examined and

oriented samples taken to provide absolute data on the orientation of structures, and to constrain drill core interpretations.

Mount Novit

One deep drill hole, H830, has been logged in detail, and two other deep holes in its vicinity, Vw 810 and Tw 846, drilled to follow-up the H830 intersection, have been examined. 1:5000 mapping across a surface strip about 1200 metres wide over the H830 section has been checked and modified.

FEATURES OF THE DEPOSITS

Mount Isa

The stratigraphic setting at Mount Isa is detailed in Neudert, (1983), and the structural environment is from Mathias and Clark, (1975); Perkins, (1984); Swager,(1985); Bell et al. (1988); and Proffett, (1990).

Detailed correlation of highly mineralised stratigraphy into relatively barren sequences has only been successfully done north of Isa mine (Part A). In parts of the 7 orebody sequence a lamina-by-lamina correlation has been extended for five kilometres (J. Landmark, pers. comm., 1992). This continuity casts doubt on the current deposit origin for the laminites (Neudert, 1983). The 7 orebody "B" sequence has a clear distinction between the discontinuously laminated layers and laminites. Neudert (1983) had proposed that the discontinuously laminated layers became the laminites laterally by a process of stylolamination. Since this is not the case, it indicates that individual laminations are distinct, presumably pelagic, events that may be basin-wide. It is these laminated horizons which become the mineralised layers along strike.

A more complete description of alteration, mineral distribution and textures is given in Parts A and B, and argument is presented therein for all sulphides, including the oldest phase of finely laminated fine-grained pyrite, having been deposited by replacement towards the close of the ductile deformation history. In terms of folds and cleavages identifiable in the altered siltstone hosts, sulphides were deposited in a paragenetic sequence which largely overprinted the D_3 structures. Younger structures, which concentrate in a zone closer to the Basement-Buck Quartz fault systems, are not developed in the lead-zinc zones, so timing relative to them is equivocal.

Hilton

Host stratigraphy:

As at Mount Isa, ore is contained within the Urquhart Shale, and the host unit exhibits the same facies (Neudert, 1983). Not only is there not an exact correlation between the sequences at Mount Isa and Hilton, a detailed correlation from a mineralised

zone through to a barren zone, such as for 7 orebody at Mount Isa, has not been achieved. Mineralised and non mineralised sequences can be compared on the stoping block scale. For example, major changes along strike occur in 4 pod on 11c sublevel (Fig. 3a,b), and a laminated sequence must become mineralised between holes 4 and 5 in Figure 3b.

Structure

Most mesoscopic folds have gentle plunges and more shallowly dipping axial planes than at Mount Isa. Cleavage correlation is more difficult as there are generally more cleavages developed at Hilton. Fig. 4 illustrates a range of fold styles in moderately to strongly mineralised sequences. These can be compared with folds illustrated by Valenta (1994a); figs 9b, 10b, and 11), who grouped mesoscopic folds into two generations, with the reclined folds called F_3 and the steep folds F_2. In general, this overprinting relationship is confirmed, although some of the reclined folds were reassessed following the recognition south of Hilton by T. Bell (pers. comm., 1991, Bell and Hickey, 1997) of folds with shallow axial planes that were overprinted by north-south steep axial plane folds with the same style as Mount Isa mine D_3. These have been called $D_{2.5}$ folds, and are distinguished from the D_3 folds of Valenta (1994a) by having an opposite sense of vergence. Once aware of the existence of large-scale structures, smaller flexures which would have been previously ignored in the Hilton mine, can now be assigned to $D_{2.5}$. A fold of this generation is sketched in Fig. 4b.

Close to the dyke on 10 level, an isoclinal syncline with an overall steeply east dipping axial trace is refolded by open folds dipping intermediate west (Fig. 5). Examination of a sample from the west limb of this syncline suggests that the gross structure is the result of three cleavage-forming events (Fig. 6). The syncline on the south wall has its hinge zone sheared out, and, except for the closure on the north wall, would not have been recognised. An intermediate west dipping cleavage defined by sericite and quartz shapes is the strongest foliation visible (Fig. 6b). It is overprinted by a steep west dipping cleavage also shown around patches of quartz-rich alteration (Fig. 6c). Pyrrhotite is the only sulphide occurring in these "buff-altered" rocks, and its growth seems to be controlled primarily by elongate dolomite grains across veins and the intermediate west-dipping cleavage. The structure is interpreted as an isoclinal D_2 syncline with the west limb refolded with $D_{2.5}$, and overprinted by a weak s_3 cleavage (Fig. 6c). The vergence of the D_2 syncline is not uniquely defined, since a corresponding anticline was not located. There is some suggestion of westwards younging on the west limb, which would give the same vergence to the west as that illustrated at Mount Isa (Part A, Fig. 7).

At Mount Isa, folds with gently dipping axial planes are generally restricted to smaller scale intrafolial structures within ore zones, whereas at Hilton such structures can

have amplitudes of 5m (Valenta, 1995a). Another difference appears to be the formation at Hilton of intrafolial folds on the normal west dipping long limb with west dipping axial planes and a westerly vergence, best observed in 2 orebody, 11c sublevel, 4900N. All intrafolial folds observed to date at Mount Isa on the western long limb have an easterly vergence.

A cleavage at a high angle to bedding (dipping intermediate to shallow east, and developed best in sideritic zones) was called s_3 by Valenta (1988). A sample from the hinge zone of the fold which has a profile similar to Mount Isa D_3 folds, and an axial plane orientation of 79 -> 052, is shown in Fig. 7. Here lenticular concretionary structures show the intensity of cleavage parallel to bedding. Narrow shear zones, which are bedding-parallel above and cut across bedding beneath them, are also deformed around the fold. A weak carbonaceous cleavage lies parallel to the axial planes of the folds in layers which have dilated off their neighbours and are separated by curved fibrous dolomite and quartz. A better developed cleavage has a pitch of 37^0 east in a vertical east-west plane. In orientation and character it appears to correspond with s_3 of Valenta (1988, 1994a). The sense of shear on this cleavage is dextral (looking north).

Locally, there are additional cleavages associated with shear on bedding, occurring in the pillar between 4 orebody and 4 pod. A spaced crenulation cleavage, which from character and orientation correlates with s_3 of Valenta (1995a), deforms two directions of fine (0.3mm) dolomite veins, and is in turn deformed by kink-style spaced crenulations at 45^0 to each other (Fig. 8). These cleavages are not recorded by Valenta (1995a) and do not appear to be extensively developed. Younger cleavages at Mount Isa intensify towards the greenschist contact fault (Bell et al., 1988).

Alteration and Mineralization

This study does not systematically address the distribution of alteration associated with lead-zinc ore. The distribution of some of the alteration features on the 5180N section is illustrated in Wilson (1992), along with the distribution of sulphides and metal grades. All of the components, such as siderite and ankeritic dolomite, sericite and biotite, and stilpnomelane and magnetite, occur at Hilton but appear have a more restricted development than at Mount Isa.

There is an obvious distinction between the intersections of 4 Pod and the pillar sequence between it and 4 orebody on 11c sublevel (Fig. 3). The well banded siltstones in the pillar are greenish grey reflecting chlorite alteration, with a gradual lightening in colour over 200mm into the ore zones, which are characterised by coarser-grained dolomites, creamy brown siderite zones and strongly baritic intervals. Although Ba levels are elevated in some Mount Isa ore, none has been observed which has semi-massive barite as at Hilton. The ore zones contain pyrrhotite in excess of pyrite, and have sporadic magnetite.

Irregular coarse-grained carbonate along bedding is associated with the bulk of the ore grade mineralisation, as also exists at Mount Isa. Staining shows that most of this carbonate examined in the 4 pod sequence is dolomite, with minor calcite. Much of this carbonate elsewhere, particularly in more distal sites, may be calcite (R. Myers, pers. comm., 1993). In DDH H820 E. Dec. #1B, this carbonate with only about 40% sulphide, mostly sphalerite, reaches thicknesses up to 60mm between carbonaceous laminated layers. It is associated with wavy lamination and a spaced cleavage, with common divergence of laminae around it. Adjacent siltstone layers are commonly bleached. The boundaries of the carbonate layers, where abrupt, are distinctly scalloped and replace the adjacent carbonaceous siltstone layer. As discussed in Part A, these carbonate layers can be interpreted as carbonates after nodular evaporite minerals (Neudert, 1984), early diagenetic carbonate growths, or bedding-controlled metasomatic alteration. The distribution and form at Mount Isa favoured a metasomatic interpretation, and the preferential occurrence on one limb of folds (Fig. 8e), supports this interpretation at Hilton.

"Buff alteration" similar to that described from Mount Isa (Part A) is extensively developed at Hilton. It is characterised by oxidation of carbonaceous matter, neomorphic dolomite formation, and sericitization. Its distribution is not well documented. It occurs in three 0.5m bands over a width of 15m on 10 level AI522 stope, in a folded zone, (Fig. 5).

Valenta (1994b) described the various textural relationships of chalcopyrite, and interpreted it to occupy the paragenetically latest, commonly extensional, sites in ore zones. Generally, this relationship appears to hold. However, some samples from 3 centre lens have disoriented clasts of massive finely laminated chalcopyrite in a matrix of coarse-grained galena and sphalerite, with the appearance of the chalcopyrite being paragenetically earlier (Fig. 9a). Sulphides more commonly form breccias at Hilton, at least in the lenses wide enough to be mined (e.g. Figs 4a and 9b). In narrower zones separated by continuous siltstone layers, the sulphide-rich zones are very similar to those at Mount Isa (Fig. 9c). Further out towards the margins and particularly at Hilton North, sphalerite is in bands of nodular carbonate (Fig. 9d).

Large-scale structural relationships of sulphides

Valenta (1994a) and Wilson (1992) described the zoning pattern of copper away from the Hangingwall fault and dyke system, and interpreted it to be controlled both by that system and strain rate incompatibility between the lead-zinc lodes and the barren siltstones. In addition, there is a zoning of lead and zinc patterns around the same structures. The ratio of Pb/Zn increases in a parallel fashion from around 0.5 about 50m from the fault to about 1.0 or greater adjacent to the fault/dyke system (Fig. 10). This suggests that the ratio change is also related to control on the fault system.

Microstructural timing of mineralisation

The main part of the sulphide system at Hilton, to which timing criteria have been applied, is the significant chalcopyrite which occurs within the hangingwall orebodies (Valenta, 1988,1994b). This work concluded that chalcopyrite, even where it was fine-grained and intimately associated with sphalerite and galena, was deposited subsequent to the gross bedding being rotated to its present steep orientation (F_2). Valenta (1988) studied in detail the relationship between all styles of veins and breccia veins and chalcopyrite deposition. There were five classifications of vein types, two of which were pre or syn-D_2. Chalcopyrite in these vein types was regarded as being deposited in the veins subsequent to a deformation event. Consequently, in his local deformational scheme, Valenta (1988) interpreted the copper mineralisation to have begun depositing in pre-existing veins during the later stages of the F_2 episode, after dyke intrusion, and to continue depositing with subsequent veins syn-to late F_3, with the final deposition as large open space veins at unknown time during or after F_4.

Relationships indicating mineralisation timing are illustrated in Figure 11. Extensional veins containing chalcopyrite cut across a thrust fault which has the same character as those which are deformed around the Mount Isa fold at Mount Isa. They have the same relationship as east-dipping silica-dolomite veins high in the Mount Isa copper system. In this development face, high grade galena/pyrrhotite ore also cuts across similar faults with 0.3m displacement. Cross-cutting and discontinuous mineralisation, both sphalerite-rich and galena-rich, is shown in Figures 11b,c,d. Although the sulphides are distributed broadly parallel to bedding, and different layers have different average concentrations, these sulphides are distinctly cross-cutting even at this hand specimen scale. Sphalerite is unevenly distributed across a $D_{2.5}$ fold (Fig. 11b) and a D_3 fold (Fig. 11c). Galena-rich fronts have advanced across a D_3 fold (Fig. 11d).

Microstructural relationships of sulphides to alteration minerals and cleavage events indicates a consistent overgrowth by sulphides (Fig.12). In these examples, which relate to cleavage events s_2, $s_{2.5}$, s_3 s_4, there seems to be a consistency in that the sulphides illustrated, pyrite, pyrrhotite and sphalerite, either overprint the cleavages directly or overprint alteration gangue minerals which were formed either during or after the cleavage. If the correlation of the high angle s_3 cleavage of Valenta (1988) as being younger than the Mount Isa s_3, an additional younger constraint is placed on timing

H.Y C.

Host Stratigraphy

The McArthur host stratigraphy is described by Croxford (1968) and, in contrast to the Reward dolomite above it, contains finely parallel-laminated units that host the

sulphides. Where the effects of sequence-repeating and sequence-removing structures can be accounted for, there is remarkable continuity and similarity of the host siltstones (Fig. 13). The sequence (Fig. 13) was correlated by R. Logan using a unit of 40mm to 120mm non-laminated siltstone with a graded polymict breccia at the base, and an approximately 40mm banded zone with a chert above it, as the underlying and overlying sequences respectively. Four of the correlated intersections are very similar, but the J15 sequence at the south is quite different and contains bands of nodular dolomite. The non-laminated carbonaceous beds can still be correlated into this sequence. Nodular dolomite in J15 spans a stratigraphic width of at least 7 m containing the sequence in Fig. 13a.

Structure

A broad U-shaped syncline with a steep western limb and an interpreted near vertical to overturned eastern limb (Figs 2d,e) contains the deposit. Two generations of thrust faults are ubiquitous throughout the H.Y.C. mineralisation. In underground exposure, although it appears at a superficial level that stratigraphy is continuous, it is normal for individual laminae not to be traceable across the development opening. They are displaced by healed faults, where those that repeat stratigraphy, predominate over those that remove stratigraphy (Fig. 14). Clear overprinting relationships exist between the two sets of thrusts (Fig 15). On the steeply east dipping limb, the earlier set, which may be related to folds, dip more shallowly than bedding, and the later set which are commonly related to folds, dip more steeply than bedding. The first phase of extensional structures are truncated and displaced by the second phase of thrusts with distances measured up to 0.5m. Early thrusts are deformed around folds which vary in wave-length from 2 cm to 1.0m (in exposure). These folds locally have extensional microfaults parallel to the axial plane. In drill core, the set at the lowest angle to bedding is presumed to be the earliest, and maintains a consistent vergence relationship along the flat hinge of the basinal fold. In the 25m of underground development, the intersections of both thrusts with bedding plunge very gently due south, indicating that, at least in the core of the deposit, the first phase of thrusting is essentially west over east, and the second phase is reversed.

These two generations of structures were recognised by Hinman (1994) and Hinman et al. (1995). Their study used oriented drill core and obtained a direction of 'top to NE' for the first phase and subdivided the second into two distinct kinematic phases " a SE-NW shortening phase characterised by 'top to NW' kinematics and a later NE-SW shortening phase characterised by 'top to SW' kinematics'.

Alteration and Mineralisation

With such fine-grained rocks, and non-unique interpretion of some of the textures, it is difficult to establish which changes are due to primary depositional features and

which are due to subsequent alteration. Some samples of distinct lithologies such as the Cooley Dolomite, polymict breccias, concretionary structures and "nodular dolomite" have been examined to see if there are distinctive features that give information on their origins.

Cooley Dolomite

The Cooley Dolomite (Fig. 2) is shown in Walker et al. (1977) as the Cooley Dolomite Member. It has been interpreted as a talus slope breccia (Walker et al., 1977; Logan, 1979) which formed adjacent to a fault scarp delineating the eastern edge of the H.Y.C. sub-basin. This body has now been traced (D. Wilson, pers. comm., 1994) on drill sections for 6500m from east of the main deposit northwards. It contains a variety of rock types, but the typical form is a fractured rock grading to breccia, consisting of buff-cream weakly recrystallised mostly angular dolomite clasts separated by brown-grey fine-grained fracture seams or matrix. The matrix is commonly host to fine-grained pyrite, and rarely chalcopyrite and barite. Chalcopyrite also occurs in white dolomite veins which cut across this breccia.

There are three broad interpretations of the Cooley Dolomite. Murray (1975) and Walker et al. (1977), regarded it as a block of contemporaneously deposited and brecciated dolomites which stratigraphically replaced the H.Y.C. Pyritic Shale member. Interpretation of the Cooley Dolomite body by Hinman et al. (1994), has it as a brecciated and altered uplifted block of lower sequence Emerugga Dolomite, thrust against the mineralised H.Y.C. sequence on the Mount Stubbs Fault. According to this interpretation, the apparent displacement on the Mount Stubbs Fault in section ranges from almost nil on 181900N to greater than 1000m on 183500N. A major constraint on the timing of all mineralisation, according to Hinman et al., (1994), is the interpretation of an high angle unconformity of McArthur Group over this upfaulted sequence of strongly brecciated Teena, Mitchell Yard and Mara Dolomite units. The onlap interpretation is derived from shallow fences of holes, such as the I series (approx. 186700N), G series (approx. 185900N), E series (approx. 185100N), and Emu 14, Emu 16 (approx. 184700N). There is debate about the stratigraphic level of "onlap" but now most agree that it is upper Barney Creek Formation, with Mara Dolomite beneath it adjacent to the Mount Stubbs Fault (Hinman et al., 1994).

An alternative third interpretation is indicated by this study (Appendix 1). Some diamond cores intersecting the Cooley Dolomite have been examined, both near the main part of the deposit and further north at 183900N. Drill holes S32/05 ND and R27 both appear to show extensive Cooley-style alteration of H.Y.C. carbonaceous laminites. In S32/05, the zone examined was between 28m and 47m. The interval from 28m to 32.9m consists of a breccia with angular to ragged-edged buff-cream fragments in a darker carbonaceous matrix. This is logged as normal Cooley breccia. From 32.9m to 41m

contains about 50% strongly pyritic carbonaceous H.Y.C. shale and 50% irregular Cooley breccia. Samples, in particular at 36.1 (Fig 16) and 36.5m, seem to show a transition from laminated sediment to Cooley alteration, with transgressive darker zones obliterating the bedding, overprinted by sharp-edged but irregular vein-like zones and angular blocks of Cooley dolomite. The sequence from 41m to 47m is again Cooley-style breccia, but with angular relics of carbonaceous shale. R27 has a wide zone of very pale breccia with interstices containing carbonaceous matter, fine-grained pyrite, and chalcopyrite. This matrix composition and the up dip continuation from the H.Y.C mineralised sequence indicates that the Cooley Dolomite is derived from it. Thus, this interpretation is that the Cooley Dolomite is an *in situ* alteration body, but is contiguous with, and derived from, the H.Y.C. sequence, rather than being separated from it by a thrust fault.

Polymict breccias

Layer-parallel breccias occur throughout the H.Y.C. sequence (Fig. 2). They have been interpreted as primary sedimentological features (Cotton, 1965; Croxford and Jephcott, 1972; Murray, 1975; Logan, 1979; Logan and Williams, 1990). Characteristics of the polymict breccias are such that a sedimentary origin seems obvious. These include: 1) lateral continuity along bedding; 2) size grading of clasts both up sequence and laterally; and 3) the existence of coarser-grained non-laminated and frequently cross-bedded sequences directly above them. In many areas, particularly the outcropping breccia in Barney Creek, individual clasts have an interpreted provenance from underlying sequences, some large blocks up to 3 metres across are stromatolitic, and suggestions have been made of reverse stratigraphy in clasts indicating hinterland uplift on basin margin faults (Walker et al., 1977).

Examples of polymict breccias are illustrated in Figure 17 Clasts in the polymict breccias are generally non-laminated to poorly laminated, with some containing layering defined by chalcedonic silica in zones up to 3 mm thick (Fig. 17b). There is a range of clast colour variations, with the most common being buff-brown, greyish-green, cream and light green. They are mostly angular and commonly tablet-shaped with their long axis sub-parallel to the top and bottom of the unit. The breccia layers mostly have finely laminated siltstone at the base with thicker sandy layers at the top, although one has a 15 mm. graded bed at the base. The thickest polymict breccia bed examined in this study was 0.37 m (N18, 319.5 m.), but they have been recorded by Logan(1979) to be up to 3 metres. The O.37m bed is well graded except for "clasts" of laminated high-grade mineralisation up to 27mm across, which are at the top of the sequence.

Despite the many features indicating a sedimentary origin for the breccias, there are other characteristics which are difficult to explain by sedimentary processes. The most important of these are the mostly pyritic, but commonly galena/sphalerite-bearing "clasts"

and their relationship to overlying and underlying similar lithologies. The existence of adjacent laminated "clasts" that are rotated through high angles with respect to each other, yet still contain the same lamination spacing even when lamination is orthogonal to gross bedding, is hard to reconcile with a sedimentary "rip-up clast" origin. As Williams (1978c) pointed out, shortening of these laminated rocks takes place during the formation of concretionary bodies, which must at least represent a sediment load. It is difficult to envisage these compacted laminites being then available for erosion and incorporation into a sedimentary breccia, with no further differential compaction of laminite. A range of polymict breccias (Fig. 17) show different proportions of laminated mineralisation within the breccia, and there seems to be a continuous gradation from isolated "clasts" (Fig. 17a) to sequences of fine-grained laminated or non-laminated sediment which could represent *in situ* stratigraphy (Figs. 17d,e). This gradation and the corroded but semi-continuous nature of the "clasts" (Fig 17c) is supporting evidence that they represent residuals of essentially *in situ* sediment rather than sedimented "clasts" In addition, the laminated mineralisation within the breccias contains the same folding and microfaulting structures as the normal mineralisation away from the breccias. Thrusts and cleavage-parallel microfaults, which may be associated with folds, show no displacement of the boundary against breccia clasts (Fig 18a). This indicates that irrespective of how the breccia formed, these structures were in the laminated "clasts" beforehand. One possibility is that the mineralised fragments represent matrix residuals resulting from almost complete incorporation of folded and thrusted laminated siltstone in the breccia.

An alternative interpretation for at least some of the polymict breccias is that the non- laminated clasts have not been transported and sedimented but have grown in situ, largely within laminated siltstone. This is supported by the following criteria: 1. The changes in colour and texture constituting the polymict nature of the breccia commonly takes place within what is most likely to be a single continuous "clast" (Fig. 17b; Fig. 18b). 2)There is a jigsaw-like fitting together of adjacent clasts with commonly quite elaborate interlocking, particularly involving green presumably chloritic shapes (Fig. 17a). This can only be explained in a sedimentary breccia by invoking substantial dissolution along clast boundaries. However, such an interpretation is not supported by concentration of insolubles along boundaries or stylolitization. In some cases (Fig. 17b), there is an interlocking shape match between adjacent "clasts" with a thin strip of laminated carbonaceous sediment between. Many clasts (Fig. 17c.) exhibit angular protrusions which would be very difficult to maintain during mass slurry flow, even over short distances. K. Woolfe (pers comm., 1995) has examined specimens of the breccias and found that the relationships of clasts, in particular the fitting together of adjacent clasts with similar textures, and the necessity for the same clasts to exhibit rigid behaviour (angular shapes) and yet show plastic behaviour (interpenetration), are not consistent with sedimentary processes. It is possible to envisage a sedimentary model involving the

build-up of a fan adjacent to a fault which is subsequently slurried by tectonic instability, to produce breccias having some of these features. However, the observed breccia textures would still necessitate some subsequent unusual alteration and deformation processes. Deformation subsequent to clast incorporation is shown by bending of laminations around clasts (Figs. 16b,d), and this seems to account for strain changes between clasts, but not for gross differential transport of them.

Polymict breccias on the surface (in the Teena and Caranbirini areas) although broadly stratabound, are shown not to be sedimentary because of their cross-cutting relationships to both overlying and underlying sequences. One polymict breccia observed underground in the footwall sequence (Fig. 19), was almost orthogonally discordant to the overlying sequence. Such relationships show that non-sedimentary polymict breccias exist at McArthur. The bulk of the polymict breccias interpreted as sedimentary occur in drill core, where their field relationships are not obvious. In some core intersections, however, (e.g. Fig 17e), the strongly cross-cutting upper breccia boundary could not be generated with a sedimentary origin.

Relationship between the polymict breccias and the Cooley Dolomite

It is the relationship with Cooley dolomite which is most intriguing for the origin of the polymict breccias. The polymict breccias extend towards the anticlinal high to become contiguous with the Cooley Dolomite. No convincing evidence has been seen that the Cooley Dolomite overprints the polymict breccias. Rather, it appears that the polymict breccias become monomict as they enter the Cooley Dolomite, where much of the breccia has the same clast shape and disposition, but the clasts are more uniformly textured and pale coloured. The breccia at the base of DDH L18/00 from 316.5 to 317.4 is an example of a zone logged as a sedimentary breccia which contains only light colored fragments supported in a brown colored matrix which appears indistinguishable from Cooley Dolomite. That part of the Cooley Dolomite which is most similar to the above breccia is from the Amelia area (DDH's A35 and A44- D. Wilson, pers comm. 1991).

Alternative interpretations for a drill section assuming the Hinman et al., (1994) model of an upthrust block prior to the unconformity (Fig. 20a), present quite a different picture from a model whereby the polymict breccias and the Cooley Dolomite are contiguous (Fig. 20b). With this latter model, there is also no necessity to interpet blocks of creamy dolomitic rock, up to several metres in thickness, within the polymict breccias as gigantic clasts from an adjacent fault. In an interpretation with only minor Cooley-style alteration affecting polymict breccias (M. Hinman, pers. comm., 1993), rather than wholesale Cooley alteration of laminated sediments (this interpretation), there is also the geometric difficulty of positioning a Mount Stubbs Fault with substantial displacement.

Concretionary structures.

Another feature of the H.Y.C. succession whose relationship to both the Cooley Dolomite and the polymict breccias remains enigmatic, are the concretionary structures (Williams, 1979c). Most of these are ovoid in shape, with their long axes in the plane of bedding (Fig. 21). Some, however, have shapes that are transitional to isolated clasts in the polymict breccias, with truncated boundaries and protruberant extensions. They show both overprinting of bedding and bifurcation of outer layers around them. They have not been observed to occur in base metal mineralised layers (R. Logan, pers comm, 1991), but are common in pyritic layers, and have been used by Williams (1979c) to argue for a post-early diagenetic formation of the pyrite. Figure 21 supports this interpretation, with much diminished pyrite concentration inside the concretion where the thickness of the containing unit is nearly 100% greater. The size of dolomite grains is about 40 microns which is similar to the dolomite in the Cooley zone, and the textures are similar to the initial stage of Cooley Dolomite. By analogy with modern deposits, the ovoid concretions form during diagenesis. However, some may form or be modified during the alteration associated with Cooley Dolomite formation.

Nodular Carbonate

Nodular zones from H.Y.C. are shown in Figure 22. The zones are bulbous and associated with disruption of the laminae. Although it is not possible to match individual laminations with certainty, correlation of nodular dolomite with mineralised zones (Fig.12) shows that along strike the nodular layers pass into the bitumen-rich mineralised bands, with the weakly mineralised layers continuing. In some samples (e.g. N18, 392.7m), nodular dolomite occurs completely within the 3mm non-laminated siltstone bands as well as in the bituminous layers. Although on the specimen scale, the growth of nodular dolomite is associated with minor thickening of the sequence, the broad development of nodules in drill hole J15 shows that there is little thickness change overall.

It is difficult to establish the timing of growth of the nodular dolomite. No unequivocal timing relationships have been located with respect to the Phase I thrusts. Nodular dolomite has been interpreted to be a pseudomorphism of sulphate evaporites (Croxford and Jephcott, 1972; Neudert, pers. comm., 1995). Logan (1979, in prep.) concluded that it had grown as dolomite but was a very early diagenetic form related to the lake shoreline. Eldridge et al. (1993), interpreted the nodular dolomite as hydrothermal and recorded in some cases the coexistence of recrystallised primary dolomite, with hydrothermal ferroan dolomite and ankerite. Nodular dolomite was regarded as forming at the same time as the base metal mineralisation.

Characteristics of sulphide mineralisation

Styles of sulphide mineralisation have been well described by Croxford and Jephcott (1972) and Eldridge et al. (1993). By far the most important is the finely stratiform style involving pyrite, sphalerite, galena, with minor chalcopyrite and tetrahedrite. As emphasised by Eldridge. et al., these sulphides do not form monomineralic bands, although in some bands there may be only trace amounts of other sulphides present. Sulphide intergrowths are also described by Eldridge et al., in particular the growth of chalcopyrite inside both galena and sphalerite in the form of "chalcopyrite disease" It is very common for very fine-grained galena to assume a similar habit inside sphalerite, suggesting that it too may have deposited subsequently to the sphalerite.

All stratiform sulphides are intimately associated with bituminous matter, which, although separating fine siltstone bands approximately along the bedding planes, produce both ragged cross-cutting boundaries and progressively thinner parallel lenses of siltstone within the more massive bands of carbonaceous material. Individual fine bands containing sulphides may be laterally persistent for hundreds of metres, although the absolute amount and proportions may vary considerably. Within the correlated layers of Figure 13, sulphide bands can best be matched around layer A. Inside this layer, an individual 30 mm wide correlated sulphide-bearing band shows the following changes:

N18; 50% galena, 5% sphalerite, 2% pyrite.

K18; 35% galena, 10% sphalerite, mnr chalcopyrite.

L21; 40% galena, 40% sphalerite, 10% pyrite, mnr coarser chalcopyrite.

L26; 5% galena, 5% sphalerite.

The other main styles of sulphide are those associated with nodular dolomite, and as matrix and clast replacement in breccias (Williams, 1979a). Textural relationships between sulphides and ferroan dolomite are well illustrated in Eldridge etal., (1993), where it is argued that the dolomite has been progressively replaced by the sulphides, particularly sphalerite. This interpretation appears to hold for all examples of sulphides in nodular dolomite zones. Where sulphides occur in polymict breccias, the pyrite is commonly in the carbonaceous breccia matrix, whereas the sphalerite generally forms rim replacement on the more dolomitic clasts. This rim replacement appears to be later than clast incorporation into the breccia (Williams, 1976; Logan, 1979). Inside the Cooley Dolomite fine-grained pyrite and chalcopyrite are within the carbonaceous matrix between the buff-coloured clasts.

Microstructural timing of mineralisation

The distribution of sulphides can be related to both the first and second phases of thrusting and microfolds. The carbonaceous matter, and its included sulphides, appears to invade and overprint first phase folds, with the resulting lenses of siltstone parallel to both the gross bedding and the axial plane (Fig. 23a). With respect to the later phases of

folds, these ragged boundaries and transgressive digestion are still observed, but it is more difficult to establish whether they were formed earlier and refolded or whether they transgress the later folds. Figure 23b, showing sulphide protrusion into a fold hinge, suggests that the mineralisation has deposited after the fold has formed.

Additional evidence for the timing of mineralisation with respect to the first phase of structures comes from observation of aggregates of sulphides and thrusts. An overprinting relationship beween aggregates of sphalerite, of the same textural form as that parallel to the laminations, and the fine phase I shear planes (Fig. 23b), suggests that the lamina-parallel sulphides are younger than these thrusts. Convincing evidence of this relationship is rare, as, in general, the sphalerite aggregates are so fine-grained, and the thrust surfaces so narrow, that it is not possible to establish a clear timing relationship. However, what is commonly seen is a narrow strip of apparently unreplaced siltstone between layers and along the thrust surface (Fig. 23c). Abrupt changes occur in the position of sulphides with respect to bedding either side of structures. Figures 23d and 23e show changes across early extensional faults and late vein systems respectively. Veins such as these cut across the second phase of thrusts. The net suggestion of these relationships is that the sufides are younger than the phase I thrusts, and seem to be late in, or post-date, the second phase of thrusts and folds.

Mount Novit

Host sequence.

The host sequence is mostly parallel-laminated with some wavy-laminated carbonaceous siltstones (Fig. 24). Correlation of individual horizons has not been possible at Mount Novit, although samples containing variably developed veining, which host mineralisation, generally have finely parallel-laminated wall rock residuals.

Over a strike length of 2.5 km, there are two zones of high grade lead-zinc mineralisation, the easterly one known as Copalot. North of the Copalot shaft it appears that the sulphidic zone to the west is not continuous with the main intersection in H830, but is a separate lens of sulphide.

Structure

The highest grade part of the deposit plunges at about 55^0 south, parallel to fold hinges with a strongly developed rodding lineation (Fig. 25a). These folds are well developed in an anticline-syncline pair about 400 metres north of the H830 section, and adjacent to the Mount Isa Fault. They are characterised by highly cylindrical profiles on the scale of the outcrop. The vergence is synform east indicating that they probably belong to the regional D_2 syncline. Folds with the opposite vergence on the same limb as the Novit zone, are developed throughout the block. Good examples are in the Copalot

shaft and level development (C. Robertson, pers. comm. 1982). They are correlated with D_3 folds east of the Mount Isa-Paroo Fault block. The sliver of chlorite schist and green-buff sericitic silicified sandstone between the Mount Isa Fault and the Satellite Fault is only 3 metres wide, and the fault itself in the H830 core is a healed boundary separating carbonaceous schist to the west from chlorite schist to the east. It has a similar appearance to the steeper part of the Paroo Fault at Mount Isa Mine.

West of the Mount Isa Fault, there are generally two cleavages present. The first is intense and at a low angle to bedding, with the second consistently steeper than bedding. These have been correlated with s_2 and s_3 cleavages across the Mount Isa Fault.

Alteration and Mineralisation

The Mount Novit mineralised zone is notable for the formation of ragged aggregates of both nodular calcite and dolomite, which when less extensively developed, take the form of sigmoidal extensional microveinlets at a high angle to bedding (Fig. 24). These microveinlets (locally termed 'birdswing' texture) are calcitic to the west and more dolomitic to the east in the mineralised zone. They are associated with breccias and zones of more pervasive dolomitization. The two main generations of cleavage are much better developed at Mount Novit than at the other three deposits, and microveinlets can be much more readily related to cleavages. The veinlets are folded about the crenulation cleavage axial plane (Fig. 24) and in planes parallel to cleavage are folded about the rodding mineral lineation which plunges steeply south parallel to the second generation fold hinges (Fig. 25b). Veinlets are very irregular in wall outline and progressively consume increasing proportions of the rock, indicating that although they may initiate on extensional microfractures, they form dominantly by wall rock replacement. The proportion of veinlets increases from about 10% of the rock volume at 45 metres from the high-grade sulphide intersection to about 40% within 10 metres of it. The proportion of siderite increases to about 40% at 7 metres from the intersection and this is associated with coarsening of the siltstone.

Within the sulphidic zone, samples have fine sericite which is crenulated and overgrown by more magnesian phlogopitic biotite. Biotite occurrs both along the bedding and along coarser veins. Coarse feldspars consist of both microcline and albite, and the fine carbonate groundmass is ankeritic. They have a very similar appearance to the buff alteration at Mount Isa and Hilton.

There is an abrupt ten-fold increase in the sulphide content across the boundary at 327.5 metres into the main Pb-Zn zone, which contains about 40% pyrte, 10% pyrrhotite and minor magnetite in conjunction with lead and zinc grades. The bulk of the high grade zone consists of two types of breccia (Fig. 26). At Copalot, the main sulphide-rich rock is a breccia consisting of ragged wispy fragments generally in a range of 4 to 15mm, supported within a matrix of quartz, galena and sphalerite. Fragments are very strongly

foliated carbonaceous schist, tightly folded with a spaced axial plane crenulation cleavage. There is a range of crenulation cleavage directions between isolated fragments, but, in one instance, the dominant crenulation cleavage direction is overprinted by an orthogonal crenulation cleavage which passes into an intense foliation within 50 mm which is in turn gently warped. The other main sulphide-rich type (Fig, 26c), contains semi-rounded fragments of fine strongly foliated sericite and albite with a weak crenulation ranging from 0.7mm to 4mm, in a matrix of dolomite, quartz, and sulphides. The sulphides vary in texture from a fine interconnected network to masses about 0.7mm across with few dolomite and quartz inclusions which average about 30 mm.

To the east of the galena-sphalerite rich intersection is a pyrite-bearing zone which is 33 metres thick with an average sulphide content of 50% of which 15% is pyrrhotite, sphalerite is variable up to 10% and magnetite is up to 10%. The bulk of the pyrite, although banded, is quite euhedral and granular, and is associated with bleaching of the siltstone. Only minor fine-grained pyrite (around 30 mm) occurs, in bands up to 3mm (Fig. 26). To the footwall of the sulphide zone is a 6 metre thickness of breccia with much more silica-dolomite characteristics. It consists of residuals of variably laminated partly carbonated siltstone cut by veins of coarse grained ferroan dolomite and quartz. The dolomite is variable in grain size with the finer grained (1-2mm) dolomite being rich in carbonaceous inclusions and the coarser (up to 10mm) being cleaner with sutured grain boundaries. Silicification of the dolomite matrix has the same textural relationships as partially silicified dolomite breccias at Mount Isa (Perkins, 1984), although only minor pyrite was associated with this textural type in this hole.

The gross form of the sulphide zone, at least in the area examined, is indicated by the two holes drilled beneath H830. The intersection in hole Vw810 vert.#1 is 700m below and 250m further south. It contains 3.8m of medium grade lead-zinc in an intersection of 10m of pyrite. The next intersection 400m north of this contains only disseminated pyrite and trace sphalerite, although there is no change in the host rock of the zone. This confirms that the plunge of mineralisation, including the semi-massive bedding-parallel pyrite, at this locality is steeply south-west approximately parallel to the plunge of the mesoscopic folds.

The Native Bee siltstone beneath the Mount Novit Fault block has a distinct banded appearance with vaguely structured blue-grey calcareous bands, within the brownish-grey finely laminated carbonaceous siltstones and grossly parallel to bedding. Where the laminated siltstones are thin (1-3cm) they commonly exhibit both extensional and contractional structures somewhat similar to the style of structures developed in shaley bands when surrounded by lead-zinc sulphides at Mount Isa (Part A, Fig. 20). These structures are extensional rotated blocks on strongly refracted microfaults, boudins, intrafolial folds, and microthrust repeats (Fig. 27). The strong refraction and "streaming" of cleavages along the calcareous layers and edge effects of progressive

calcitization of folded laminated siltstones indicate alteration synchronous with deformation. The microfolds in this sequence have well developed axial plane cleavage which dips steeply west (steeper than bedding) and is correlated with s_3. Pyrite is preferentially associated with both the calcitic zones and quartz-calcite veins crossing the laminated siltstones. It is postulated, because of these textural and timing similarities, that this zone of alteration may represent a peripheral precursor to later lead-zinc mineralisation, with the calcitic layers being overprinted in the orebodies by later dolomite and sulphides.

Microstructural timing of mineralisation

Although the microveinlets appear to have part of their history as dolomitic zones that are folded about the crenulation cleavage (s_3), the sulphides do not seem to have participated in their deformation history (Fig. 28). Sphalerite, galena and pyrrhotite seem to have overprinted both the deformed and partly recrystallised dolomite as well as later overgrowth dolomite. There is no reflection of the intense bedding-parallel schistosity (s_2) in the sulphides, which should be present if the sulphides were precipitated earlier. (Fig. 28a).

Where the sphalerite-pyrrhotite rich zones are strongly discordant to the relict bedding (Fig. 28b), they are related to differential microvein development which is strongly controlled by original lithology. The microveins are related to both the bedding-parallel and cross-cutting foliations, and the sulphides reflect these controls, although they replace the alteration minerals developed in these veins.

DISCUSSION

Comparison of mineralisation styles-the degree of strata-parallelism

Concentrations of sulphides along layers parallel to bedding at all scales, and in particular, different sulphide ratios and assemblages in adjacent layers, have been the main evidence used to infer a synsedimentary timing (Croxford, 1962; Williams, 1976). There are two aspects of the extent of stratiform nature to sulphides along the bedding. They are related to grain size of individual sulphides, and the continuity and concentration along individual correlatable layers. To take extreme cases, for example, it is possible to envisage fine-grained homogenous aggregates of sulphides which on the scale of a drill core, are uniformly distributed across the core within the layer and yet do not extend for more than a few metres from it. Conversely, a particular layer may have irregularly distributed sulphides along it, but this relationship may persist for hundreds of metres. The former style would generally be termed stratiform and the latter stratabound.

It is very difficult to measure these relationships in any consistent way, and yet it is the stratiform nature of these deposits which is used as the main evidence that they are synsedimentary. As described for the correlated sequence in the H.Y.C. deposit, at least two layers which can be correlated are mineralised in the four intersections over 800m, although the proportions of the different sulphides varies. There is only limited information in the second dimension, although the K18-N18 intersections show at least some continuity. Given that there are many lines of evidence that the sulphides are not strictly syngenetic, any timing model must still account for such remarkable selectivity. No layers have been located at Mount Isa which have anything approaching that degree of continuity of fine-grained sulphides (excluding fine-grained pyrite). Instead, even the entire B sequence only has sphalerite over a maximum distance of 400m (Part A; Fig. 10d). Stratiform sulphides which are not continuous over the width of core or hand specimen, where the host layers themselves are continuous, are relatively common compared with the H.Y.C. deposit.

In order to establish timing of formation, the degree of stratiform or stratabound sulphide development cannot be used. Intuitively, workers (e.g. Williams, i976) reasoned that in order for layers to have stratiform sulphides over any distance, the host requirements were for pre-lithification porosity and the availability of connate fluid. These conditions were most likely satisfied in sediments which still had an overlying water column. Stratiform sulphides were interpreted to be already in the sediments prior to any deformation, which was itself interpreted as synsedimentary (Williams, 1976; Hinman, 1973). These relationships are discussed below.

Comparison of mineralisation styles-the relationship of copper.

As well as Mount Isa having huge copper orebodies in its own right, both Isa and Hilton lead-zinc orebodies have areas of significant chalcopyrite. Hilton has a greater proportion of layer-parallel forms, and certainly has proportionally more finely laminated and finer grained chalcopyrite than Mount Isa (Valenta, 1988, 1994b). This is mostly on the margins of lead-zinc layers, and is particularly concentrated around the dyke (Fig. 5 and 9a).

The higher concentrations of copper at HYC are in the Cooley Dolomite (best intersection of 50m @ 1.49%), and at HYC north, as coarse readily visible concentrations in the galena-rich stratiform mineralisation. An average concentration of copper in the H.Y.C. lead-zinc orebodies is 2000ppm. Most of the chalcopyrite in the lead-zinc ore is not visible, but occurs as fine filigree textures in the sphalerite, in apparently very much the same textural form as the galena in sphalerite. It is quite irregular with sphalerite patches containing perhaps 40% chalcopyrite adjacent to others with no chalcopyrite. Alternatively, some chalcopyrite in the lead-zinc rich zone occurs in quite different sites. In the sample shown in Fig. 13b, (K18) chalcopyrite forms coarser grains, although still not visible, inside the steep 0.25mm-wide dolomite vein. Chalcopyrite grains in this vein vary in long axis from 40 mm to 120 mm. The vein also contains galena and sphalerite, with more galena than chalcopyrite, and considerably less sphalerite than chalcopyrite.

Minor chalcopyrite occurs in the Mount Novit zone, but seems not to show any consistent relationship. Micro-inclusions of chalcopyrte occur in sphalerite. There seems to be an increase in copper in sections to the south, where it has formed in separate zones to the main lead-zinc bands and commonly associated with actinolite.

All four deposits thus contain copper mineralisation, which at Isa, Hilton, and HYC shows a zonal pattern away from the main fault zone, with copper concentrating closest to the fault in most altered rocks. In all four deposits, chalcopyrite occurs in the most cross-cutting relationships, with least distribution along the bedding, and most common occurrence in structures at a high angle to the extension direction, relative to the other sulphides. Although Mount Isa is unique, not only in this group, but in deposits throughout the world, in having such a massive copper system closely associated but little mixed with lead-zinc, all deposits have significant chalcopyrite indicating that it does not represent a separate event but belongs to the same mineralising stage.

Breccia Development at each deposit

All deposits have a range of breccia types which are both lead-zinc ore-forming and as separate bodies. This section concentrates on the associated breccias which do not form in the lead-zinc ore. Lead-zinc ore breccias and their origin are discussed in Part A

and elsewhere in this section. At HYC, polymict breccias outcrop in Barney Creek and, although they show some of the features suggesting alteration, they contain large stromatolites and thus are evidence of the introduction of exotic material. Thus it must be concluded that at least some of the polymict breccias are of sedimentary origin. The Cooley Dolomite, however, has features which are better interpreted as a massive fracture-controlled alteration body. The contiguity with, and lack of overprinting relationships between, the Cooley Dolomite and the polymict breccias, in conjunction with evidence in the breccias themselves, suggests that many of the latter may have an alteration origin. This has major implications for the tectonic setting of the H.Y.C. deposit. Arguments for the syndepositional origin for the Emu Fault and other major faults in the district, refer to the massive development of turbidite breccias, and the existence of karsted unconformities (e. g., Neudert and Sheppard, 1993). If the polymict breccias and the abrupt oxidised fronts, including the Cooley Dolomite, are explained as the result of alteration, then evidence for the syndepositional origin for the major faults breaks down.

The silica-dolomite breccia system at Mount Isa is intimately related spatially to the lead-zinc lodes, interdigitating between them and having the same gross trends as their enveloping surfaces. There seems to be no evidence of prior significant facies changes controlling the breccia (Perkins, 1984), although some workers (especially M. Neudert, pers. comm. 1985) suggest that there is preferential sulphate evaporites pisolites in the silica-dolomite.

Both Mount Isa and Hilton are associated with *in situ* breccias in the hangingwall units, (Neudert, 1983), which are not dissimilar to the cross-cutting breccias at McArthur. They are best developed in outcrop at the Kennedy Quarry, Spear Creek and south-west of Hilton. At Hilton, they may have a bleached and buff-altered appearance much like the Cooley Dolomite. There is commonly a foliation with clasts elongate in the direction of the cross-cutting (s_3) cleavage. In drill core, the hangingwall breccias at Mount Isa are overprinted by silica-dolomite veins.

All deposits are therefore closely associated with breccias which have been interpreted in different ways. It is possible that all of these breccias have an alteration origin, although the more polymict breccias are distinctly earlier than the silica-dolomite style.

Depositional Features or Alteration

Mount Isa, Hilton, and H.Y.C. deposits all contain layer-parallel development of neoformed carbonate which can vary considerably in grain size but has many features in common. It both overprints and expands laminations, and may vary from isolated unconnected bodies to almost complete overprinting of sequences up to 25mm thick. The

term "nodular dolomite" has been used frequently in the past, but is not strictly applicable unless the mineral chemistry has been established. The neoformed carbonate in the 7 orebody "B" sequence samples is all dolomite, and Logan (1980) established that the term nodular dolomite was appropriate at H.Y.C. At Hilton, however, D. Clark (pers. comm. 1993) has established that much of the coarser-grained white carbonate is calcite.

The most significant aspect of these nodular carbonate zones is whether they represent precursor sulphate evaporites. This interpretation has been argued at McArthur by Logan (1979) and Neudert (pers. comm., 1994), and at Mount Isa by McClay and Carlile (1978), and Neudert (1983) for at least some of the carbonate parallel to bedding. In contrast, Eldridge et al. (1993) and Hinman (1994) have interpreted the nodular dolomite at HYC to be the result of hydrothermal alteration which is part of the mineralising process. As noted above, the limited HYC nodular dolomite investigated in this study is interpreted to represent an alteration zone. In part A, arguments were presented for Mount Isa bedding-parallel neoformed carbonate being an early part of the alteration system, associated with dilation during folding along the bedding. At all deposits, this form of carbonate is spatially closely associated with the base metal sulphides, but appears to be consistently replaced by them.

Timing of ore formation.

Factors relevant to timing of Mount Isa mineralisation, such as the concepts of remobilisation and recrystallisation, the possibility of a series a lead-zinc mineralising events, and coincidence of copper and lead-zinc were discussed in Part A. Many of these arguments have relevance at the other three deposits, and will be related to them where appropriate.

Hilton:

If a correlation of D_2(Valenta,1988) with D_3 (Perkins, 1984), is used, then the periods of copper formation between Mount Isa and Hilton correspond closely. As Valenta(1994b) states "in both mines, copper mineralisation occurs late in the syndeformational alteration-veining history"p.1049.

In the case of the main ore system at Hilton, the lead-zinc lodes, however, the interpretation of this study and that of Valenta (1988, 1994a, 1994b), differ entirely. Valenta (1994a) concludes "Pb-Zn mineralisation records the entire deformation history" p438, and op. cit (1994b) p.1043. The argument is mostly based on the striking differences in styles of structures in strongly mineralised zones compared with barren or weakly mineralised zones. In addition, Valenta (1994b) states, "lead-zinc mineralisation.....is at least partially overprinted by the early bedding-parallel foliation, suggesting that the earliest lead-zinc deposition preceded deformation" p.1043. No

illustrations are provided to support this contention, and no evidence of it has been seen in this study.

On the scale of underground exposure and hand specimen, [(e.g. Valenta, 1994a), Figures 9,10,11, and (1994b), Figure 6], the interpretation provided that such structures are the result of brittle behaviour of shale layers alternating with plastic sulphide layers, seems reasonable, if not obvious. However, when examined microtexturally, particularly if including the possibility of replacement, the alternative interpretation that sulphides are superimposed on zones that have had a different alteration and deformation history, is preferred. In fact, many of the relationships illustrated by Valenta(1994b), in support of chalcopyrite being deposited late in the deformation history, also apply to galena and sphalerite.

H.Y.C.

Stratiform mineralisation has hitherto been interpreted as forming strictly syngenetically (e.g. Croxford, 1968, Lambert, 1976), or within the sediments, (Williams, 1976, 1978b) with discussion centering on the stage of diagenesis and depth of sediment deposited before metals were introduced. A limiting constraint that has governed ideas of maximum pre-ore sediment thickness has been the existence of polymict breccias between orebodies, and the presence of mineralised clasts within them (Logan et al., 1984). Hinman et al. (1994), presented arguments to constrain the stratiform mineralisation to being earlier than "the formation of abundant and kinematically distinctive drill-core scale structures". They hypothesised that each shale package was mineralised before the subsequent package above the overlying breccia "was either deposited or became diagenetically amenable to mineralisation". This limited ore-forming processes to depths of the order of ten to a couple of tens of metres below the sediment-water interface. Mineralization was envisaged to be an episodic process, with the breccias punctuating metal introduction. An upper constraint on timing of both the fine stratiform ore and the more obvious cross-cutting Cu-Pb-Zn sulphides was argued to be provided by a high angle unconformity with upper Barney Creek Formation onlapping over steeply dipping and mineralised Teena, Mitchell Yard and Mara dolomite of the Western Fault Block. The former style was regarded as being earlier than the structures with "top to NE" kinematics, whereas the latter was associated with transpressional structures forming the Western Fault Block.

In the discussion of Eldridge et al. (1993), no mention was made of mineralisation in clasts in the breccias which has been a feature of the evidence for early diagenetic mineralisation (Logan et al., 1984). Neither was mention made of the "permeation model" of Williams (1992, 1993), where it was argued that the base metals from each successive pulse of mineralisation displaced the previously deposited pyrite into successively higher stratigraphically levels. Eldridge et al. (1993) examined their data in

the light of five models of pyrite and base metal sulphide genesis, and related observed textures to those expected from each of the models. They concluded that the textural evidence was indicative of the processes and sequence of mineralising events, and that these were unlikely to be "altered by diagenesis or metamorphism" These textural relationships indicate a straightforward sequencing of Py1->Py2-> base metal suldides. It appears from the discussion of Eldridge et al., that they favored the mineralising event occurring not far below the sediment-water interface, involving the permeability-controlled migration of basinal brines along bedding.

Crick(1992), from a detailed study of organic matter in sequences of the McArthur Basin, concluded that the heat from hydrothermal solutions associated with formation of Pb-Zn mineralisation at H.Y.C., had raised reflectances in migrabitumen adjacent to the mineralisation. The raised reflectances extended for at least 50 metres above the mineralised zone in DDH M17/08.

Evidence on timing of pyrite formation relative to compaction around concretionary structures is presented in Williams (1978c; 1979a,b), but is not addressed in Eldridge et al. (1993). Similar relationships have been observed in this study (Fig. 21), and, although base metal sulphides do not occur with pyrite in these concretions, paragenetic overprint of pyrite elsewhere (Williams, 1978a,b) indicates them to be even younger. These above studies do not address the question of the relationship of sulphide precipitation to deformation events.

The separation of two kinematic phases from this limited study agrees with the interpretation of Hinman(1993). What is in question, however, and has critical bearing on the timing of mineralisation, is firstly, whether the sulphides have deposited prior to either, or both, of these sets of structures, and secondly, whether either, or both, of these kinematic phases were active during sedimentation and were complete before upper Barney Creek Formation time, as concluded by Hinman et al. (1994). At the scale of hand specimen, their notion that the sulphide banding is established before the development of any of the drill-core scale structures appears inarguable. There seems to be perfect matching of fine sulphide bands across the structures. At the micrograph scale, this interpretation becomes equivocal, and some evidence is presented above that the base metal sulphides are deposited after the formation of the Phase I thrusts, and possibly also after the second.

Timing of both phases of thrusts obtained by Hinman et al. (1994) depends entirely on evidence for an unconformity on top of the "Western Fault Block" According to their interpretation, both sets of structures are earlier than the upper part of the Barney Creek Formation or locally the Reward Dolomite. An alternative to the sedimentary onlap interpretation across the top of a syndepositional fault, is that the boundary is an abrupt oxidative alteration front, similar to the steep western front of the Cooley Dolomite (see Appendix 1)

As is the situation at Mount Isa and Hilton, timing relationships between sulphides in late veins and those distributed along the bedding, can be interpreted in a number of ways. The most common interpretation (e.g. Gustafson and Williams, 1980) is that the veins represent younger "remobilisation" of synsedimentary sulphides. Alternatively, they could represent a younger epigenetic pulse of mineralisation (Neudert, 1984), or part of the same late phase as bedding-parallel replacement (Part A). The continuity of sulphide from the laminations to the veins, the replacive nature of sulphides in both sites, and the lack of any evidence of dissolution or destruction of sulphides in the laminations, are suggestive of the fractures being in existence before the deposition of sulphide in the laminations, and both styles belonging to one event.

Mount Novit:

Base metal sulphides replace the arrays of replacive veinlets which were deformed by the second deformation event in the area. This is correlated with the cleavage-forming D_3 event at Mount Isa. No previous published works on Mount Novit discuss timing relationships, although an internal project by Chi Minh (pers. comm., 1986) concluded that the deposit was hydrothermal and replacive.

Depositional Conditions

Eldridge et al. (1993) detailed a paragenetic history for H.Y.C. samples which is compatible with a model of bacteriogenic reduction of sea water sulphate to form py1 and py2, with a subsequent overprint of base metal sulphides precipitated from H_2S-poor hydrothermal fluids. They suggested that influx of a carbonate-, iron bearing ore fluid could have dissolved dolomite in the original sediment which was reprecipitated as ferroan dolomite in nodules which were partially replaced by base metal sulphides. They also speculated that the warmer fluids bearing Zn, Pb, Ag, Cu could have been toxic to the bacteria, so clearly envisaged an early diagenetic timing of mineralisation.

This environment and that postulated by Hinman et al. (1994), with deposition within a couple of tens of metres of the sediment-water interface, restricts the conditions of sulphide deposition to one of limited temperatures because of the availability of the overlying water column. A post-McArthur Group depositional timing places increased importance on the availability of bituminous matter for sulphate reduction, in concert with Hinman et al. (1994), although the sulphate has an alternative source from either the water column or sulphate minerals precipitated in the sequence. This much greater depth of burial is consistent with a thermal anomaly within the oil window as envisaged by Crick (1992).

A far greater proportion of sulphides at Mount Isa, Hilton and Mount Novit which appear to have replaced phases other than bituminous matter, particularly dolomite,

indicate different depositional conditions at these deposits. Only the fine-grained pyrite seems to share the same relationship to carbonaceous material, and similar depositional conditions are possible.

Controls on orebody formation

Hilton, Mount Isa and Mount Novit all occur adjacent to the Paroo and Mount Isa Faults and H.Y.C. is adjacent to the Emu Fault. These are all major structures, with movement on the Mount Isa Fault being at least 5 km, on the Paroo Fault at least 3 km, and the Emu Fault at least 2 km. An interesting empirical relationship is that all deposits have formed close to a fault block which represents a narrow sliver of older sequence between younger host units. Hilton north block, Hilton, and Mount Isa lead-zinc centres of mineralisation all occur where the Paroo Fault is locally closest to the host horizon. At Mount Isa, this also corresponds to the domal surface of the Basement Fault. In terms of gross relationships, all four deposits, Hilton and Hilton North, Mount Isa, and Mount Novit, are all exposed at approximately the same structural level, with the base of higher grade mineralisation extending from 1500m to 2000m below the present ground surface, extending to gossans at the surface. Such a relationship would require a large element of coincidence if the deposits were synsedimentary and, after folding, were to finish at the same structural level.

As Valenta(1995b) illustrates, the Cu/Pb+Zn ratio increases towards the hangingwall fault system, and he uses this spatial relationship as well as the overprinting of copper on the altered dyke to interpret this fault system as a major controlling structure for copper.

CONCLUSIONS

Hilton and Hilton North have many features in common with Mount Isa. They share a similar structural setting, but do not have an equivalent ramp structure in the Paroo Fault, at least at comparable depth. Similar arguments apply to timing of mineralisation between the deposits, although clearly defined structurally controlled mineralisation fronts similar to those documented at Mount Isa (Part A), have not been discovered at Hilton. Similar arguments apply as to whether the distribution of the sulphides is the result of two distinct episodes, consisting of a synsedimentary accumulation followed by "remobilisation" or whether there is a single late episode of mineralisation. The simplest interpretation of all relationships observed is that there is a single late mineralising episode. The similarity in both mesoscopic appearance and microscopic textural relationships between Mount Isa and Hilton, negate the argument that Mount Isa lead-zinc has only apparent epigenetic characteristics because of its proximity to a giant metasomatic silica-dolomite system.

The Mount Novit mineralisation appears to be related to carbonate metasomatism which nucleated on extensional veins, subsequent to a crenulation cleavage development in a zone of high strain within the overturned Moondarra Siltstone sequence. This high strain zone is closely related to the Mount Isa Fault.

At McArthur, the H.Y.C. orebody is significantly more stratiform at all scales than the three Mount Isa area deposits. The highly sulphidic sequences are, in general, not directly associated with coarse-grained gangue minerals, particularly ferroan dolomite, as they are at the other deposits. Instead, they are associated with fine-grained bituminous matter which is lamination-parallel on all but the microscopic scale. Only the fine-grained pyrite at Mount Isa and Hilton shares this association with carbonaceous material.

For the Mount Isa deposit, looked at the scale of the district, mine, or individual cross-section and plan, the bedding-parallel distribution of lithologies, including the sulphides, is compatible with the notion of the sulphides being a syndepositional accumulation. When examined in conjunction with relationships at the scale of the exposure, hand specimen, or microscope, however, the alternative interpretation of structurally controlled replacement late in the deformational history, is more consistent (Part A). In terms of timing, this conclusion appears to be also applicable at the other three deposits. The evidence for this at Mount Isa, Hilton, and Mount Novit, is much more conclusive than at the fine-grained McArthur River deposit.

PART D.

Processes in the Formation of Stratiform Lead-Zinc Ore at Mount Isa and Hilton, Queensland.

TABLE OF CONTENTS

INTRODUCTION

Until the processes involved in the formation of ore deposits can be quantified, our understanding of their formation is, at worst, erroneous, or, at best, incomplete. While the debate continues to be limited to whether stratiform lead-zinc deposits, are deposited syngenetically or diagenetically, for example, Solomon et al. (1994), existing models are essentially concerned with processes which involve supply of at least some component of the fluid from the overlying water column. Models of formation generally involve fluid/fluid interaction, with one of the fluids being an evolved basinal brine. If the system forms as the result of late replacement as argued in Parts A and B, however, an overlying water body is not available, and the only fluid mixing concepts relate to meteoric/connate fluids and introduced hydrothermal fluids. A fluid-rock reaction model is much more likely, and understanding the reactions involves determining such fundamental relationships as paragenetic sequences on all scales, and the extent of dilation versus wall rock replacement.

In this study, understanding of chemical changes associated with the lead-zinc mineralising systems at Mount Isa and Hilton has been approached from two different directions. As part of the study of 7 orebody at Mount Isa, a series of intercepts have been analysed on logged splits, which have, as closely as practicable, been divided on the same stratigraphic intervals. Unfortunately, the northernmost reference intercept from drill hole QZ10, was not split on these intervals. Both the full 7 orebody interval (Fig. 1) and many more intercepts of the B sequence in the hangingwall of 7 orebody (Fig. 2), give an empirical idea of chemical distributions in selected zones.

A more interpretive analysis of the geochemical data, involves using the textural and paragenetic relationships observed and reported in Part A. The model derived from that interpretation involves the deposition of sulphides as the result of fluid-rock reaction, rather than fluid mixing. The second major constraint is the paragenetic sequence whereby at each site the succession of non-sulphide and sulphide deposition can be inferred.

Creating a model for the entire deposit depends on what assumptions are made about depositional relationships in time and space. For example, how diachronous were depositional events throughout the rock volume now occupied by the orebodies? At any time, t_1, what was the relationship between the development of the gangue alteration system, and the deposition of sulphides? Assuming that the interpretation presented in Part A is correct, and that any locality (at time t_1) the precursor gangue alteration is complete, containing both deformed earlier phases and undeformed later phases, before the deposition of at least the economic sulphides, are there other localities in the system where either other sulphides, or undeformed gangue minerals, were precipitating at the

same time? In an outwards growing model, these areas could be towards the core or, alternatively, precipitation of initial sulphides could be at the periphery.

CHEMISTRY OF THE LEAD-ZINC OREBODY ZONES

Carbonate chemistry

There is a lack of comprehensive carbonate chemistry data from Mount Isa mine, although some idea of the distribution of carbonate species can be gained by combining data from a variety of sources. The main sources are Neudert (1983), Croxford (1962), Patterson (1982), Waring (1990), and Swager et al. (1987). There is a large range of carbonate compositions, commonly within quite small areas. Phases from calcite to dolomite (ferroan to ankeritic), siderite and magnesian siderite and/or pistomesite (Swager et al., 1987), are located in the boundary zone between the silica-dolomite and lead-zinc orebodies. Swager et al. found that there was a correspondence between the MgO/(MgO + FeO) ratios of the carbonates and the adjacent phyllosilicate, especially stilpnomelane.

M. Painter (pers. comm., 1994) has obtained consistent analyses for carbonates from the 8 orebody sequence in correlated holes north of Isa Mine. These can be related to a paragenetic sequence of carbonate growth.

Chemistry of the B sequence

In order to remove the bias of facies differences as much as possible, samples for chemical analyses were taken from correlated sequences. Where the sequences are not only constrained by tuff marker beds, but also by fine laminae which are correlatable over many kilometres, time lines are perfectly parallel to facies boundaries, and chronostratigraphy and lithostratigraphy are identical. Samples were selected across the B sequence, which meets these criteria, to exhibit a pattern of geochemical distribution. The samples included the uppermost "tuffaceous marker bed" but not the one at the base of the sequence. The sample locations and results are shown as a series of longitudinal projections in Figure 2b, and are tabulated in Appendix 2.

Geochemical profiles can be compared with Figure 10 (Part A) which shows the distribution of alteration and mineralisation. Highest silica is zonally arranged around the silica-dolomite, whereas Fe_2O_3 appears to be more zoned away from the greenschist basement contact. Potash is enriched in a band which is closely associated with high zinc, but extends beneath it. Elements As, Bi, and Sb show a similar distribution to Cu, as found for previous studies of pathfinder elements for the copper orebodies. Pb has a much more restricted range than Zn, which seems to have better halo-forming

characteristics than Tl. Organic carbon depletion reflects the bleaching and "buff-altered" zone which forms a front south of the anticlinal hinge of the Mount Isa Fold.

Chemistry of 7 Orebody

Four drill holes and two development intersections of 7 orebody were used to obtain an overview of chemical changes associated with the mineralisation in this stratigraphic interval. The locations of the intersections are shown in Figure 1a, and the two development intersections on 11 level are related to the Mount Isa fold in Figure 1b. The 11 level locations lie either side of a very rapid diminution of ore grade in 7 orebody, with the northern-most in the anticlinal hinge of the Mount Isa Fold. The most southern intersection (M657) is on the edge of massive silica-dolomite, with the footwall tmb having been overprinted by coarse-grained dolomite. The other three drill holes are outside the main sulphide zone, with one south of the Mount Isa fold and the other two north of it. Drill hole QZ10 was not plotted in Figure 1c because it lacks major element data.

Inspection of Figs. 1b and 1c show some of the major features of chemical distribution. In particular, they show the massive changes in alteration and mineralisation between the orebody and intersections just outside the periphery. Silica is depleted in the orebody zone (7174) relative to the hangingwall and footwall and the intersections north of the orebody. Potash is likewise depleted in the mineralised zone. The major decrease in organic carbon between the orebody (7174) intersection and the marginal silica-dolomite intersection corresponds with the bleaching and "buff alteration". The M657 intersection has a high Pb/Zn ratio which is consistent with its location on the edge of the silica-dolomite, and has copper relatively higher than zinc. Pyrrhotite predominating over pyrite is a characteristic of the 7172N intersection, and barium is strongly enriched in this section, commonly over 2000ppm.

Chemistry of 4 Pod-Hilton

As illustrated in Figure 3b of Part C, the highly altered and mineralised zone of 4 pod transgresses correlatable laminites. In this case, the intersections have not been sampled on correlatable layers, but the mineralised zones and the footwall well-bedded zones have been bulked for analysis (Appendix 2). Such a procedure highlights the massive changes in composition associated with alteration and mineralisation. The same trends as in 7 orebody are evident, but in this case rapid changes can be seen from hole to hole. In particular, there is high concentration of barium, reaching 14.4% in hole No 6.

REPLACEMENT PROCESSES

Review of Replacement

Stanton(1962, 1965) claimed that geochemical evidence showed that the sulphides were an addition to the non-sulphide component rather than being selective replacement. He utilized the technique developed by Croxford (1965), to show that with increasing sulphide content, the ratios of the non-sulphide components remained the same. Plots on ternary diagrams included SiO_2, MgO and CaO. Samples were taken from all copper orebodies and selected lead-zinc orebodies.

How can the data of Croxford (1965) and Stanton (1962, 1965) be reconciled with the petrographic and microtextural evidence of Part A, that all sulphides are consistently replacive of the gangue mineralogy? There are two fundamental assumptions inherent in the above geochemical work. The first is that sulphide-rich rocks can be directly compared with barren unmineralised Urquhart Shale, rather than with variably altered rocks. The second is that the only replacement model allowable is one of selective replacement of only one phase. Mathematically, the model is sound providing that these requirements are met However, arguments in Part A indicate that, in general, the mineralogical composition differs between precursor lithologies and barren Urquhart Shale, and that phases other than carbonate are replaced. What the above studies did not attempt is the method utilised in this study, namely to analyse specific stratigraphy either side of a sulphide front. The results of this approach are illustrated in the section below.

Chemical changes involved in replacement

Sharp discordant fronts of mineralisation allow samples to be taken close together of mineralised and unmineralised sequences. In these circumstances, none of the variation in chemistry is likely to be primary depositional or diagenetic in origin. Such a sample is that from the A sequence illustrated as Figure 23c in Part A. The only assumption made is that there has been insignificant change in volume. This assumption is supported by the maintenance of stratigraphic thickness across the front, and the lack of any structures such as extensional microveinlets on one side, or orthogonal dissolution on the other to indicate differential changes in the along-bedding direction. The comparison in bulk chemistry is illustrated in Figure 3. Mineralogically, the main difference is the large increase in sphalerite on the mineralised side. Minerals showing a decrease on the mineralised side were quartz, K-feldspar and dolomite. Chlorite also is identifiable on the mineralised side and not the other. Chemically the Zn increase is associated with significant increases in Pb, Ba, As, Sb, Ag, Cd, Cu, and Na_2O, and decreases in SiO_2, Fe_2O_3, MnO, MgO, CaO, CO_2,, and Ni. TIO_2, Tl and P_2O_5 remained essentially unchanged.

In terms of the analyses of Croxford(1965), and Stanton(1962, 1965), the results measured across the front conflict with their observations of maintainance of group ratios, and are consistent with replacement rather than addition.

DEPOSITIONAL CONDITIONS IN THE COPPER OREBODIES

A series of studies has been done to attempt to model the depositional conditions in the formation of the copper orebodies. In approximate order of the work, these are reported as McGoldrick and Keays, (1989); Heinrich et al., (1989); Waring, (1990); and Hannan et al. (1993). The model of McGoldrick and Keays (1989) differed from the other three in that, although they interpreted the copper and lead-zinc systems to be cogenetic, they regarded both these systems to be early diagenetic, and the copper to be unrelated to a syndeformational "silica-dolomite" system. Thus conditions involved in formation of the silica-dolomite were not relevant to depositional conditions for the copper system.

Heinrich et al. (1989) hypothesised, from fluid inclusion and stable isotope studies, that there was an earlier independent stage of dolomitic alteration associated with moderate amounts of two fluids, represented by $CaCl_2$-rich and CO_2-rich fluid inclusions. Subsequent to this was a phase of silicification and copper introduction imposed by externally derived, weakly $CH_4 + CO_2$-bearing, NaCl-rich fluid at high fluid/rock ratios and over a range of temperatures. The copper deposition stage was apparently bracketed by an earlier higher salinity (10-20 wt %) and later low salinity (4-9 wt %) variant of this fluid. The mineralising fluid was modelled to be reduced and acid, with deposition involving a pH increase and slight cooling. Using the sulphur isotope data, an additional hypothesis (Andrew et al. 1989) was that the fluids were sulphur-deficient and obtained the bulk of their sulphur for chalcopyrite deposition from pre-existing fine-grained pyrite.

The author now accepts that the interpretation of the silica-dolomite as involving distinct dolomitisation and silicification stages (Heinrich et al., 1989), rather than a contemporaneously evolving system (Perkins, 1984), is more compatible with the geochemical data. However, the constraint on input fluid composition as being sulphur-deficient, is not accepted, for reasons given in Part A.

Fluid compositions and depositional conditions in the silica-dolomite are no longer regarded in this study as being irrelevant to the formation of the lead-zinc orebodies. Instead, the two ore types and associated alteration should be regarded as an integrated system, with all base metal sulphides sharing many of the same depositional conditions. What remains to be explained is the zonal pattern of sulphides.

ISOTOPE GEOCHEMISTRY OF THE ORE SYSTEMS

Lead Isotopes

A comprehensive data base of lead isotopes on both lead-zinc and copper orebodies exists for Mount Isa (Gulson et al., 1983; Vaasjoki, 1986). There is a tight clustering of lead isotope ratios for the lead-zinc orebodies with a mean of:

8/6 2.2226 +/- 0.0011

7/6 0.9588 +/- 0.0003

6/4 16.108 +/- 0.009

On 8/6 vs 7/6 diagrams a series of arrays from the copper orebodies lie on regression lines which pass through this point, representing different calculated U/Th ratios, which can then be related to source rocks. The initial interpretation of these data was that the lead-zinc and copper orebodies were part of a single hydrothermal system. In the light of the new data at the time that the copper orebodies were late and epigenetic, this was rationalised in Gulson et al. (1983) that the later copper fluids inherited the progressively more of the lead-zinc isotopic signature with increasing interaction. The possibility that the lead-zinc orebodies could be formed at the same late stage as the copper orebodies, was not considered at that time.

Some of the samples for the study by Vaasjoki came from three different levels in 7 orebody, in order to test for a lead isotope halo to the lead-zinc orebodies. That work found there was an along-strike halo, but that this did not extend across the stratigraphy. The halo in lead isotopes did not appear to be as good a discriminator as trace lead geochemistry. Unfortunately, reports relating to this study could not be located in the MIMEX library, so detailed analysis is not possible.

The lead isotope data of Gulson et al., (1983) plot exactly on the growth curves of Cumming and Richards (1975) and have a calculated model age of 1510 m.y., according to that model.

Lead isotopes and deposit ages

One of the main arguments advanced recently in favour of a syndepositional origin for stratiform lead-zinc deposits in northern Australia, is based on the apparent congruence between stratigraphic ages and lead isotope model ages (Page, 1994, Page et al., 1994, Sun, S-s et al., 1994, Carr et al., 1994). It is argued that trends are consistent between U-Pb in zircon ages for tuffaceous horizons in the orebody sequences and the Pb-Pb model ages derived from the ores. This consistent relationship to stratigraphic age is taken to indicate that the ore formation is syndepositionally related to the host sediments. These publications further argue that Pb-Pb model ages, calibrated where U-

Pb ages exist, should be used to estimate the ages of enclosing sequences, such as indicating Cannington is hosted in Cover sequence 3.

Without these additional data, the Pb-Pb model age using the Cumming and Richards (1975) model (1510Ma) could be used to support a ~1500Ma age for an epigenetic Mount Isa system (Perkins, 1984). In fact Sun, S-s et al. (1994) claim that attempts to fit deposits throughout time to a single growth curve should be abandoned, and that constraining model ages as for the North Australian deposits should be done for each terrain.

Superficially, the consistent relationship of model ages to stratigraphic ages, agreeing as they appear to with stratigraphic ages from the Soldiers Cap Group, Mount Isa Group, McArthur Group and Lawn Hill Formation, apparently supports a syndepositional origin, opposed to the syndeformational origin of Perkins(1993). How can these conflicting lines of evidence be accommodated?

Model ages for Mount Isa and other stratiform deposits are shown in Appendix 3 from Carr et al. (1994). In addition, Nutman et al., (1995) have calculated ages based on a revised model of 1575 +/-20 m.y. for Mount Isa and 1574 +/- 20 m.y. for Broken Hill, which do not correspond with the stratigraphic ages.

There are a number of problems with the approach of 'correcting' the model ages to agree with the stratigraphic ages. As the authors themselves admit, Lady Loretta data indicates epigenetic processes. Mount Novit has the same isotopic ratios as Mount Isa, and is clearly in older stratigraphy. The Silver King deposit at the Lawn Hill field apparently has the same isotopic ratios as the nearby Century Deposit, and yet is clearly epigenetic, in a fault zone cross-cutting the north-south folds. At this stage, there are only three deposits for which lead isotope ratios can be tied directly in with stratigraphic ages, Mount Isa, HYC, and Century. Given the paucity of data, and the similarity of ages for deposits in the Eastern fold belt to Mount Isa, Hilton, and Mount Novit, an alternative relationship may exist more with geographic position than stratigraphic age. In fact, the similarity in new model ages for Broken Hill and Mount Isa, appear to give support to a late epigenetic replacement model for both deposits.

Sulphur Isotopes.

Previous analyses

A very comprehensive data base of sulphur isotope determination exists for both the copper and lead-zinc areas of the mine. The gross sulphur isotope composition, utilizing all data, of the lead-zinc orebodies is very similar to that of the copper orebodies (Andrew et al., 1989). Much of the more recent work was done to address the question of sulphur source for the copper orebodies. Both conventional and ion microprobe techniques were used (Andrew et al. 1988). $\delta^{34}S$ results for fine-grained pyrite in and around the copper

orebodies varied from 0.8‰ to 16.9‰ and chalcopyrite from 8‰ to 21.1‰. These authors concluded that the greater percentage of the sulphur for chalcopyrite deposition was inherited from pre-existing stratiform pyrite. Their argument was based on an estimation of an initial sulphur isotope signature, either for a pyritic system only, or for pyrite plus lead and zinc.

Some evidence against the derivation of sulphur from fine-grained pyrite for chalcopyrite precipitation was given in Perkins (1984). Essentially the arguments were that: 1) the proportion of chalcopyrite that directly overprinted fine-grained pyrite was miniscule compared to the total volume of chalcopyrite; 2) even assuming that pyrite components were originally released on replacement by dolomite, there was insufficient sulphur released at the core of the system with high copper grades, and it would have to be transported downwards in the system; and 3) where chalcopyrite had obviously replaced former dolomite, both copper and sulphur were being transported in solution, and could therefore have been exotic. Waring (1990,1991) presented arguments for exotic derivation of much of the sulphur for chalcopyrite deposition, but also claimed that there was substantial lead-zinc in the area now occupied by the silica-dolomite, and that significant copper orebody sulphur was derived from the overprinting of these lead-zinc orebodies.

SHRIMP ion microprobe analyses

Only fine-grained pyrite was analysed using SHRIMP Three correlatable horizons in the B sequence of 7 orebody were selected. The results are shown in Appendix 4. In keeping with results from earier studies (Eldridge, 1991), there is a very large range overall and a large variation in $d^{34}S$ over short distances. In addition, there is a lack of consistency of variations between adjacent layers along strike.

One sample with good development of pyrite along the s_3 cleavage direction was analysed, to check whether there was greater consistency along the bedding laminae, or along the cleavage direction. All of the results from this initial study were inconclusive, and a decision was made not to proceed with additional analyses. The large variation over small distances and lack of continuity along strike may give some support to a zonal distribution along specific layers of sulphur isotopes in pyrite. However, the approach now being used by M. Painter, (pers. comm., 1995) in applying conventional analyses to correlatable samples should produce more meaningful results.

DISCUSSION

This study has not produced a geochemical model of the Mount Isa/Hilton lead-zinc ore systems. Instead, data are available from it which remove the effect of different stratigraphy on the distributions. It shows what changes are represented across fronts of alteration and mineralisation. If the arguments are accepted, that these relationships

represent the primary deposition of base metal sulphides, rather than later "remobilisation" during deformation, then these changes indicate reactions involved in lead-zinc ore formation.

The direct relationship between fine-grained pyrite and carbonaceous matter concentrated along cleavage planes, in conjunction with other sulphides, especially galena and chalcopyrite, having their intitial deposition controlled by carbonaceus boundaries and inclusions between quartz and dolomite support, but do not prove, that sulphate reduction by inorganic processes is an important control on mineralisation.

Given a single late period of ore formation, the difficulty still remains of whether there is an outward-growing process of copper-lead-zinc deposition, as modelled in Part A, or whether there is a sequential deposition of all sulphides. A dynamic geochemical model will differ substantially between these two alternatives.

CONCLUSIONS

Processes involved in the formation of the Mount Isa and associated deposits can not be established until it is known whether there are two periods of lead-zinc deposition, involving an earlier diagenetic form which is "remobilised" during deformation, or a single late period of deposition as argued in this study. Lead isotope and sulphur isotope data from Mount Isa can be used to support a direct link between the lead-zinc lodes and the copper orebodies.

In addition, further work such as is now in progress must be continued in order to resolve fundamental questions raised in the introduction to this part. That is, how did the alteration and mineralisation system develop with time, and what were the controls in detail on sulphide precipitation?

There are still many problems with the direct application of lead and oxygen isotopes as used to provide countervailing arguments against the bulk of structural and distributional criteria which suggests a late deformational replacement origin for the lead-zinc deposits in the Mount Isa district and in Northern Australia.

REFERENCES

Andrew, A.A., Heinrich, C.A., Wilkins, R.W.T. and Patterson, D.J., 1989, Sulphur isotope systematics of copper ore formation at Andrew, A.S., Heinrich, C.A., Wilkins, R.W.T., and Patterson, D.J. Mount Isa. Econ. Geol., 84: 1614-1626.

Atkinson, B.K., 1976. The temperature and strain rate-dependent mechanical behaviour of a polycrystalline galena ore. Econ. Geol., 71: 513-525.

Bell, T.H., 1983. Thrusting and duplex formation at Mount Isa, Queensland, Australia. Nature, 304; 493-497.

Bell, T.H., Perkins, W.G. and Swager, C.P., 1988. Structural controls on development and localization of syntectonic mineralisation at Mount Isa, Queensland. Econ. Geol., 83: 69-85.

Berner, R. A., 1970. Sedimentary pyrite formation. Am. Jour. Sci., 268: 1-23.

Berner, R. A., 1972. Sulphate reduction, pyrite formation and the oceanic sulphur budget. In Dryssen, D. and Jagner, D.,(eds), The changing chemistry of the oceans. (Nobel Symposium 20): Stockholm, Almquist and Wiskell: 347-361.

Bethke, C.M., 1986. Hydrologic constraints in the genesis of the Upper Mississippi Valley mineral district from Illinois Basin brines. Econ. Geol., 81: 233-249.

Blake, D. H, 1987. Geology of the Mount Isa Inlier and environs, Queensland and Northern Territory. BMR Bulletin 225.

Blanchard, R., and Hall, G., 1942. Mount Isa ore deposition. Econ. Geol., 32: 1042-1057

Carr, G. L., Page, R. and Sun, S., 1994. Lead isotope and U-Pb studies relating hydrothermal activity and stratigraphy in the Proterozoic basins of Northern Australia: Abs. AMF Mt. Isa Inlier seminar No 902/94.

Chi Minh T., 1987. Results of the Mount Novit Project. Unpublished report for Mount Isa Mines Limited. Aust. Nat. Univ.

Crick, I. H., 1992. Petrological and maturation characteristics of organic matter from the Middle Proterozoic McArthur Basin, Australia. Aust Jl. Earth Sciences, v. 39, no.4, p 501-519.

Croxford, N. J. W., 1962. The mineralogy of the no. 7 lead-zinc orebody, Mount Isa, and its interpretation: Unpub. PhD thesis, Armidale, Univ. New England, 284 p.

Croxford, N. J. W.,1964. Origin and significance of volcanic potash-rich rocks from Mount Isa: Inst. Mining Metallurgy Trans.,v.74,p.34-43.

Croxford, N. J. W., 1965. Sulphide-sediment relationships at Mount Isa. Nature, London. 206: 4989, p1144-1145.

Croxford, N. J. W., Draper, N., and Harraway, D. H., 1958. Some aspects of the carbonaceous fraction of the Mount Isa lead concentrate. Proc. Australas. Inst. Min. Metall., No. 197: 149-161.

Croxford, N.J.W., and Jephcott, S., 1972. The McArthur lead-zinc silver deposit, N.T., Australasian Inst. Mining Metallurgy Trans. Proc., no 243, p 1-26.

Croxford, N.J.W., Gulson, B.L. and Smith, J.W.,1975. The McArthur River deposit: a review of the current situation. Mineralium Deposita, v. 10, p. 302-304.

Croxford, N.J.W.,1968. A mineralogical examination of the McArthur River lead-zinc-silver deposit; Australasian Inst. Mining Metallurgy Proc., no. 226, p. 97-108.

Cumming, G.L., and Richards, J.R., 1975. Ore lead isotope ratios in a continuously changing earth; Earth Planet. Sci. Letters, v. 28, p. 155-171.

Eldridge, C.S., 1991, Sulphur isotopes in 7 orebody. SHRIMP unpublished Report to Mount Isa Mines Limited.

Eldridge, C.S., Compston, W., Williams, I.S., Patterson, D.J., Ohmoto, H., Walshe, J.L., and Both, R.A., 1985. SHRIMP ion microprobe determination of sulphur isotopic ratios in some sediment hosted massive sulphide ores: variability in their timing and formation. Abs. ICOG VI Univ. of Cambridge.

Eldridge, C.S., Williams, N., and Walshe, J.L., 1993. Sulphur isotope variability in sediment-hosted massive sulphide deposits as determined using the ion microprobe SHRIMP: II. A study of the H.Y.C. deposit at McArthur River, Northern Territory, Australia. Econ. Geol., 88: 1-26.

Finlow-Bates, T., Croxford, N.J.W. and Allan, J.M.,1977. Evidence for, and implications of, a primary FeS phase in the lead-zinc bearing sediments at Mount Isa. Miner. Deposita, 12: 143-149.

Grondijis, M.F., and Schouten, C., 1937. A study of the Mount Isa ores. Econ. Geol., 32: 407-450.

Gulson, B.J., Perkins, W.G., and Mizon K., 1983. Lead isotope studies bearing on the genesis of the copper orebodies at Mount Isa, Queensland. Econ. Geol. 78: 1466-1504.

Gustafson L.B., and Williams N.,1981. Sediment-hosted stratiform deposits of copper, lead and zinc. Econ. Geol. 75th Anniversary Volume. 139-178.

Hannan K.W., Golding, S.D., Herbert, H.K., and Krouse, H.R., 1993. Contrasting alteration assemblages in metabasites from Mount Isa, Queensland: implications for copper ore genesis. Econ. Geol., 88: 1135-1175.

Hannan, K.W., 1989. Fluid-rock interactions recorded in metabasites near Mount Isa; Implications for copper ore genesis. Unpublished PhD thesis, Univ. of Queensland, Brisbane.

Heinrich, C.A., Andrew, A.S., Wilkins, R.W.T., and Patterson, D.J., 1989. A fluid inclusion and stable isotope study of synmetamorphic copper ore formation at Mount Isa, Australia. Econ. Geol., 84: 529-550.

Hewett, R.L., and Solomon, P.J., 1964. The role of mobilisation in silver-lead-zinc sulphide assemblages, with particular reference to Mount Isa, Australia. Internat. Geol. Cong. 22nd, New Delhi, 1964, sec. 5.

Hinman, M., 1994. Structure and kinematics of the H.Y.C.-Cooley zone at McArthur River, Northern Territory: AGSO record 1995/5.

Hinman, M., Wall, V., and Heinrich, C., 1994. The interplays between sedimentation, deformation, and hydrothermal activity at the McArthur Pb-Zn(-Cu) deposit. Extended abstract 37. 12th. AGC, Perth.

Knight, C. L.,1953. Regional geology of Mount Isa. Empire Mining Metall. Cong., 5th, Melbourne, Pub., 1: 352-360.

Lambert, I.B., 1976. The McArthur zinc-lead-silver deposit; features, metallogenesis and comparisons with some other stratiform ores, in Wolf, K.H., ed., Handbook of stratabound and stratiform ore deposits, v.6: Amsterdam, Elsevier, p. 535-585.

Lambert, I.B., 1982. Constraints on the genesis of major Australian lead-zinc-silver deposits: from Ramdohr to recent, in Amstutz, G.C., Gorsey, A., Frenzell, G., Kluth, Moh, G., Wauschkuhn, A., and Zimmerman, R.A., eds. Ore genesis, the state of the art: Springer-Verlag, Berlin, p. 625-636.

Logan, R. G., 1979. The geology and mineralogical zoning in the H.Y.C. Ag-Pb-Zn deposit, McArthur River, Northern Territory, Australia: Unpub. M. Sc. thesis, Aust. Natl. Univ., 187p.

Logan, R. G., 1980. Mineralogical zoning in the H.Y.C. deposit, McArthur River (abs):, Fourth Australian Geol. Convention, Hobart 1980, Programmes and Abstracts, p. 45.

Logan, R. G., and Williams, N., 1984. Sedimentary controls on the hydrothermal system that formed the H.Y.C. deposit at McArthur River, Northern Territory (abs): Geol. Soc. Australia, Seventh Australian Geol. Convention, Sydney 1984, Programmes and Abstracts, p. 339-340.

Love, L. G., 1964. Early diagenetic pyrite in fine-grained sediments and the genesis of sulphide ores. In; Amstutz, G.C. (Ed.), Sedimentology and ore genesis. Elsevier, Amsterdam.

Love, L. G., and Zimmerman D. O., 1961. Bedded pyrite and micro-organisms from the Mount Isa Shale. Econ. Geol., 56: 873-896.

Love, L. G.,1965. Micro-organic material with diagenetic pyrite from the Lower Proterozoic Mount Isa Shale and a Carboniferous shale. Proc. Yorkshire Geol. Soc., 35: 187-202.

Marshall, B. and Gilligan, L.B. 1987. An introduction to remobilisation. In Mechanical and Chemical (Re)mobilizion of Metalliferous Mineralization. Ore Geology Reviews 2, 87-131.

Mathias, B.V., and Clark, G.J., 1975. Mount Isa copper and silver-lead-zinc orebodies. Isa and Hilton mines., In Knight,C.L., ed., Economic geology of Australia and Papua New Guinea, I Metals: Australasian Inst. Mining Metall. Mon. 5: 351-372.

Mathias, B.V., Clark, G.J., Morris, D., and Russell, R.E., 1973. The Hilton deposit - stratiform silver-lead-zinc mineralisation, in Metallogenic Provinces and Mineral Deposits in the south-western Pacific. Bull. Bur. Miner. Resour. Geol. Geophys. Aust., v.141, p. 33-58.

McClay, K. R., 1983a. Fabrics of deformed sulphides. Geol. Rundschau. 72, 2: 469-491.

McClay, K. R., 1983b. Deformation of stratiform lead-zinc deposits. *in* Sediment-hosted Stratiform Lead-Zinc Deposits. Mineral. Assoc. Can., 283-307.

McClay, K. R., and Ellis, 1983. Deformation and recrystallisation of pyrite. Min. Mag., 47: 527-38.

McClay, K.R., 1979. Folding in the silver-lead-zinc orebodies, Mount Isa, Australia: Inst. Mining Metallurgy Trans.,v. 88,p.5-14.

McClay, K.R., and Carlile, D.G., 1978. Mid-Proterozoic sulphate evaporites at Mount Isa Mines, Queensland, Australia: Nature, v. 274, p. 240-241.

McDonald, J.A., 1970. Some effects of deformation on sulphide-rich layers in lead-zinc orebodies, Mount Isa,. Queensland. Econ. Geol., 65: 273-298.

McGoldrick, P. 1986. Volatile and precious metal geochemistry of the Mount Isa ores and their host rocks. Unpublished PhD thesis, Univ.of Melbourne.

McGoldrick, P.J., and Keays, R.R., 1989. Mount Isa copper and lead-zinc-silver ores-coincidence or cogenesis? Econ, Geol., 85: 641-650.

Muir, M., 1983. Depositional environments of host rocks to Northern Australian lead-zinc deposits, with special reference to McArthur River. Mineralogical Assoc. of Canada Short Course Notes. 9: 141-174.

Murray, W. J.,1961. Notes on Mount Isa geology. Australas. Inst. Mining. Metallurgy Proc., no. 197: 105-136.

Murray, W.J., 1975. McArthur River H.Y.C. lead-zinc and related deposits, N.T. *in* Knight C.L., ed., Economic geology of Australia and Papua New Guinea.-metals, Australian Inst. Mining Metall., Melbourne, p. 329-339.

Neudert, M.K., 1983. A depositional model for the Upper Mount Isa Group and implications for ore formation. PhD thesis, Aust. Nat. Univ. published by Sedcon Publs.

Neudert, M.K., 1984, Are the Mount Isa lead-zinc ores really syngenetic? [abs.]: Geol. Soc. Aust. Jl, 12: 402-404.

Neudert, M.K., 1988. A new sedimentation concept for the Urquhart Shale and constraints on the timing of silver-lead-zinc ore genesis at Mount Isa, Queensland, Australia. submitted to Nature.

Neudert, M.K., and Russell, R.E., 1981. Shallow water and hypersaline features from the Middle Proterozoic Mt Isa sequence. Nature, 293: 284-286.

Neudert, M.K., 1984, The sedimentology of the Mount Novit and East Sybella areas. unpublished internal report to Mount Isa Mines Limited.

Neudert, M.K. and Sheppard, W A., 1993, unpublished report to MIMEX.

Nutman, A.P., Foster, J., and Ehlers, K., 1995. The Broken Hill ore body: Concentration of the lead during high grade metamorphism. Abstract for 1995 structural conference.

Oehler, J.H., and Logan, R.G., 1977. Microfossils, cherts, and associated mineralisation in the Proterozoic McArthur (H.Y.C.) lead-zinc-silver deposit: Econ. Geol. v.72, p. 1393-1409.

Page, R., 1994. Geochronological results from the Eastern Fold Belt, Mount Isa Inlier. AGSO Research Newsletter, 19: 4-5.

Page, R., Sun, S-s., and Carr, G., 1994. Proterozoic sediment-hosted lead-zinc-silver deposits in northern Australia-U-Pb zircon and Pb isotope studies: Geol. Soc. Aust. Abs. Ser. 37, p 334-335.

Page, R.W., 1981. Depositional ages of the stratiform base metal deposits at Mount Isa and McArthur River, Australia, based on U-Pb zircon dating of concordant tuff horizons, Econ. Geol., 76: 648-658.

Perkins, W G., and Poole, J. R., 1980. A re-interpretation of the structural and stratigraphic relationships across the Mount Isa Fault. MIM Ltd. Internal report (unpubl.) 12p.

Perkins, W.G., 1981. Mount Isa copper orebodies - evidence against a sedimentary origin [abs.]: BMR Jour. Australian Geology and Geophysics, v. 6, p. 331.

Perkins, W.G., 1984. Mount Isa silica-dolomite and copper orebodies: The result of a syntectonic hydrothermal alteration system: Econ. Geol., v. 79, p. 331.

Plumb, K.A., Derrick, G.M., and Wilson, I.H., 1980. Precambrian geology of the McArthur River-Mount Isa region in northern Australia, in Henderson, R.A., and Stephenson, P.J., eds. The geology and geophysics of northeastern Australia: Brisbane, Geol. Soc. Australia (Queensland Division), P. 71-88.

Proffett, J.M., 1990. Some new observations on the geologic structure southwest of Mount Isa. (abs) Mount Isa Inlier Geology Conference, Victorian Institute of Earth and Planetary Sciences, Monash University, 29-31.

Sawkins, F.J., 1984. Ore genesis by episodic dewatering of sedimentary basins: Application to giant Proterozoic lead-zinc deposits. Geology, 12: 451-454.

Schieber, J., 1990. Pyritic Shales and microbial mats: Significant factors in the genesis of stratiform Pb-Zn deposits in the Proterozoic? Mineral. Deposita, 25: 7-14.

Skinner, B.J., and Johnson, C. A., 1987. Evidence for movement of ore materials during high-grade metamorphism. Ore Geology Reviews, 2: 191-204.

Smith, J.W., and Croxford, N.J.W., 1973. Sulphur isotope ratios in the McArthur lead-zinc-silver deposit. Nature Physical Science, 245: 10-12.

Smith, J.W., Burns, M.S., and Croxford, N.J.W., 1978. Stable isotope studies of the origins of mineralisation at Mount Isa. Mineral. Deposita, 13: 369-381.

Smith, S.E. and Walker, K.R., 1972. Primary element dispersions associated with mineralisation at Mount Isa, Queensland: Australia Bur. Mineral Res., Geology Geophys. Bull. 131.

Smith, W.D., 1969, Penecontemporaneous faulting and its likely significance in relation to Mount Isa ore deposition: Geol. Soc. Australia Spec. Pub. 2, p. 225-235.

Solomon, M., and Heinrich, C.A., 1990. Are high heat-producing granites essential to the origin of giant lead-zinc deposits at Mount Isa and McArthur River, Australia? Jl. Mining and Exploration Geol., 1: 85-91.

Solomon, M., Groves, D.I., and Jacques, A.L., 1994. The geology and origin of Australia's mineral deposits. Oxford monographs on geology and geophysics, Oxford University Press, 24.

Solomon, P.J., 1965. Investigations into sulphide mineralisation at Mount Isa, Queensland. Econ. Geol., 60: 737-765.

Stanton, R. L., 1962. Elemental constitution of the Black Star orebodies, Mount Isa, Queensland, and its interpretation: Inst. Mining Metallurgy Trans., v. 72, p. 61-144.

Stanton, R.L., 1963. Constitutional features of the Mount Isa sulphide ores and their interpretation. Australasian Inst. Mining Metallurgy Proc., 205: 31-153.

Stanton, R.L., 1964. Mineral interfaces in stratiform ores. Trans. Instn. Min. Metall., 72: 61-144.

Stanton, R. L., 1965. Composition and textures of conformable ores as guides to their formation. 8th Commonwealth Mining and Metall. Congress, 35th Tech. Session.

Strauss, H., and Schieber, 1990. A sulphur isotope study of pyrite genesis: The Mid-Proterozoic Newland Formation, Belt Supergroup, Montana. Geochemica et Geocosmica Acta, 54: 197-204.

Sun, S-s., Page, R., and Carr, G.R., 1994. Lead-isotope-based stratigraphic correlations and ages of Proterozoic sediment-hosted Pb-Zn deposits in the Mount Isa Inlier. AGSO Research Newsletter, 20: 1-2.

Swager, C.P., 1983. Microstructural development of the silica-dolomite and copper mineralisation at Mount Isa, NW-Queensland, with special emphasis on the timing and mechanism of mineralisation: Unpub. PhD thesis, Townsville, Australia, James Cook Univ., 258 p.

Swager, C.P., 1985a. Syndeformational carbonate-replacement model for the copper mineralisation at Mount Isa, north-west Queensland: A microstructural study. Econ. Geol., 80: 107-125.

Swager, C.P., 1985b. Metamorphism, alteration and deformation of Eastern Creek Volcanics in the Mount Isa Mine area and their implications for syntectonic copper mineralisation. Report to MIM Ltd. James Cook Univ.

Swager, C.P., Perkins, W.G., and Knights, J., 1987. Strata-bound phyllosilicate zones associated with syntectonic Cu orebodies, Mount Isa, Queensland. Aust. Jl. Earth Sci., 34: 463-476.

Tourtelot, C.B., and Vine, J.D, 1976. Copper deposits in sedimentary and volcanogenic rocks. U.S. Geol. Survey Prof paper 907C. 34p.

Trudinger, P. A., and Williams, N.,1982. Stratified sulphide deposition in modern and ancient environments. Mineral deposits and the evolution of the biosphere, eds. H.D Holland and M. Schidlowski, Report of the Workshop on Biospheric Evolution and Precambrian Metallogeny; Springer-Verlag, Berlin, 177-178.

Valenta, R.K., 1988. The dynamics of deformation, fluid movement, and mineralisation in the Hilton area, Mount Isa, North-west Queensland: Unpublished PhD Thesis, Monash University, 270 p.

Valenta, R.K., 1989. Vein geometry in the Hilton area, Mount Isa, Queensland:- implications for fluid behaviour during deformation. Tectonophysics, v.158, p. 191-207.

Valenta, R.K., 1994a. Deformation of host rocks and stratiform mineralisation in the Hilton Mine area, Mount Isa. Aust. Jl. Earth Sciences, 41, p. 429-443.

Valenta, R.K., 1994b. Syntectonic discordant copper mineralisation in the Hilton Mine, Mount Isa. Economic Geology , 89, p. 1031-1052.

Van Dijk, P.M., 1986. Copper mineralisation and regional structural geology of the western Mount Isa block, Australia: Unpublished PhD thesis, James Cook University, 241 pp.

Walker, R.N., Logan, R.G., and Binnekamp, J.G., 1977. Recent geological advances concerning the H.Y.C. and associated deposits, McArthur River, N.T. Geol. Soc. Australia Jour.,v. 24, p. 365-380.

Waring, C.L., 1990. Genesis of the Mount Isa Cu Ore System. Unpublished PhD thesis, Monash Univ. Melbourne.

Waring, C.L., 1991. The distinction between metamorphosed stratiform Pb-Zn-Ag mineralisation and metamorphic syntectonic Cu mineralisation at Mount Isa. SGEG Ore Fluids Conf. Bur. Mineral Resources, Geology and Geophysics, Record No. 1990/95. Abs.

Williams, N.,1976. The formation of sedimentary-type stratiform sulphide deposits. PhD thesis, Yale University (unpublished), 330p.

Williams, N., 1978a. Studies of the base metal sulphide deposits at McArthur River, Northern Territory, Australia. I. The Cooley and Ridge deposits. Econ. Geol., 73: 1005-1035.

Williams, N., 1978b. Studies of the base metal sulphide deposits at McArthur River, N.T., Australia. 2. The sulphide-S and organic-C relationships of the concordant deposits and their significance. Econ Geol., v.73, 1036-1056

Williams, N., 1978c. The timing and mechanism of emplacement of sulphide minerals into the H.Y.C. Pyritic Shale Member at McArthur River, N. T. Abs. Progr. 3rd Aust Geol Conv.,p.32. Geol. Soc. Aust., Q'ld. Div., Brisbane.

Williams, N., 1979a. The timing and mechanisms of formation of the Proterozoic stratiform Pb-Zn and related Mississippi Valley-type deposits at McArthur River, N.T.,Australia. Presented at the A.I.M.E. Annual meeting New Orleans; Society of Mining Engineers of A.I.M.E. Preprint Number 79-51.

Williams, N., 1979b. Precambrian mineralisation in the McArthur-Cloncurry region, with special reference to stratiform Pb-Zn deposits. The Geology of NE Australia, (edit. by Henderson, R.A. and Stephenson, P.J.), James Cook Univ. Press, Townsville.

Williams, N., and Rye D.M.,1974. Alternative interpretation of sulphur isotope ratios in the McArthur lead-zinc-silver deposit. Nature Physical Sciences, 247: 535-537.

Wilson, A. 1992. Metal distribution in the Hilton Mine, Mount Isa, and its genetic implications. BSc. Hons thesis (unpublished), Monash Univ.

Wilson, I.H., Derrick, G. M., and Perkin, D.J., 1985. Eastern Creek Volcanics: their geochemistry and possible role in copper mineralisation at Mount Isa, Queensland. B.M.R. Jl. Aust. Geol. Geophys. v9, p.317-328.

Zimmerman, D.O., 1961. A thesis entitled "mineralisation of the northern leases, Mount Isa, Queensland, and its surface expression" London Royal School of Mines. PhD thesis, unpubl. 345p.

TITLE PAGE

A Study of the Nature, Timing, and Processes in the Mount Isa Lead-Zinc Orebodies; their Relationship to Adjacent Copper Orebodies and the Lead-Zinc Systems at McArthur River, Hilton, and Mount Novit.

VOLUME II

Thesis submitted by

William George PERKINS BSc.*U.N.E.* B. Econ.*U of Q'ld* MSc. *JCUNQ.*

in June 1996

for the degree of Doctor of Philosophy

in the Department of Earth Sciences

James Cook University of North Queensland

PART A.

Mount Isa Lead - Zinc Orebodies: Replacement Lodes in a Zoned Syndeformational Copper Lead - Zinc System?

Figures 1-26

Table 1

DEFORMATION	ALTERATION-MINERALIZATION
D_1 Foliation parallel to layering. Fine dolomite veins. Only locally observed by Swager (1995). Local folds with vergence anticline east.	Replacement veins and possibly first stage bedding-preserving dolomitization. K-Feldspar alteration (esp of tuff layers)
D_2 Foliation s_2 parallel or subparallel to layering. Shear on cleavage is west block up. Healed thrusts probably associated. Foliation and healed thrusts folded around the Mount Isa fold. East-dipping dolomite veins giving extension in the plane of bedding, alternating with reverse shear on bedding. No folds in Mine but form major Mount Isa syncline (Fig. 1).	Replacement veins, recrystallization along bedding, porphryoblastic dolomite. Phengite I, "buff alteration" Chloritization of metabasalts.
$D_{2.5}$ Folds with axial planes at a high angle to bedding. May have shear sense of top to east or west. No cleavage visible except in thin section. Poorly developed at Mount Isa Mine, much more strongly at Hilton (Bell and Hickey, 1997, Perkins, 1997b).	
D_3 Foliation s_3 sub-vertical. Axial planar to mesoscopic folds (incl. Mount Isa Fold) with vergence syncline west.	Silica-dolomite breccia. Phyllosilicates, magnetite, silcification. Sulphides at close of deformation to post-deformation.

Figure 1. Map of the Mount Isa area showing the main geological features and the relationship of the ore environment to the major structures. Only the basic volcanic sequences of the Eastern Creek Volcanics have been highlighted (rock symbol v). East of the Paroo Fault are formations of the Mount Isa Group. Lead-zinc orebodies in the Urquhart Shale have been projected from the closest data in unweathered rock to show an estimate of original ore at the current erosion level. Silica-dolomite is from the 1966 surface mapping by W.D Smith (pers. comm. 1994), updated by more recent drilling (S. de Kruijff, pers. comm., 1983). The unconformity west of the Mount Isa fault was mapped by J.M. Proffett in 1989 (Proffett, 1990). Modified from 1:2500 map compiled by P. Stoker, 1991. Outcrop boundaries are not shown west of the Mount Isa Fault, which is generally an area of good exposures. Inset. Location of Mount Isa.

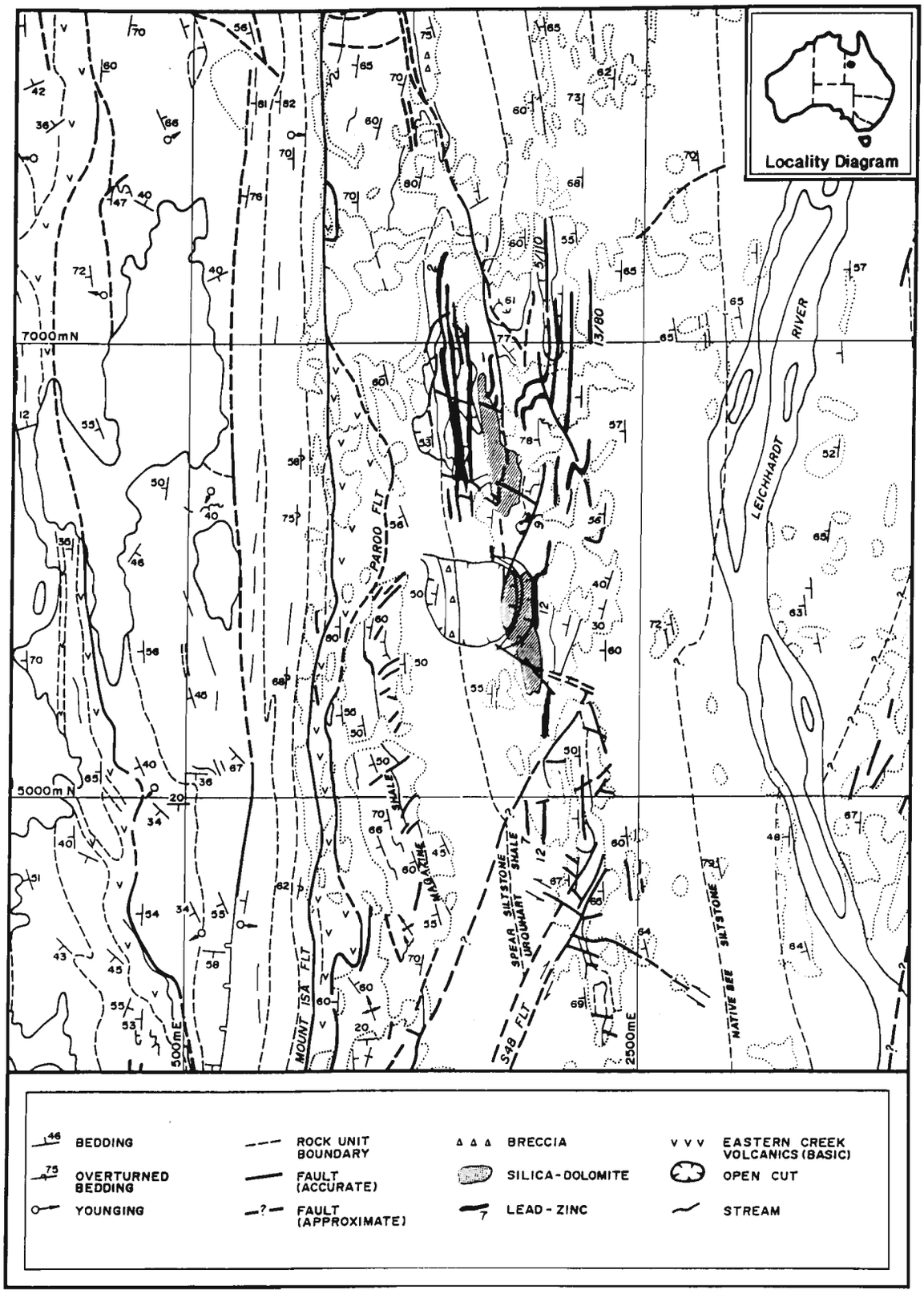
Locality Diagram
7000mN
5000mN
500mE
2500mE
PAROO FLT
MOUNT ISA FLT
SYN 13/80
SYN 5/110
LEICHHARDT RIVER
MYRAPINE SHALE
SPEAR SILTSTONE
URQUHART SHALE
NATIVE BEE SILTSTONE
BEDDING
OVERTURNED BEDDING
YOUNGING
ROCK UNIT BOUNDARY
FAULT (ACCURATE)
FAULT (APPROXIMATE)
BRECCIA
SILICA-DOLOMITE
LEAD-ZINC
EASTERN CREEK VOLCANICS (BASIC)
OPEN CUT
STREAM

Figure 2 a. Plan of the north end of 17 Level showing fold zones, faults and shear zones, and their relationship to lead-zinc orebodies. The enveloping surfaces of the terminations of the lead-zinc orebodies which trend at 345 degrees, transgress across the stratigraphy, parallel with the fold hinges and the limits of silica-dolomite. 6500mN refers to metres north on the Mine grid.

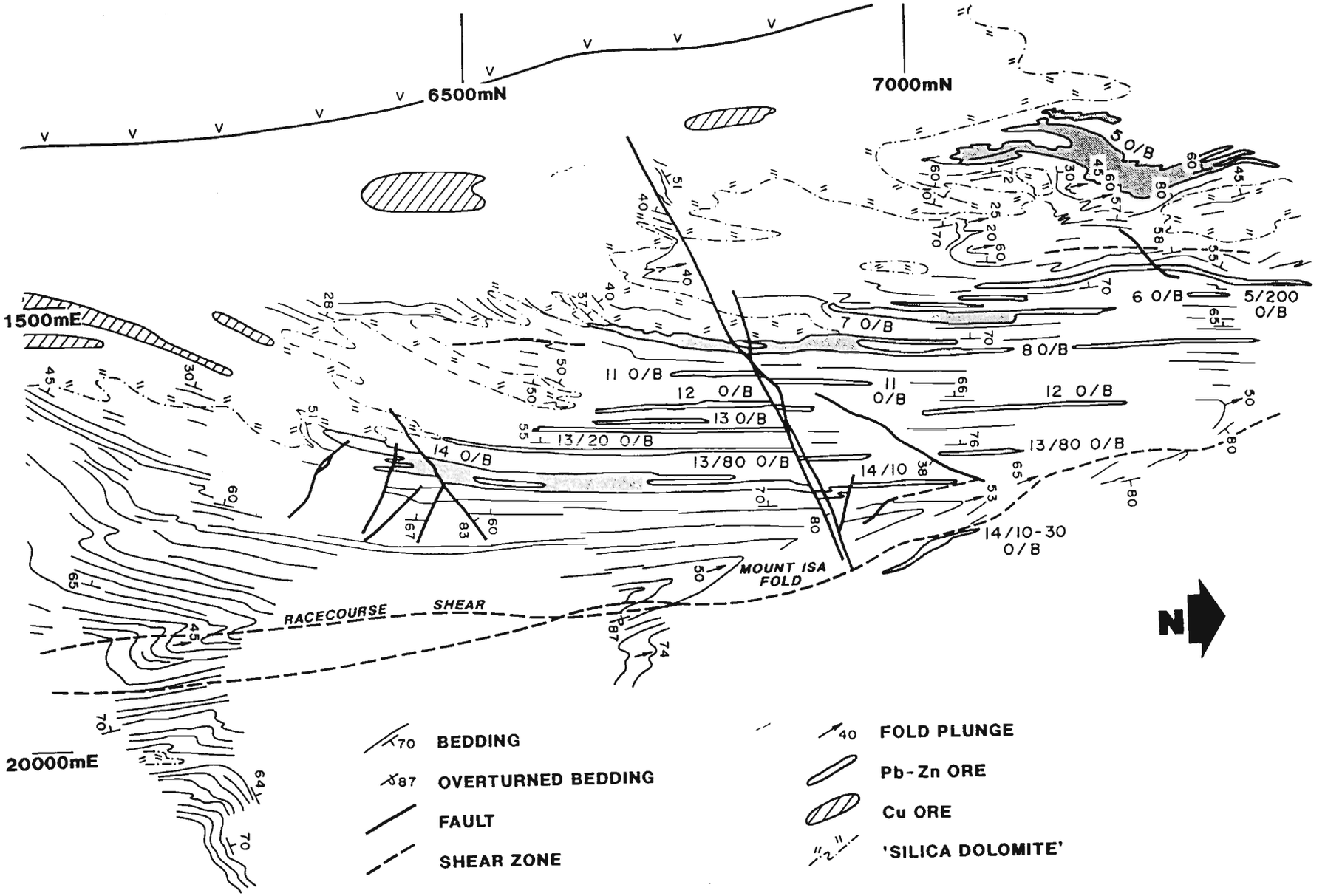
6500mN
7000mN
1500mE
20000mE
5 0/B
6 0/B
5/200
0/B
7 0/B
8 0/B
11 0/B
12 0/B
13 0/B
13/20 0/B
14 0/B
13/80 0/B
14/10
14/10-30
0/B
MOUNT ISA
FOLD
RACECOURSE SHEAR
N
BEDDING
OVERTURNED BEDDING
FAULT
SHEAR ZONE
FOLD PLUNGE
Pb-Zn ORE
Cu ORE
'SILICA DOLOMITE'

Figure 2 b. Longitudinal projection of 7 orebody (vertical north-south section onto which all positions have been projected orthogonally). It shows the locations of cross-section profiles in Figure 5. (A and B).

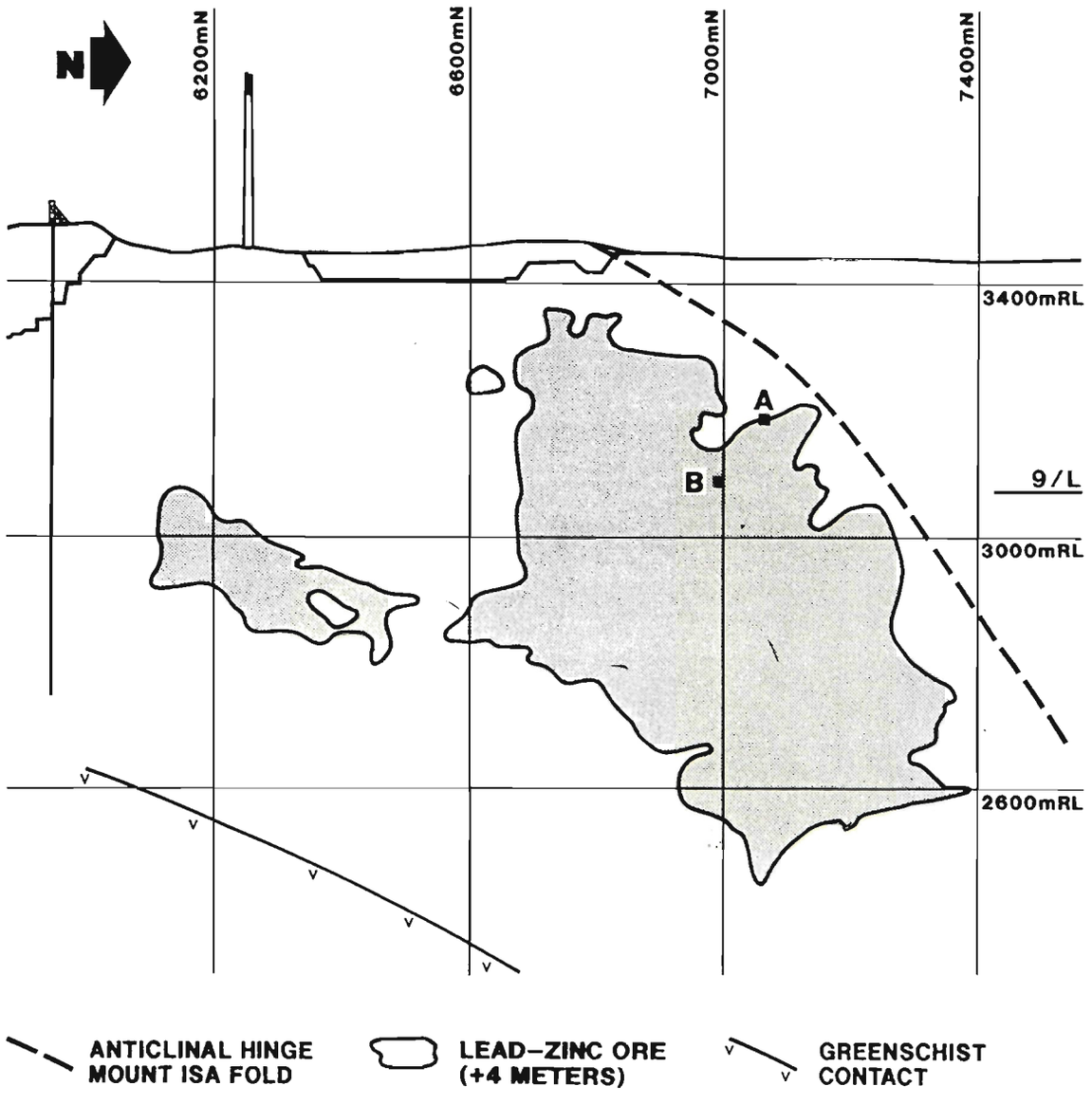
N
6200mN
6600mN
7000mN
7400mN
3400mRL
3000mRL
2600mRL
9/L
A
B
ANTICLINAL HINGE
MOUNT ISA FOLD
LEAD–ZINC ORE
(+4 METERS)
GREENSCHIST
CONTACT

Figure 3 a. Styles of galena-rich mineralization in a single sample. 1. Finely laminated gray bands are rich in galena. 2. Folded remnant layers with galena-transitional to breccia ore. 3. Breccia ore with only vague remnant layers and scalloped edges replacing adjacent non-laminated layer, and cutting across faults within it. 4. Galena-rich microbreccia. 5. Fine-grained galena replacing host siltstone around veins. Looking north - approximate horizontal shown. Location; 5 Orebody, 15B Sublevel, 6960N, 1407E.

Figure 3 b. Stratiform sphaleritic ore. 1 Banded carbonaceous siltstone. 2. Bands of fine wavy-laminated pyrite. 3 Neomorphic dolomite with sphalerite-similar bands also contain sphalerite. Location; 7 Orebody, 7 Level, 7050N.

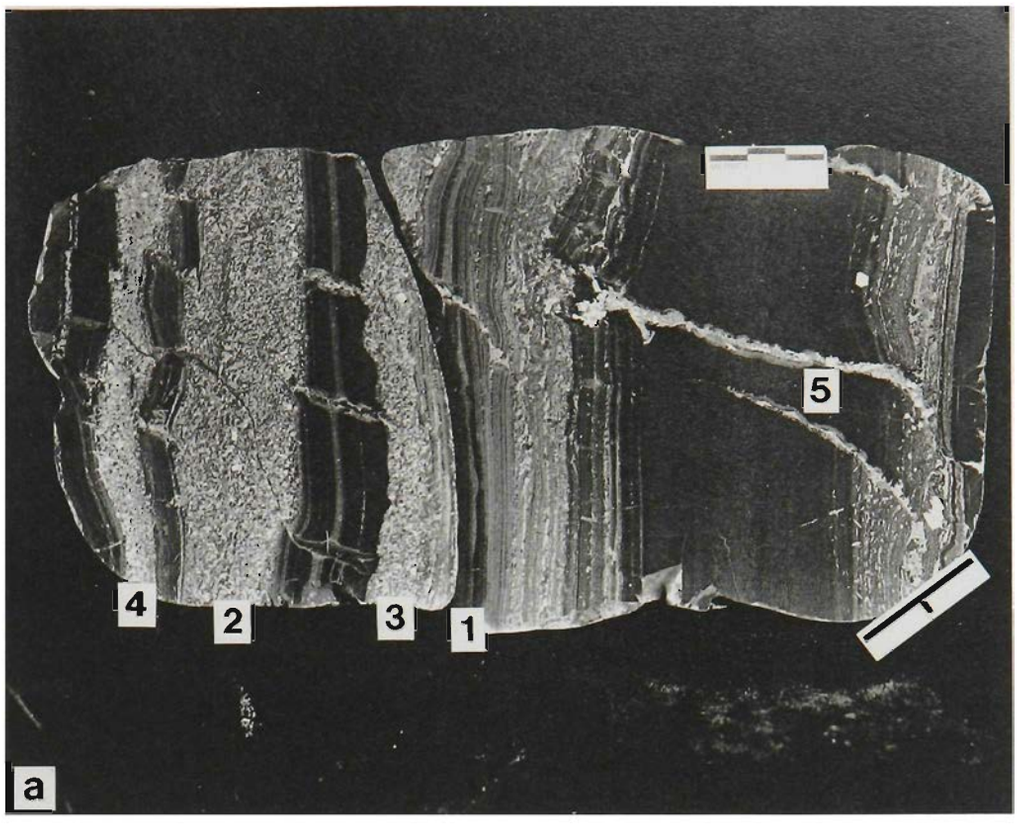
4
2
3
1
5
a

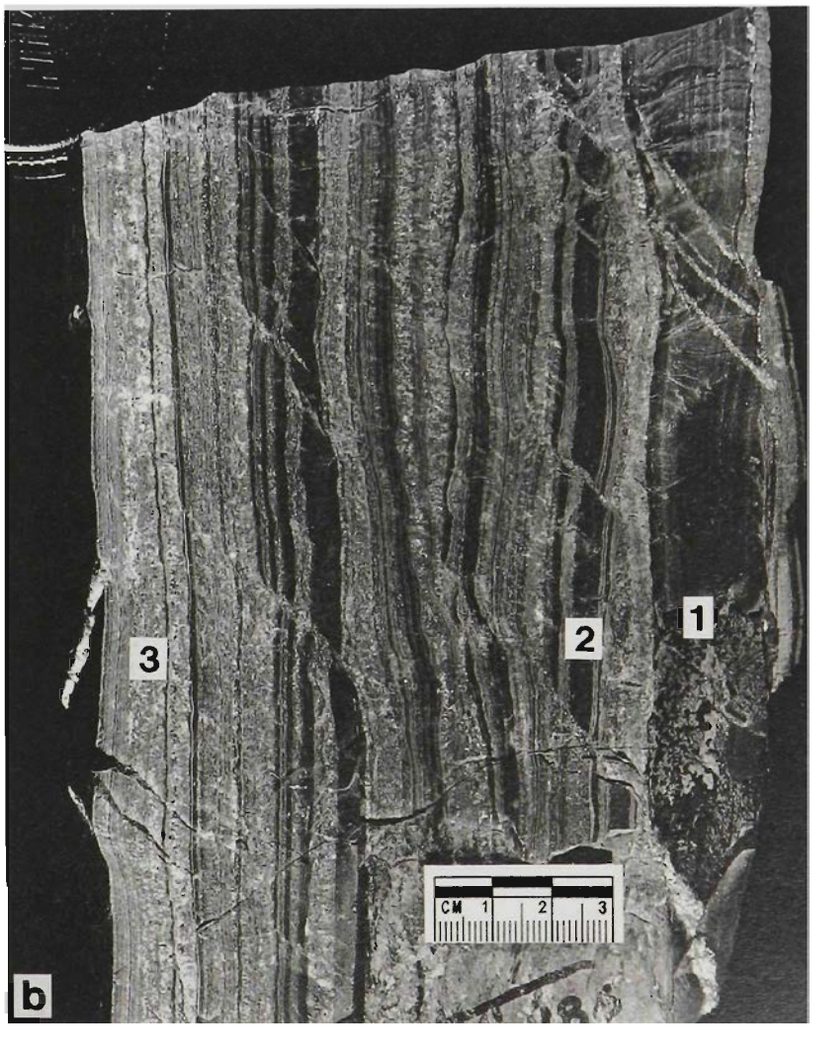
3
2
1
CM 1 2 3
b

Figure 4. Correlation of fine (sub-millimetre) laminae in the 7 orebody zone over three kilometres. This sequence correlates with ore grade banded lead-zinc, one kilometre south of (a). Such detailed correlation indicates that each lamination is a depositional unit, and is extremely difficult to interpret as a current deposit. This laminite was used to establish correlation of a carbonaceous layer 150mm below (b) as a TMB, although it showed none of the normal characteristics in hand specimen. a. Location, DDH M815, 38150mN, 1039.2m. true thickness 39mm. b. Location, DDH QZ10, 41,000mN. true thickness 50mm.

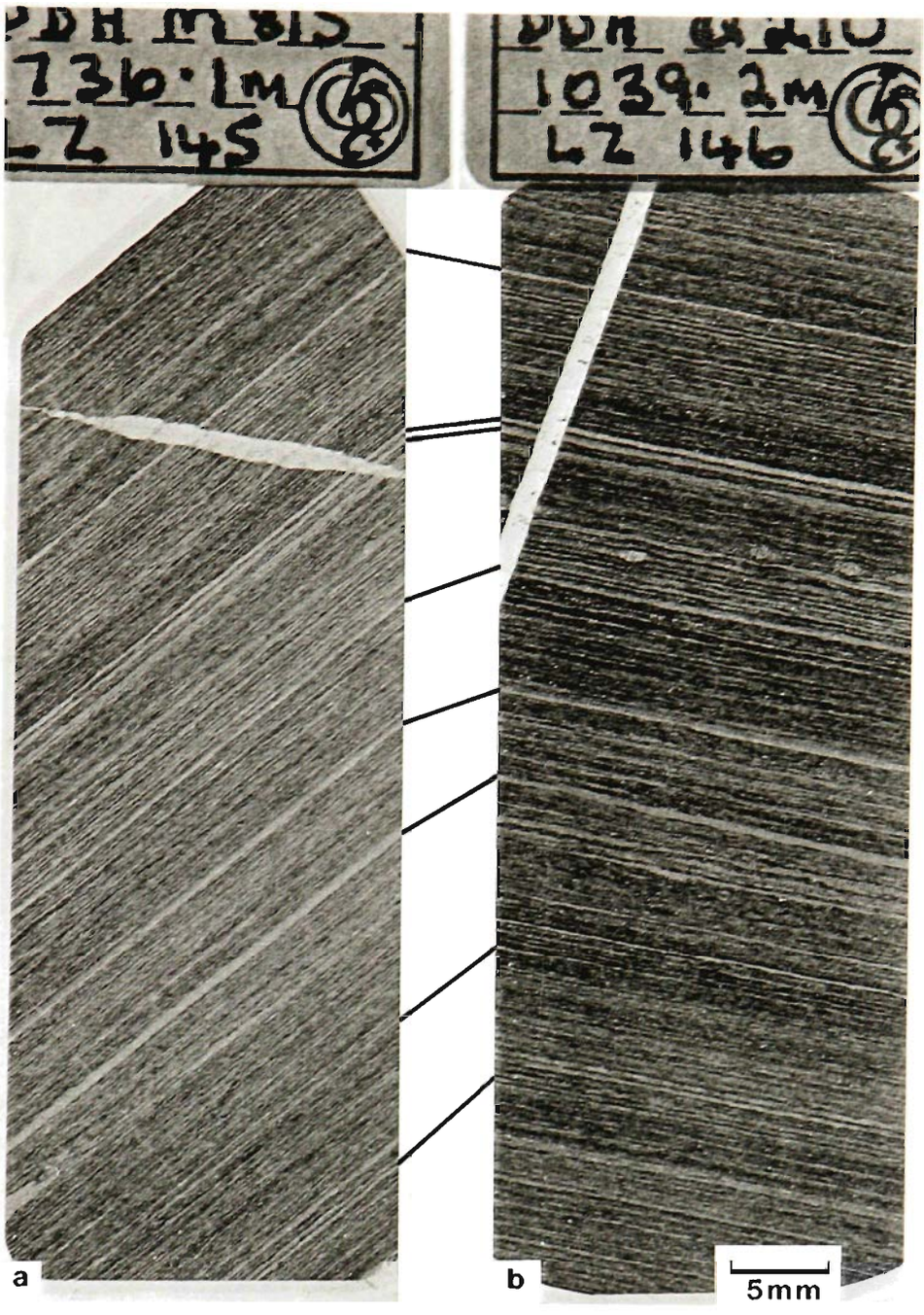
7360.1m
LZ 145
1039.2m
LZ 146
a
b
5mm

Figure 5. a. Wall section (narrow strip looking north) across 7 orebody, 7 Level, with a range of styles of lead-zinc mineralization. The pyritic zones contain very little sphalerite, but the sphaleritic layers contain pyrite and some galena, and the galena breccia contains substantial sphalerite, with minor pyrite. b. Wall section across 7 orebody, 9A Sublevel, showing a change in distribution of mineralization relative to 5a,(approx. 100m below, see Figure 2b.), and the development of a healed fault and anticline which repeat stratigraphy. The galena breccia zones, in particular, are in a different position in the sequence from the intersection shown in 5a. Correlation of the footwall marker bed and other non-laminated units is indicated. Note the variation in density of east-dipping veins between the two exposures.

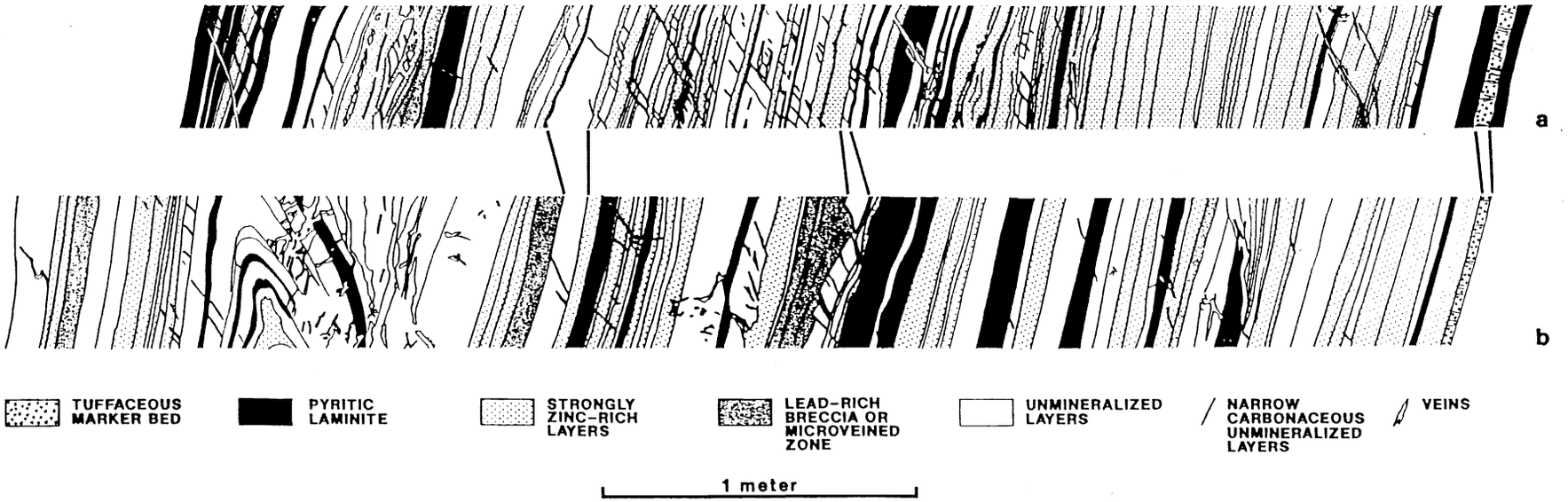

7 OREBODY PROFILES

Figure 6. Longitudinal projection of 12 orebody with a selected diagonal profile indicating the change in stratigraphic position of sulphide concentration relative to correlated stratigraphic markers (TMB's). Mineralization is preferentially developed at higher stratigraphic levels in an upwards and northwards direction.

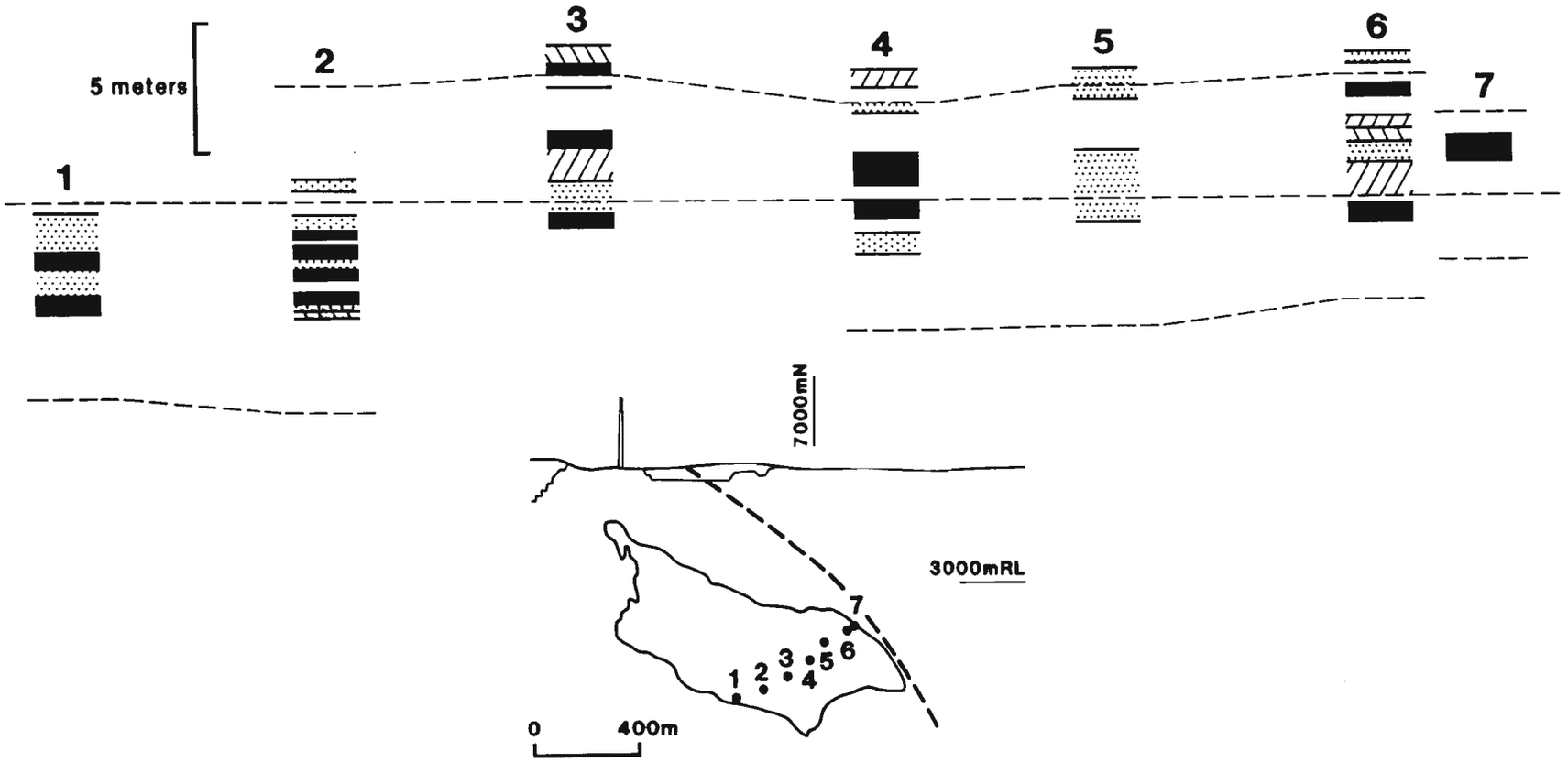
5 meters
1
2
3
4
5
6
7
7000mN
3000mRL
0
400m
MARKER BED
>10% LEAD
5–10% LEAD
2–5% LEAD
>10% ZINC,<2% LEAD
DRILL HOLE INTERSECTIONS
ORE (+4.0m)
ANTICLINAL HINGE

Figure 7. a. Part of hinge and long limb of early fold with axial plane carbonaceous cleavage parallel to bedding in the limbs, and cross-cutting cleavage(s_3) highlighted.

Figure 7 b. Anticline looking north with the early fold A shown on the western limb, but having the wrong vergence to it. The bedding-parallel cleavage is deformed around the anticline, and an axial plane cleavage(s_3) is axial plane to it. Extensional shears are also deformed around the fold, and they form the margins of carbonate-altered laminites. Sphalerite occurs in the hinge of the fold where much of it replaces coarse-grained albite, in the large vein on the limb, and also irregularly in the fine veins cutting across the fold. b. Location; No 6 orebody, 19C Sublevel, 7350 N.

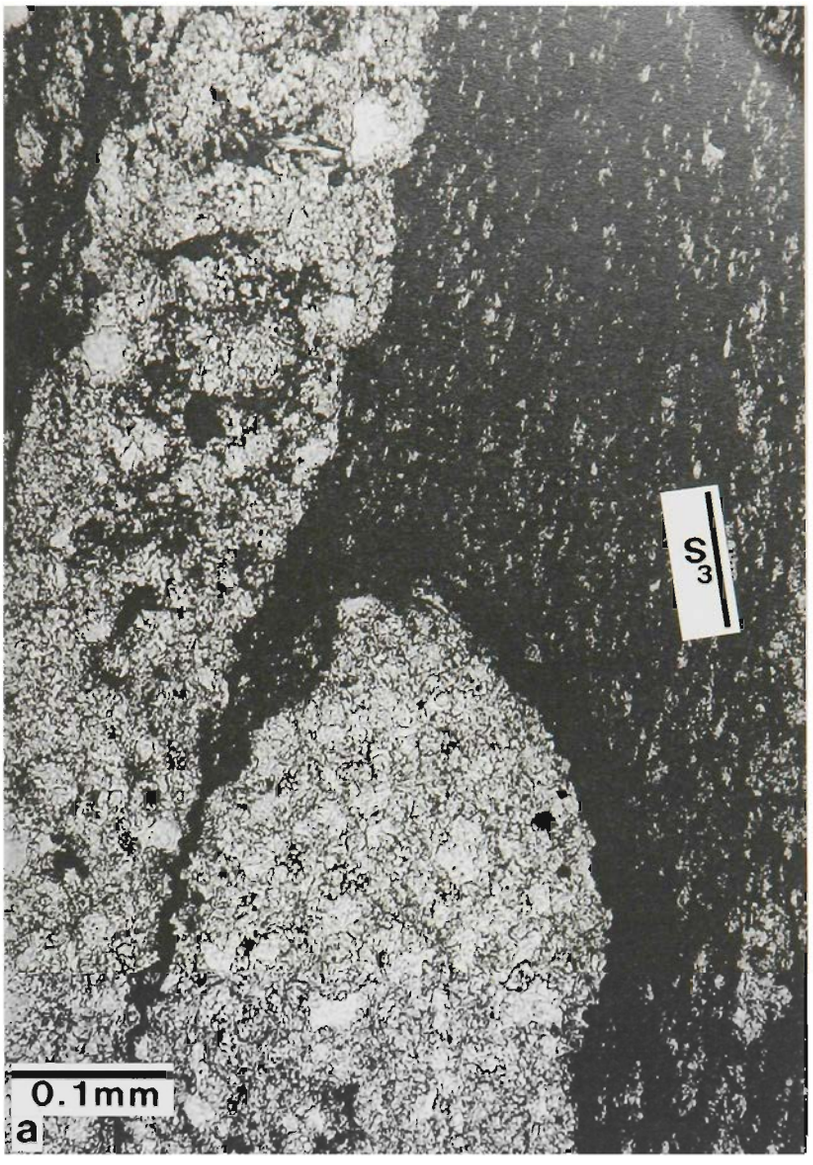
S3
0.1mm
a

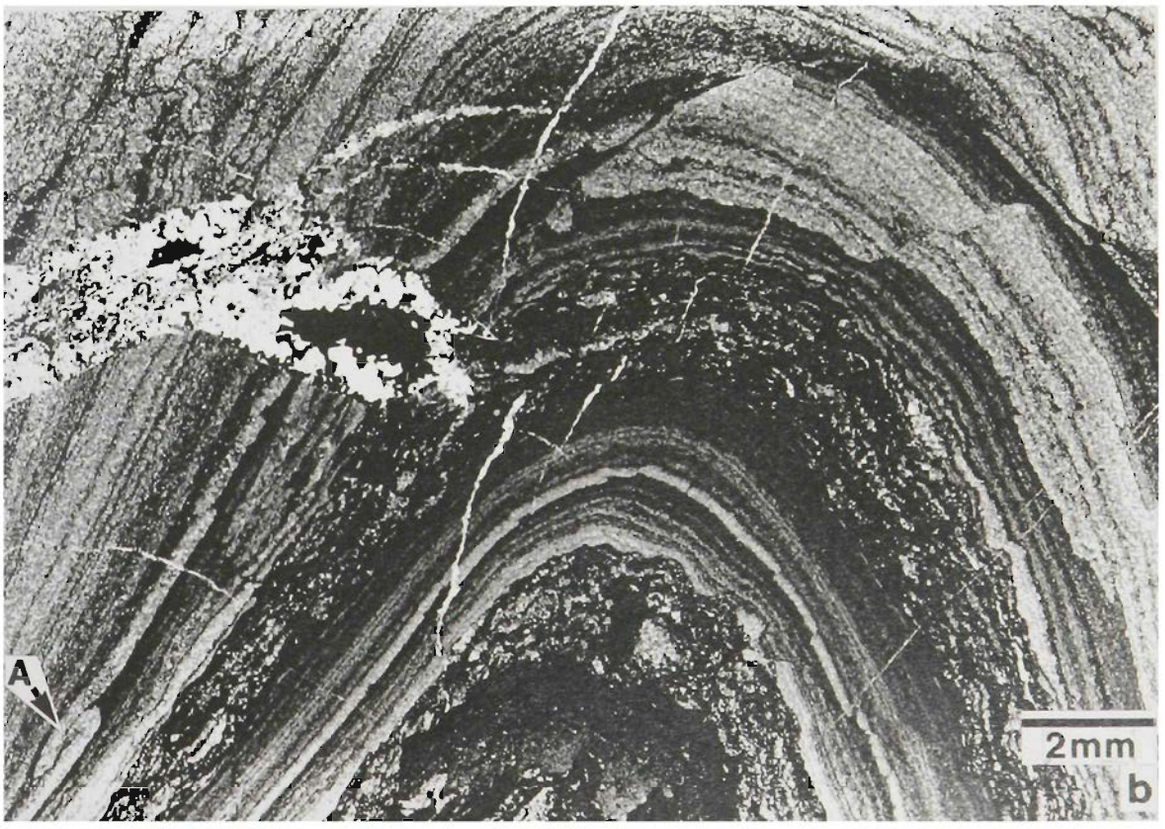
A
2mm
b

Figure 8. Fold zone in lead-zinc ore. Larger folds have axial planes which dip from vertical to steeply west sub-parallel to bedding, and all have a vergence indicating anticline east. One small fold at A has an axial plane which dips gently west at a high angle to bedding. Intrafolial folds have the same sense of vergence as the large folds. The galena band immediately above A transgresses across stratigraphy and removes it over about 0.5m. Looking south. Location; 8 Orebody, 15 Level, 6294N, 1600E.

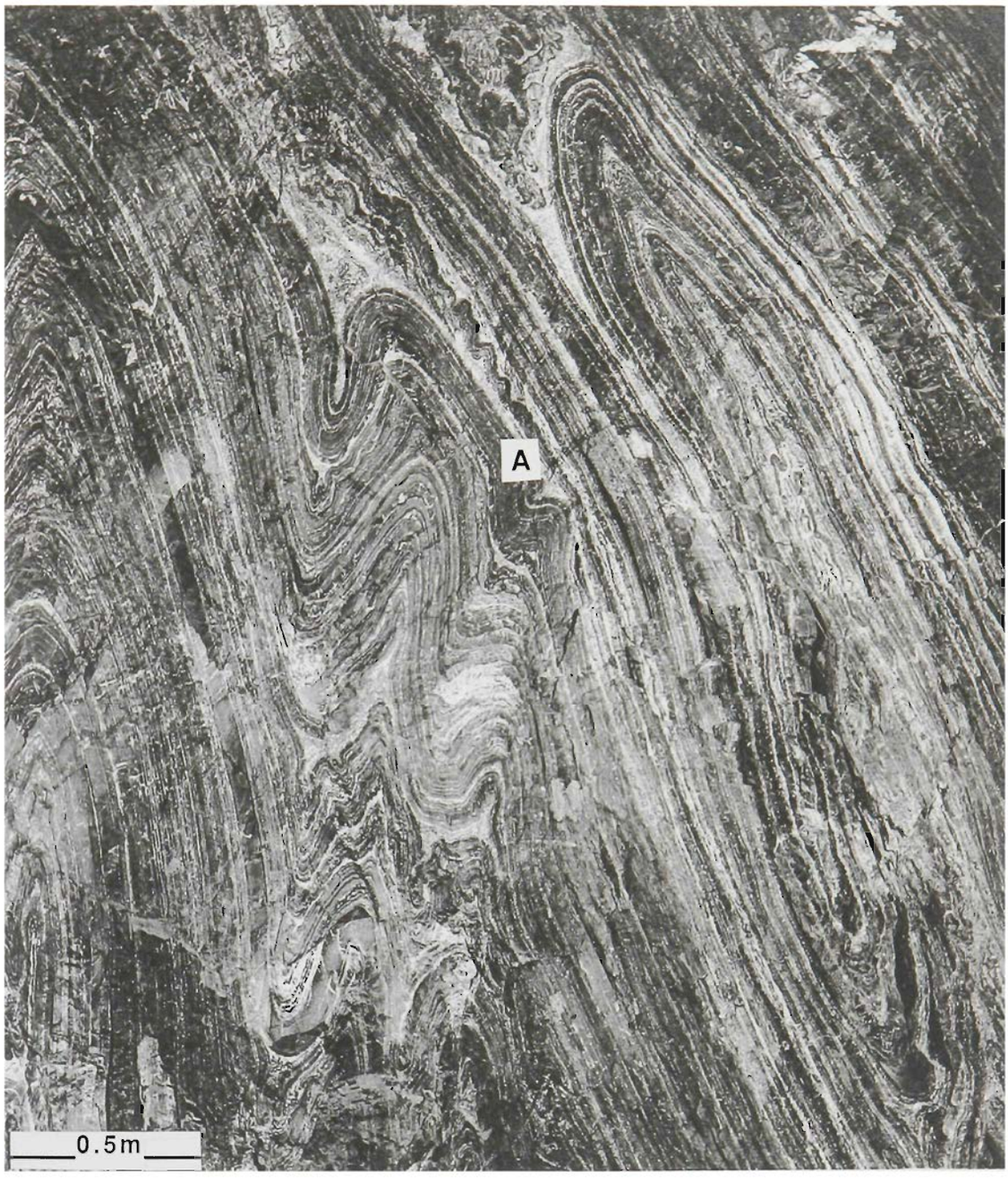
A
0.5m

Figure 9. Dolomite vein systems in a lead-zinc mineralised sequence looking northwards. Most veins dip moderately east and strike either slightly easterly or westerly from bedding. In this example, most have a reverse (ie. east block up) sense of displacement. Vein A has a slight normal displacement. Location; 7 orebody, 7 Level, 7050N.

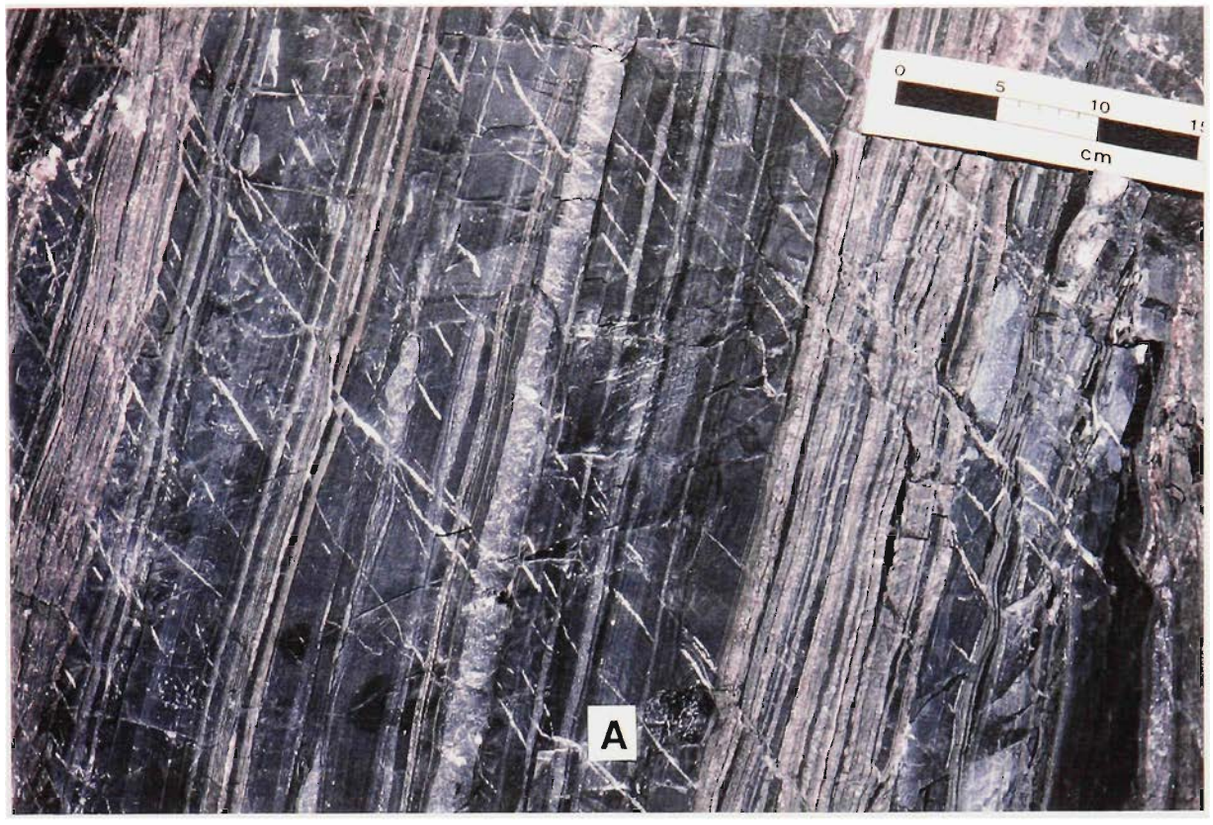
0
5
10
cm
A

Figure 10 a. Longitudinal projection of 7 orebody sequence with observation locations, and stratigraphic thickness measurements of the hangingwall "B" sequence. All samples are from the western long limb of the Mount Isa Fold. Location of samples in Figure 11 are shown. b. Alteration overprint on the "B" sequence: Coarse-grained "nodular" dolomite growth similar to unit 1, Figure 11b, bleaching and "buff alteration" (lacking gray carbonaceous appearance, similar to Figs. 11c and 11d); biotite alteration (brown or green biotite confirmed in thin section); chlorite alteration (enough chlorite to give characteristic green color to hand specimen), and silica-dolomite alteration, progressing from isolated porphyroblasts to almost massive dolomite. c. Iron sulphide mineralization pattern-inner limit of fine and coarse-grained pyrite, outer limit of pyrrhotite. d. Distribution of economic sulphides. N.B. Sulphides are those visible in hand specimen.

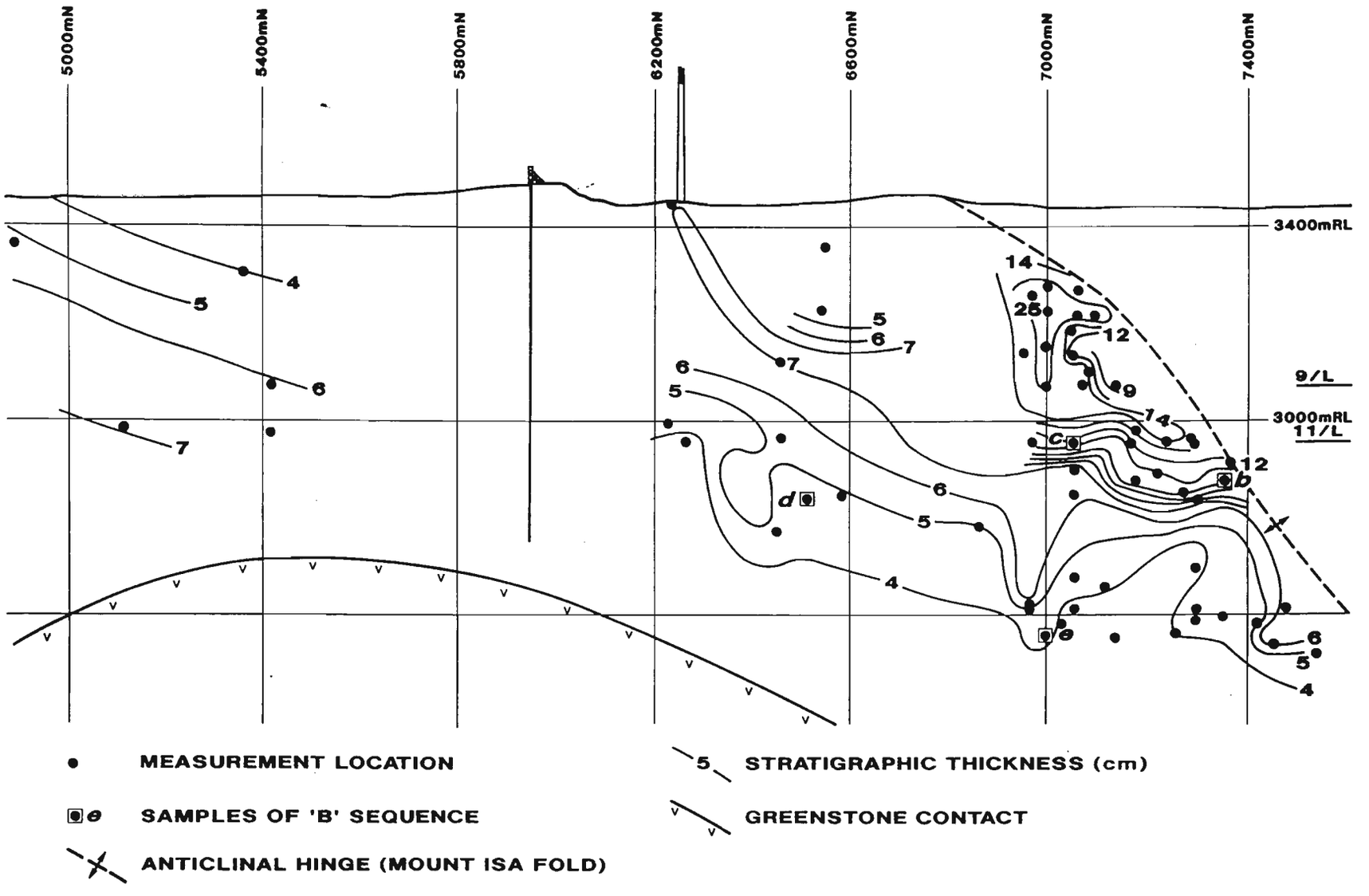
5000mN
5400mN
5800mN
6200mN
6600mN
7000mN
7400mN
3400mRL
3000mRL
9/L
11/L
a
b
c
d
e
MEASUREMENT LOCATION
SAMPLES OF 'B' SEQUENCE
ANTICLINAL HINGE (MOUNT ISA FOLD)
STRATIGRAPHIC THICKNESS (cm)
GREENSTONE CONTACT

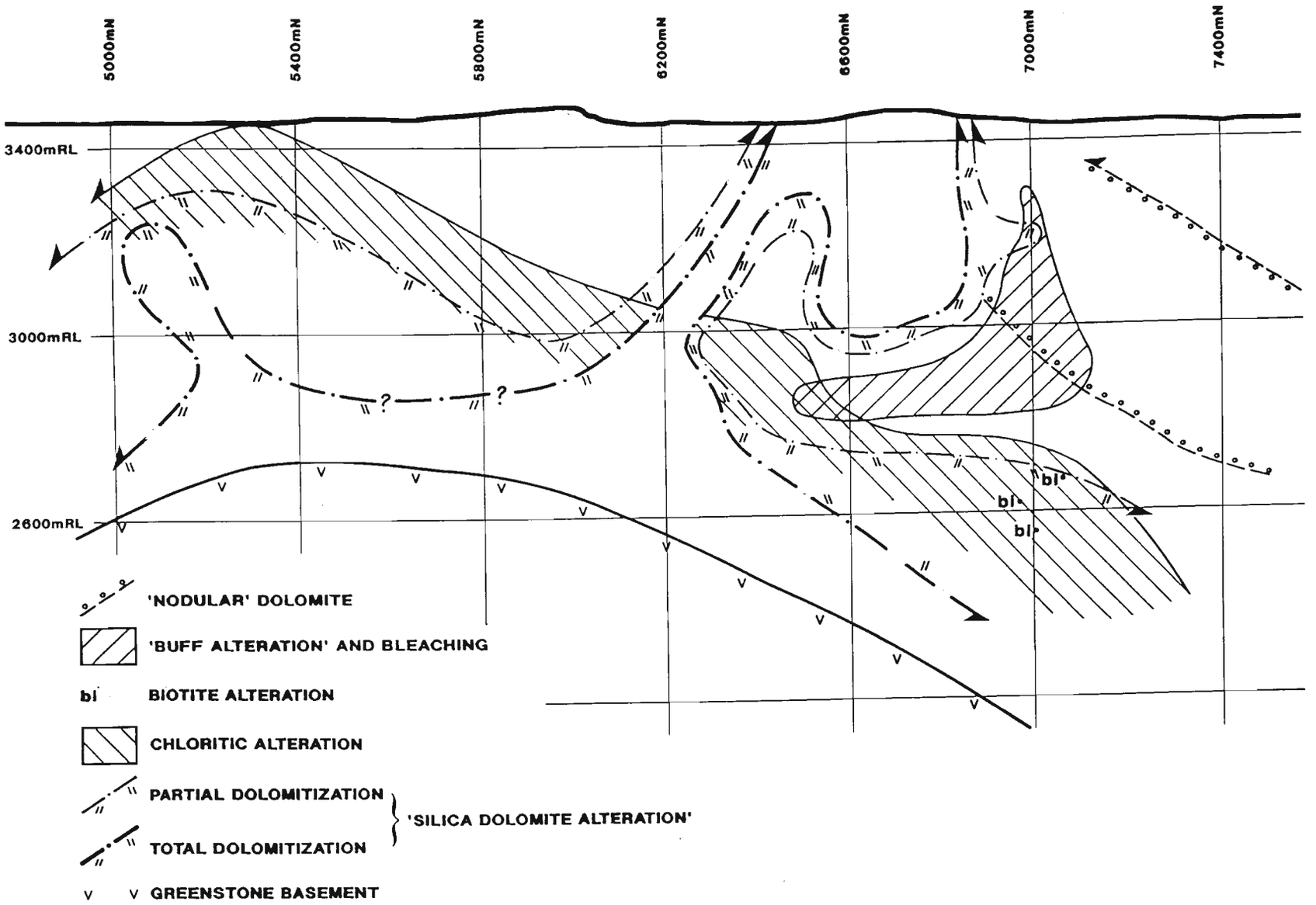
5000mN
5400mN
5800mN
6200mN
6600mN
7000mN
7400mN
3400mRL
3000mRL
2600mRL
bl
bl
bl
'NODULAR' DOLOMITE
'BUFF ALTERATION' AND BLEACHING
BIOTITE ALTERATION
CHLORITIC ALTERATION
PARTIAL DOLOMITIZATION
TOTAL DOLOMITIZATION
'SILICA DOLOMITE ALTERATION'
GREENSTONE BASEMENT

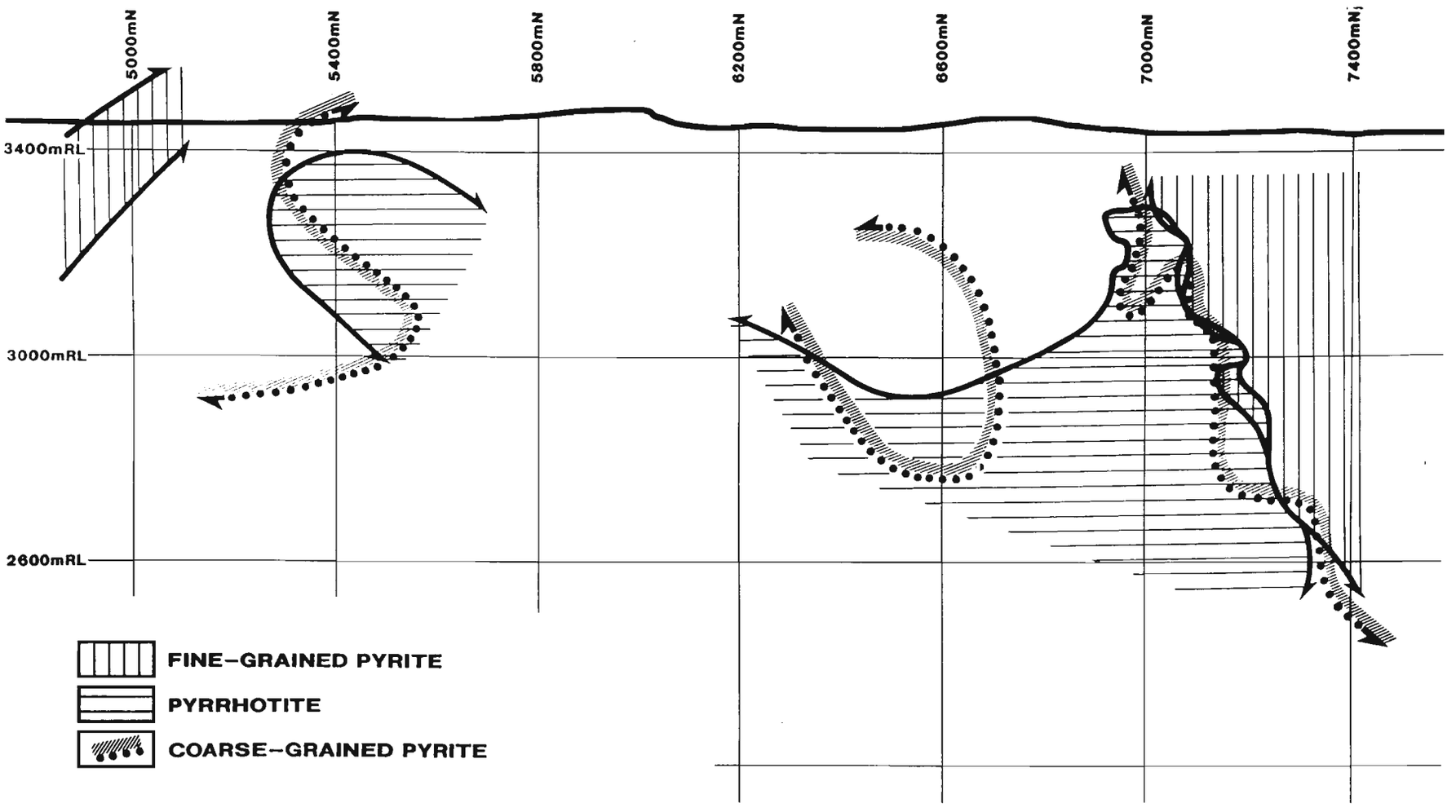
5000mN
5400mN
5800mN
6200mN
6600mN
7000mN
7400mN
3400mRL
3000mRL
2600mRL
FINE-GRAINED PYRITE
PYRRHOTITE
COARSE-GRAINED PYRITE

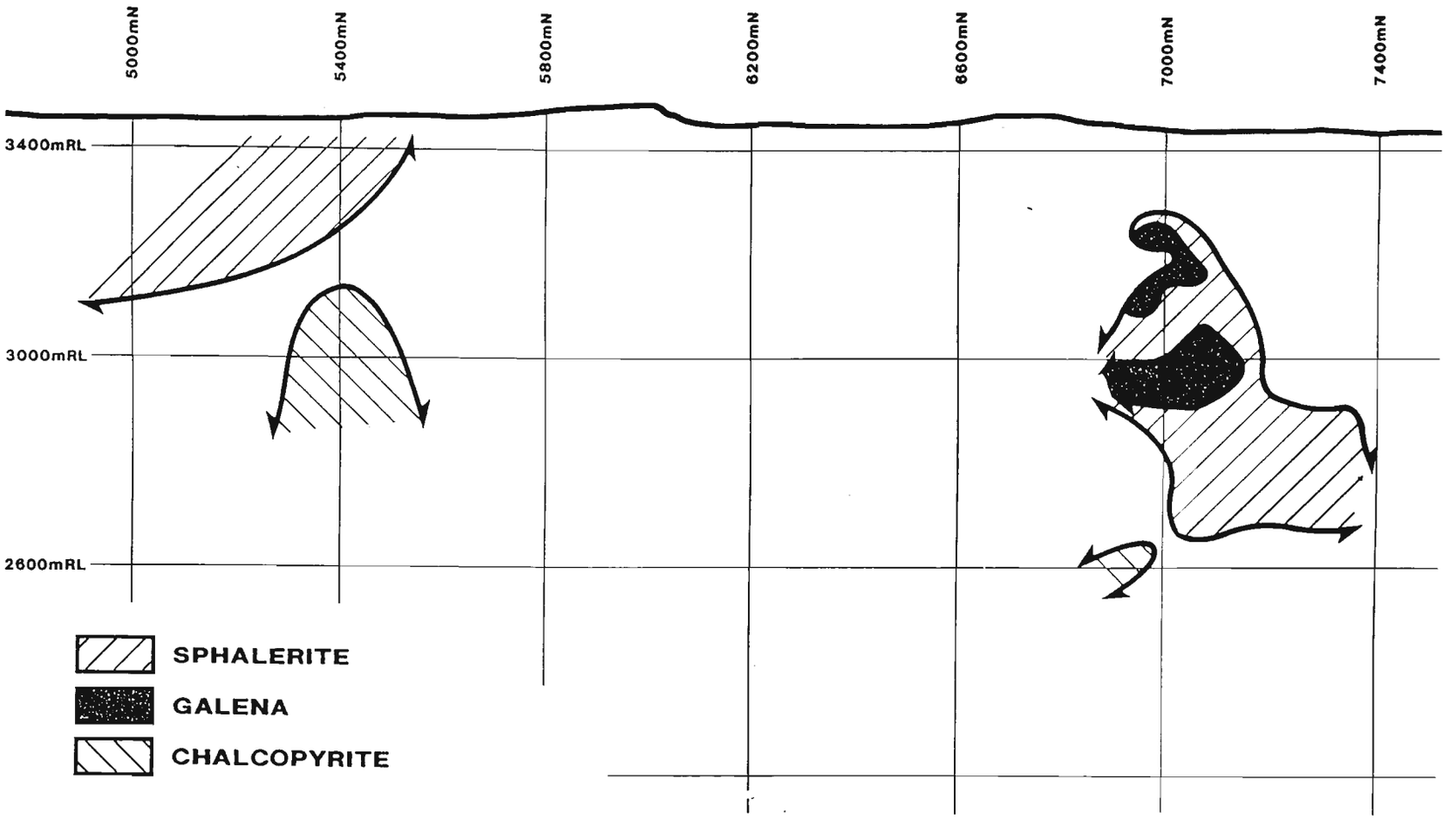
5000mN
5400mN
5800mN
6200mN
6600mN
7000mN
7400mN
3400mRL
3000mRL
2600mRL
SPHALERITE
GALENA
CHALCOPYRITE

Figure 11. Lithological variation in the "B" sequence. Examples at different locations of this sequence showing features of zoned alteration. The outer correlation lines are the bases of the bounding TMB's. The sequence contains two non-laminated to vaguely laminated layers which are the main cause of thickness variation between each location (in 11b these are layer 2 and the 30mm light gray layer above the scale marker.

a. 1. Highly pyritic laminite. 2. Carbonaceous vaguely-laminated siltstone. Location; M815 East Decline(Surface), 730.6m. N.B. 800 metres north of (b)-refer Figure 10a.

b. 1.Pyritic bands following bedding laminae and s_3 cleavage, alternating with 'nodular' dolomite layers containing variable sphalerite. 2. Double banded 15mm. mudstone-siltstone layer with minor wisps of pyrite. Location; 13D Sub. 7360N.

c. 1. Faintly laminated "buff-altered" zone with crude bands of dolomite, pyrrhotite and sphalerite. 2. Double-banded19mm "buff" bed consists of quartz, dolomite, muscovite, K-feldspar, albite, and siderite. Location; 11 Level,7058N.

d. 1.Faintly-laminated buff zone with random acicular pyrrhotite aggregates and euhedral pyrite. 2. Thin layer rich in muscovite. Location; 13 Level, 6515 N.

e. 1. Strongly chloritised and pyrrhotite/mineralised laminite. Lighter areas associated with chlorite are strongly potassic. 2 Brown biotite with chlorite alteration and pyrrhotite. Location; Above 19C sub, 6997N, 2575RL, K699 W. Inc.

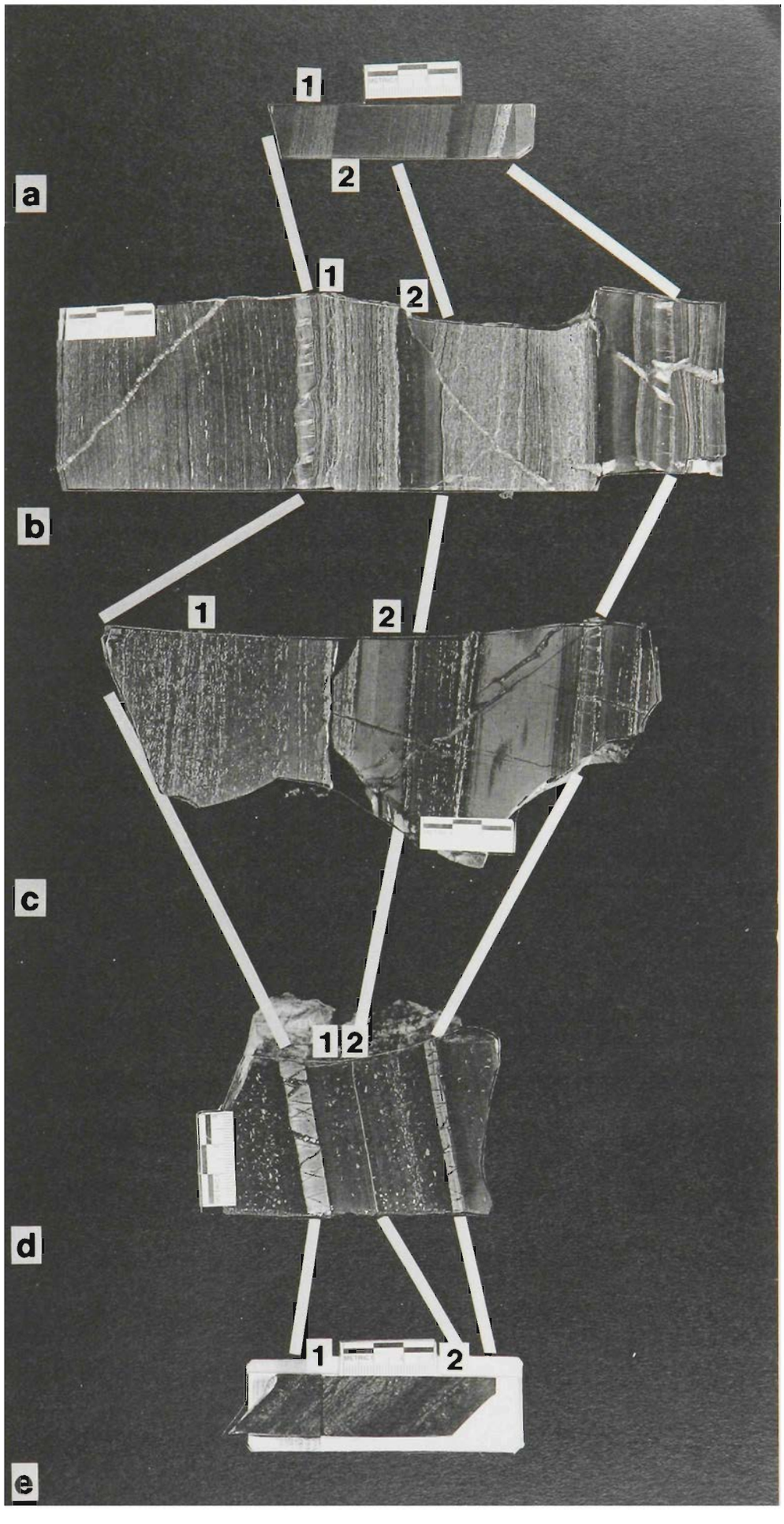
a
1
2
b
1
2
c
1
2
d
1 2
e
1
2

Figure 12. Alteration and mineralization in the northern lead-zinc orebodies, 6999N section. a. Base section with major fold zones, selected marker beds, and distribution of coarse-bedded siltstone facies subdivision after Neudert(1983). The basement ramp is that part of the Paroo Fault between approximately 1300E. and 2100mE which cuts across bedding in the overlying Urquhart Shale at a higher angle. b. Main alteration zones progressing from "buff alteration" and bleaching, to chloritisation and dolomitic and siliceous silica-dolomite. c. Iron oxide and sulphide patterns showing magnetite, fine-grained pyrite and pyrrhotite. d. Economic sulphides with low lead and zinc grades, and a range of copper grades. e. Orebody distribution. Note particularly the eastern terminations of the orebodies define a vertical plane which is adjacent to, and parallel with, the axial plane of the Mount Isa (D_3) Fold.

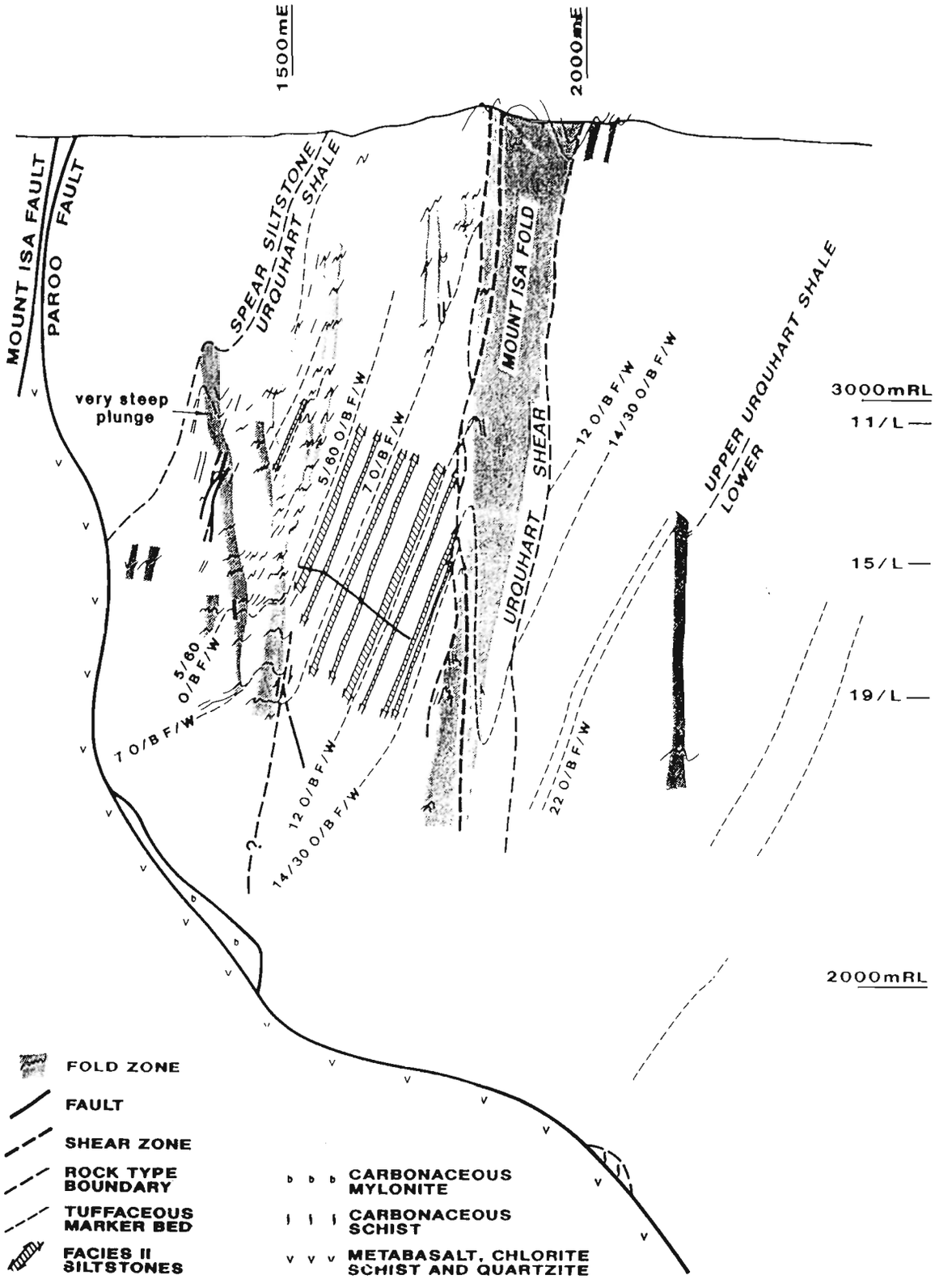
1500mE
2000mE
MOUNT ISA FAULT
PAROO FAULT
SPEAR SILTSTONE
URQUHART SHALE
MOUNT ISA FOLD
URQUHART SHEAR
very steep plunge
5/60 O/B F/W
7 O/B F/W
12 O/B F/W
14/30 O/B F/W
22 O/B F/W
UPPER URQUHART SHALE
LOWER
3000mRL
11/L
15/L
19/L
2000mRL
FOLD ZONE
FAULT
SHEAR ZONE
ROCK TYPE BOUNDARY
TUFFACEOUS MARKER BED
FACIES II SILTSTONES
CARBONACEOUS MYLONITE
CARBONACEOUS SCHIST
METABASALT, CHLORITE SCHIST AND QUARTZITE

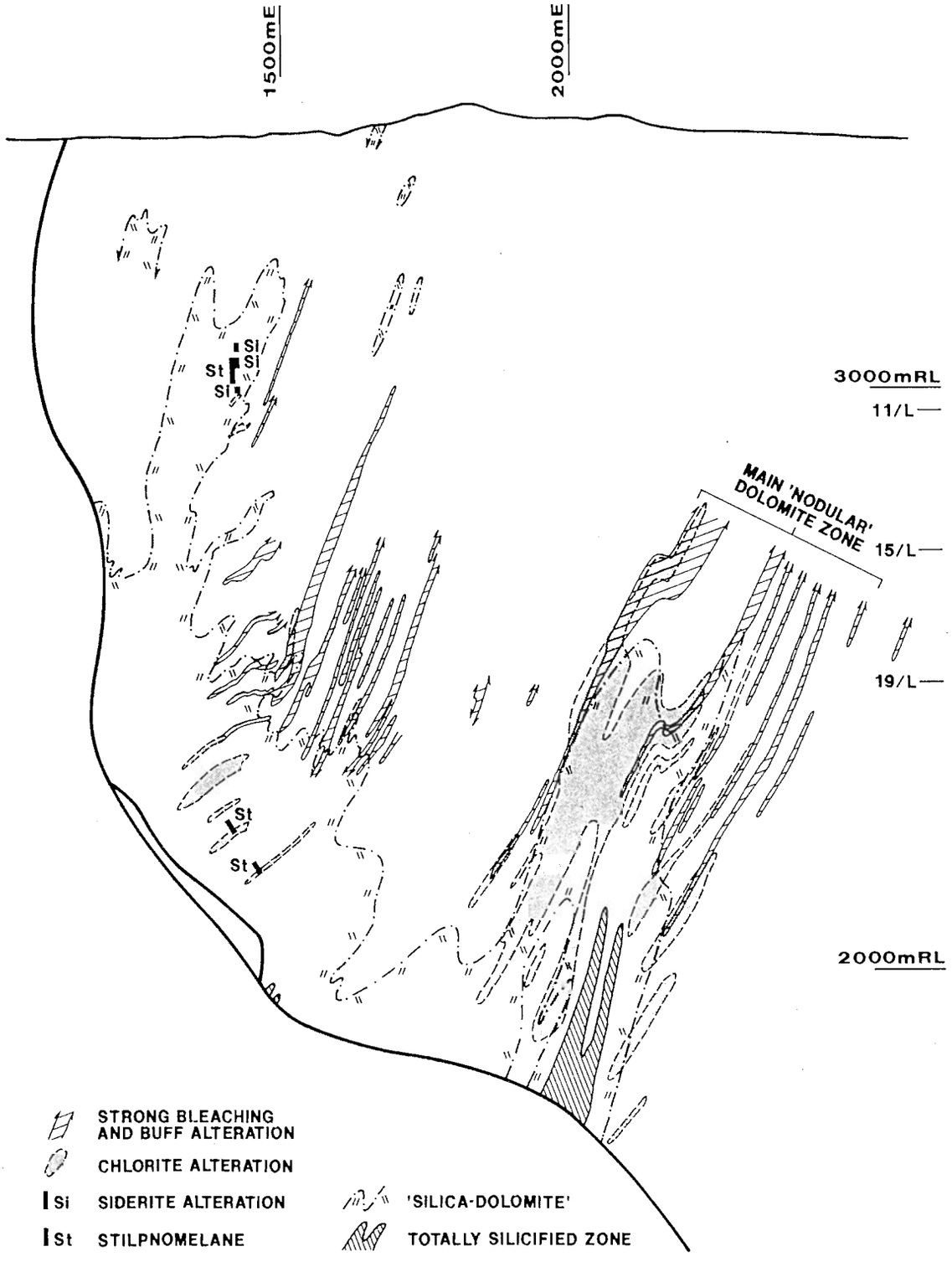
1500mE
2000mE
Si
Si
St
Si
3000mRL
11/L
MAIN 'NODULAR' DOLOMITE ZONE
15/L
19/L
St
St
2000mRL
STRONG BLEACHING AND BUFF ALTERATION
CHLORITE ALTERATION
Si SIDERITE ALTERATION
St STILPNOMELANE
'SILICA-DOLOMITE'
TOTALLY SILICIFIED ZONE

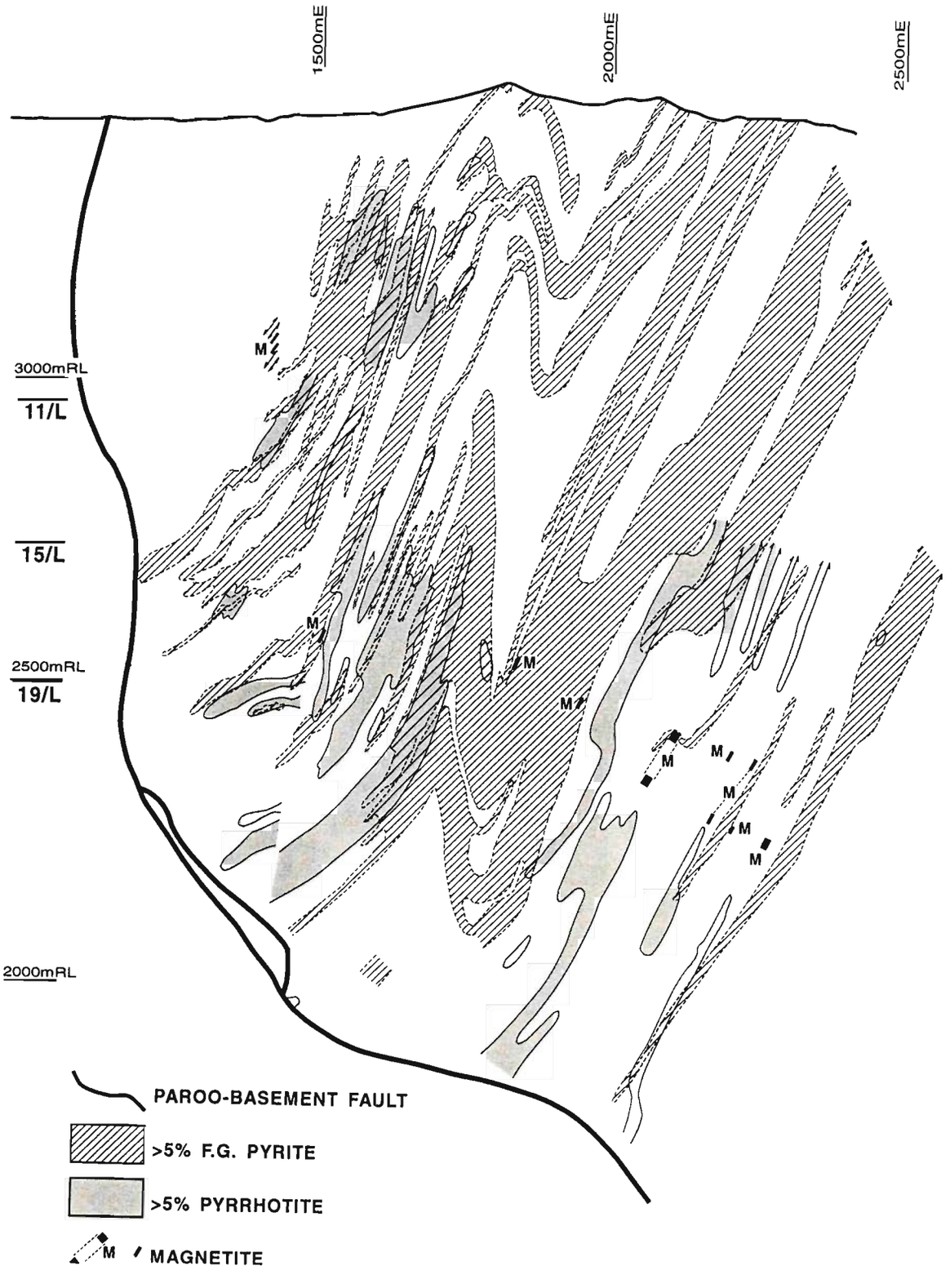
1500mE
2000mE
2500mE
3000mRL
11/L
15/L
2500mRL
19/L
2000mRL
M
PAROO-BASEMENT FAULT
>5% F.G. PYRITE
>5% PYRRHOTITE
MAGNETITE

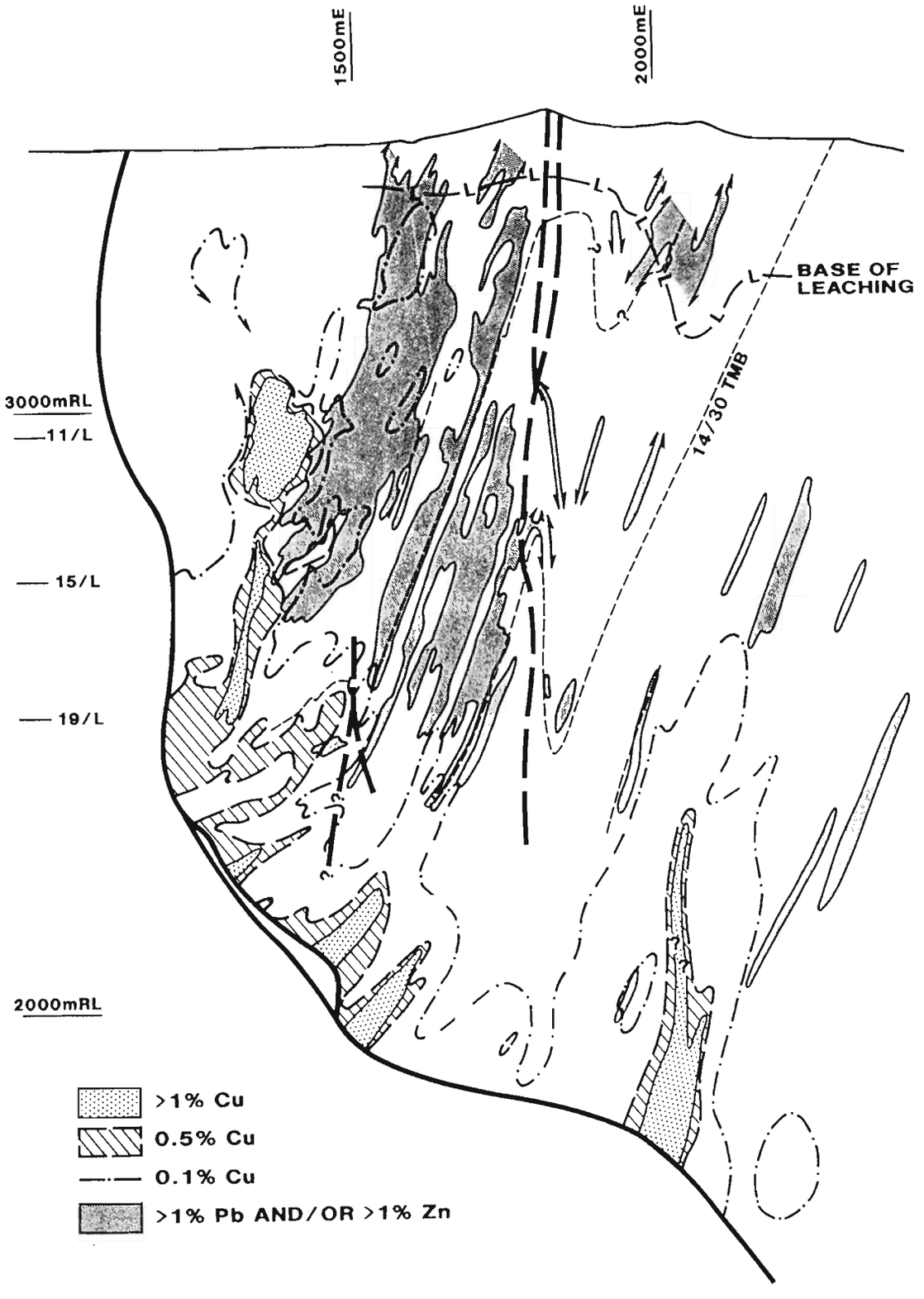
1500mE
2000mE
BASE OF LEACHING
14/30 TMB
3000mRL
11/L
15/L
19/L
2000mRL
>1% Cu
0.5% Cu
0.1% Cu
>1% Pb AND/OR >1% Zn

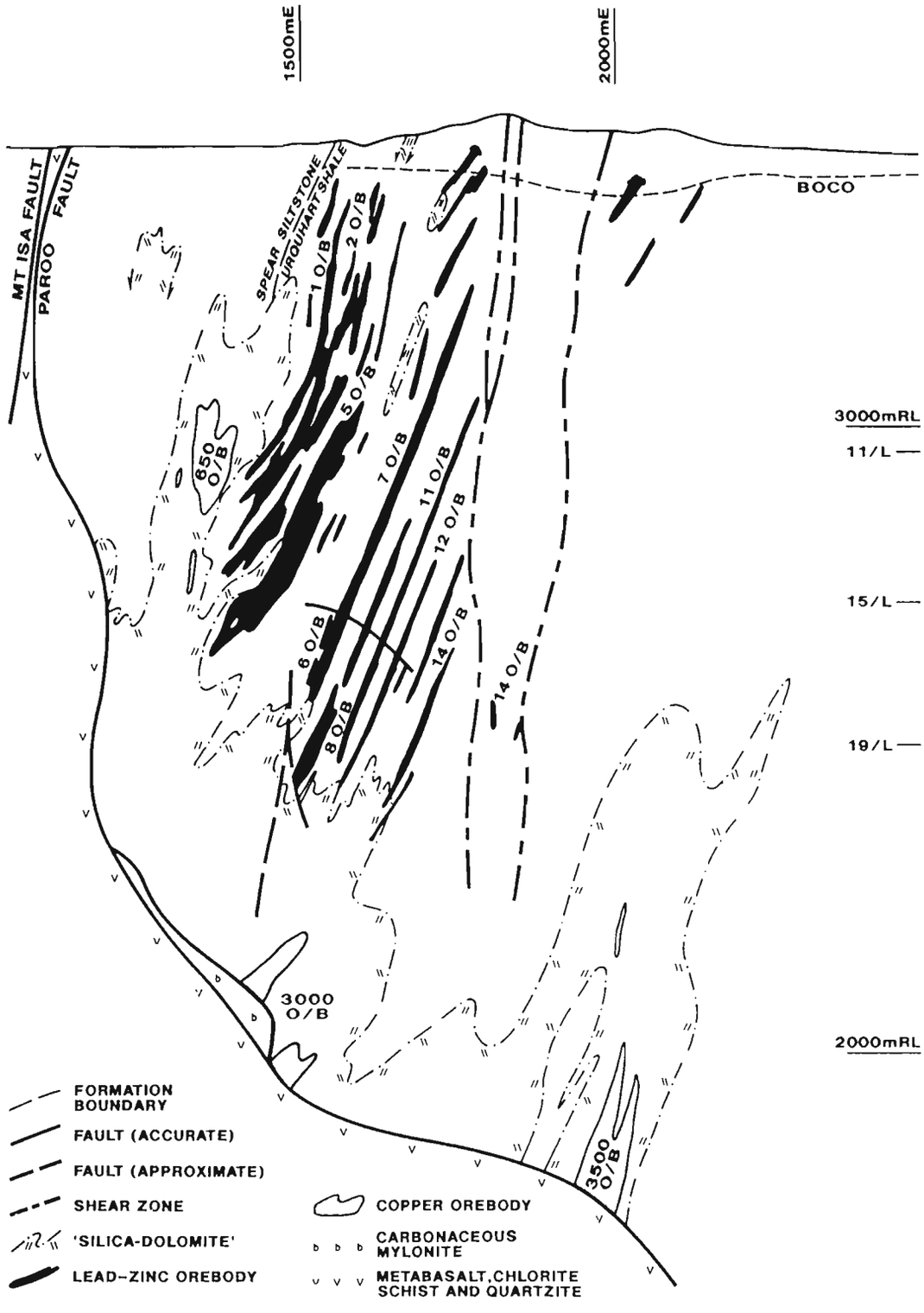
1500mE
2000mE
MT ISA FAULT
PAROO FAULT
SPEAR SILTSTONE
URQUHART SHALE
BOCO
1 O/B
2 O/B
5 O/B
650 O/B
7 O/B
11 O/B
12 O/B
6 O/B
8 O/B
14 O/B
14 O/B
3000 O/B
3500 O/B
3000mRL
11/L
15/L
19/L
2000mRL
FORMATION BOUNDARY
FAULT (ACCURATE)
FAULT (APPROXIMATE)
SHEAR ZONE
'SILICA-DOLOMITE'
LEAD-ZINC OREBODY
COPPER OREBODY
CARBONACEOUS MYLONITE
METABASALT, CHLORITE SCHIST AND QUARTZITE

Figure 13. Lath shapes pseudomorphed by a quartz-feldspar assemblage and replaced by pyrrhotite, in a vaguely-laminated bleached and buff-altered siltstone (layer 1 of Figure 11c). The more equant sulphides outside the lath shapes are pyrite. Stratigraphic up is to the left. Location; 7 Orebody "B" sequence, 13 Level, 6515 N-same sample as Figure 11d.

Figure 14. Layered coarse-grained dolomite in the "B" sequence of the type commonly interpreted have replaced sulfate evaporites, above a non-laminated fine siltstone (layer 2 of Figure 11b). The dolomitic zones contain three phases of dolomite growth, fine-grained inclusion-rich, coarser-grained inclusion-rich recrystallization, and clean dolomite around replacive aggregates of sphalerite(sp.). The dark anastomosing bands are concentrations of fine-grained pyrite following bedding-parallel and cross-cutting cleavage seams. Location; 7 Orebody, 13D Sub., 7360N. Looking south, younging to the right.


0.5mm

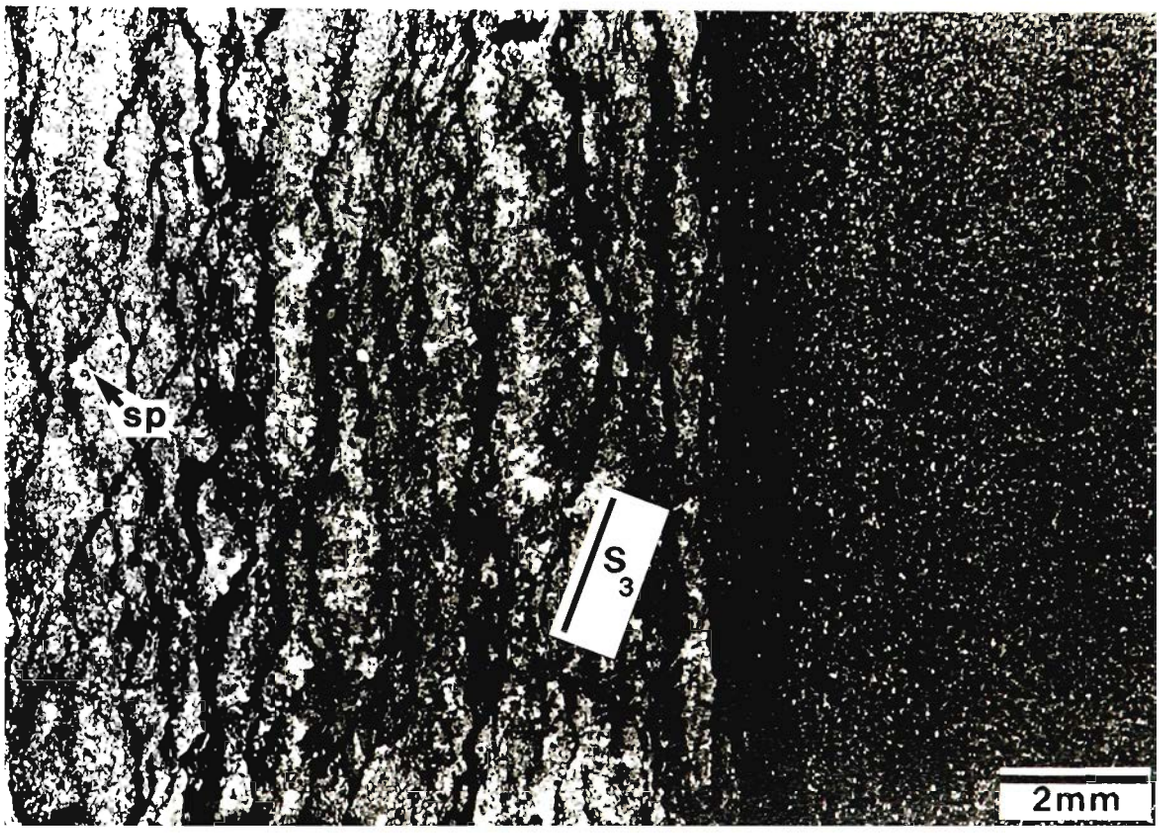
sp
S3
2mm

Figure 15. Sulphide and gangue relationships. a. Sulphide and gangue aggregate from a saddle reef zone of a small-scale fold. Sphalerite(sph) and galena(gal) form a largely connected network, mainly along grain boundaries, with some isolated fine-grained forms. The ragged and uneven boundaries of the sulphides, cutting across quartz-dolomite boundaries e.g. at A, and across twin lamellae e.g. at B, indicate that the sulphides have passively replaced the gangue minerals.

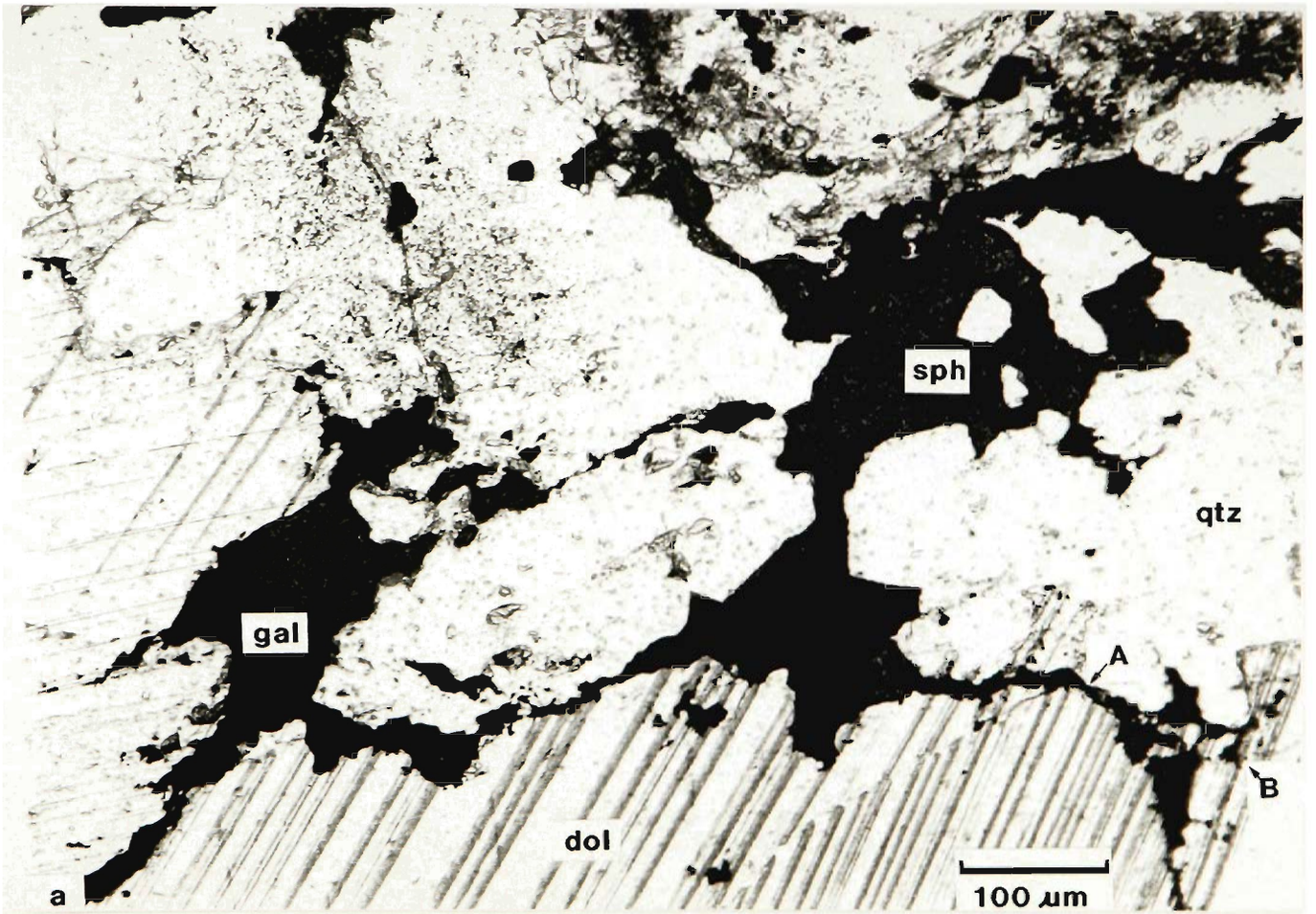
sph
qtz
gal
A
B
dol
a
100 µm

Figure 15 b. Same field as a, crossed nicols. Sulphides(black), cutting across and leaving islands of optically continuous quartz at C. Strained quartz and dolomite have been partially recrystallised. Location, 7 orebody, 8 level, 7015N.

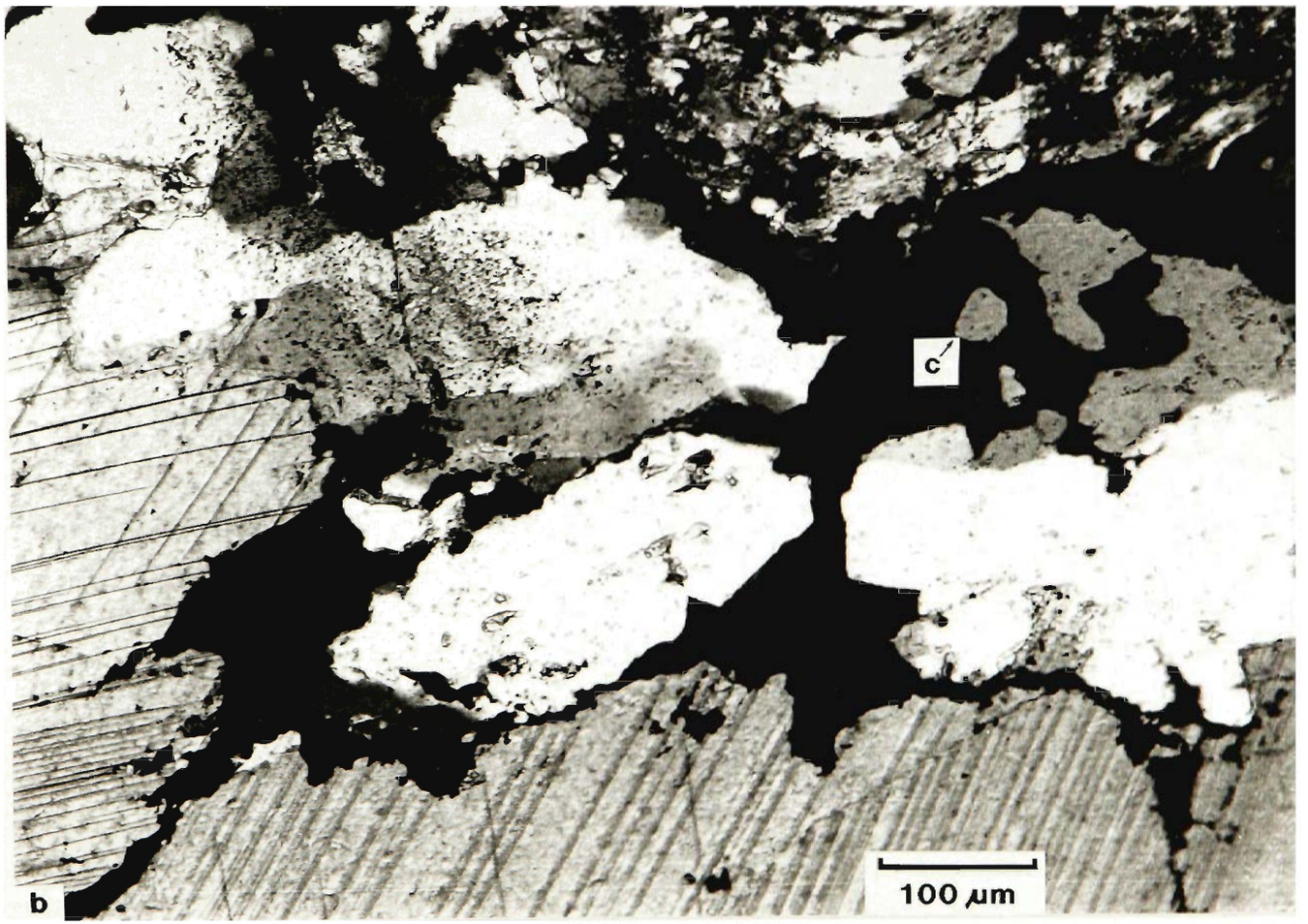
c
b
100 µm

Figure 15 c. Corner of breccia fragment (upper left quadrant) with matrix of dolomite, quartz, and sulphides. Galena (white) shows irregular protrusions into adjacent dolomite, partly along grain boundaries, and also similar protrusions into sphalerite. The fine-grained galena in the fragment has similar boundaries against adjacent gangue, and the sulphide boundaries show no evidence of subsequent deformation. Location, 8 orebody; 6910N, 2830R.L.

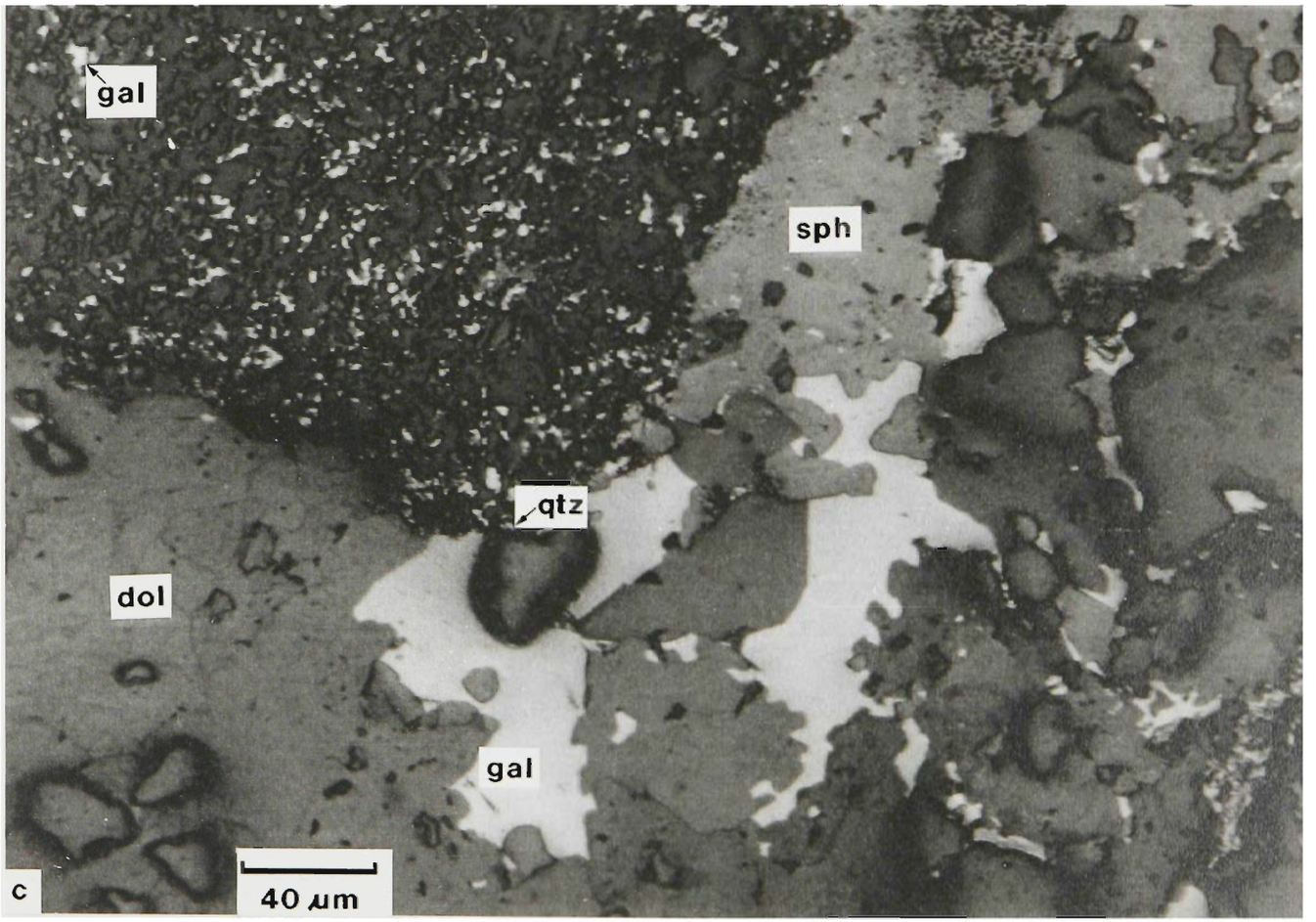
gal
sph
qtz
dol
gal
c
40 µm

Figure 15 d. Similarity in sphalerite relationships to neoformed dolomite, irrespective of whether the dolomite is along the lamination (lower left) or in a cross-cutting vein relationship. In both situations, the dolomite is interpreted to be partially replaced by sphalerite. Location; Location; K740E. Hor. 12A sublevel, 8.4m. 5 orebody.

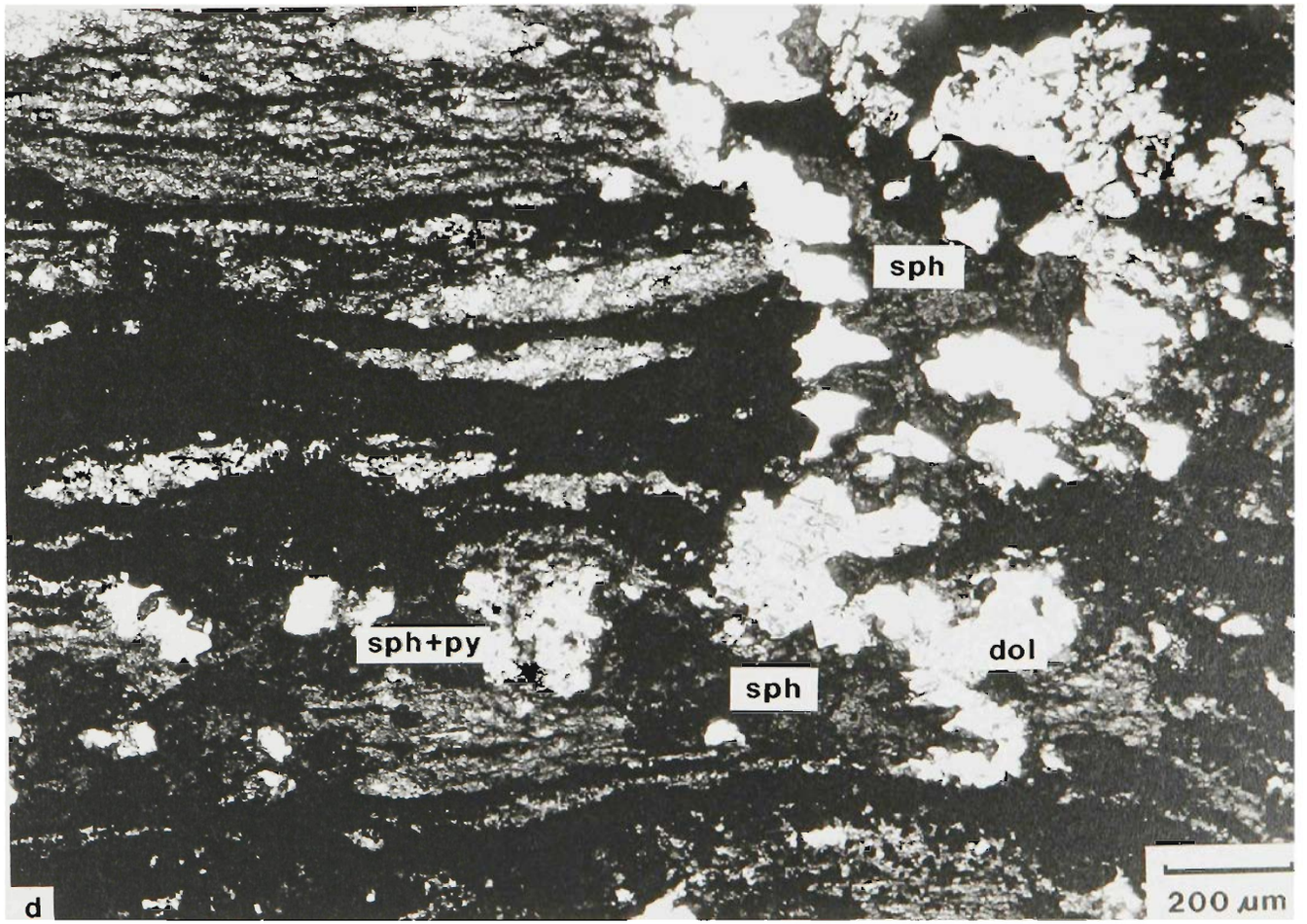
sph
sph+py
sph
dol
d
200 µm

Figure 15 e. Sulphide relationship to both deformed and recrystallised dolomite. Galena and minor sphalerite show continuity and similar overprinting relationships into and across twin planes in deformed and recrystallised dolomite, indicating growth subsequent to dolomite recrystallization. From a dilational vein in the synclinal hinge of a fold with a wave-length of 35mm. The light colored twin plane extending outwards from the protrusion of sulphide is approximately parallel to the s_3 cleavage. Transmitted light. Crossed Nicols. Location; 7 orebody, 8 Level, 7051N.

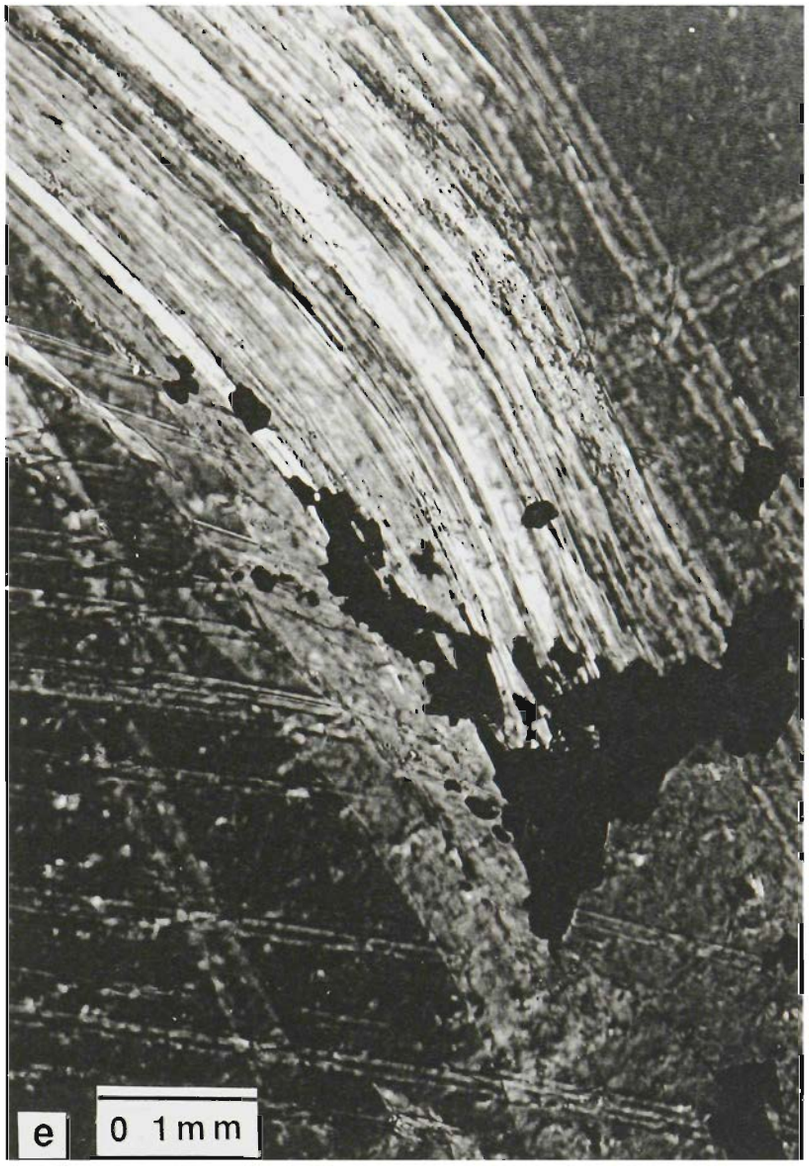
e
0 1mm

Figure 16. Typical sulphide-sulphide relationships in lead-zinc ore. a. Paragenetically earlier sphalerite(sp, dark gray) is apparently replaced by galena (black), leaving progressively smaller rounded remnants of sphalerite. Minor pyrrhotite also occurs with galena in this section, but its relationships are equivocal (ga-po). The bladed mineral on the fragment edge is chlorite. Plane polarized light. Location; 8 Orebody, 6910N, 2810R.L.

Figure 16 b. Same relationship in reflected light. Galena(ga) apparently replacing sphalerite(sp), controlled by grain boundaries. Location; 14/10 orebody, 16B sublevel, 6255N.

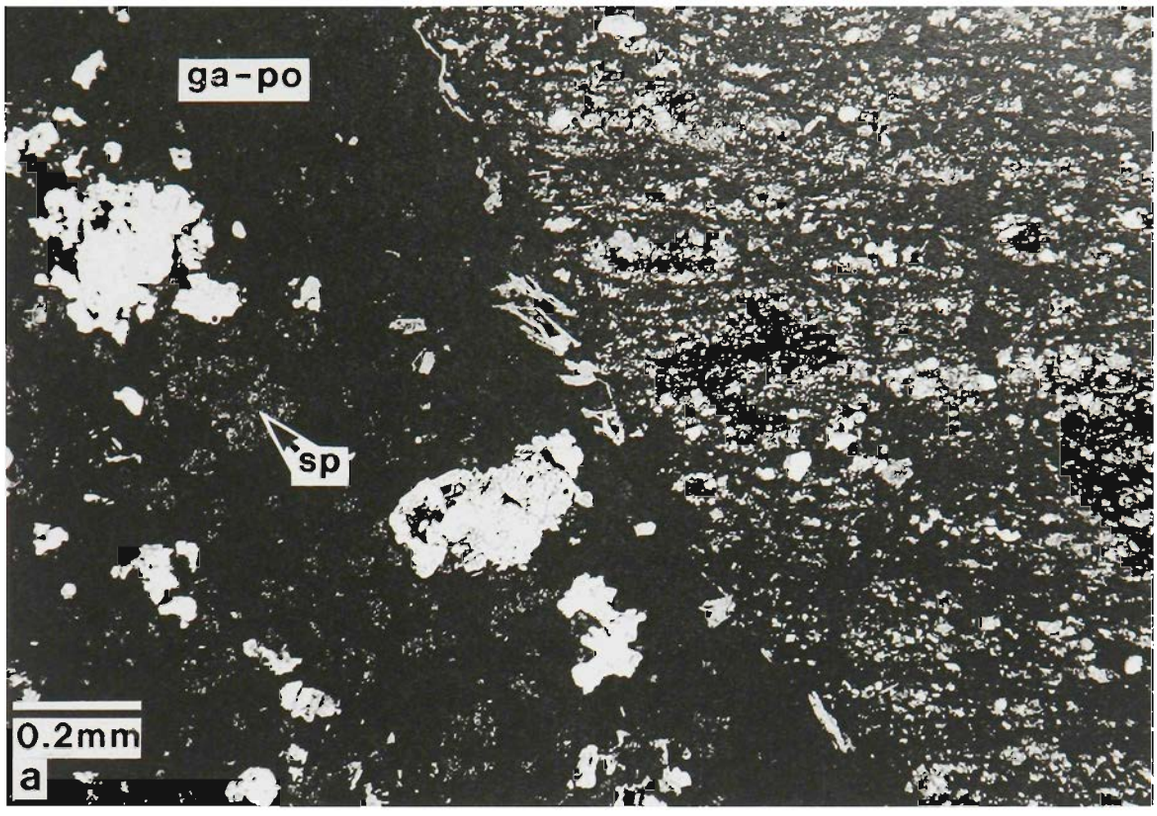
ga-po
sp
0.2mm
a

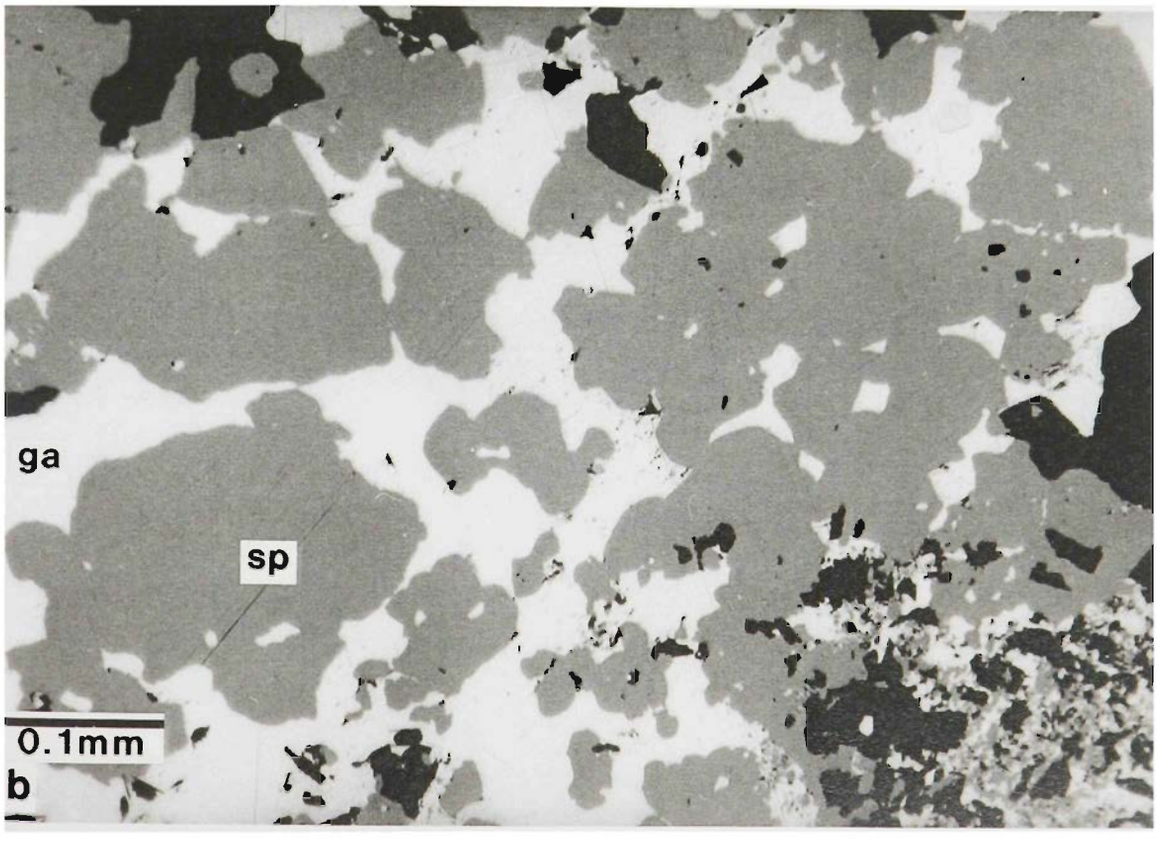
ga
sp
0.1mm
b

Figure 17. Concretionary growth of dolomite along bedding. The lighter layers contain neoformed dolomite of 10-50 micron grain size, much less carbonaceous material and exhibit vague laminations. Outside them, shortening has progressed to form lamina-parallel foliation. The lobate front 1, the thicker layer 2, and the wavy discontinuous "nodular" dolomite 3, all appear to have formed by similar processes. Location; O699W Inc, 17 Level, 58.4 m.

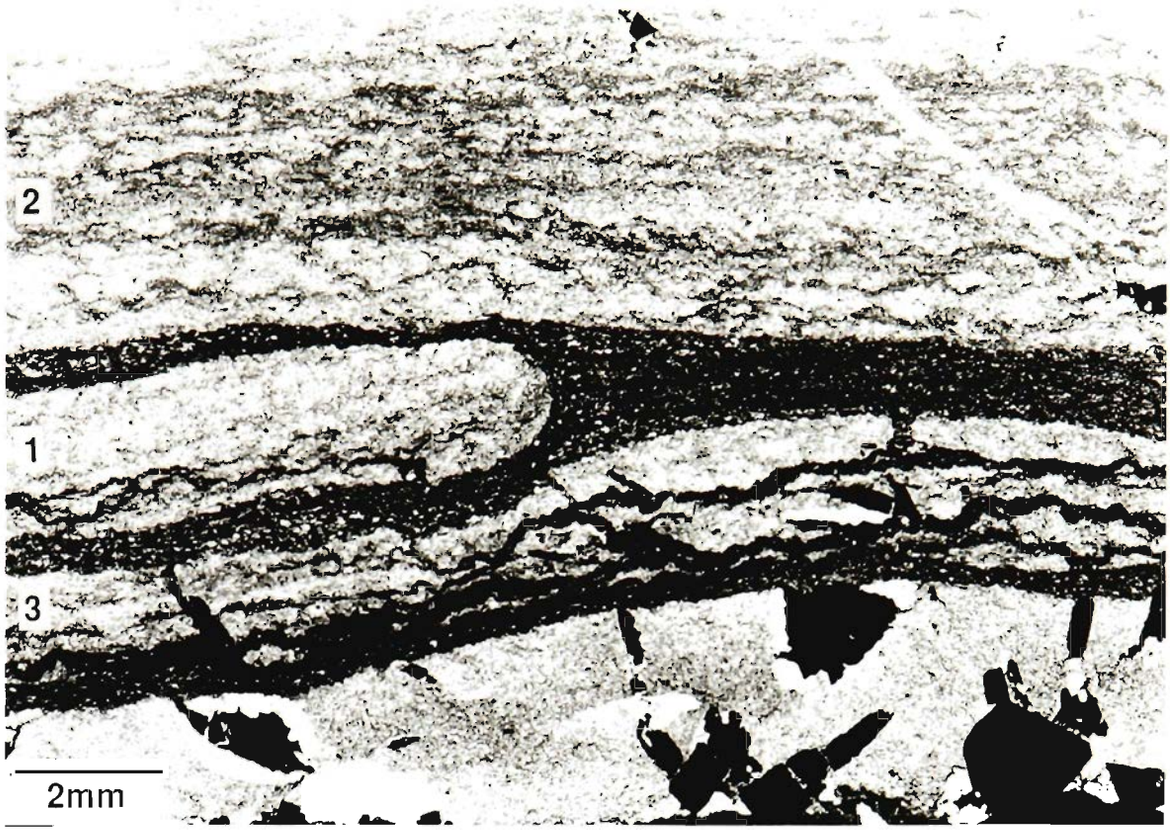
2
1
3
2mm

Figure 18a. Polished slab. Breccia with galena-rich matrix containing relict fold hinges (A). Transition from folds to breccia-characteristic extensional shears on upper breccia margin (B). Sulphide in breccia in order of abundance is galena, sphalerite and pyrrhotite.

Figure 18 b. Detail of slice beneath 18a. (approximate location shown in 18a). Transmitted light. Breccia ore with a high proportion of residual dolomite overprinting a once-continuous layer shows that fragment detachment is largely explained by dolomite replacement of the layer, with minimal transport of fragments. White areas are dolomite and minor quartz. Location; 8 orebody, 6910N, 2830R.L.

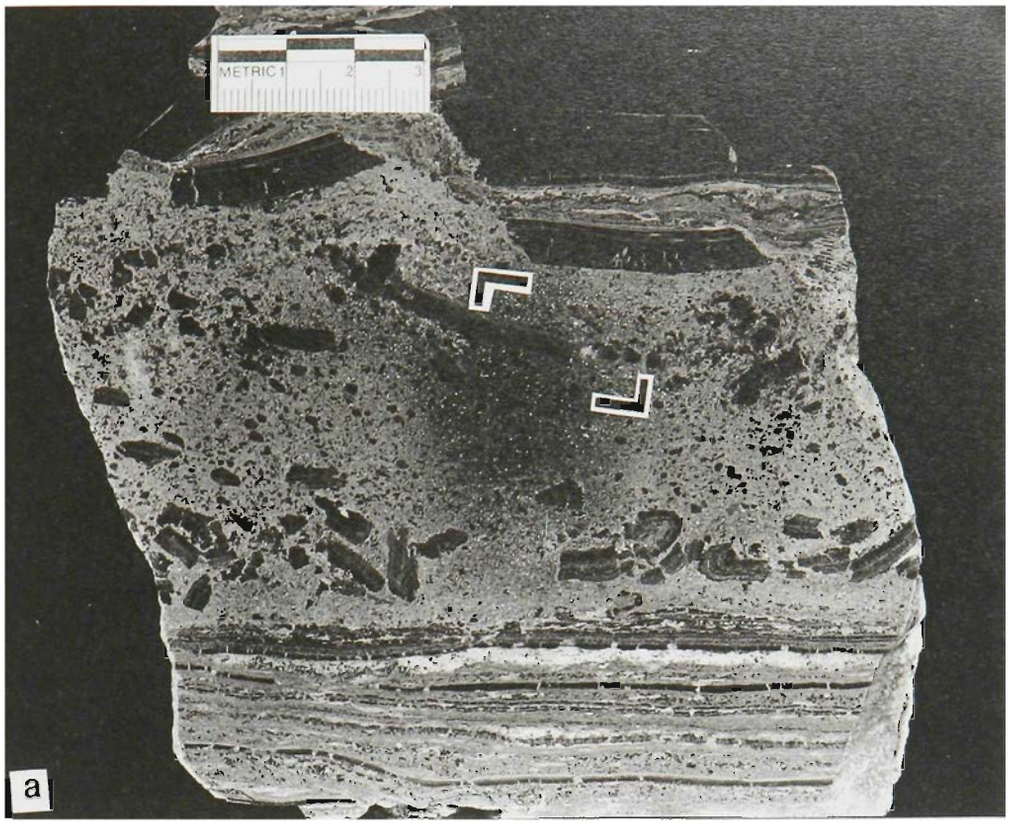
METRIC 1
2
3
a

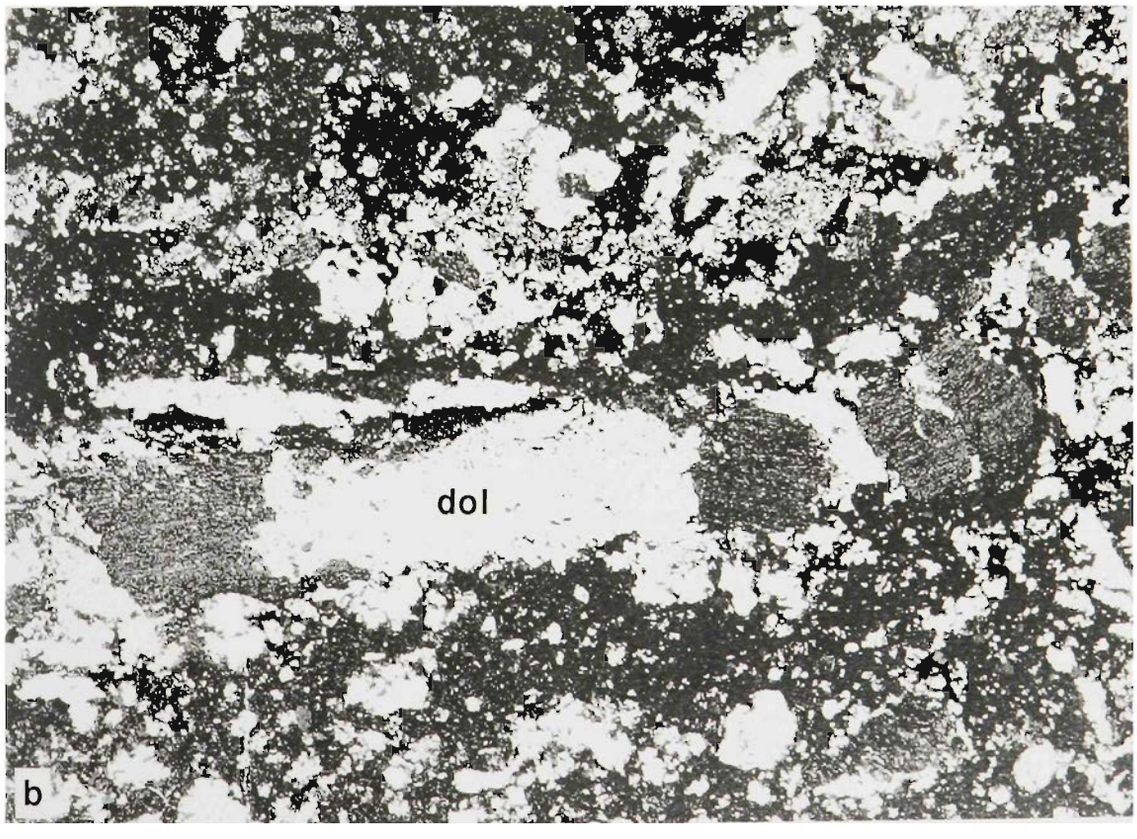
dol
b

Figure 19. Fold in carbonaceous band with fanning axial plane cleavage(s_3) surrounded by sphalerite, dolomite, quartz and pyrite. The dolomite and quartz boundary irregularly encroaches across laminations in the carbonaceous band, and on the fold limb cuts across an antithetic shear(S) which is subparallel to the axial plane cleavage. Different degrees of replacement on either side of the shear are obvious when related to the correlated light layer(A). Thin section. Location; M815 E. Decline, Surface, 870m.

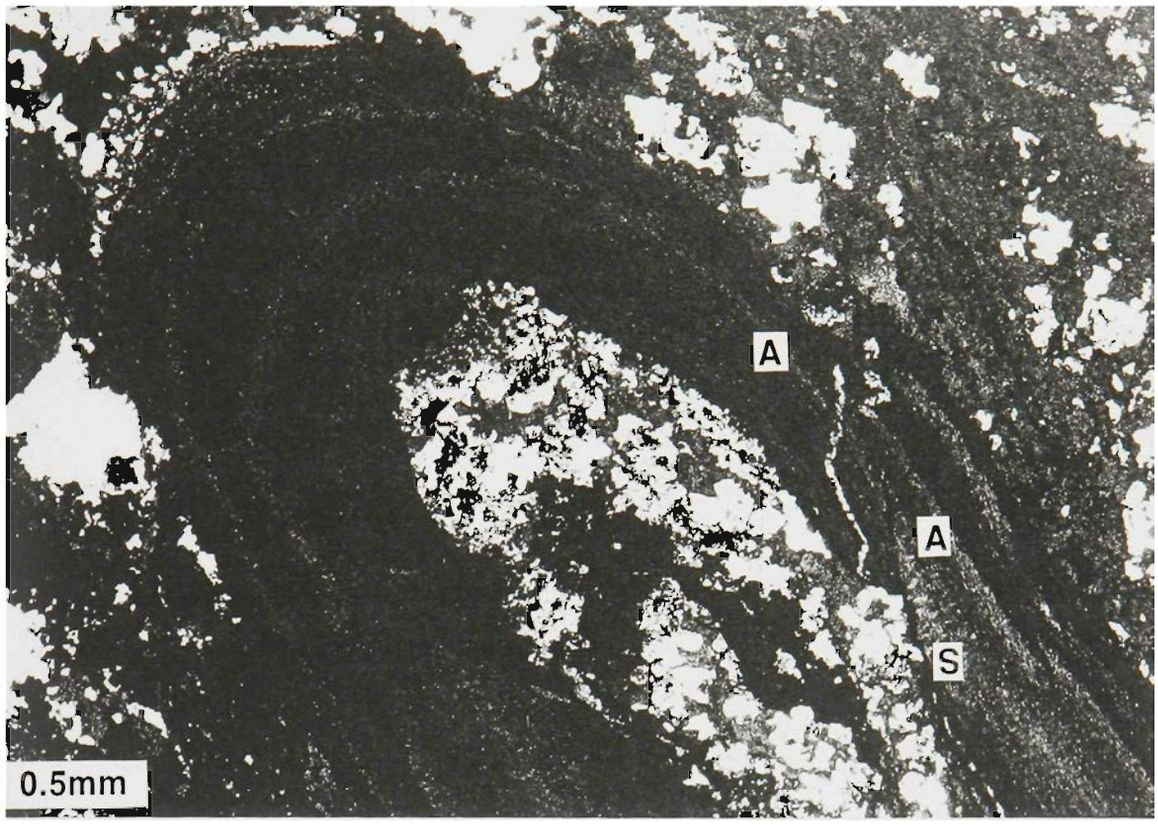
A
A
S
0.5mm

Figure 20 a. Extensional fractures, intrafolial folds and their relationship to alteration and mineralization. Shear surfaces cut through the non-mineralised layers and become more bedding-parallel in the sulphide-rich layers. These surfaces were subsequently deformed, particularly where narrower layers abut thicker ones (e.g. at A), and dilation is associated with shortening and tight folding in thin layers now surrounded by sulphide. Thin section, transmitted light.

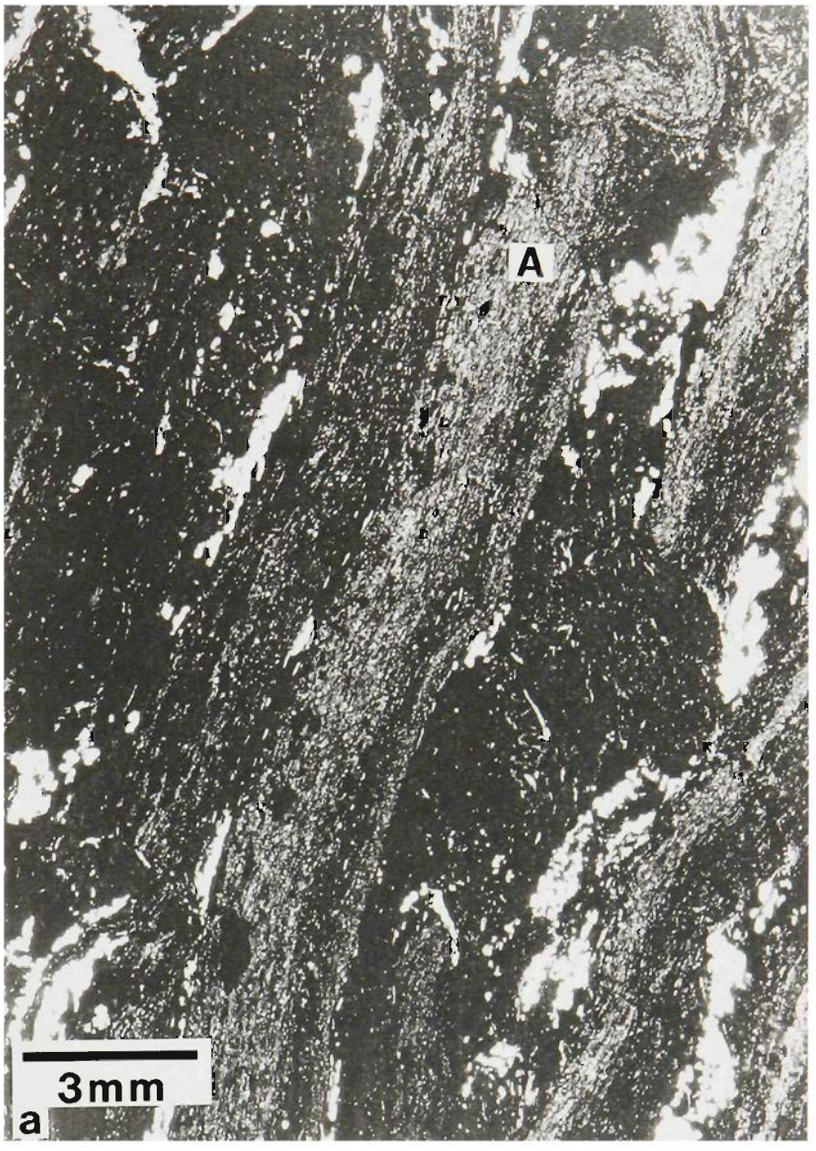
A
3mm
a

Figure 20 b. Highlighting of early shear zones from a. Light areas are quartz, dolomite, and chlorite. Shear zones are overprinted by these gangue minerals and subsequently by sulphides, with some fine-grained chlorite following the curved early shear zones. Section looking northwards. Location; 5 orebody, 14 level, 6666N, 1111E.

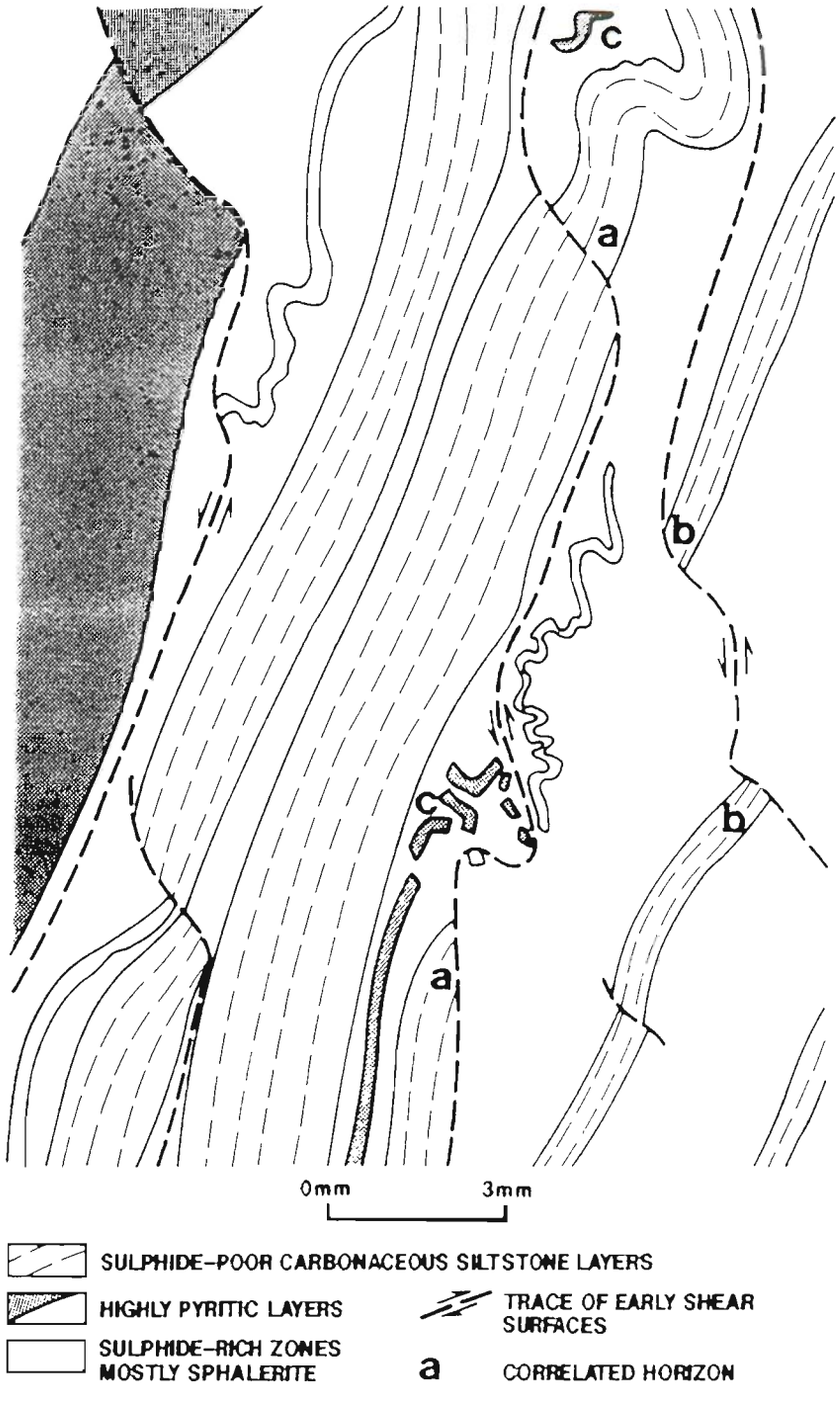
c
a
b
b
a
0mm
3mm
SULPHIDE-POOR CARBONACEOUS SILTSTONE LAYERS
HIGHLY PYRITIC LAYERS
SULPHIDE-RICH ZONES MOSTLY SPHALERITE
TRACE OF EARLY SHEAR SURFACES
a
CORRELATED HORIZON

Figure 21 a. Flexural fold around an east-dipping dolomite vein system controlling the distribution of metasomatic carbonate, pyrite and sphalerite. Correlated layers continue around the flexure as unmineralised siltstones.

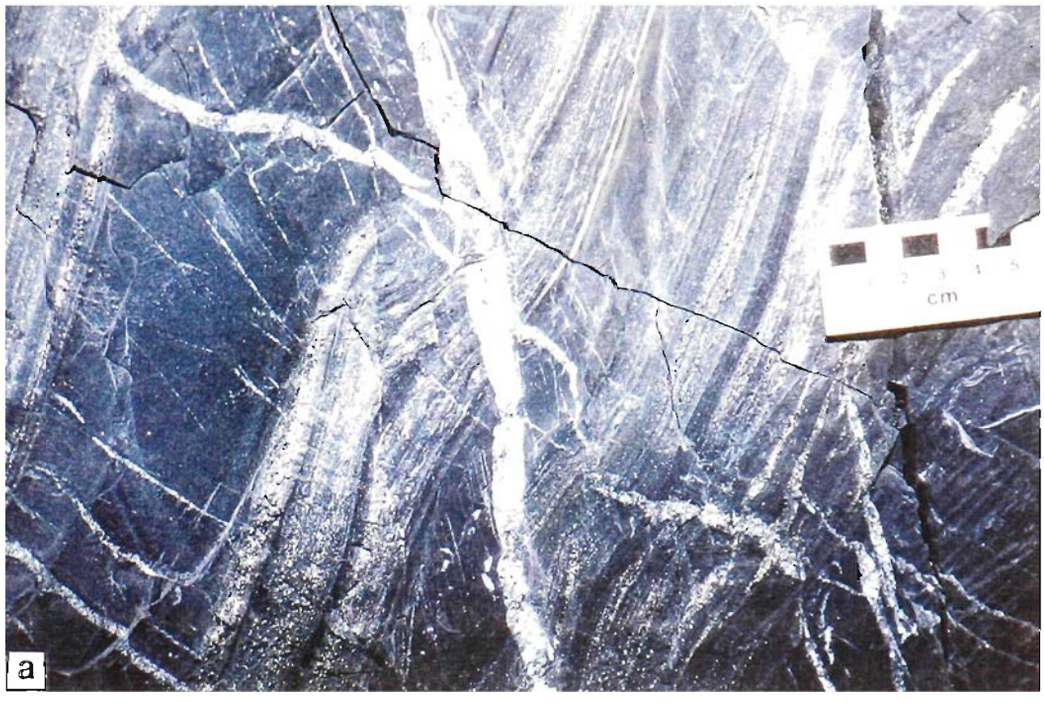
a
cm

Figure 21 b. Summary sketch, showing the abrupt diminution of pyrite and minor sphalerite along a near-vertical narrow vein. Looking north. Location; 14/10 Orebody, 6623N, 1820E, 2831R.L.

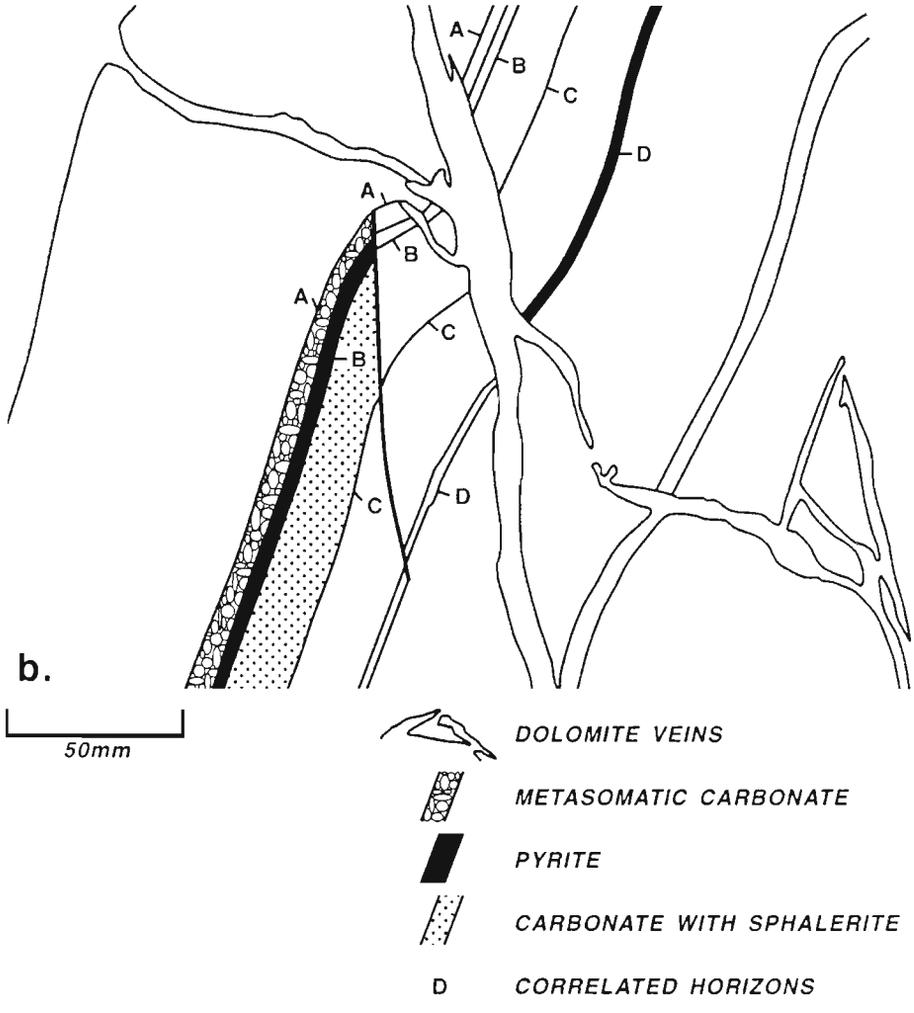
A
B
C
D
A
B
A
C
B
C
D
b.
50mm
DOLOMITE VEINS
METASOMATIC CARBONATE
PYRITE
CARBONATE WITH SPHALERITE
D
CORRELATED HORIZONS

Figure 22. Sphalerite(dark gray to black) front overprinting laminite and dolomitized mudstone. Dextral shear (by analogy with similar oriented samples) has dilated the central mudstone horizon making it amenable to dolomite replacement, leaving relict folds with cleavage S_3 at the dolomitization front. The base of the mudstone layer is also dilated and filled with coarse-grained dolomite and minor sphalerite. Randomly oriented chlorite sheaves occur around the upper sphalerite zone. Location; unknown, sample supplied by A. Rosenhein. Crossed Nicols.

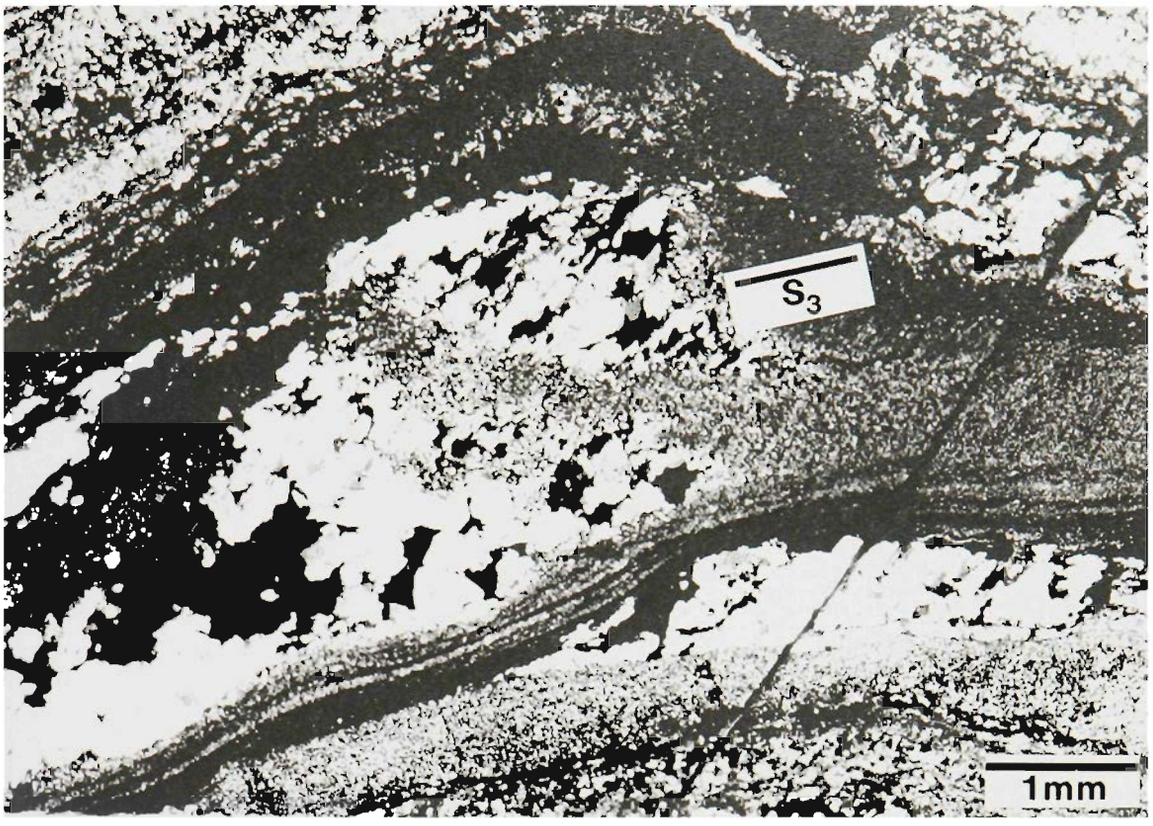
S_3
1mm

PART A.

Figure 23. a. Zone of discontinuous sphalerite controlled by east-dipping veins, in the "A" sequence. Major terminations of sphaleritic horizons are at A and B. Looking south.


A
B
a

Figure 23 b. Illustrative sketch of 23a.

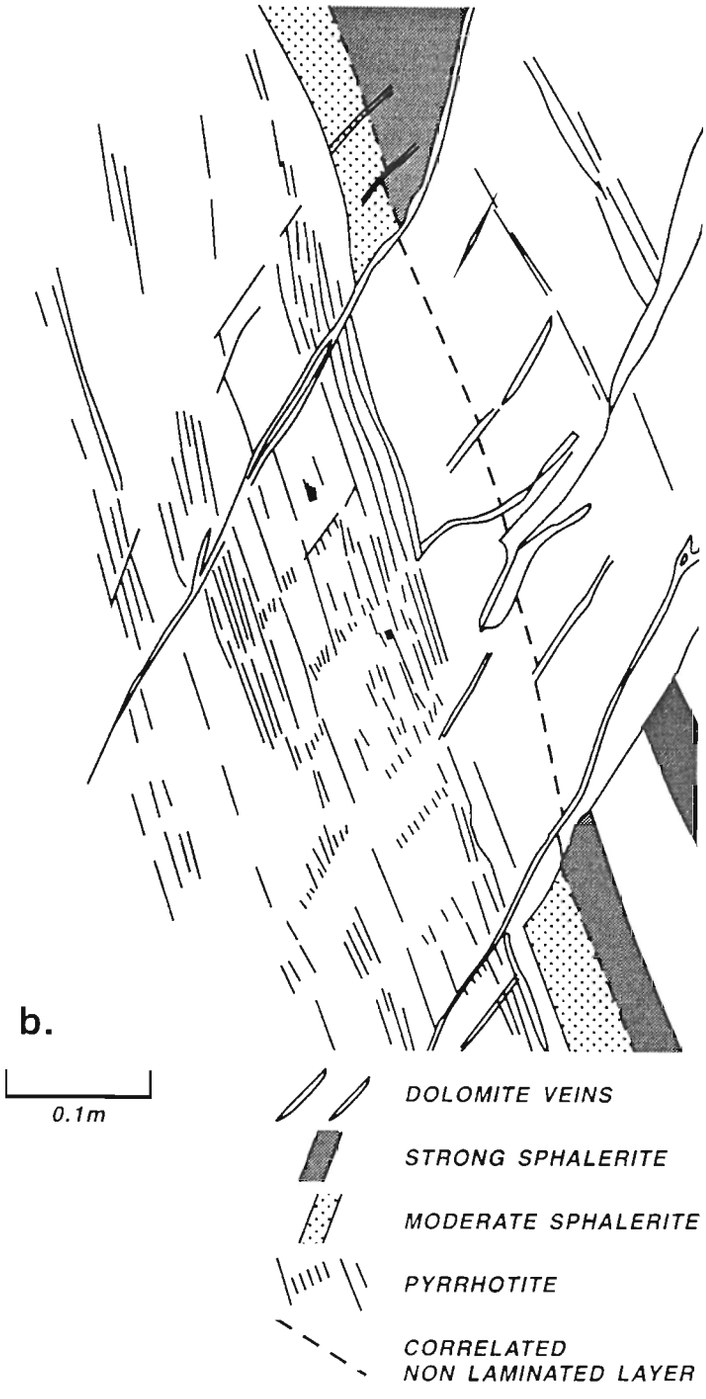
b.
0.1m
DOLOMITE VEINS
STRONG SPHALERITE
MODERATE SPHALERITE
PYRRHOTITE
CORRELATED
NON LAMINATED LAYER

Figure 23 c. Cored sample from B area of Figure 22a. Layers e.g. A match across the dolomite vein and sphalerite (yellow-brown) has formed on one side and not the other. Part of the sphalerite front coincides with a very minor vein to the right of the main vein with displacement. The highly reflective sulphide is pyrrhotite.

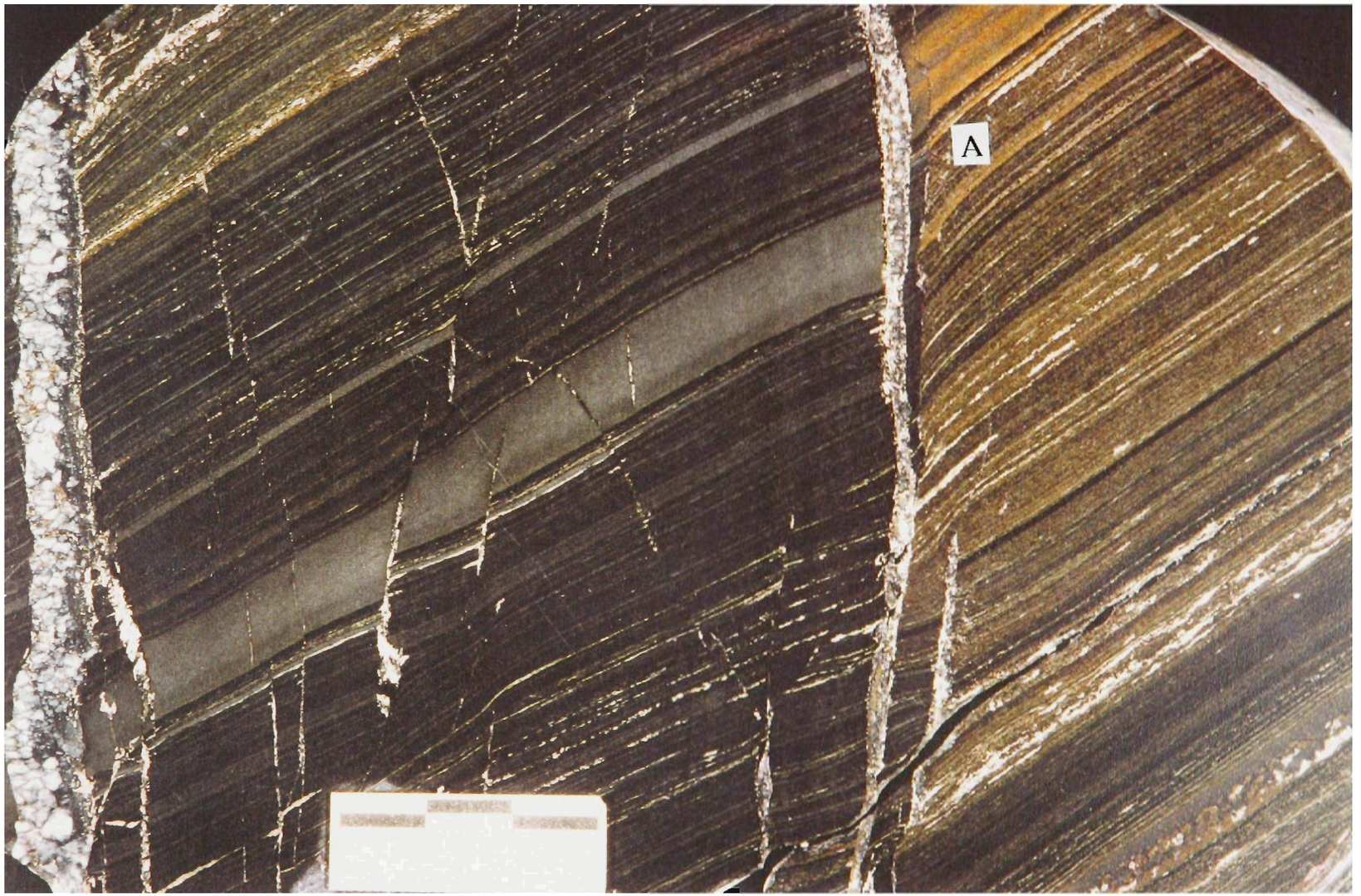
A

Figure 23 d. Sphalerite (black) front which is associated with both laminated and non-laminated units and the narrow vein within the non-laminated unit. The thicker vein away from the sphalerite front does not contain significant sphalerite. Note diminution of sphalerite associated with slight flexuring of bedding. Location; 7 orebody, 11 Level, 7174N. NB In all illustrations there is a high angle between the strike of both bedding and the veins and the observational plane.

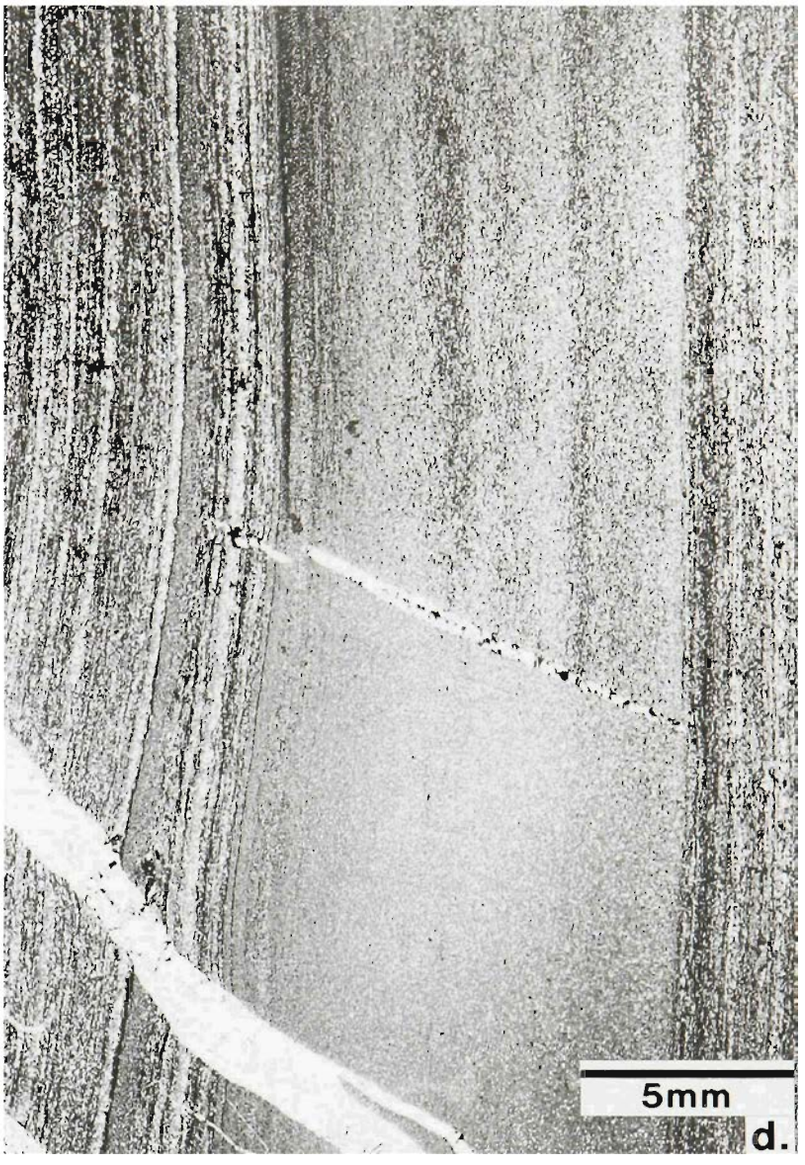
5mm
d.

Figure 23 e. Abrupt front of galena-rich (light gray) mineralization. Bedding-parallel and microvein-replacing galena is well developed on one side of the core and does not continue to the other. Chalcopyrite also occurs in veins. The host siltstone is both strongly chloritized and silicified. Location; I702 Vert. 446.4m.

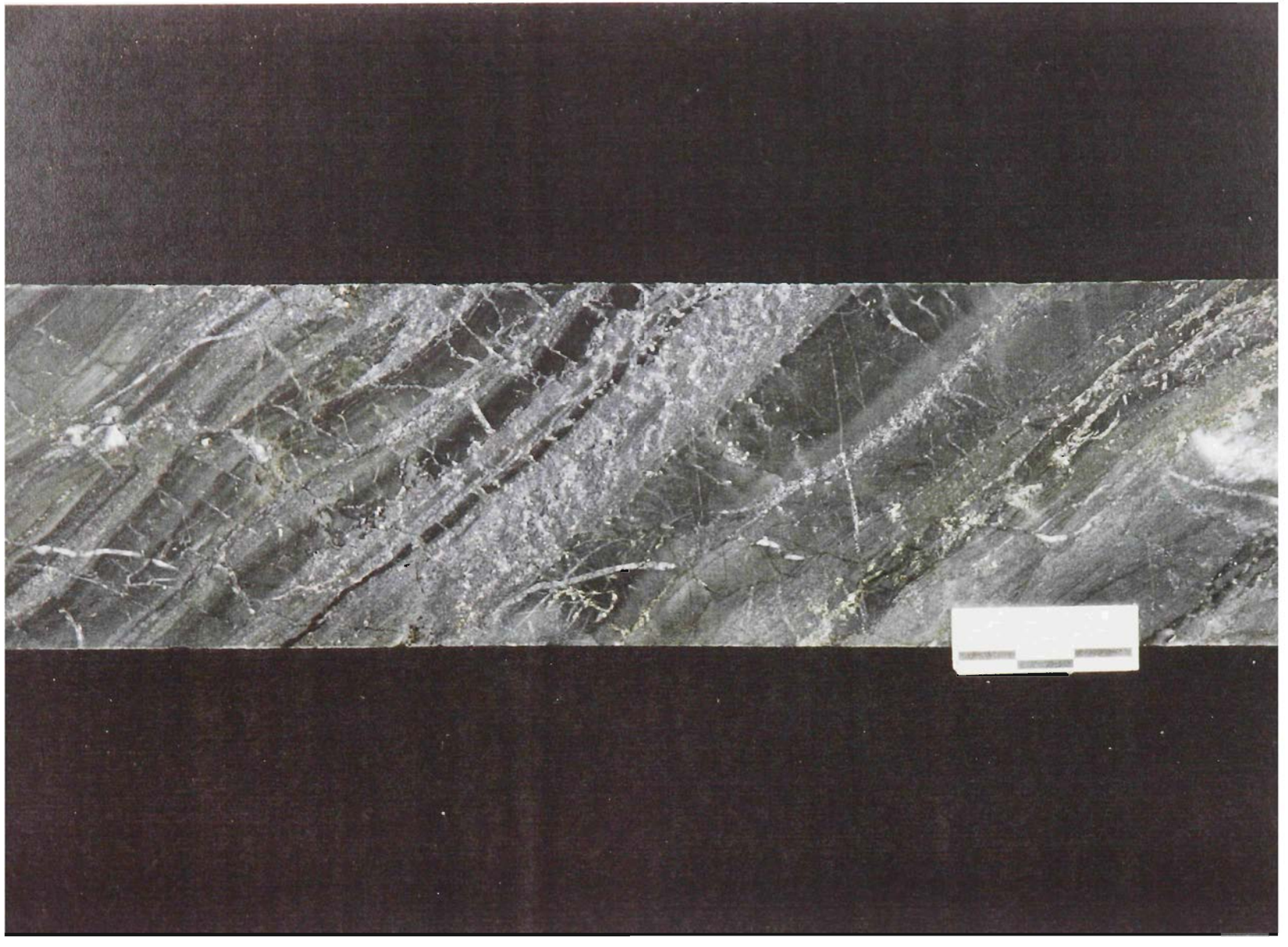

Figure 24. Orientations of fractures and veins which control replacive fronts of mineralization. Veins are related to bedding in their immediate vicinity, with corresponding notation for veins and bedding at the same locality (four sites). Poles to planes. Equal area projection.

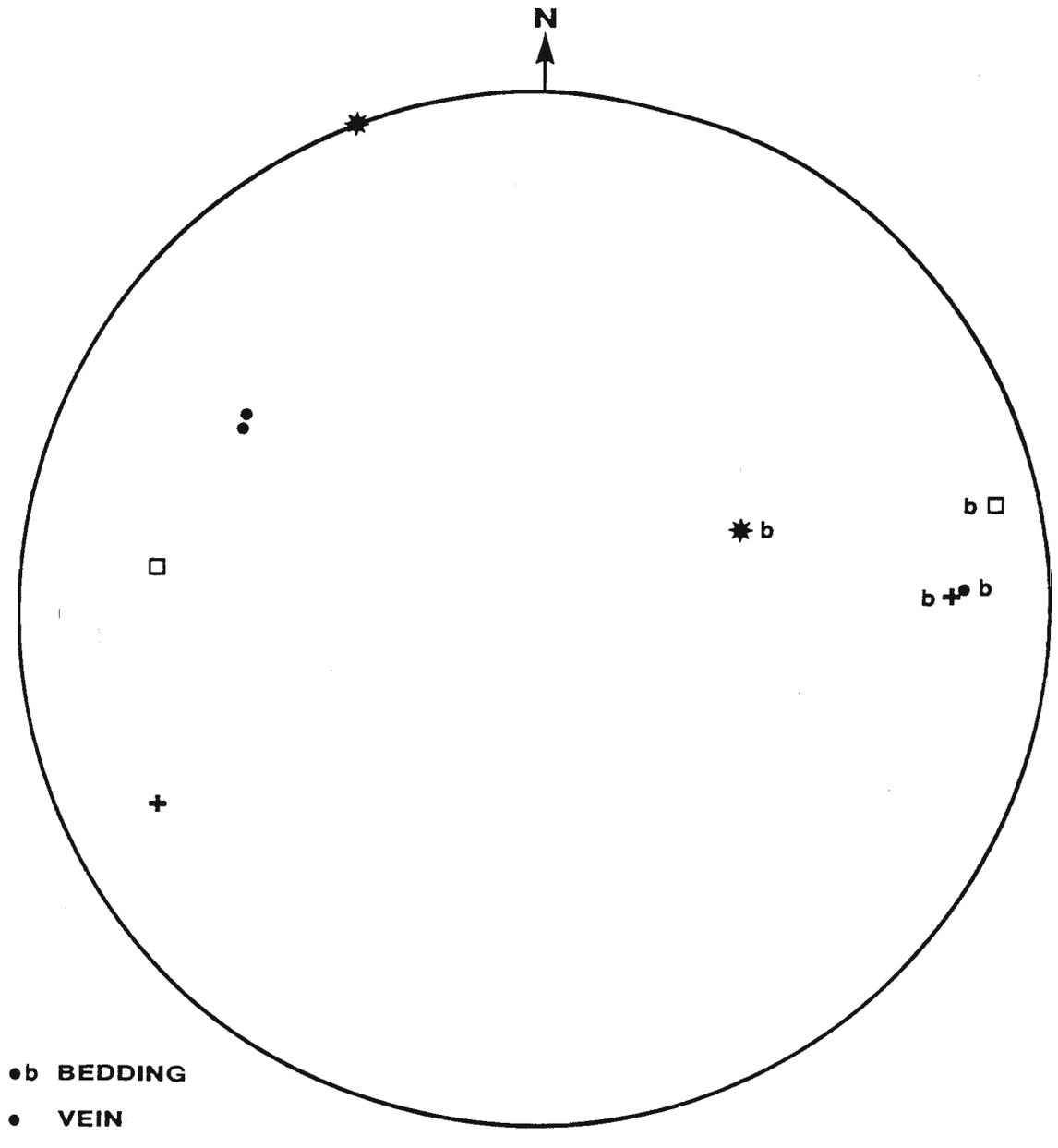
N
b
b
b
b
●b BEDDING
● VEIN

Figure 25. Illustration of the difference between the expected patterns of sulphide-gangue boundaries related to deformation. (a). deformed sulphide-gangue aggregate subsequently recrystallised. Indication of prior deformation is preserved in the gross shapes of the sulphide/gangue boundaries. (b) post deformation replacement of gangue by sulphide.

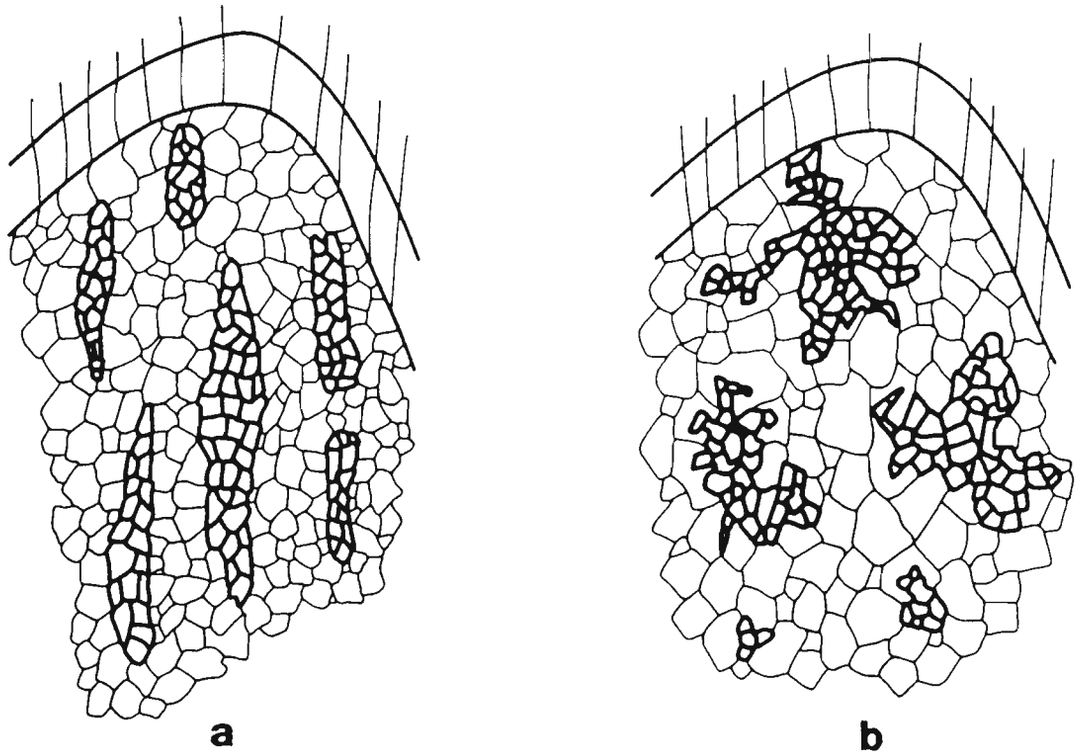
a
b
BEDDING AND CLEAVAGE
CARBONATE GANGUE
SULPHIDE

Figure 26. Diagram to illustrate the mineralization sequence of a hypothetical single-system Cu-Pb-Zn ore formation model. The alteration pattern is previously established, and the mineralizing system grows outwards from stage 1 to stage 2. Mineralization overprints along bedding, bedding-parallel dolomitic alteration, breccia veins and simple dolomite veins. Earlier-deposited fine-grained pyrite is very locally replaced by all other sulphides, and economic sulphides replace each other in the sequence sphalerite, galena and chalcopyrite. As later sulphides replace earlier-deposited sulphides, the pre-existing components migrate to precipitate in more cross-cutting outer sites.

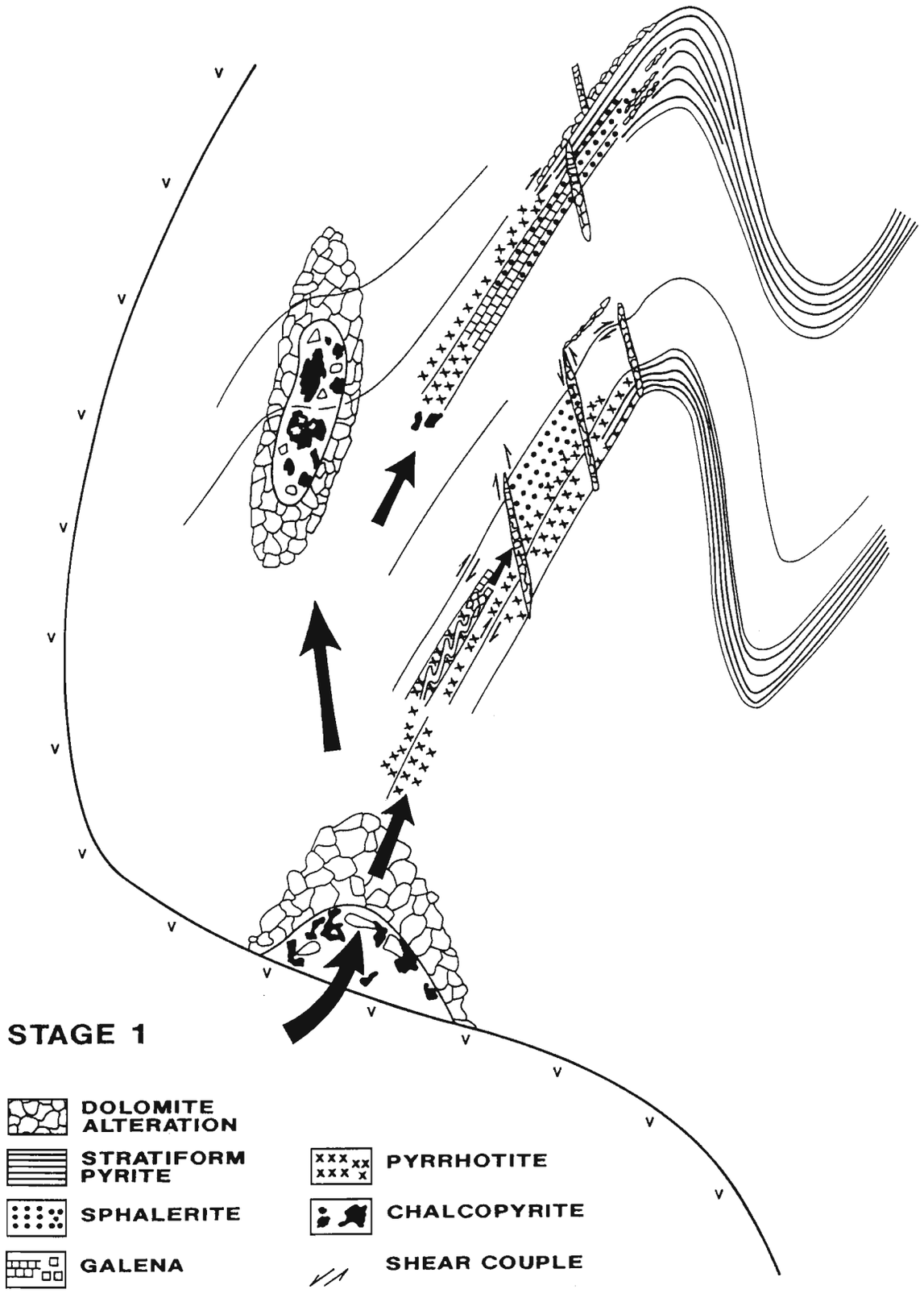
STAGE 1
DOLOMITE ALTERATION
STRATIFORM PYRITE
SPHALERITE
GALENA
PYRRHOTITE
CHALCOPYRITE
SHEAR COUPLE

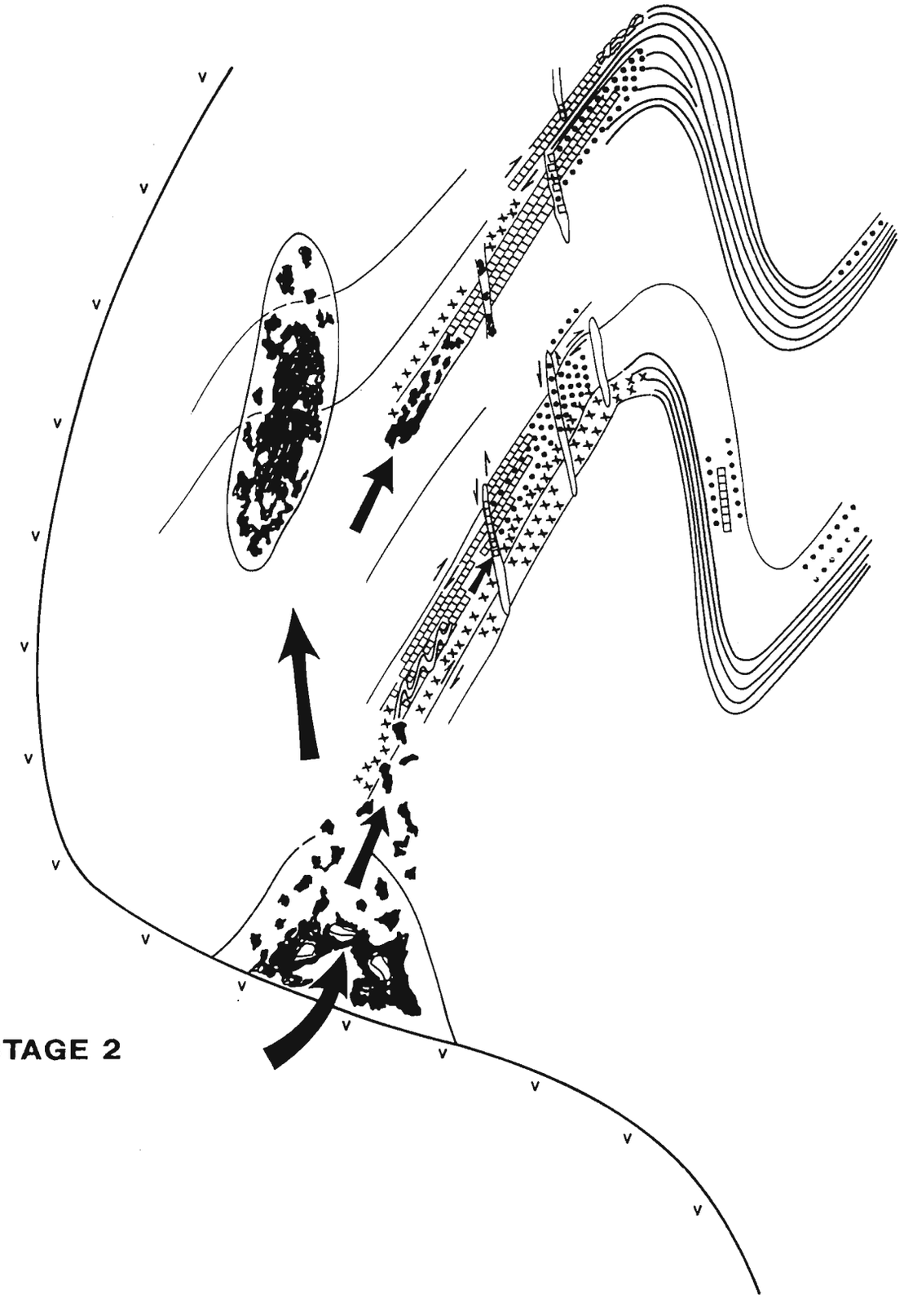

STAGE 2

PART B.

Timing of Formation of Proterozoic Stratiform Fine-Grained Pyrite: Post-Diagenetic Cleavage Replacement?

Figures 1-9

PART B.

Figure 1 a. Underground exposure of stratiform pyrite. Pyrite-rich horizons are finely laminated and separated by non-laminated carbonaceous siltstones. The more reflective "brassy pyrite" e.g. A has both uneven thickness along bedding, and abrupt discontinuities across steep veins. Laminae of finer-grained pyrite(B) are duller and more continuous along laminations. The most highly reflective sulphide (C) is pyrrhotite which is along bifurcations in the bedding and disseminated around minor faults. Location 5 orebody, 11 Level, 6540N.

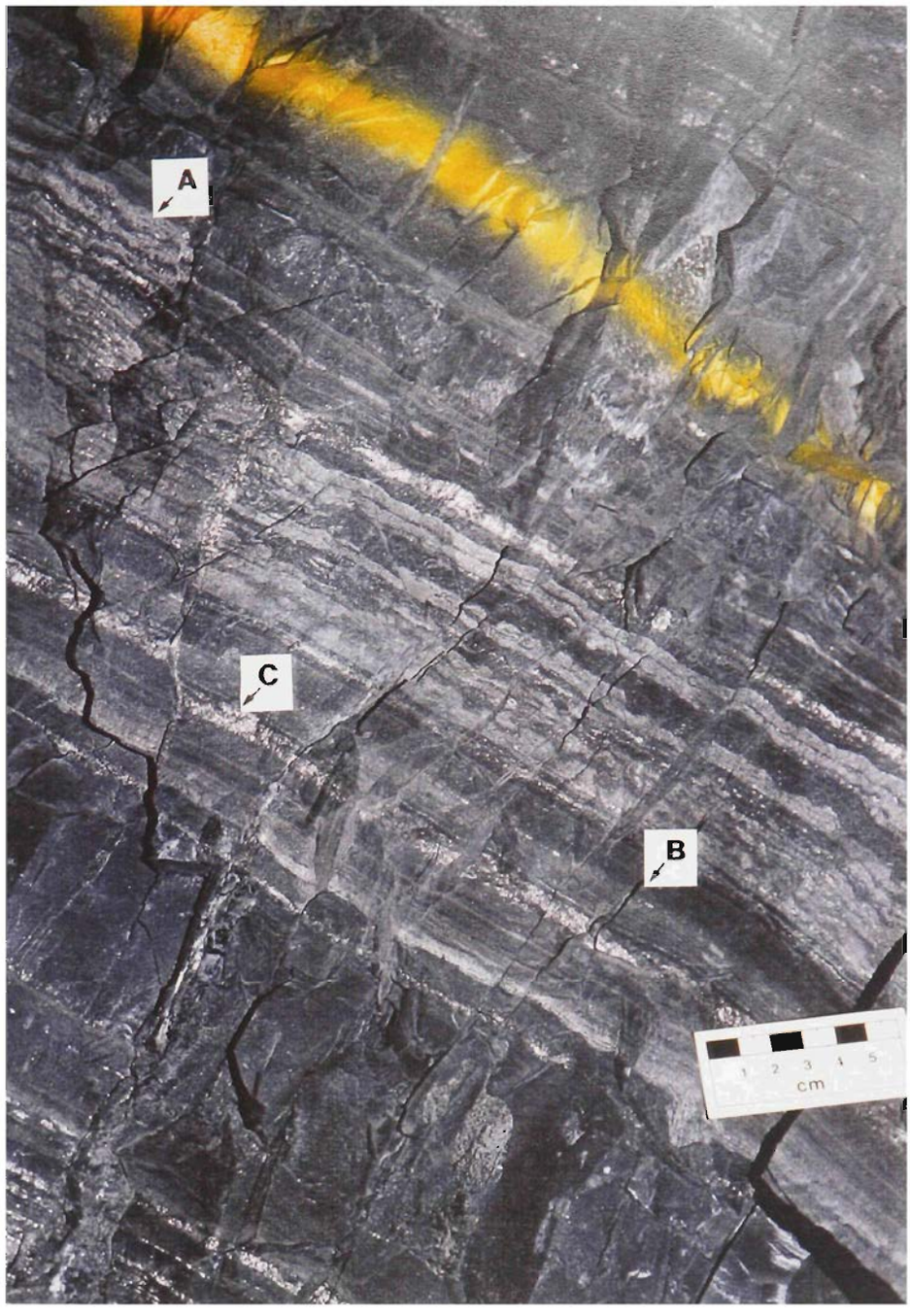
A
C
B
1 2 3 4 5
cm

PART B.

Figure 1 b. Fine-grained pyrite-rich siltstones, with dolomite veins and neomorphic dolomite along bedding. Pyrite-rich layers at A are transected by spaced pyrite bands parallel to S_3 cleavage. In the areas of greater dolomite concentration along bedding (e.g. B), similar fine-grained pyrite outlines bedding traces. Location, 7 orebody, 7 Level, 7050N.


S_3
A
B
0
5
10
15
20
cm

PART B.

Figure 2. Rock slab. Textural varieties of fine-grained pyrite in a single sample. Brassy pyrite (lightest color along bands) of variable grain size concentrates in the slightly less carbonaceous laminae and terminates on fine fractures and the larger dolomite vein. There is no differential shortening between the pyrite-rich and pyrite-free parts of the layer, showing that replacement is late in the deformation history. Fine-grained pyrite (e.g. A), in contrast, is preferentially concentrated in the darker finely laminated layers, and does not vary in density across the fractures and veins. Coarser euhedral pyrite is strung along a fracture on the left which separates different concentrations of finer euhedral pyrite. Sphalerite(sph) occurs as rounded 50-100 micron aggregates along layers. The finely laminated grey layers are galena(ga)-rich. Location; K740E. Hor. 12A sublevel, 8.4m. 5 orebody.

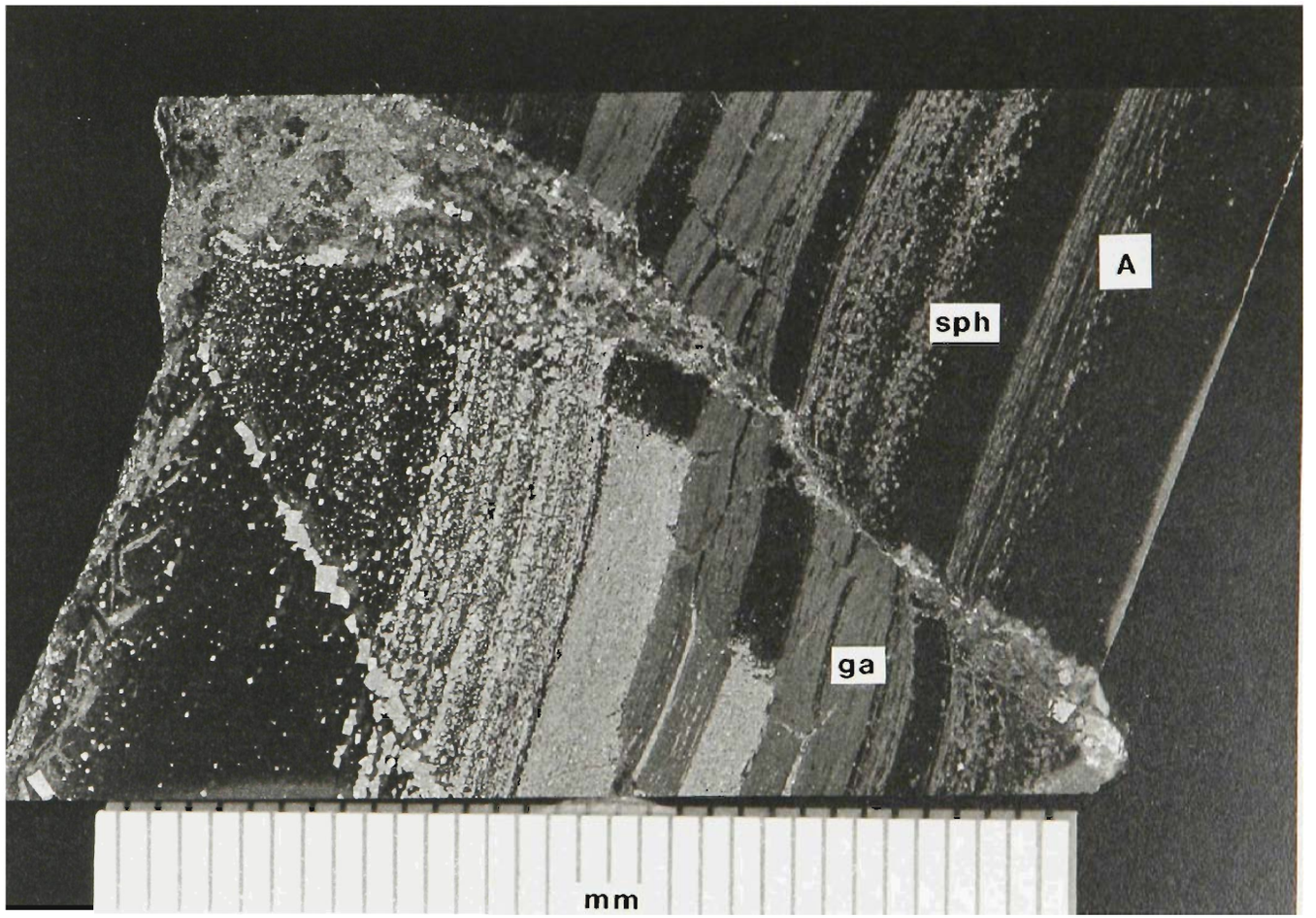
A
sph
ga
mm

Figure 3. Detail of wavy or anastomosing pattern of stratiform fine-grained pyrite. Pyrite is concentrated in carbonaceous cleavage seams which are parallel to both bedding (horizontal) and S_3 cleavage. The bulk of the fine gangue material is dolomite. Location; 6 orebody, 11 Level, 7172N,1652E.

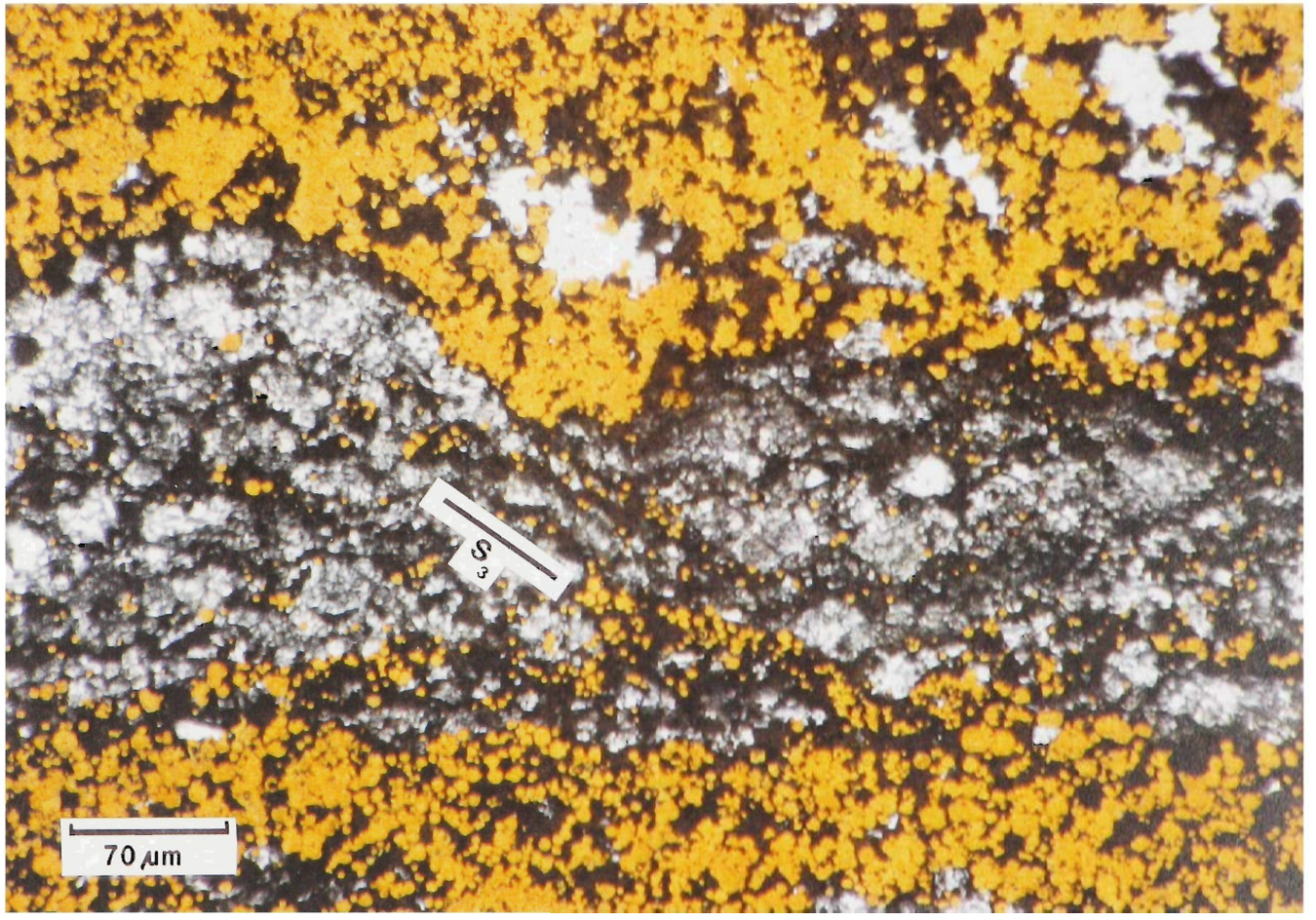
S3
70 µm

PART B.

Figure 4. Textural varieties of fine-grained pyrite. a. Mainly sub-spherical cores having a suggestion of a lighter colored rim, with central(doubly zoned), inclusion-rich annulus and irregularly developed clean outer zone.

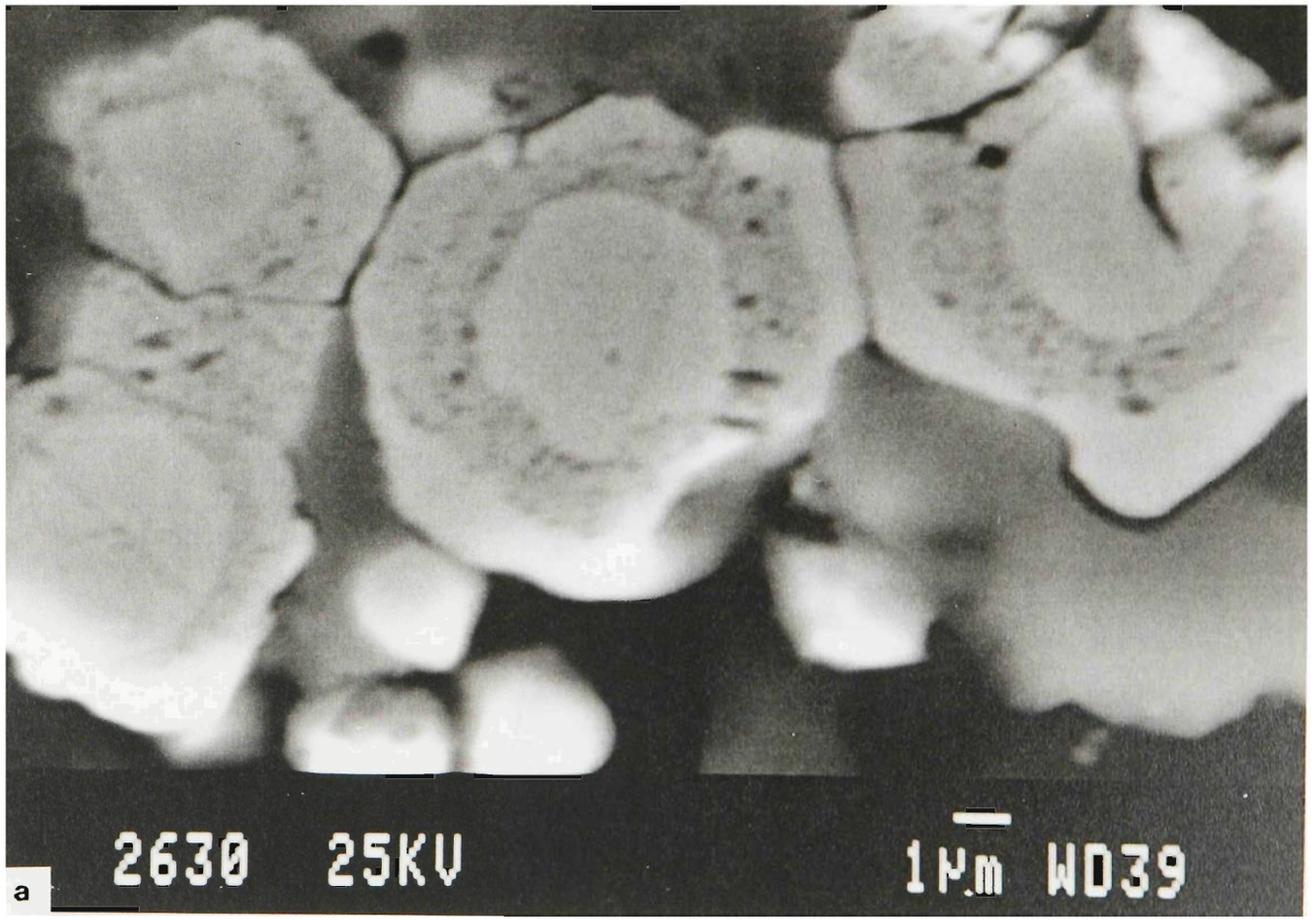

a

PART B.

Figure 4 b. Coalescing bodies with sub-spherical cores, fairly uniform inclusion-rich zone and poorly developed outer zone.

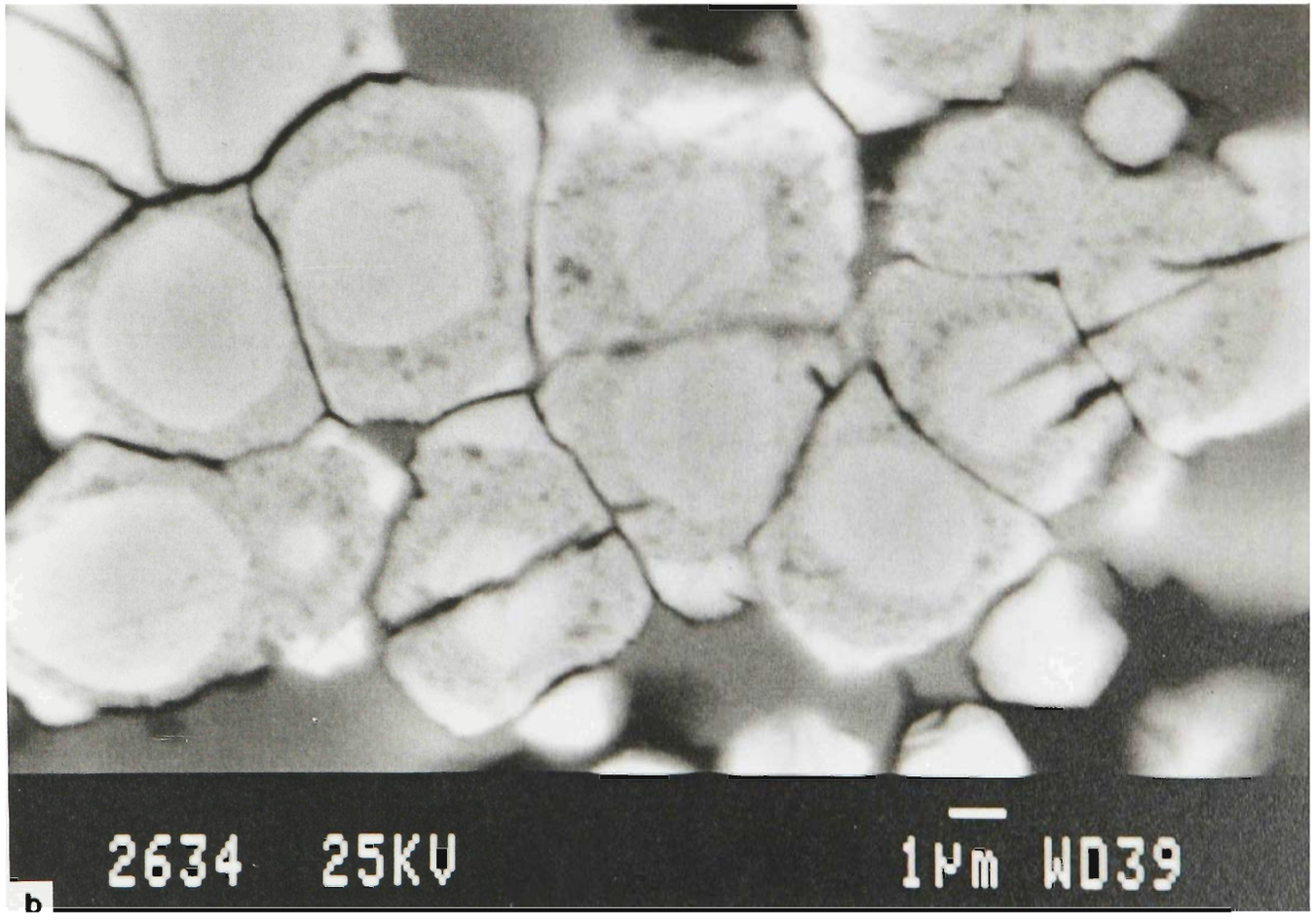
2634 25KV
1µm WD39
b

PART B.

Figure 4 c. Tetragonal body with triangular core (on left), and tendency to preferential growth of outer zone at corners. The other two bodies also show preferential growth towards "star-shaped" outer zones. SEM photomicrographs, samples etched with HNO_3. Location; same as Figure 3.

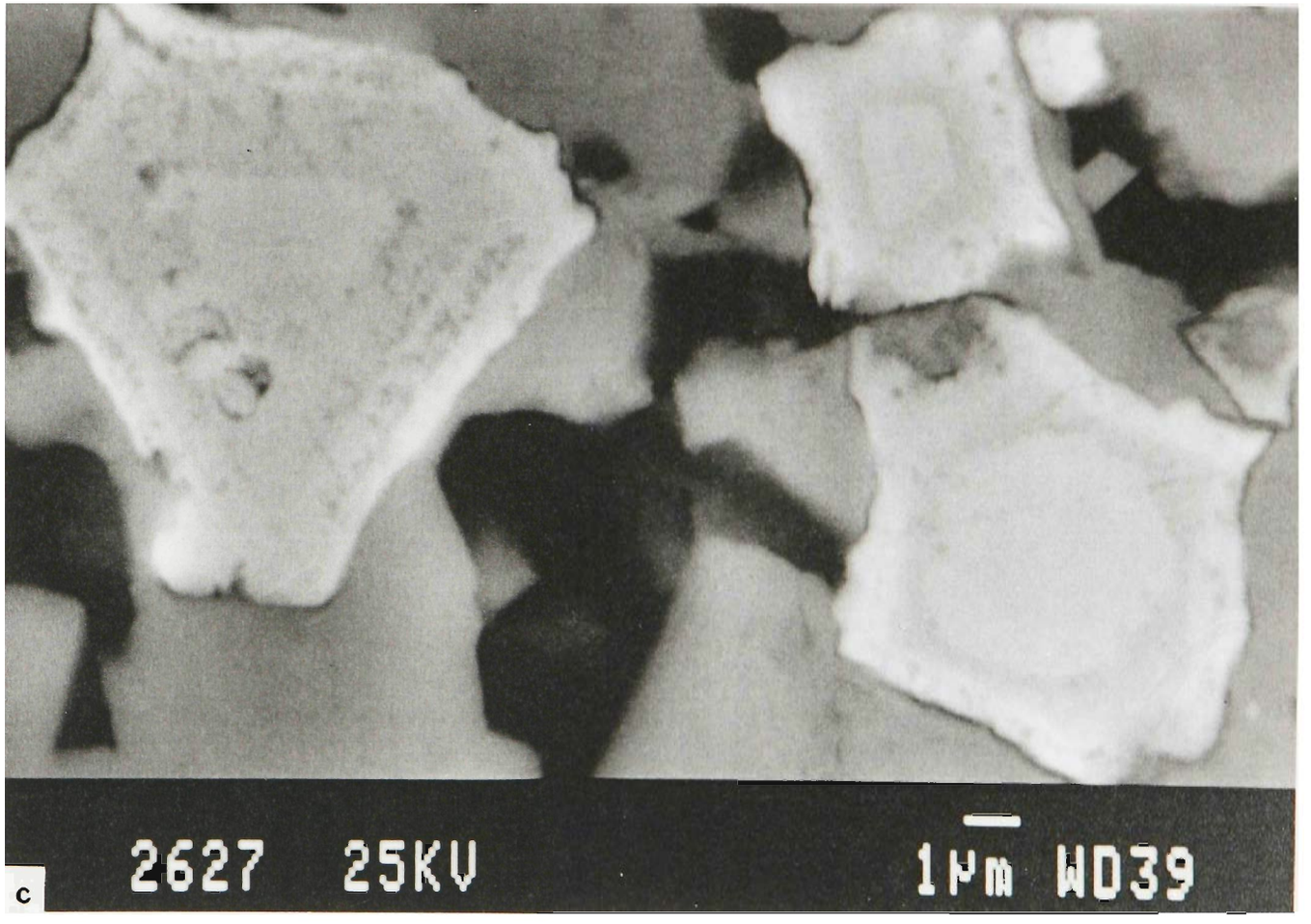

c

PART B.

Figure 5. Distribution of fine-grained pyrite (also includes bedding-parallel brassy pyrite).
a. 6999N cross-section. Pyrite concentration projected from 24 diamond drill holes on the section which have percentages of pyrite logged by mine geologists, and including development mapping and old drill holes which have pyrite quoted as 5-20% and >20%.

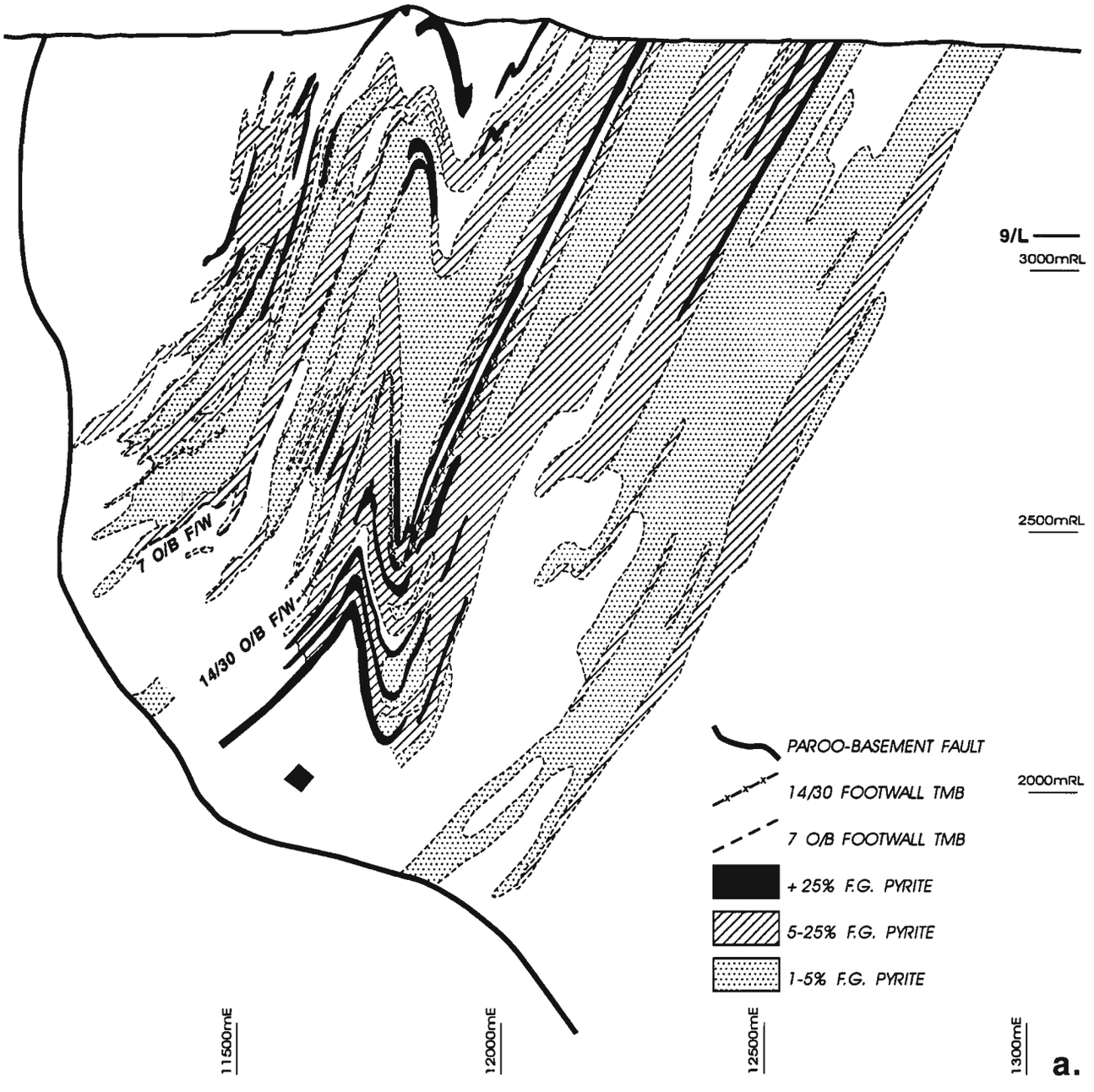
9/L
3000mRL
2500mRL
2000mRL
7 O/B F/W
14/30 O/B F/W
PAROO-BASEMENT FAULT
14/30 FOOTWALL TMB
7 O/B FOOTWALL TMB
+ 25% F.G. PYRITE
5-25% F.G. PYRITE
1-5% F.G. PYRITE
11500mE
12000mE
12500mE
13000mE
a.

PART B.

Figure 5 b. Plan of 9 level (390m. below surface). Pyrite concentration projected from diamond drill holes logged in percentages on sections shown on the right, and interpolated to development intersections mapped as 5-20% and >20%. Reference to the stratigraphic markers, in particular the 7 orebody and 14/30 tmbs, shows the transgression across stratigraphy of pyritic zones, in particular the migration of the greatest concentration of >25% pyrite from beneath 14/30 orebody in the area around S48 fault to the north-west where it lies above the 7 orebody marker.

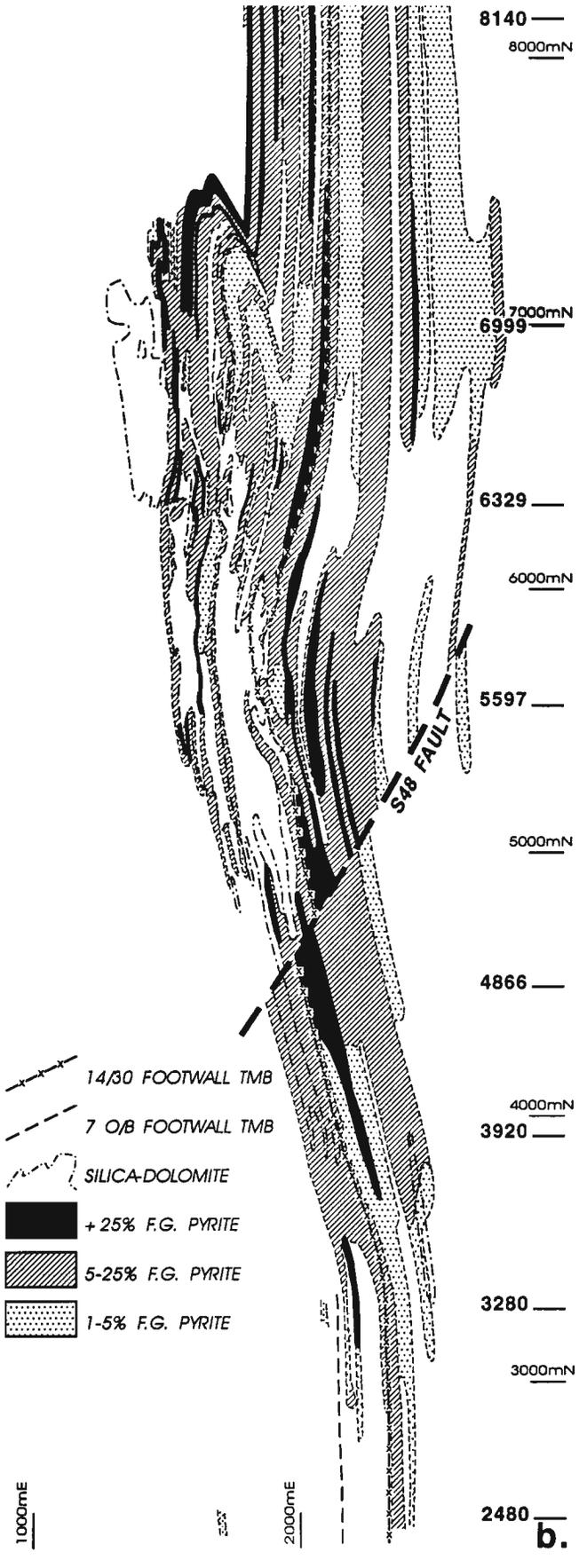
8140
8000mN
7000mN
6999
6329
6000mN
5597
S48 FAULT
5000mN
4866
4000mN
3920
3280
3000mN
2480
14/30 FOOTWALL TMB
7 O/B FOOTWALL TMB
SILICA-DOLOMITE
+25% F.G. PYRITE
5-25% F.G. PYRITE
1-5% F.G. PYRITE
1000mE
2000mE
b.

Figure 5 c. Plan of 9 level showing distribution of lead-zinc ore and the silica-dolomite boundary. In conjunction with 9b, it shows how the pyrite distribution relates to lead-zinc orebodies, and where detailed pyrite distribution data from mine development and orebody drilling is available.

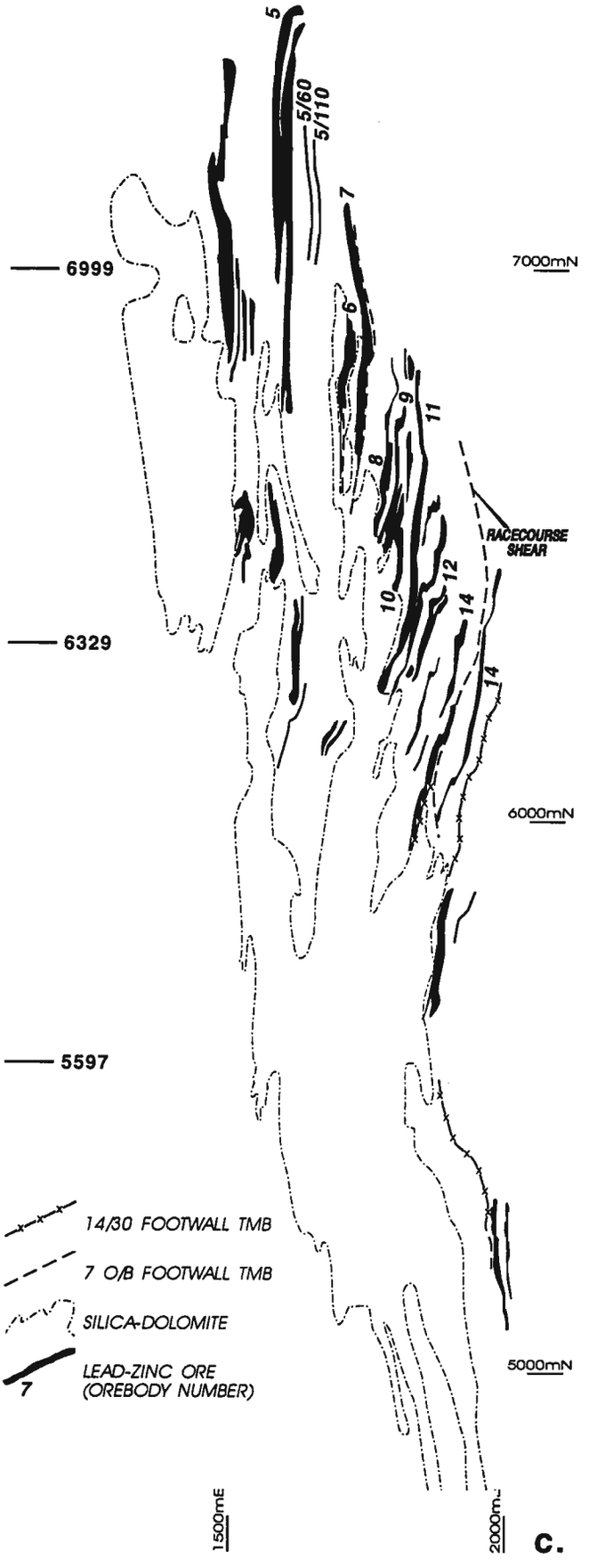
5
5/60
5/110
7
6
9
11
8
RACECOURSE SHEAR
12
10
14
14
6999
6329
5597
7000mN
6000mN
5000mN
14/30 FOOTWALL TMB
7 O/B FOOTWALL TMB
SILICA-DOLOMITE
LEAD-ZINC ORE (OREBODY NUMBER)
7
1500mE
2000mE

C.

PART B.

Figure 6 a. Longitudinal projection of 7 orebody with distribution of concentration of fine-grained pyrite. The drill holes represented have been logged in detail using the same stratigraphic intervals, and visual pyrite concentrations have been checked against Fe and S assays. The width shown is stratigraphic measured from the top of the A sequence to the footwall tmb. The approximate concentration of fine-grained pyrite comes from examination of holes shown in Fig 6b. Note that the central zone of the orebody from approximately 6800mN. to 7100mN. is highly pyrrhotitic.

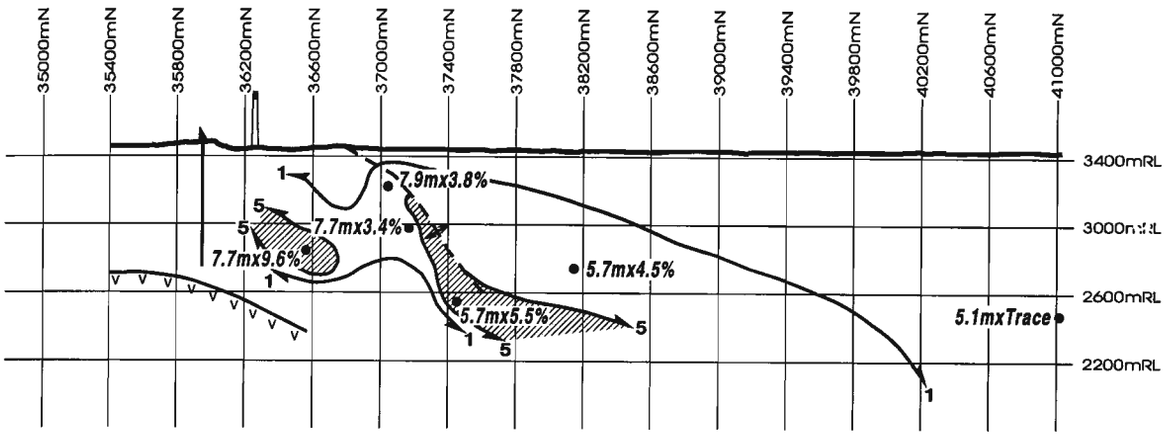

ANTICLINAL HINGE (Mt Isa Fold)

GREENSCHIST CONTACT

5.7mx4.5% DETAILED MEASUREMENT (width x pyrite %)

5% F.G. PYRITE

1% F.G. PYRITE

PART B.

Figure 6 b. Longitudinal projection of the B sequence in the hangingwall of No. 7 orebody showing boundaries and concentration of fine-grained pyrite.

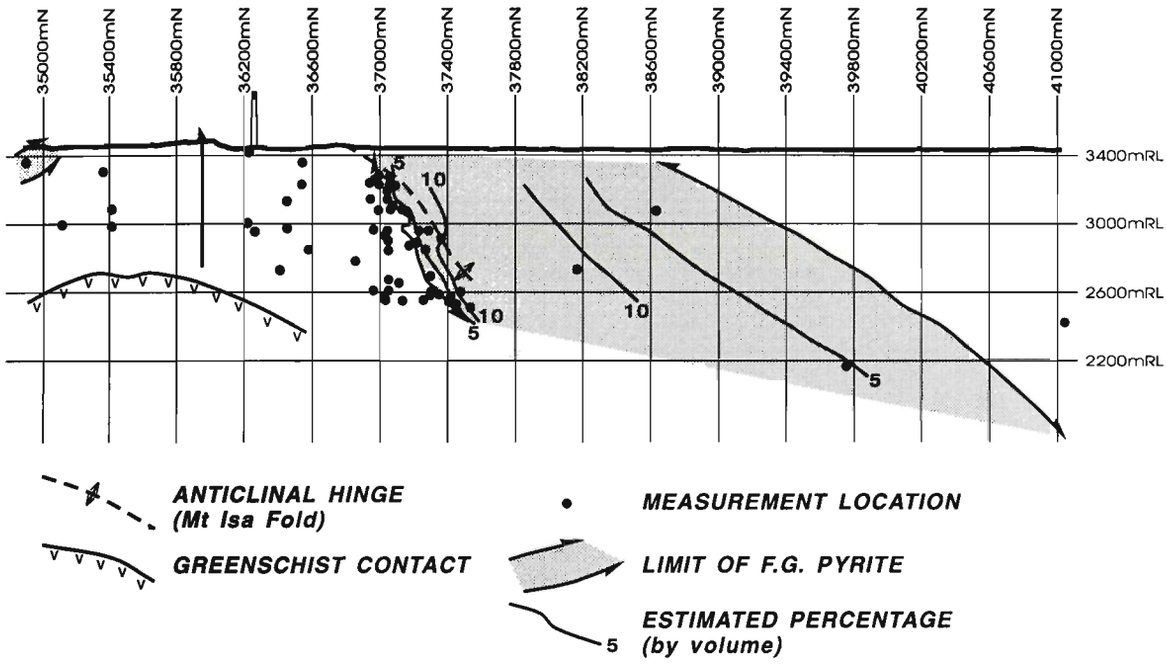
35000mN
35400mN
35800mN
36200mN
36600mN
37000mN
37400mN
37800mN
38200mN
38600mN
39000mN
39400mN
39800mN
40200mN
40600mN
41000mN
3400mRL
3000mRL
2600mRL
2200mRL
5
10
10
5
10
5
ANTICLINAL HINGE
(Mt Isa Fold)
GREENSCHIST CONTACT
MEASUREMENT LOCATION
LIMIT OF F.G. PYRITE
ESTIMATED PERCENTAGE
(by volume)
5

PART B.

Figure 7 a. Comparison of distal unmineralised laminite (A) with its pyrite-bearing correlative (B), in the B sequence. The upper light colored layer (T), which is above coarse-grained pyrite in A and contains it in B, is a TMB marker unit, in both cases consisting largely of muscovite. Shard textures are well preserved in the carbonaceous band at the base of the marker in A, and vaguely visible in the micaceous area of B. The fine-grained pyrite (P) is preferentially associated with the finely laminated zone, with the unlaminated layers being largely devoid of pyrite. True thickness comparisons are 14mm for the equivalent intersection in (A) and 13mm for the pyritic intersection in B.

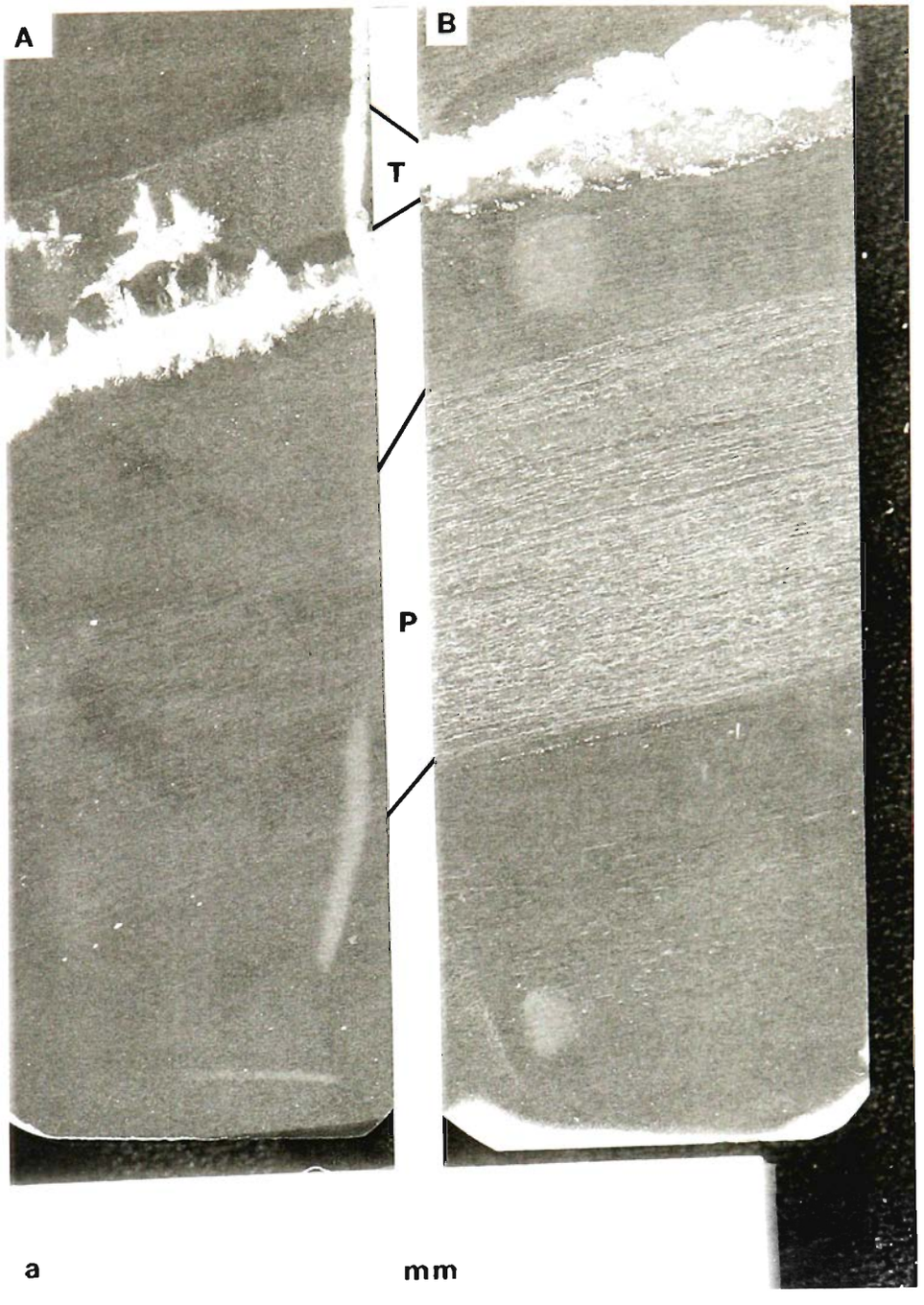
A
B
T
P
a
mm

PART B.

Figure 7 b. Thin sections of a. The zone containing fine-grained pyrite (P) in B can be matched with corresponding laminae in A. There is no change in the nature of bedding lenticles above the abrupt upper limit of pyrite, although the darker areas with pyrite are highlighted. Location (A) QZ 10, 1034.8m., (B) M815, 730.6m.

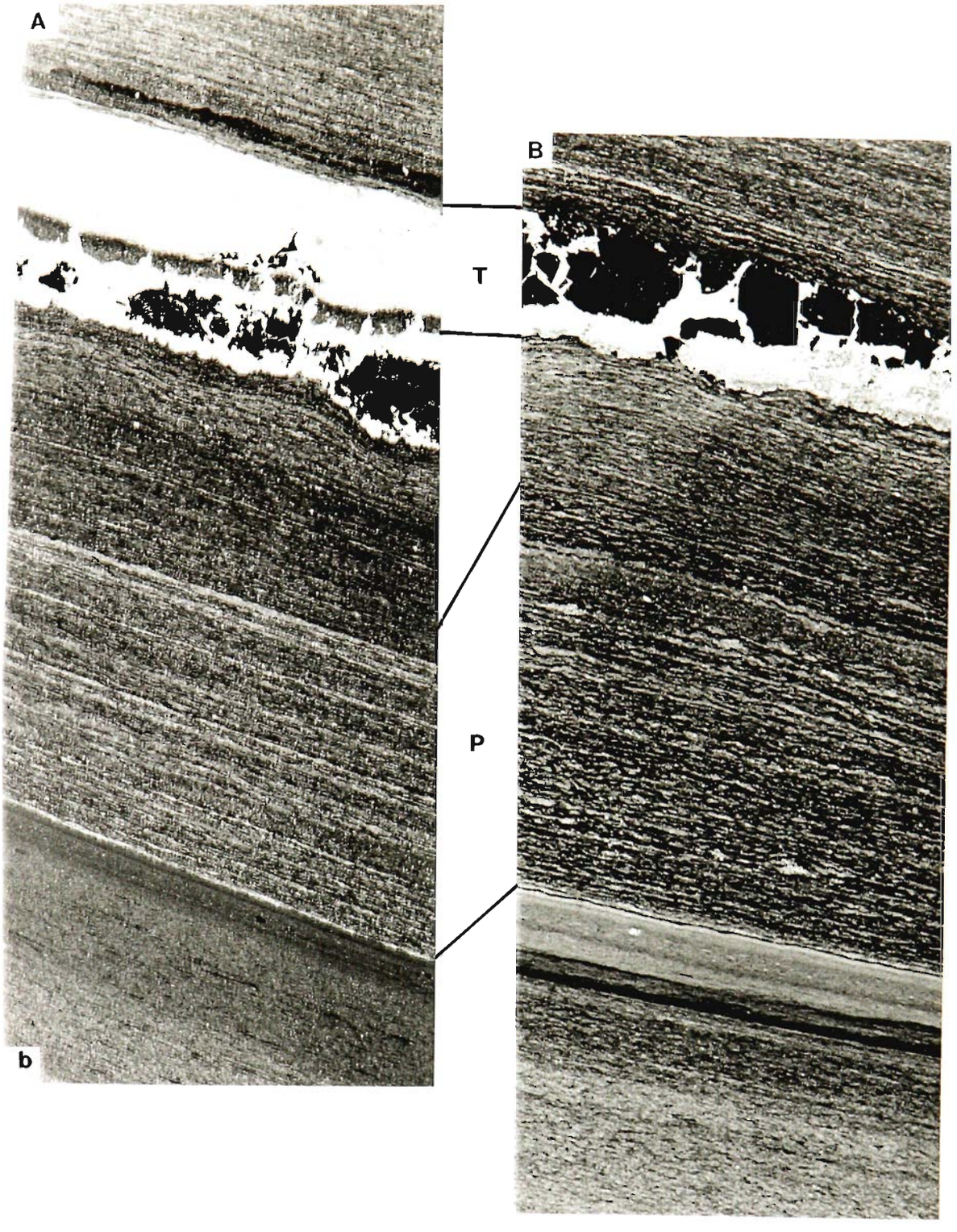
A
B
T
P
b

Figure 8. Thin section. Fine-grained pyrite (dark bands in centre) in a fold with well-developed axial plane cleavage. Although the pyrite is preferentially in the more laminated strata, it's density distribution relates to cleavage domains and cannot be caused by differential dissolution of matrix material.

Figure 8 b. Detail of a. Fine-grained pyrite density varies considerably between cleavage domains and individual pyrite spheroids overprint along cleavage seams. Bedding is approximately horizontal. Location; 17 Level, 4807N, 1804E.

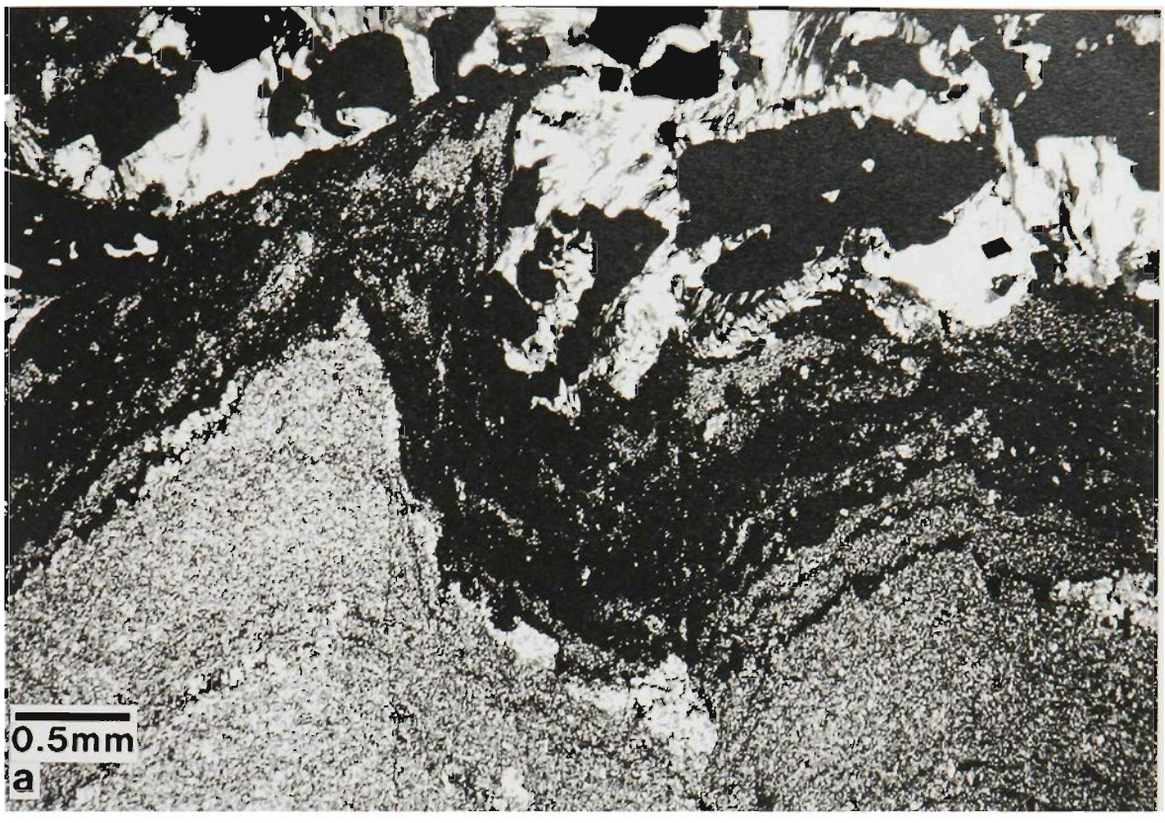
0.5mm
a


50 µm
b

Figure 9. a. Lenticular concentration of pyrite and carbonaceous material in the cleavage direction in the core of a fold (Fig 7b. of Part A) with pyrite also along bedding at a high angle to the s_3 cleavage (arcuate dark area across top). The concentration of pyrite along the cleavage direction transgresses bedding in an irregular fashion and relics of dolomitic host remain. Plane polarised light.

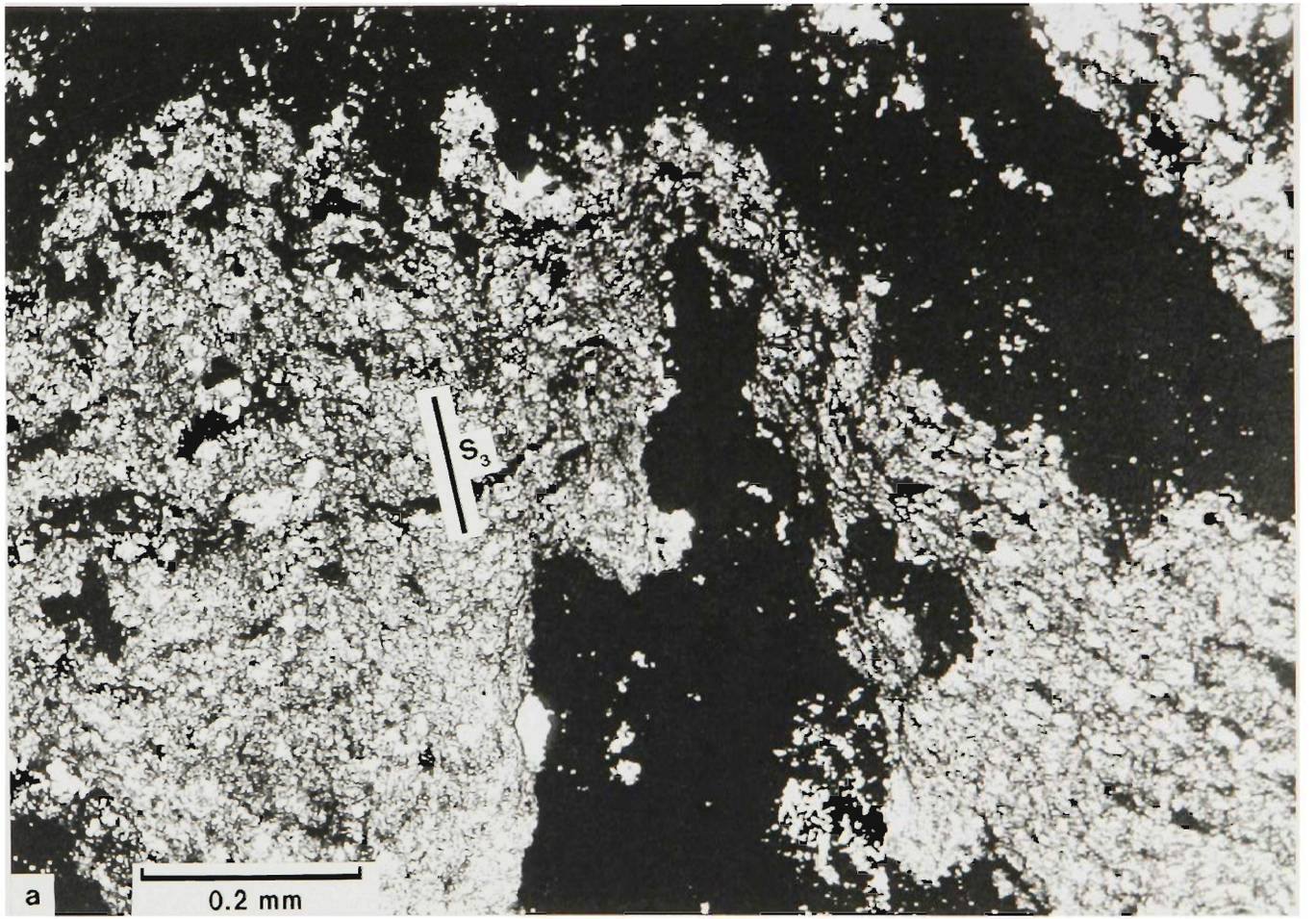
S_3
a
0.2 mm

PART B.

Figure 9 b. Enlargement of (a), using part transmitted/part reflected light, to highlight fine-grained pyrite within the carbonaceous background. Etching shows that the pyrite contains the normal growth zoning characteristic of fine-grained pyrites along the bedding, and that individual pyrites are close-packed. Carbonaceous laminations around the hinge show that the concentration of pyrite cannot be explained by concentration during deformation, although there appears to be some dissolution along pyrite boundaries.

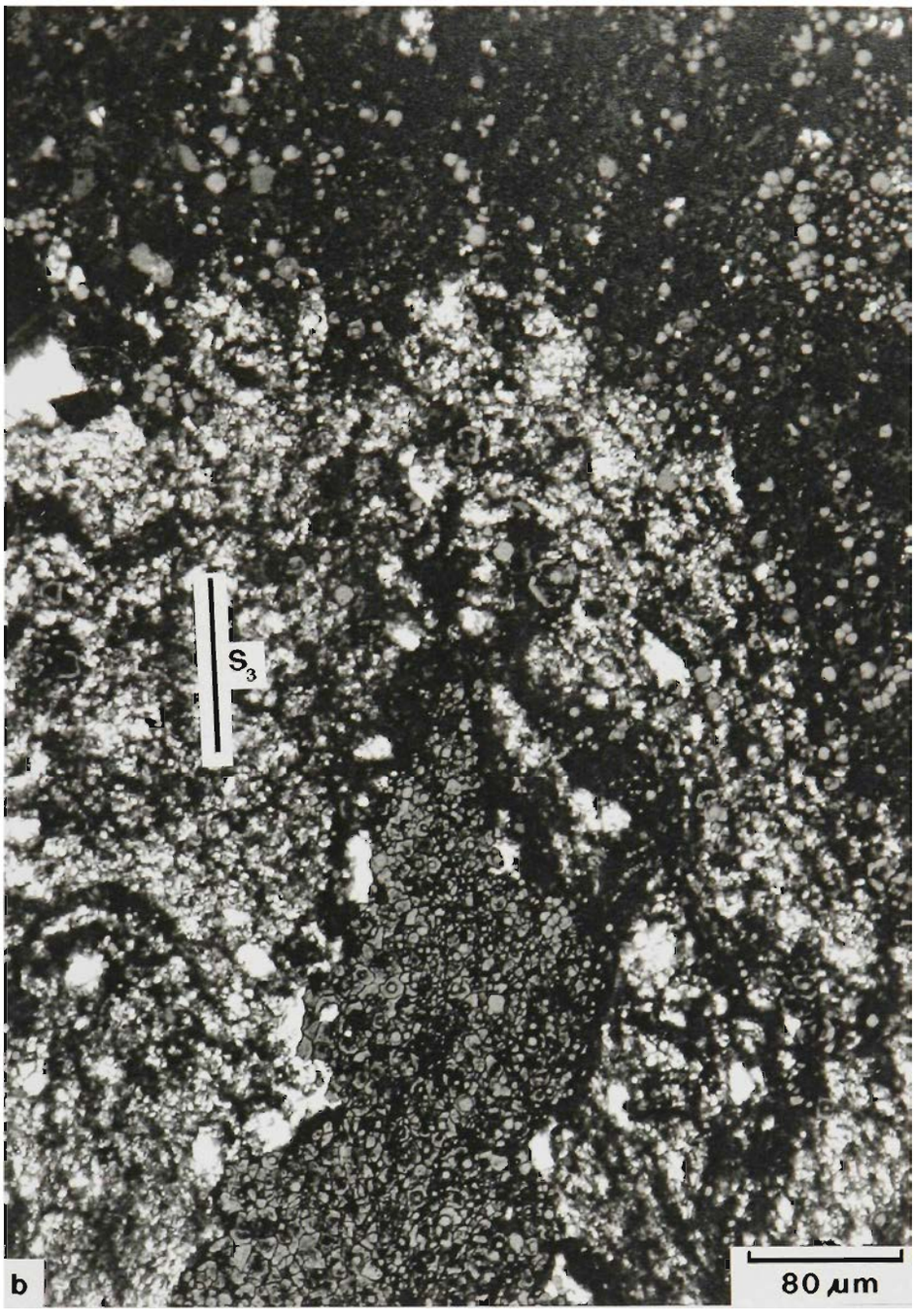
S3
b
80 µm

PART B.

Figure 9 c. Along continuation of the same pyrite aggregate as (a) and (b). Slightly elongated shapes and lack of outer growths of pyrite grains indicate some dissolution due to deformation in zones parallel to pyrite aggregates and axial plane direction. Location; No 6 orebody, 19C Sublevel, 7350 N.

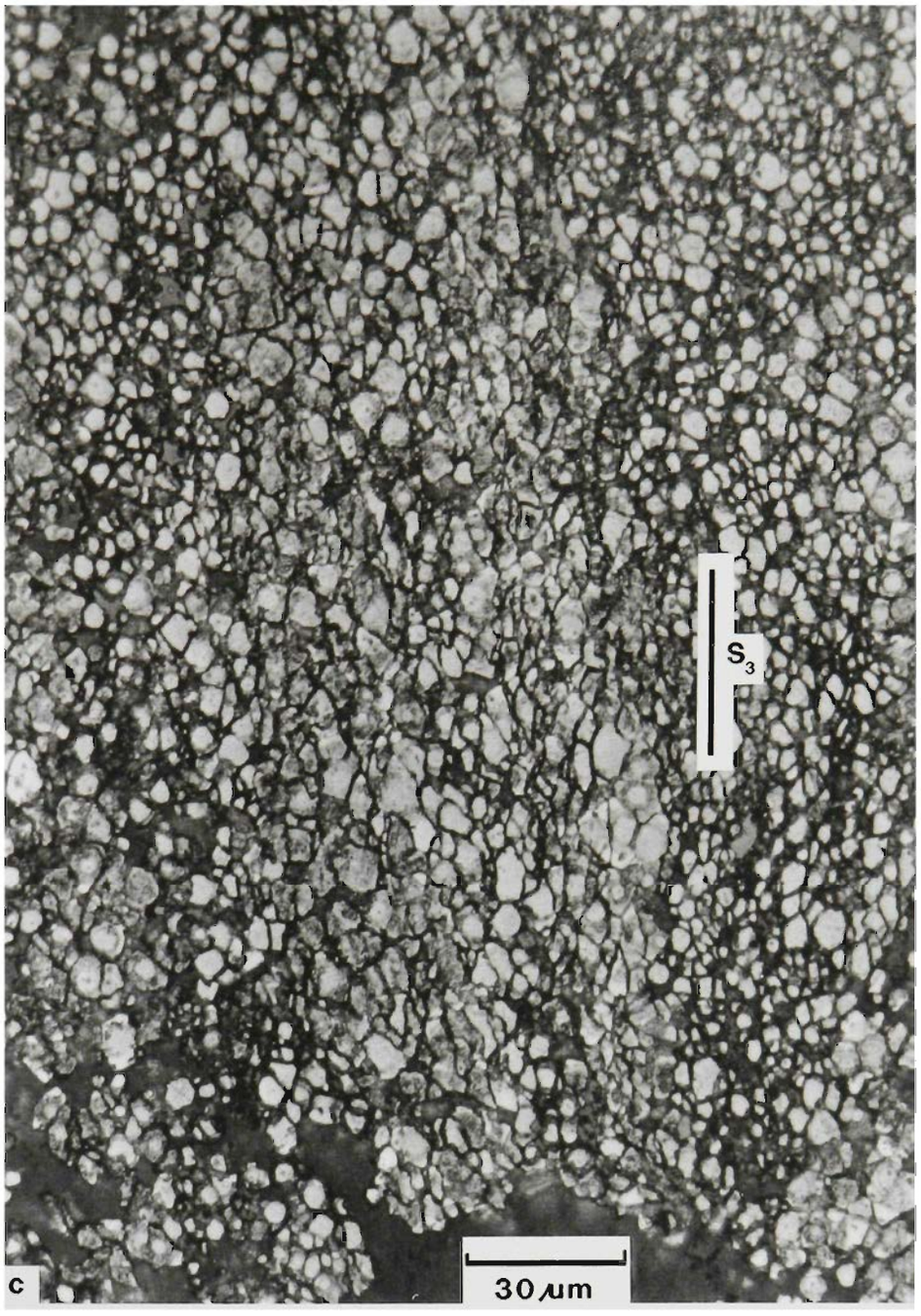
S_3
30 µm
c

PART C.

Stratiform Replacement Lead-Zinc Deposits: A comparison between Mount Isa, Hilton, Mount Novit and McArthur River.

Figures 1-28

APPENDIX 1

PART C.

Figure 1. Location map of North-west Queensland and part of the Northern Territory, showing the deposits at Mount Isa and McArthur River (HYC).

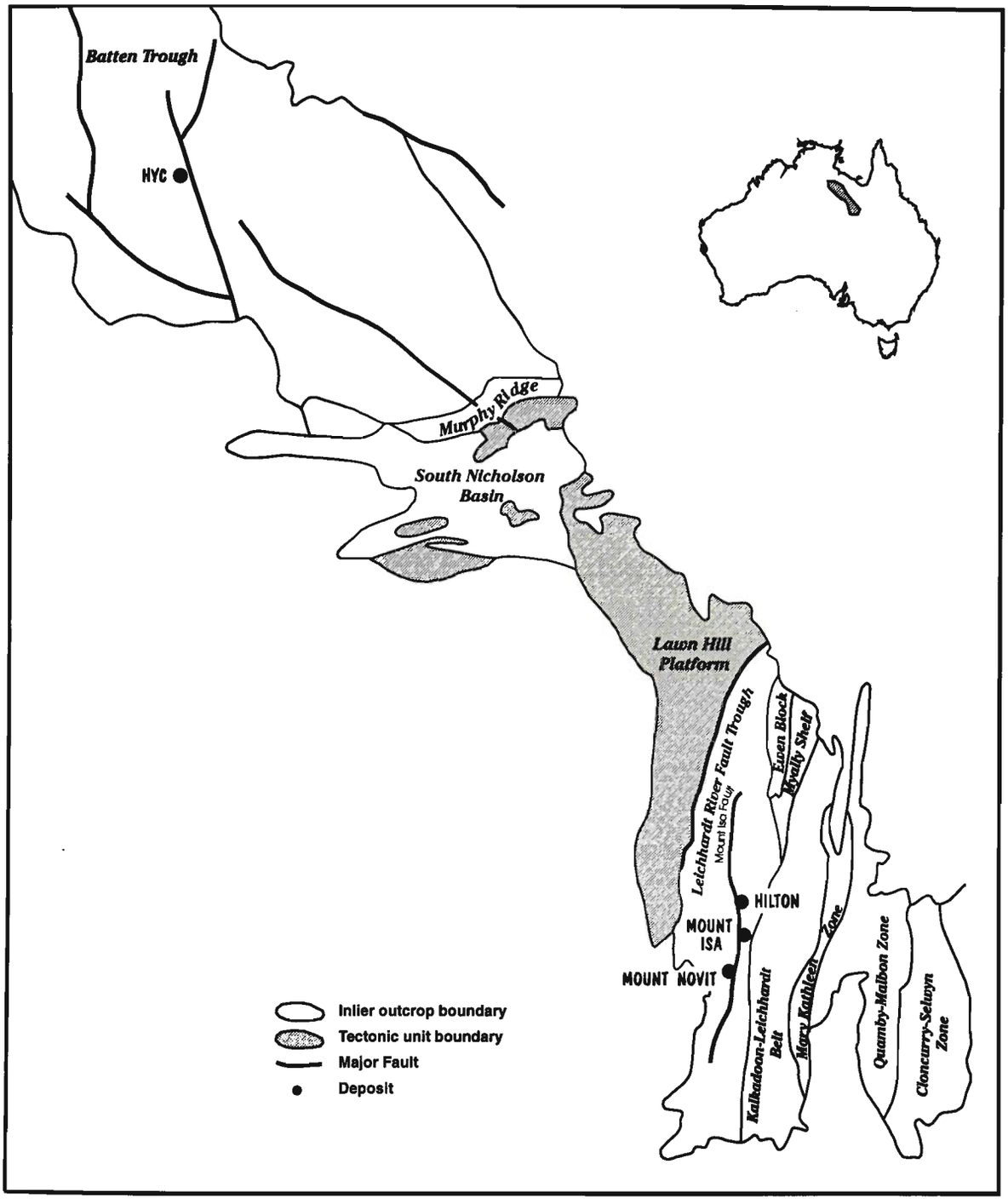
Batten Trough
HYC
Murphy Ridge
South Nicholson Basin
Lawn Hill Platform
Leichhardt River Fault Trough
Mount Isa Fault
Ewen Block
Rivalty Sheir
HILTON
MOUNT ISA
MOUNT NOVIT
Mary Kathleen Zone
Kalkadoon-Leichhardt Belt
Quamby-Malbon Zone
Cloncurry-Selwyn Zone
Inlier outcrop boundary
Tectonic unit boundary
Major Fault
Deposit

PART C.

Figure 2a. Cross-section at 6999N through northern lead-zinc orebodies at Mount Isa.

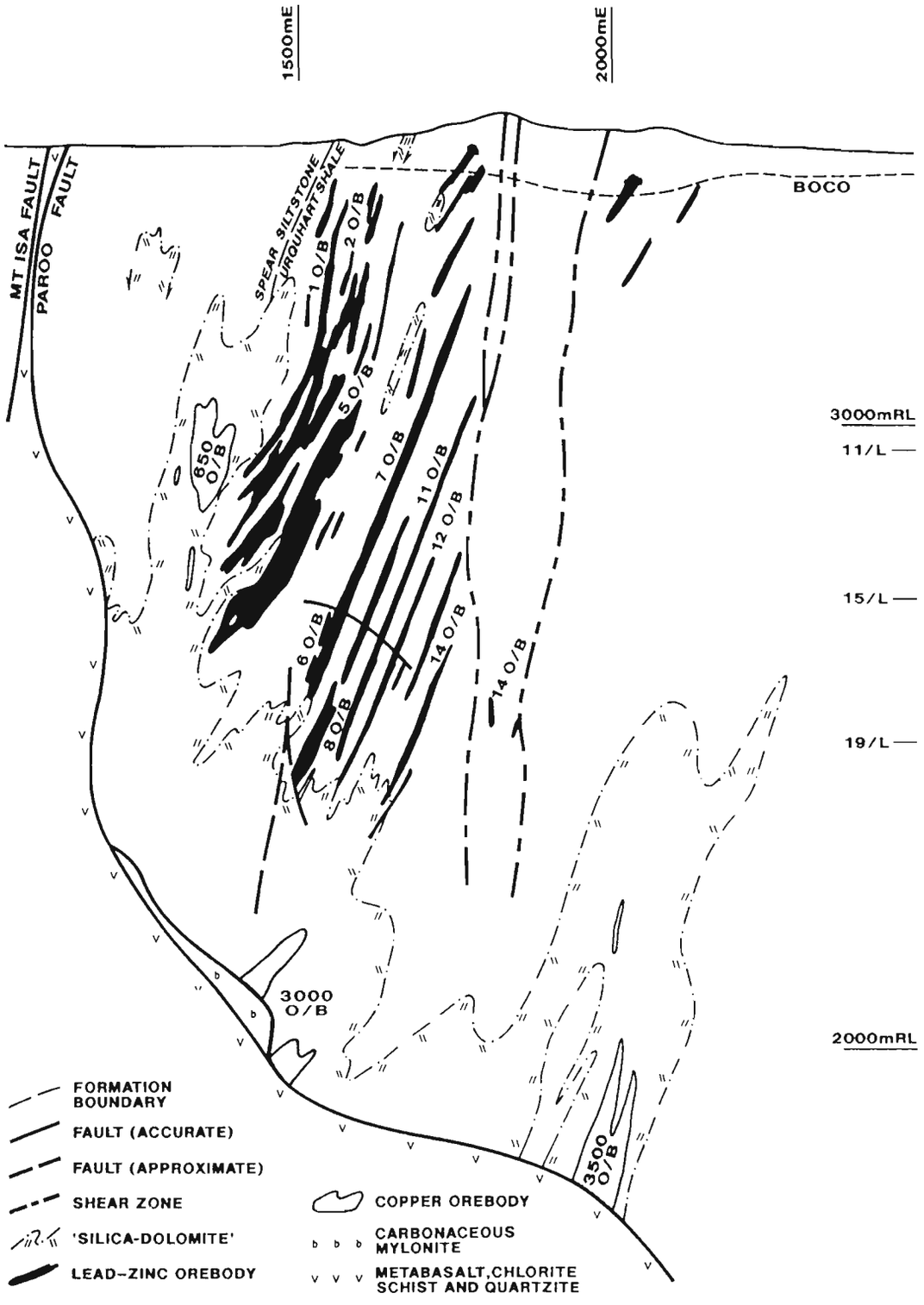
1500mE
2000mE
MT ISA FAULT
PAROO FAULT
SPEAR SILTSTONE
URQUHART SHALE
BOCO
1 O/B
2 O/B
5 O/B
7 O/B
11 O/B
12 O/B
14 O/B
14 O/B
6 O/B
8 O/B
650 O/B
3000 O/B
3500 O/B
3000mRL
11/L
15/L
19/L
2000mRL
FORMATION BOUNDARY
FAULT (ACCURATE)
FAULT (APPROXIMATE)
SHEAR ZONE
'SILICA-DOLOMITE'
LEAD-ZINC OREBODY
COPPER OREBODY
CARBONACEOUS MYLONITE
METABASALT, CHLORITE SCHIST AND QUARTZITE

PART C.

Figure 2b. Cross-section at 5220N of Hilton initial mining block.

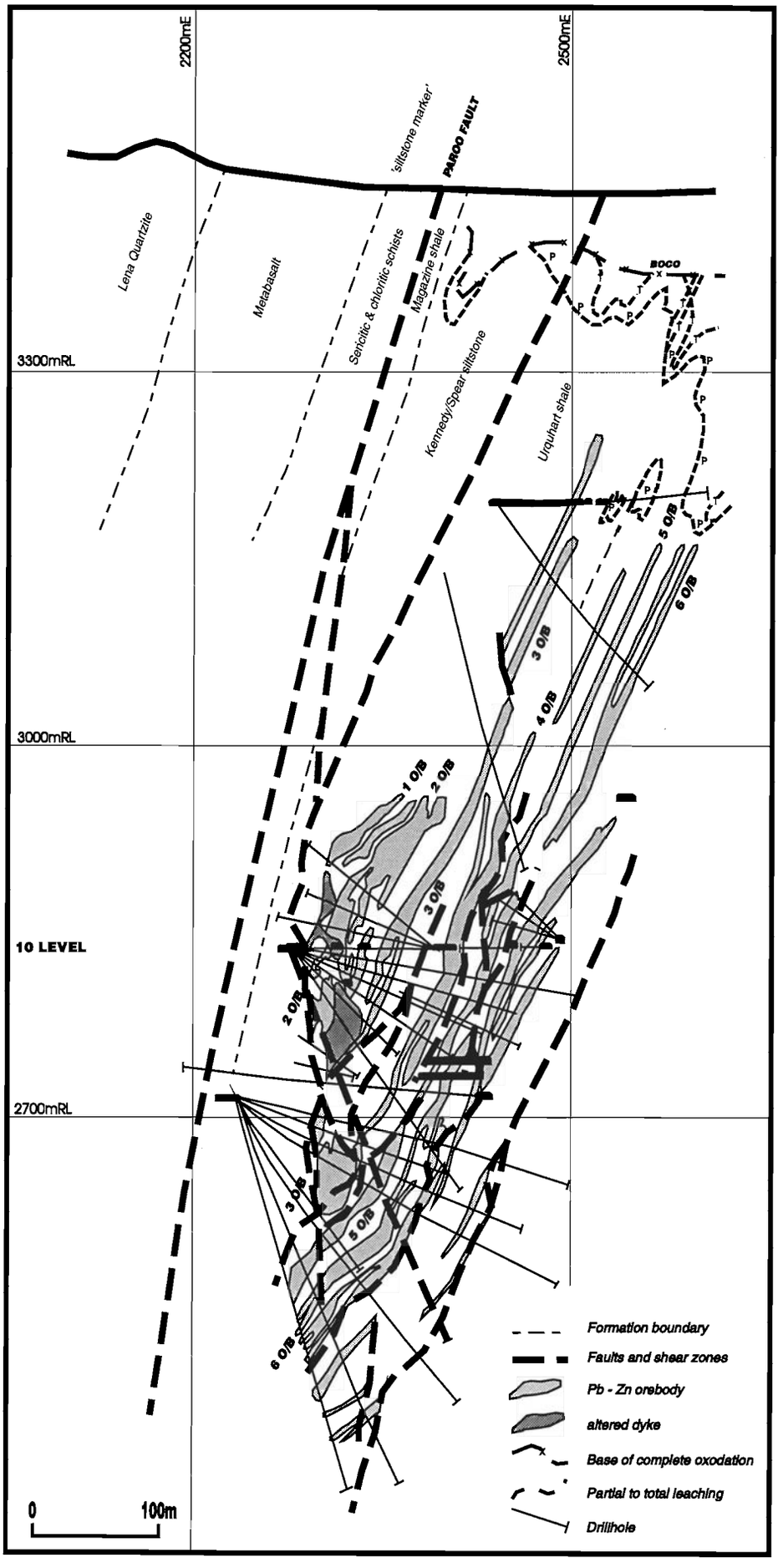
2200mE
2500mE
'siltstone marker'
PAROO FAULT
Lena Quartzite
Metabasalt
Sericitic & chloritic schists
Magazine shale
Kennedy/Spear siltstone
Urquhart shale
BOCO
3300mRL
3000mRL
10 LEVEL
2700mRL
1 O/B
2 O/B
3 O/B
4 O/B
5 O/B
6 O/B
0
100m
Formation boundary
Faults and shear zones
Pb - Zn orebody
altered dyke
Base of complete oxodation
Partial to total leaching
Drillhole

PART C.

Figure 2c. Cross-section on 18300N through the Mount Novit prospect.

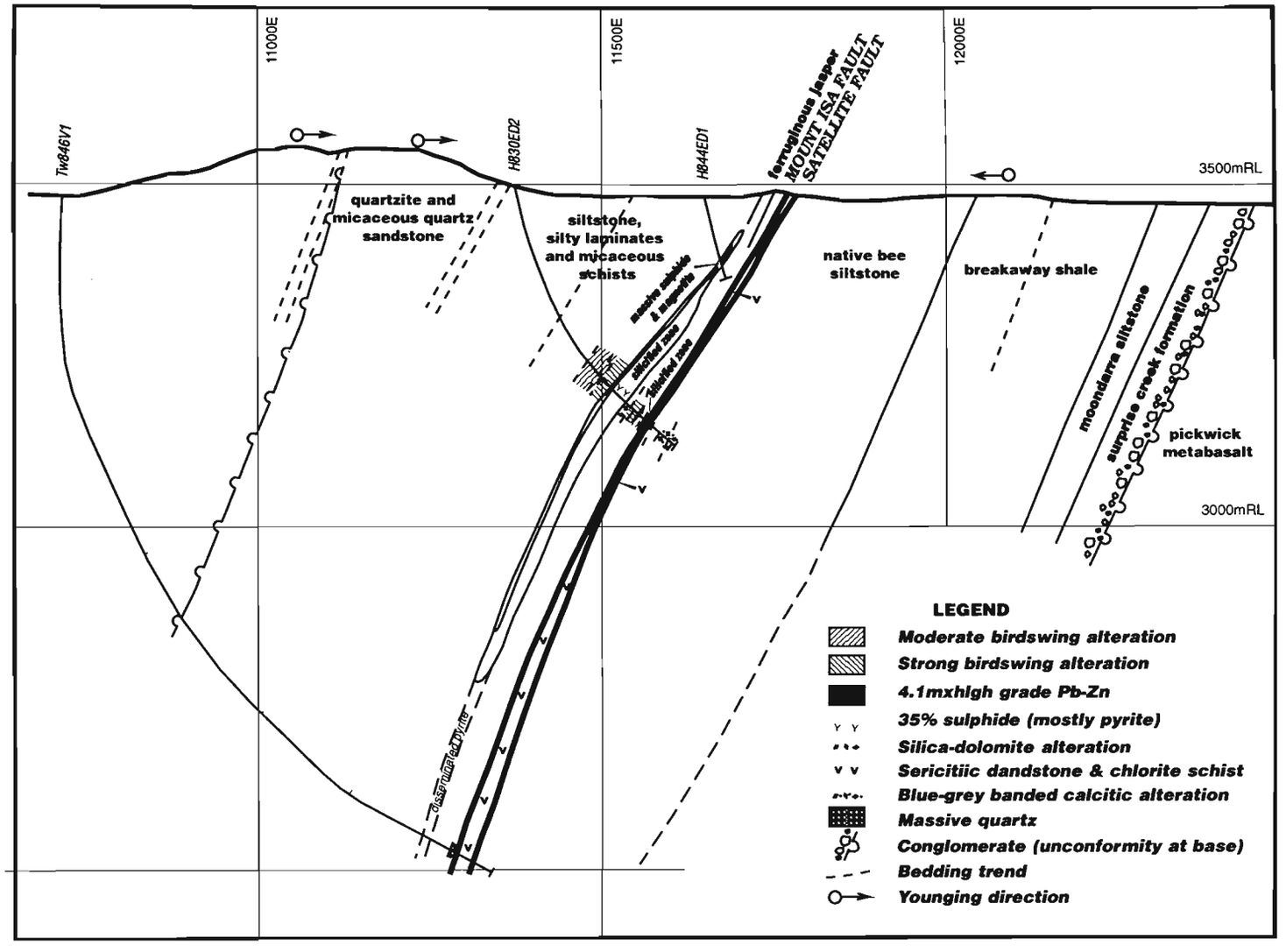
11000E
11500E
12000E
Tw846V1
H830ED2
H844ED1
ferruginous jasper
MOUNT ISA FAULT
SATELLITE FAULT
3500mRL
quartzite and micaceous quartz sandstone
siltstone, silty laminates and micaceous schists
native bee siltstone
breakaway shale
moondarra siltstone
surprise creek formation
pickwick metabasalt
3000mRL
LEGEND
Moderate birdswing alteration
Strong birdswing alteration
4.1mxhigh grade Pb-Zn
35% sulphide (mostly pyrite)
Silica-dolomite alteration
Sericitiic dandstone & chlorite schist
Blue-grey banded calcitic alteration
Massive quartz
Conglomerate (unconformity at base)
Bedding trend
Younging direction

PART C.

Figure 2d. Interpreted cross-section on 2300N through the H.Y.C. deposit. Compiled at 1:10,000 from surface mapping and drilling around this northing.

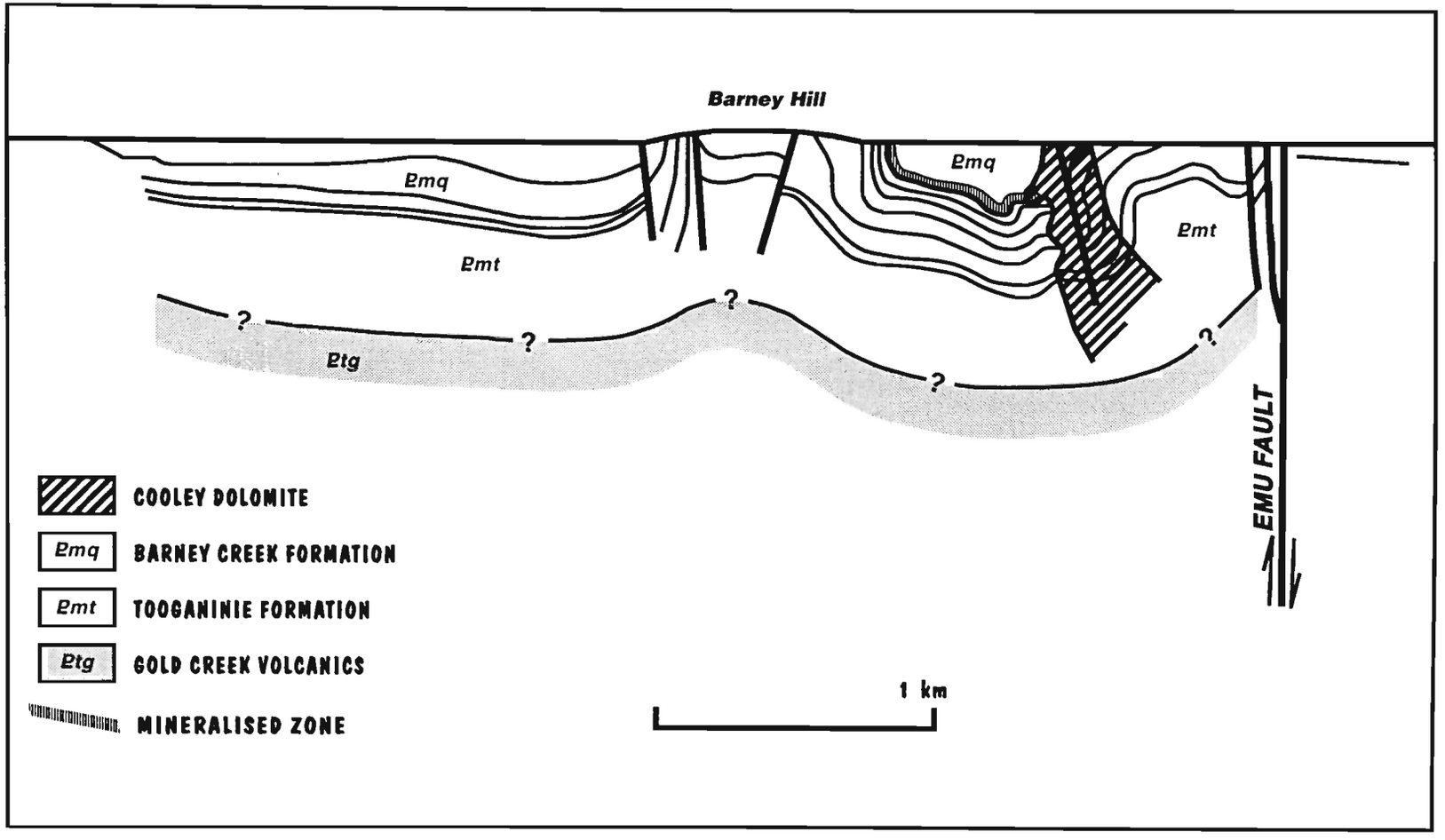
Barney Hill
Emq
Emt
Etg
EMU FAULT
COOLEY DOLOMITE
Emq BARNEY CREEK FORMATION
Emt TOOGANINIE FORMATION
Etg GOLD CREEK VOLCANICS
MINERALISED ZONE
1 km

PART C.

Figure 2e. Cross-section on 2200N through the H.Y.C. deposit.

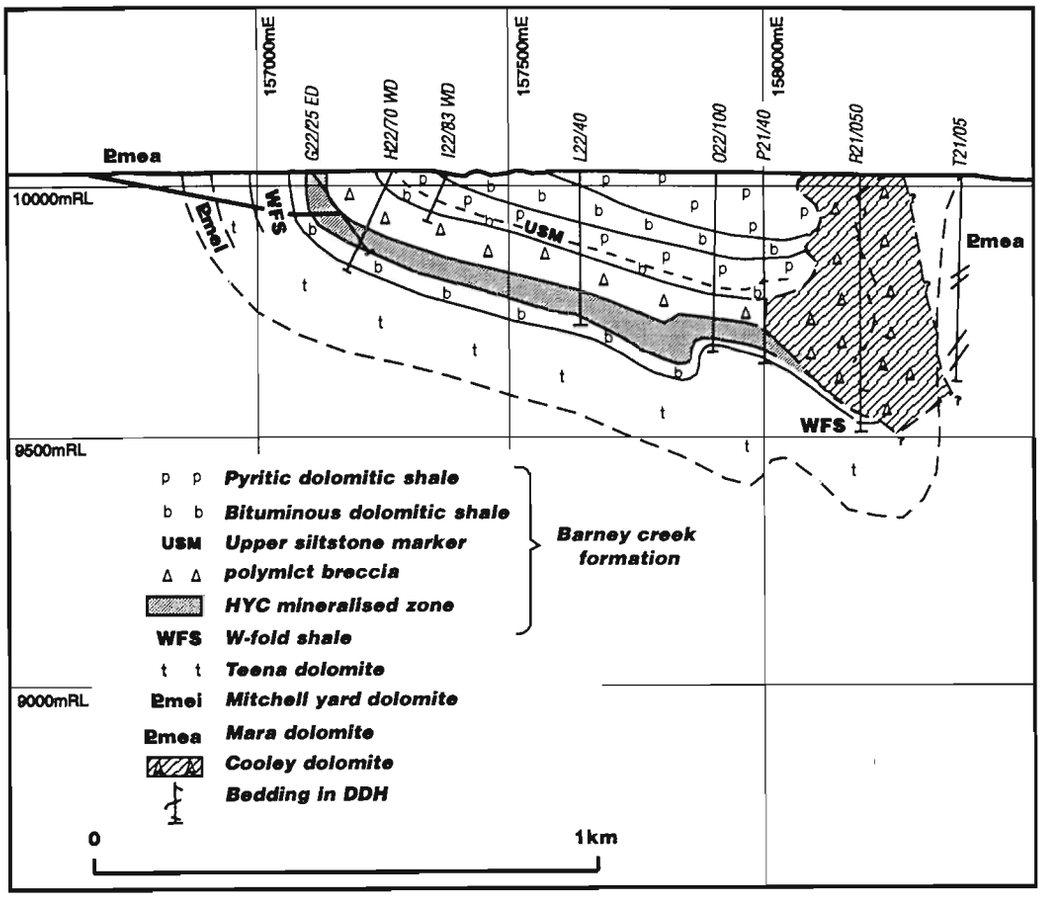
157000mE
G22/25 ED
H22/70 WD
I22/83 WD
157500mE
L22/40
O22/100
158000mE
P21/40
R21/050
T21/05
Pmea
10000mRL
Pmei
WFS
USM
Pmea
WFS
9500mRL
p p Pyritic dolomitic shale
b b Bituminous dolomitic shale
USM Upper siltstone marker
Δ Δ polymict breccia
HYC mineralised zone
WFS W-fold shale
t t Teena dolomite
Barney creek formation
9000mRL
Pmei Mitchell yard dolomite
Pmea Mara dolomite
Cooley dolomite
Bedding in DDH
0
1km

PART C.

Figure 3. a. Longitudinal projection of ore in the 4 pod, showing locations of drill holes and development examined.

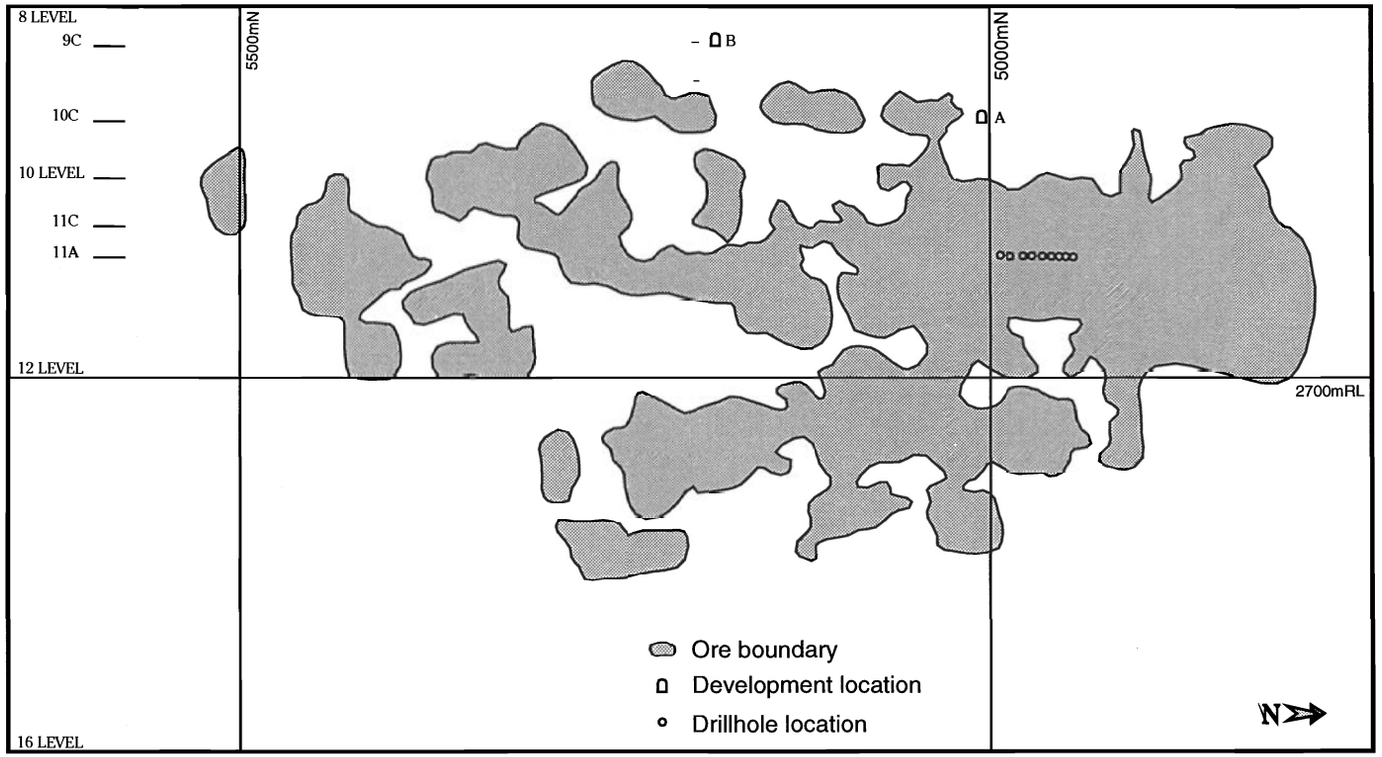
8 LEVEL
9C
10C
10 LEVEL
11C
11A
12 LEVEL
16 LEVEL
5500mN
5000mN
B
A
2700mRL
Ore boundary
Development location
Drillhole location
N

Figure 3 b. Plan of 4 pod drill intersections, drilled from 4 orebody sill drive, showing correlation of specific well-banded sequences. Pyrrhotite and economic sulphides are discontinuous and cross-cutting. Only some of the complex alteration is shown. The laminites containing the correlated horizons are partially choloritised and locally biotitic. The mineralised zones are invariably lighter coloured and contain coarser-grained carbonates. Mineralization boundaries commonly form cross-cutting breccias. Location 11c sublevel, 4900N to 5000N.

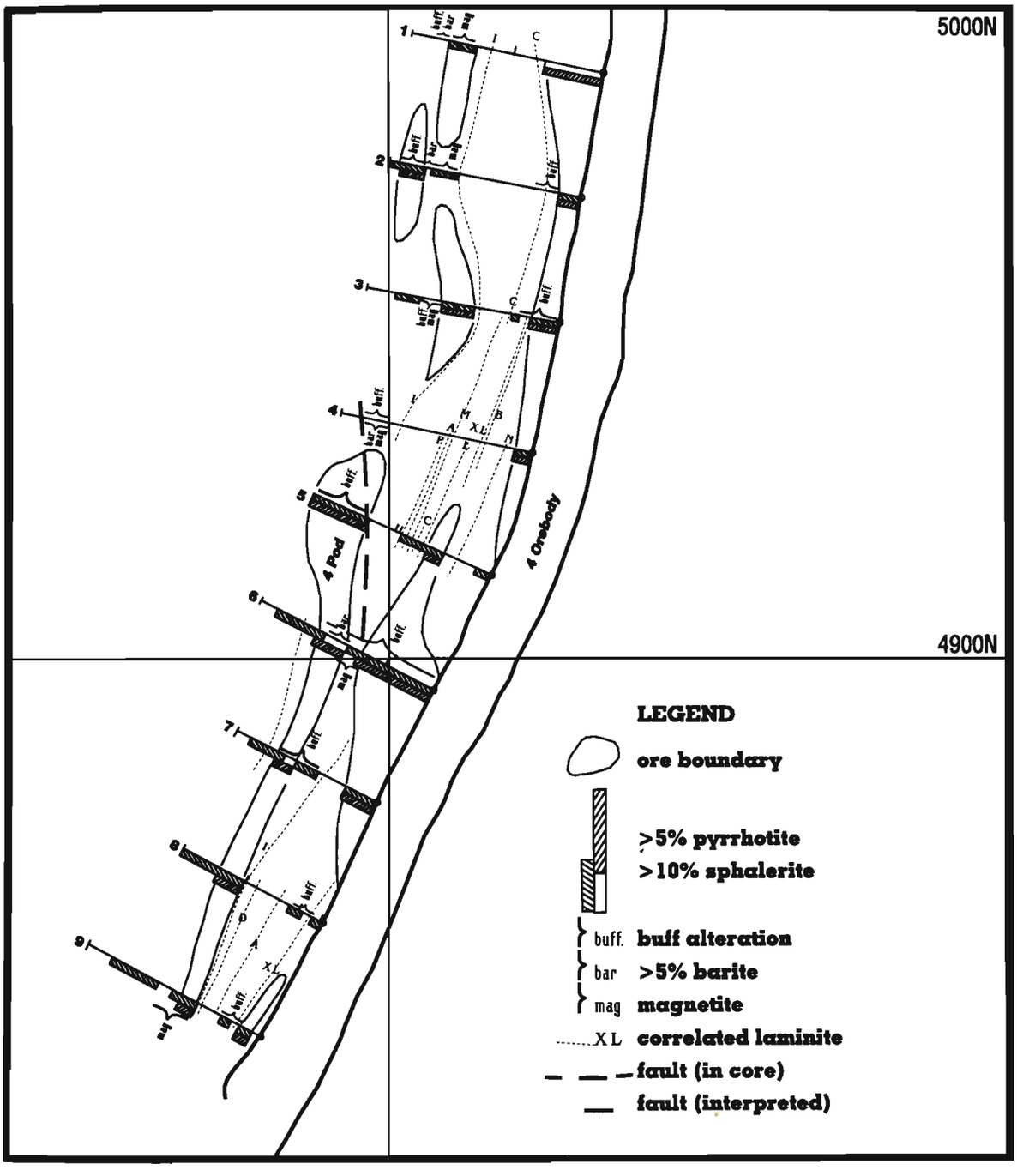
5000N
4900N
1
2
3
4
5
6
7
8
9
1 Pod
1 Orebody
LEGEND
ore boundary
>5% pyrrhotite
>10% sphalerite
buff. buff alteration
bar >5% barite
mag magnetite
XL correlated laminite
fault (in core)
fault (interpreted)

PART C.

Figure 4 a. Folds with both shallow and steeply dipping axial planes in Hilton galena-rich ore zone. Location, No 3 orebody centre lens 9c sublevel, 5195N, 2405E.


a

PART C.

Figure 4b. Interpretive sketch of a (inset), and large reclined folds, showing that the shallow axial traces (earlier) are folded about the steep folds (later).

bedding trends in less mineralized layers

short trends from broken layers

refolded axial trace

'D2½' FOLD – HILTON

PART C.

Figure 4 c. Fold with a shallow axial plane in sphalerite-rich zone. Sphalerite concentration is extremely discontinuous along bedding. Dolomite veins in the non-laminated layer are refolded with steep axial planes. Location No. 4 pod, 10c sublevel, 5006N, 2368E. (A in Fig. 3a).

C

Figure 5. Plan of AI522 stope development on 10 level, Hilton. Highly pyrrhotitic ore belonging to 2 orebody is adjacent to the dyke. The west limb of an isoclinal syncline is truncated by the dyke. Adjacent to the dyke sulphides have only limited siltstone inclusions, which are surrounded commonly by chalcopyrite. Faults which cut the dyke have only minor displacements of it, and embayments of sulphides into the dyke indicate that there has not been subsequent movement on the dyke-ore boundaries.

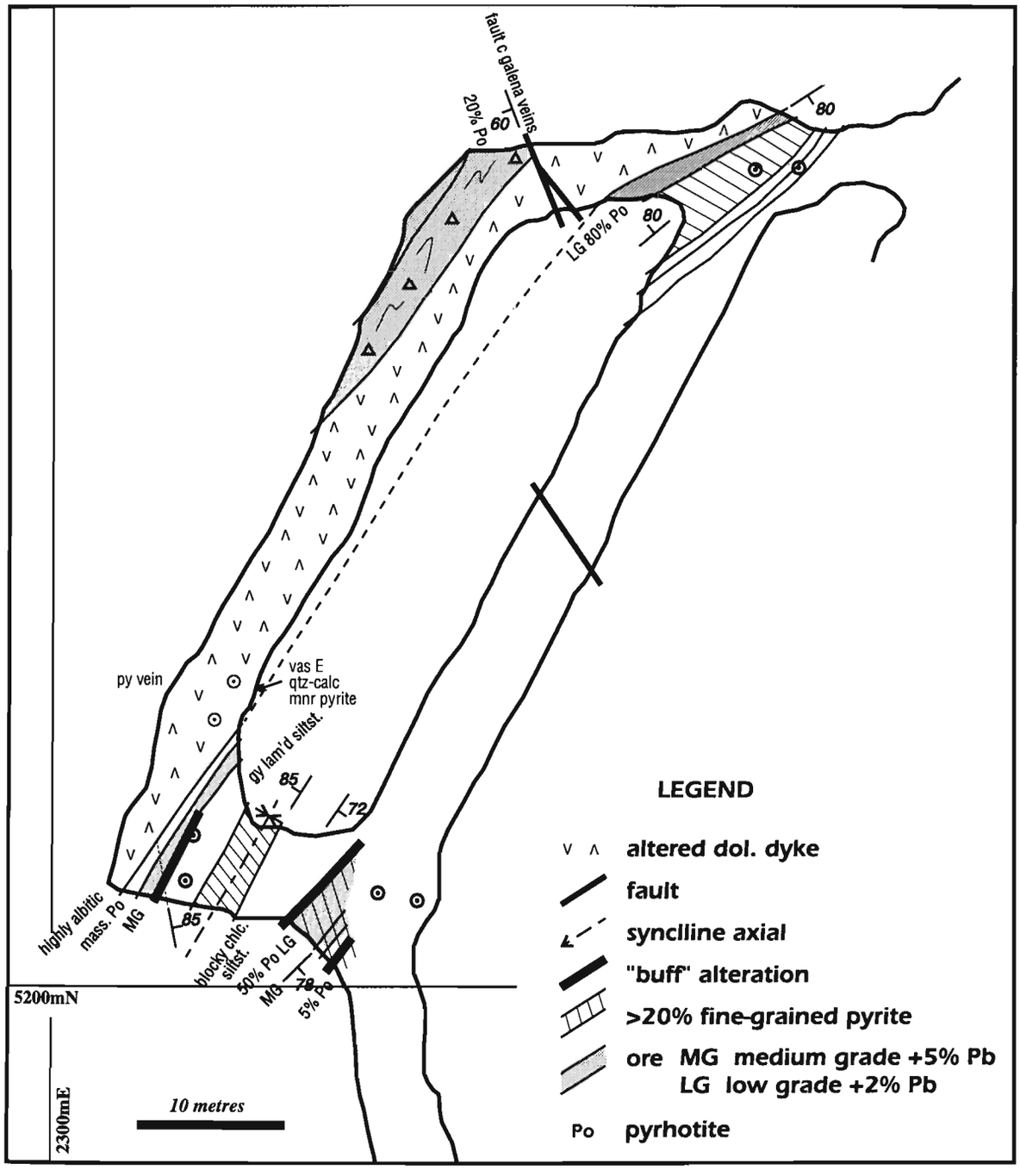
fault c galena veins
20% Po
60
80
LG 80% Po
80
py vein
vas E
qtz-calc
mnr pyrite
gy lam'd siltst.
85
72
highly albitic
mass. Po
MG
85
blocky chlc.
siltst.
50% Po LG
MG
78
5% Po
5200mN
2300mE
10 metres
LEGEND
altered dol. dyke
fault
syncline axial
"buff" alteration
>20% fine-grained pyrite
ore MG medium grade +5% Pb
LG low grade +2% Pb
Po pyrhotite

PART C.

Figure 6 a. "Buff-altered" siltstone with a flexural fold from the west limb of an isoclinal syncline. The sulphide in both the bedding parallel coarser-grained dolomite band and in the high angle dolomite veins is all pyrrhotite. Location. 10 Level AI522 stope, 5207N, 2308E. See Fig. 5.

a

Figure 6 b. Intermediate west-dipping cleavage, $s_{2.5}$, defined by shape of quartz grains and dolomite matrix. Minor biotite (bi) occurs in these altered layers. Pyrrhotite has apparently replaced both the quartz and the dolomite. Plane polarised light. Location. As for Fig.6 a.

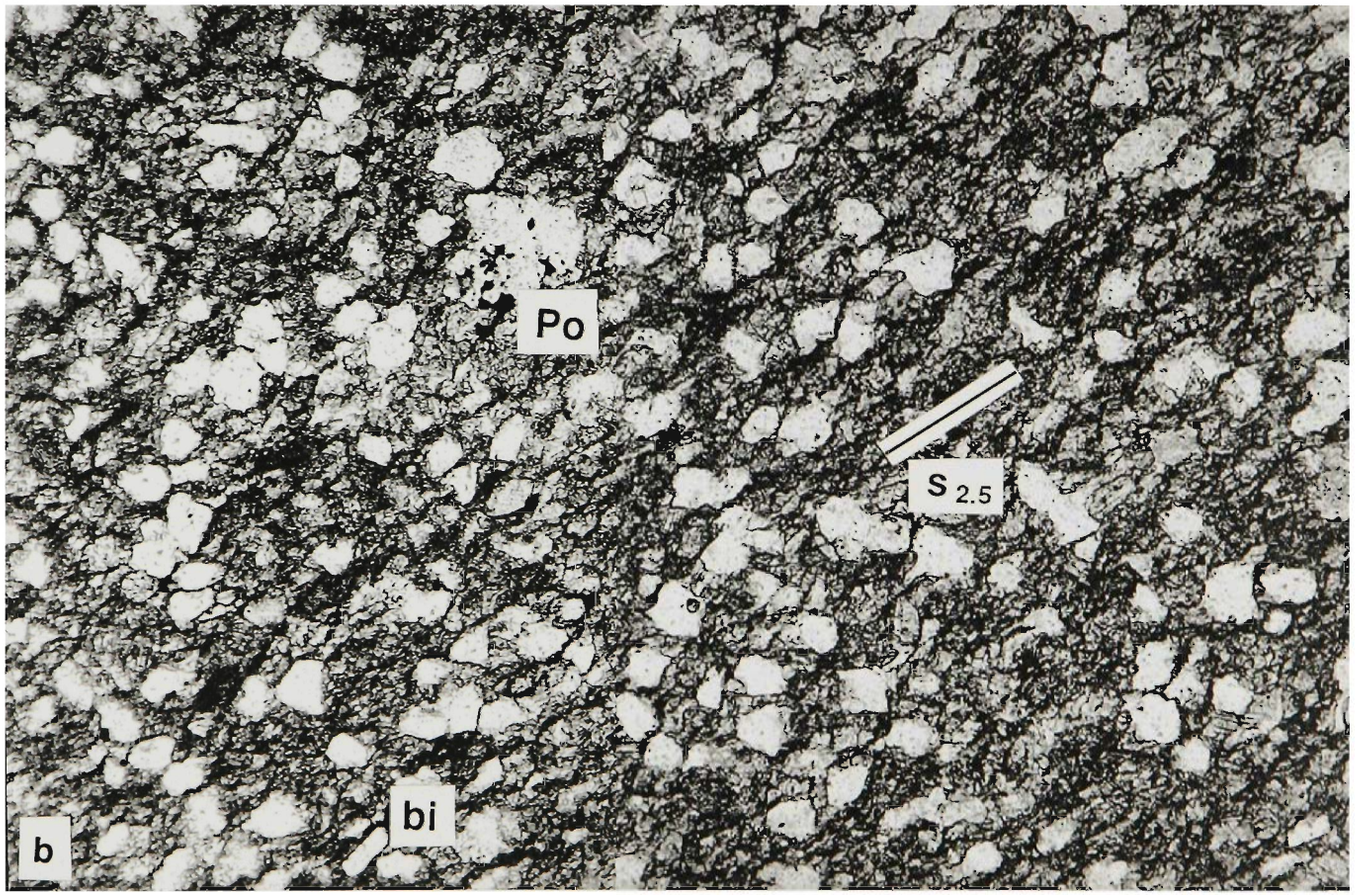
Po
S 2.5
bi
b

PART C.

Figure 6 c. Overprinting of cleavages in a zone of concentration of sericite against a pod of dolomite-quartz alteration. The earlier cleavage is parallel to that illustrated in b. ($s_{2.5}$) and the steeper is correlated as s_3. As for Fig.6 a.

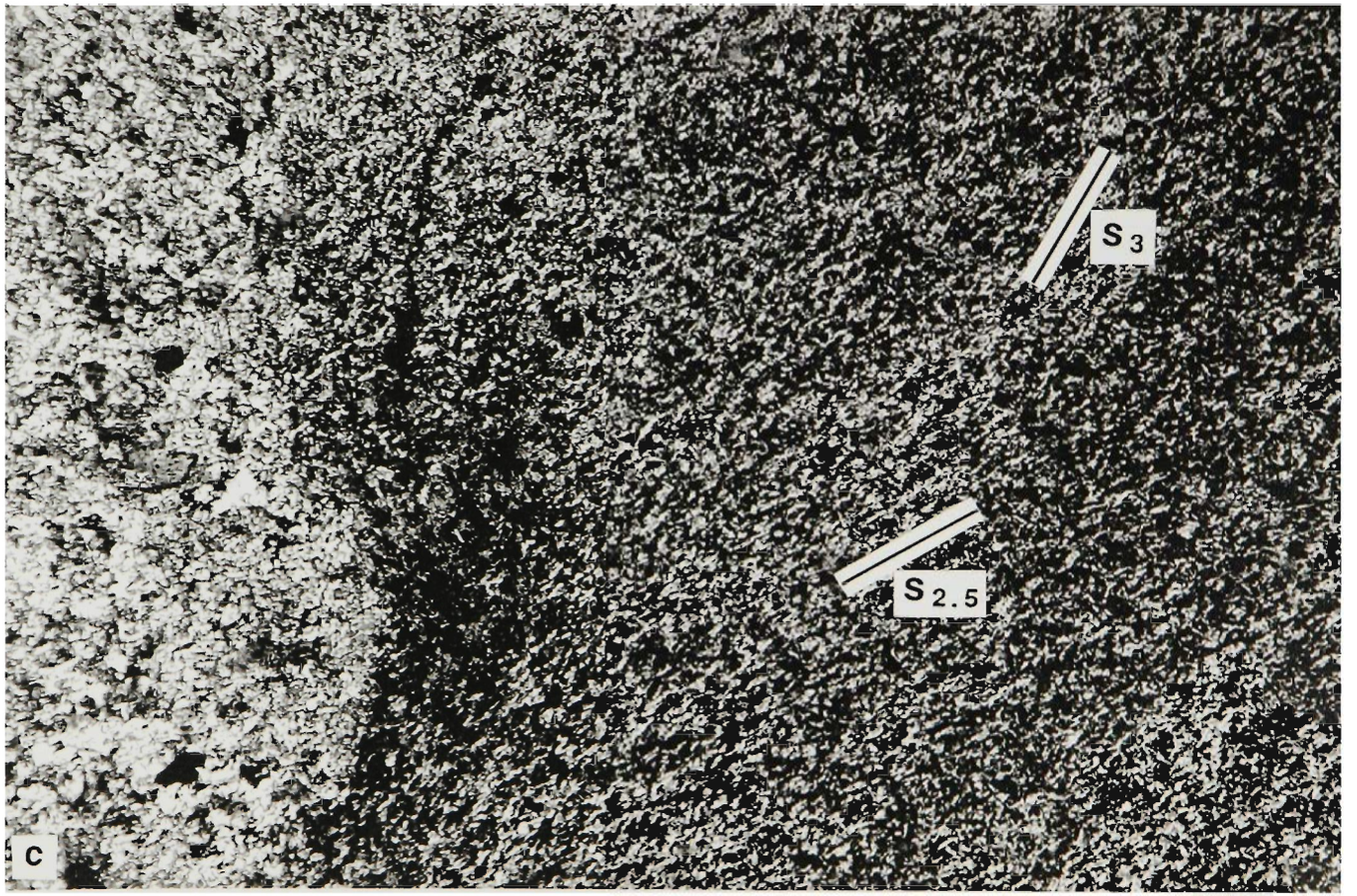
S3
S2.5
c

PART C.

Figure 7. Micaceous and chloritic dolomitic siltstone with a cross-cutting cleavage s_4 (s_3 of Valenta,1988), defined by chlorite and dolomite, which is in turn deformed by crenulation A and subsequently B. The chlorites overgrow biotite aggregates which are at a high angle to the fine dolomite veins. Location. 4 pod 10A sub. 5012N, 2359E.

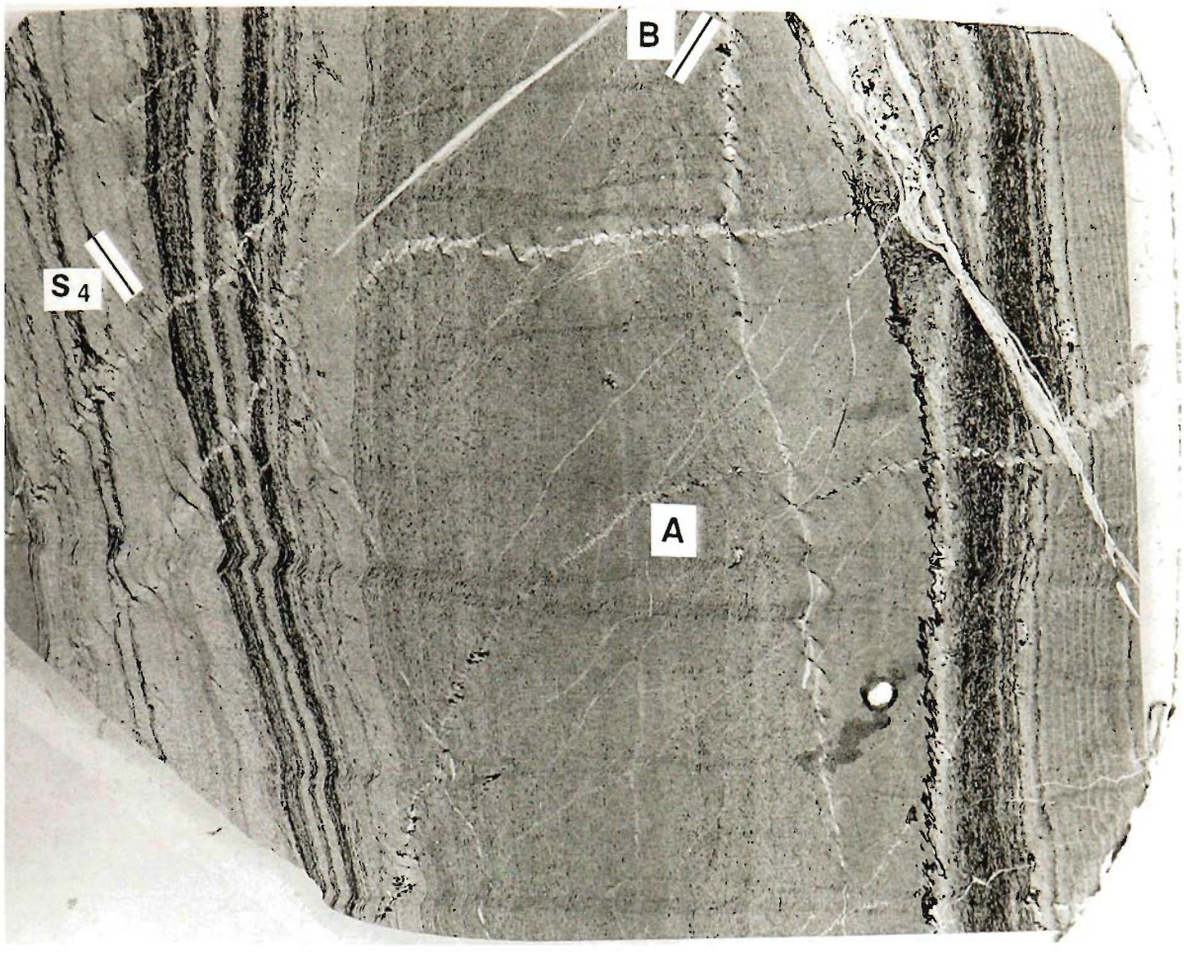
B
S 4
A

PART C.

Figure 8 a. Hinge zone of a fold with a sphalerite-rich layer and pyrite-rich layers. There is a weak steep cleavage which is axial planar to the small-scale folds in the sphalerite-rich layer. The two most obvious cleavages are parallel to bedding and dipping to the east at a shallow angle.

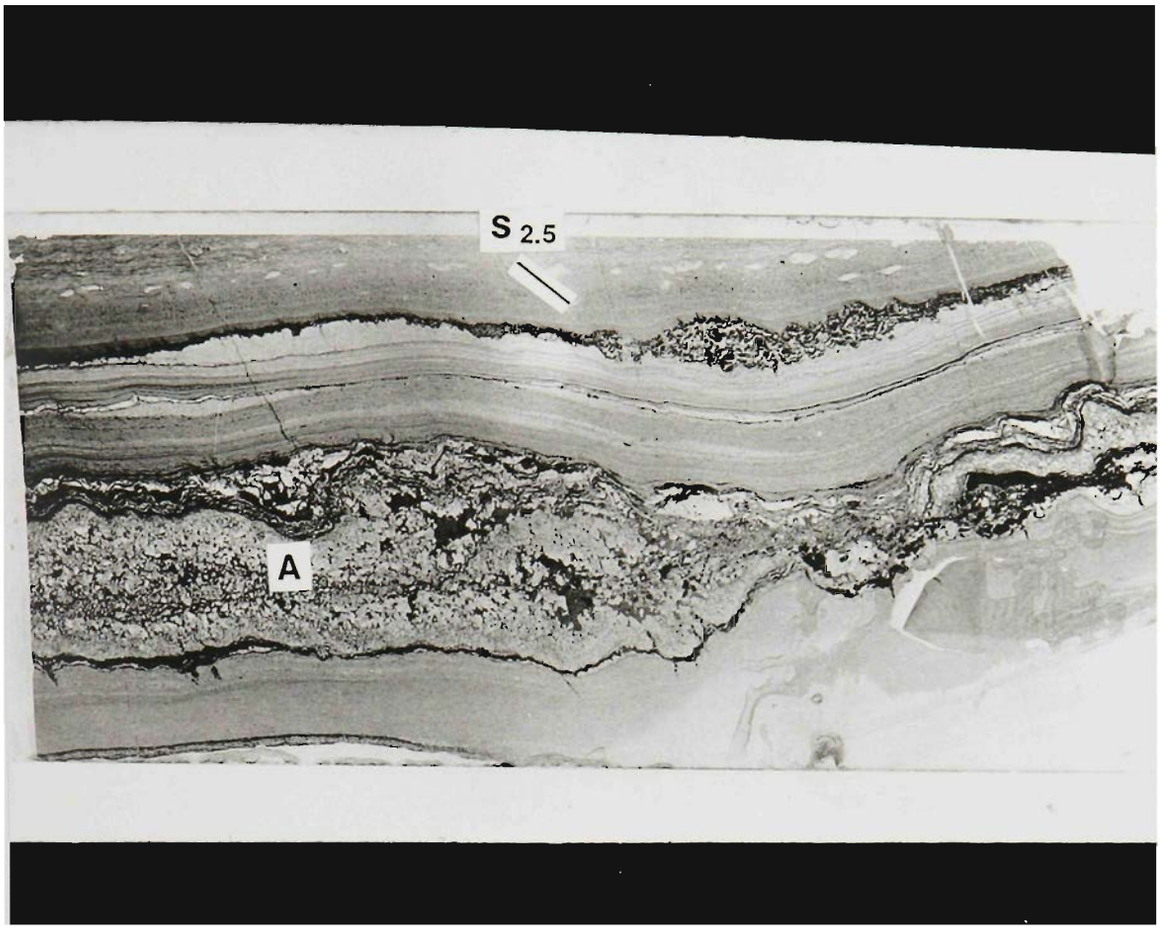
S 2.5
A

Figure 8 b. Shallow east-dipping cleavage around dolomite concretions indicating dextral shear on cleavage. Location 8 Level, 5023N, 2469E. As for Fig.8a.

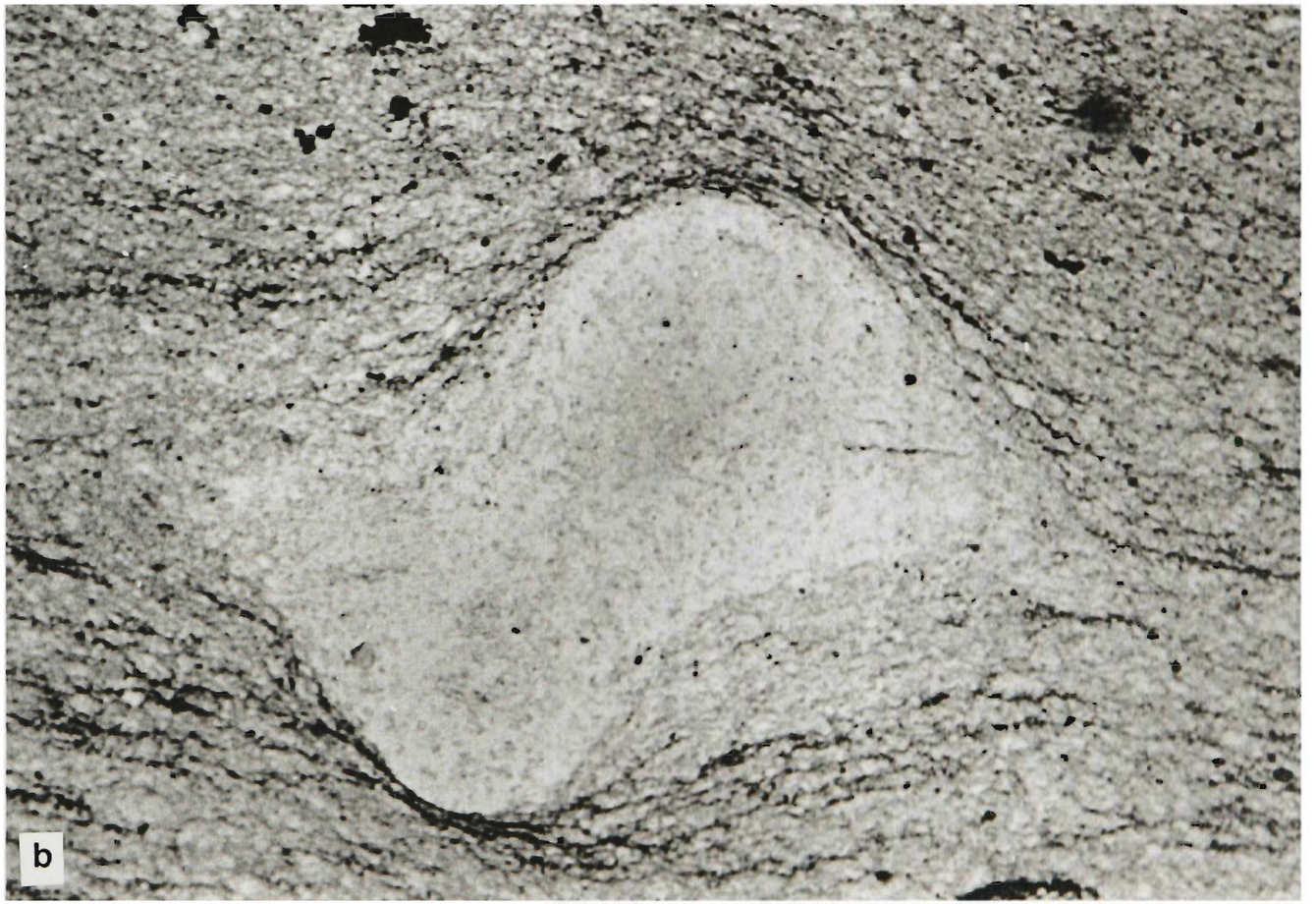
b

PART C.

Figure 9 Styles of Hilton sulphide. a. Copper-rich sulphide breccia containing blocks of laminated siltstone with discontinuous chalcopyrite and tabular blocks of massve pyrite in pyrrhotite-rich galena-sphalerite ore. Location. 10 Level AI522 stope, Fig. 5, 5262N, 23335E.

Figure 9 b. Massive banded pyrrhotite with minor dolomite. Location 9c sub. 4 pod, 5187N, 2423E (B in Fig. 3a).

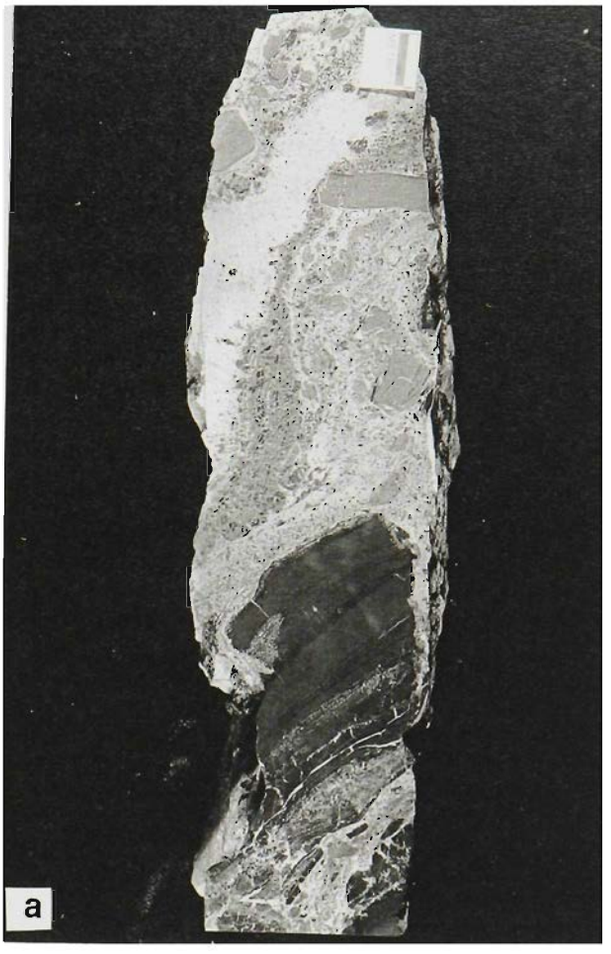
a

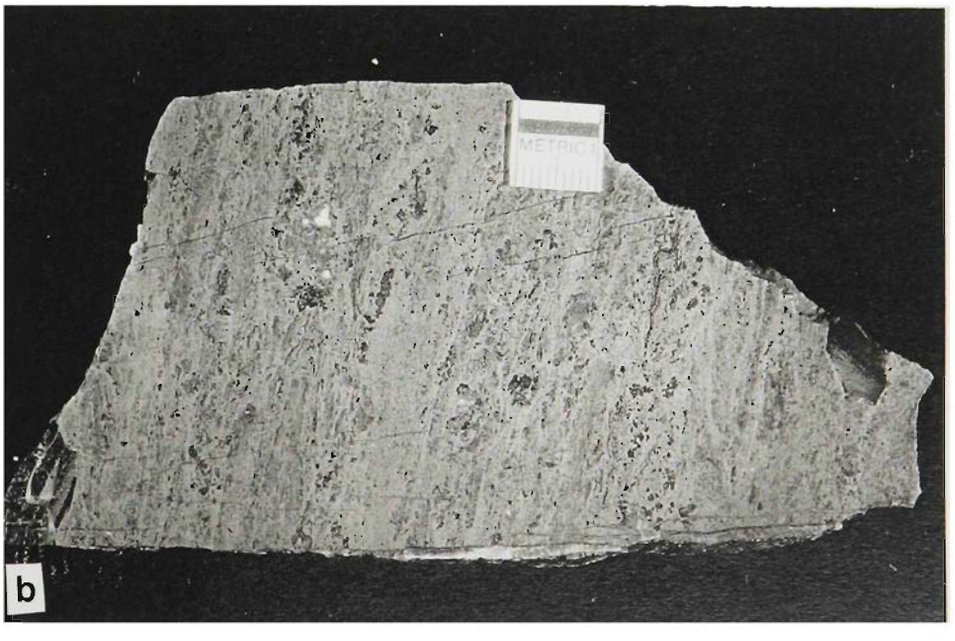
METRIC
b

PART C.

Figure 9 c. Typical coarse-grained galena-rich breccia ore, with intermediate east-dipping extension microveinlets. Location 8 level 5045N, 2446E.

Figure 9d. "Nodular" carbonate in a fold limb and synclinal hinge zone. These altered layers are associated mainly with dilation on bedding and some overprinting of laminae. In this case the alteration is related to the fold because the carbonate and quartz lenses terminate in a zone parallel to the axial plane at the short limb. The layers have been strongly silicified and sphalerite mineralised. Brassy pyrite is also better developed in the fold hinge. Location: H820 W decline at 1039.3. d. Bedding-parallel zinc-rich zone Location 9c sublevel 6 orebody.

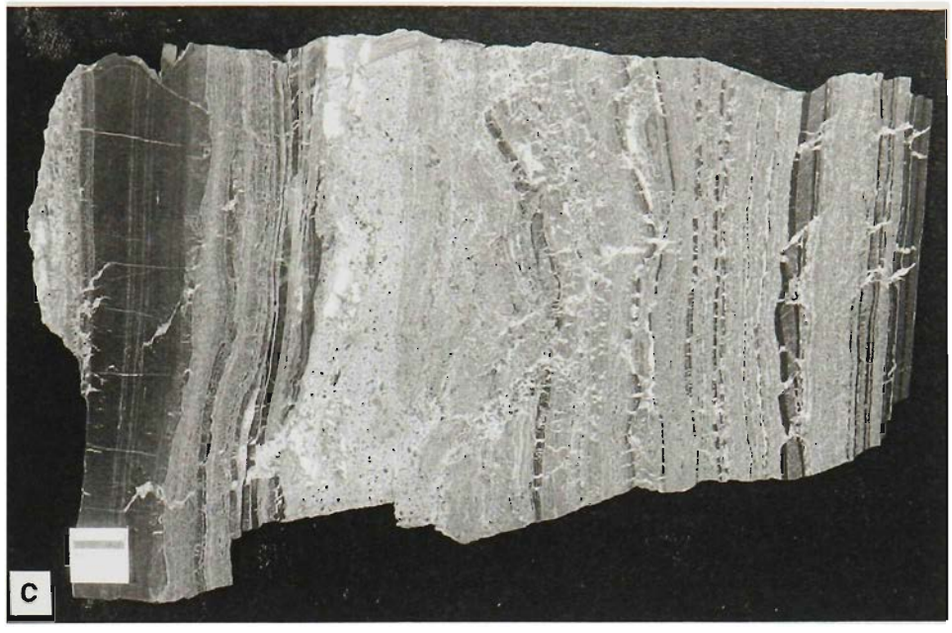
c

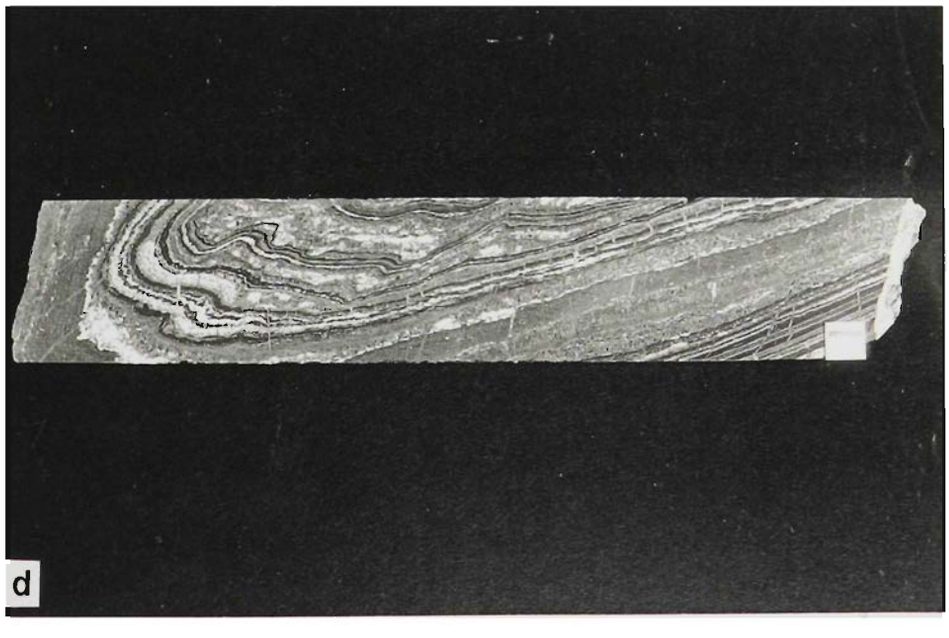
d

PART C.

Figure 10. 5220N section showing zoning of Pb-Zn ratios away from the Hangingwall fault. Compare with Fig. 2b for more detailed geology.

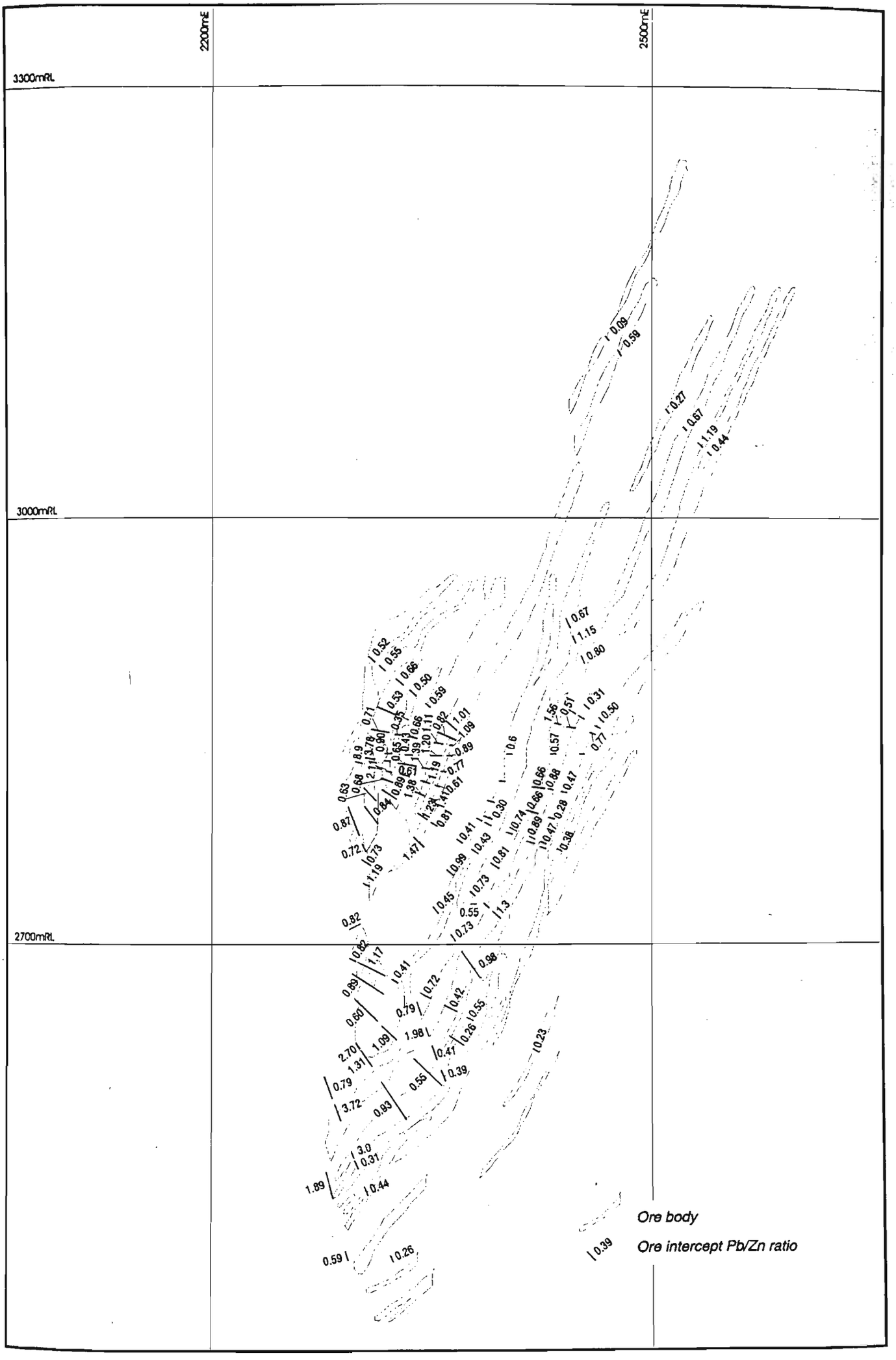
2200mE
2500mE
3300mRL
3000mRL
2700mRL
Ore body
Ore intercept Pb/Zn ratio

PART C.

Figure 11 a. Slate with a healed microfault which is cut by veins containing chalcopyrite. Location. 2 orebody, 11A sub. 4985N.

Figure 11 b. Sphalerite as very discontinuous concentrations along bedding in a zone of horizontal $D_{2.5}$ folds. Location 4 pod, 10C sub., 5006N, 2368E.

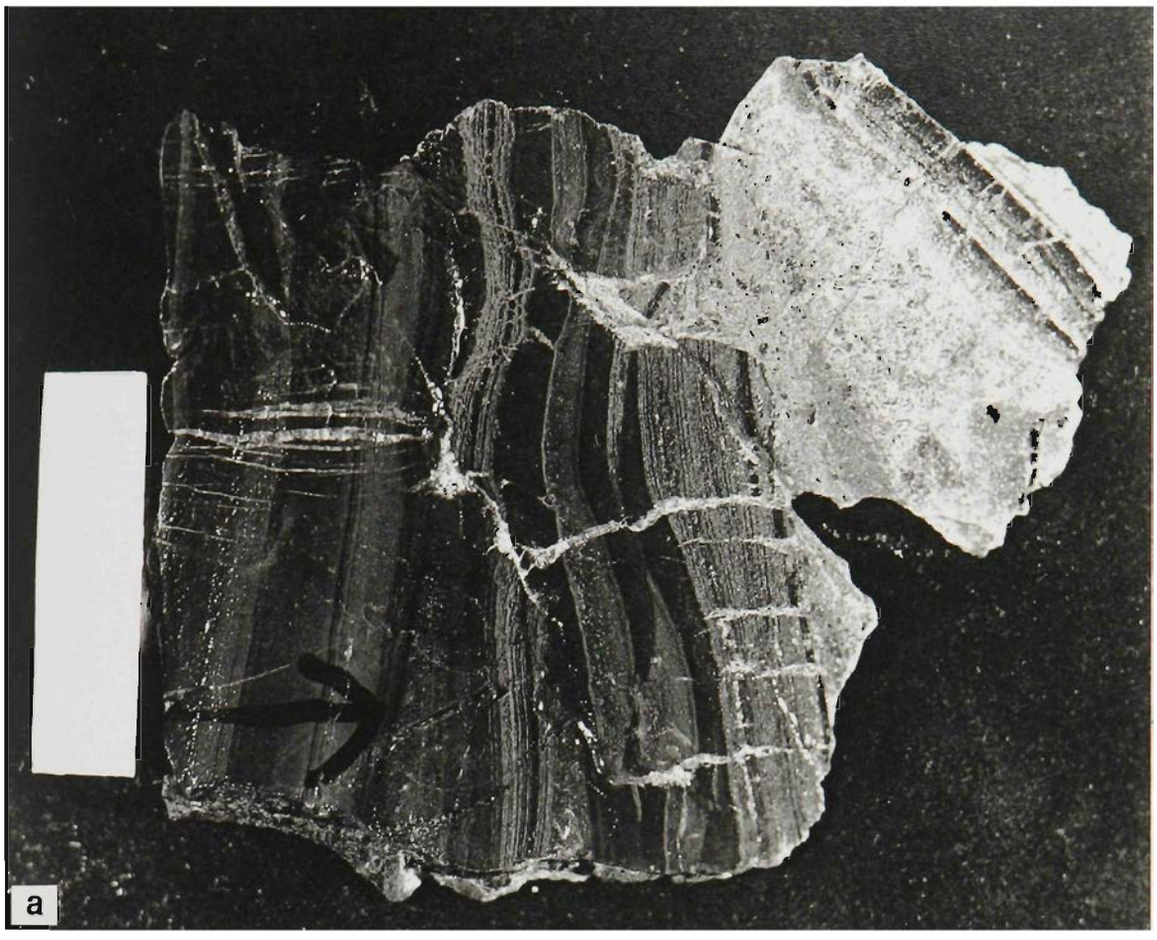
a

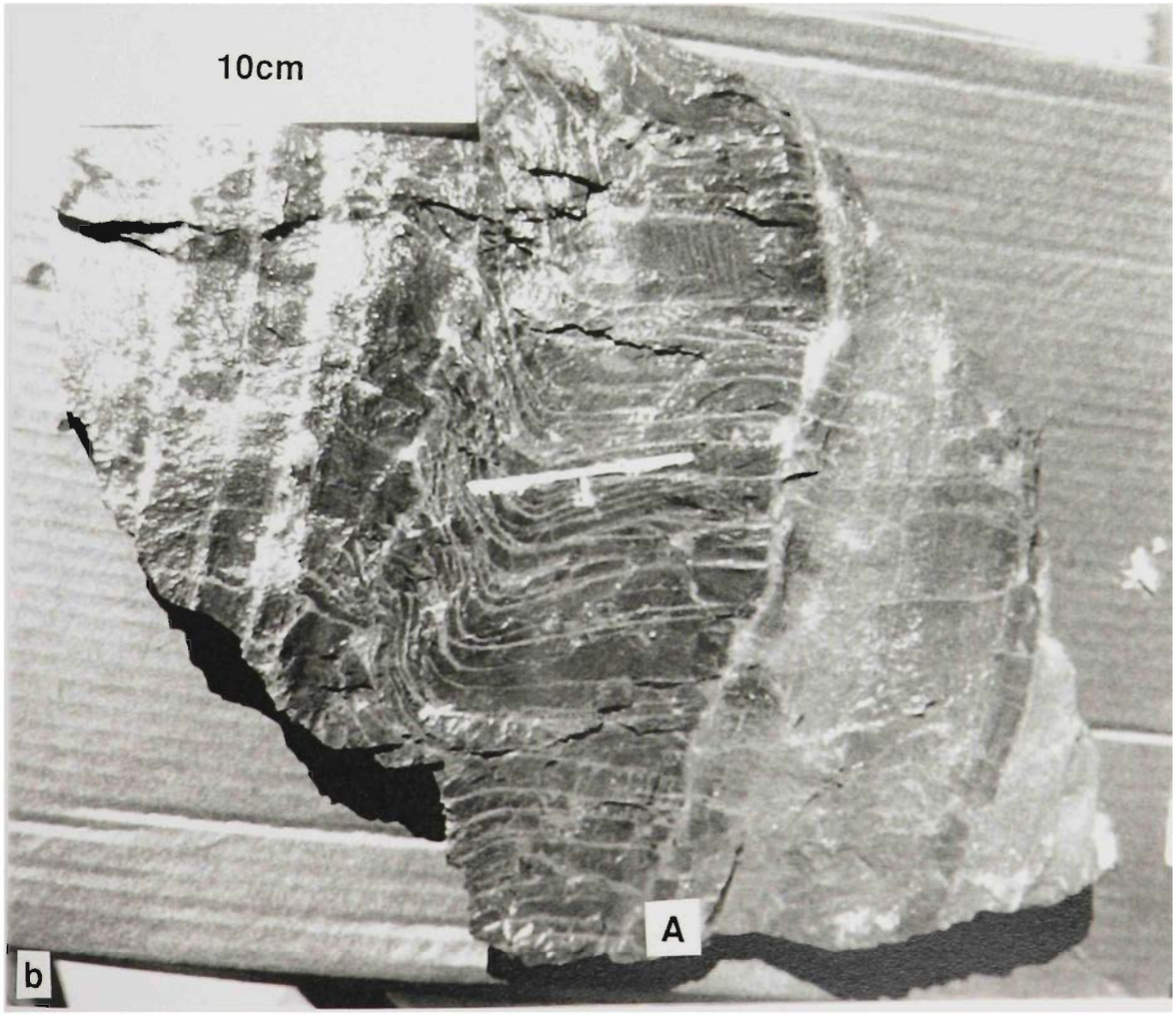
10cm
A
b

PART C.

Figure 11 c. Extremely uneven distribution of sphalerite along bedding around a D_3 syncline. The sphalerite occurs as irregular shapes along bedding, the s_3 cleavage, and along fanning veins around the fold, all with textural continuity. Location. H820 W Decline, 1216.9m, Hilton North.

Figure 11 d. Folded carbonaceous siltstone with galena-rich breccia matrix. The galena has sharp breccia margins, which transgress the D_3 folds. Sphalerite along bedding at A is cut by galena breccia. Location, 6 orebody footwall 10B sub.


c

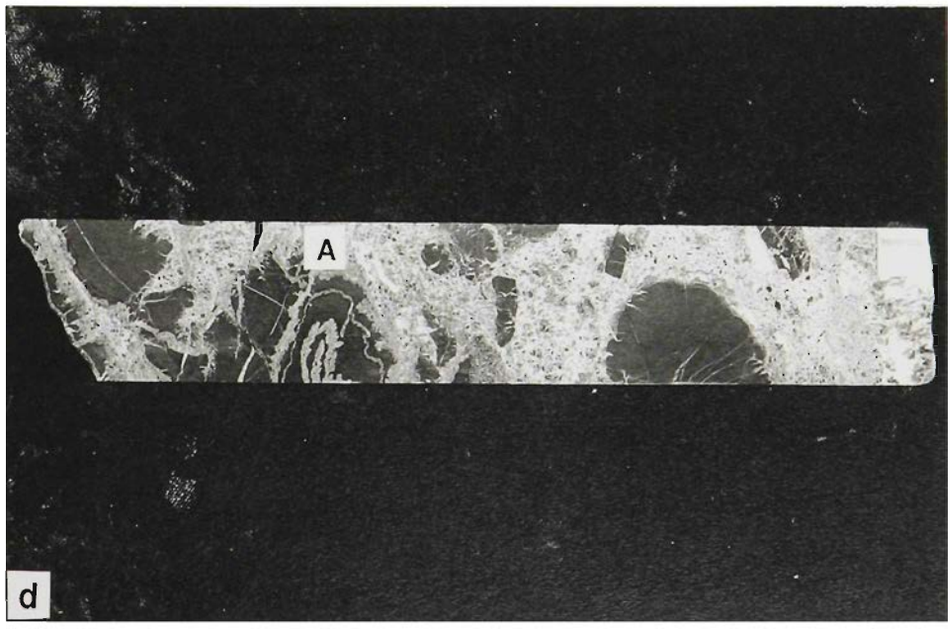
A
d

PART C.

Figure 12. Microstructural relationships of sulphides. a. Dilation on bedding is related to small-scale refolded folds with both $s_{2.5}$ and s_3 orientations. Sphalerite (sp) has overgrown the dolomite that partially overprints these folds. Location. 9c sub. 5169N, 2501E.

Figure 12 b. Sphalerite (sph) aggregates overgrowing and showing no preferred orientation in a zone where biotite is aligned along the $s_{2.5}$ cleavage. Location. As for Fig. 11c.

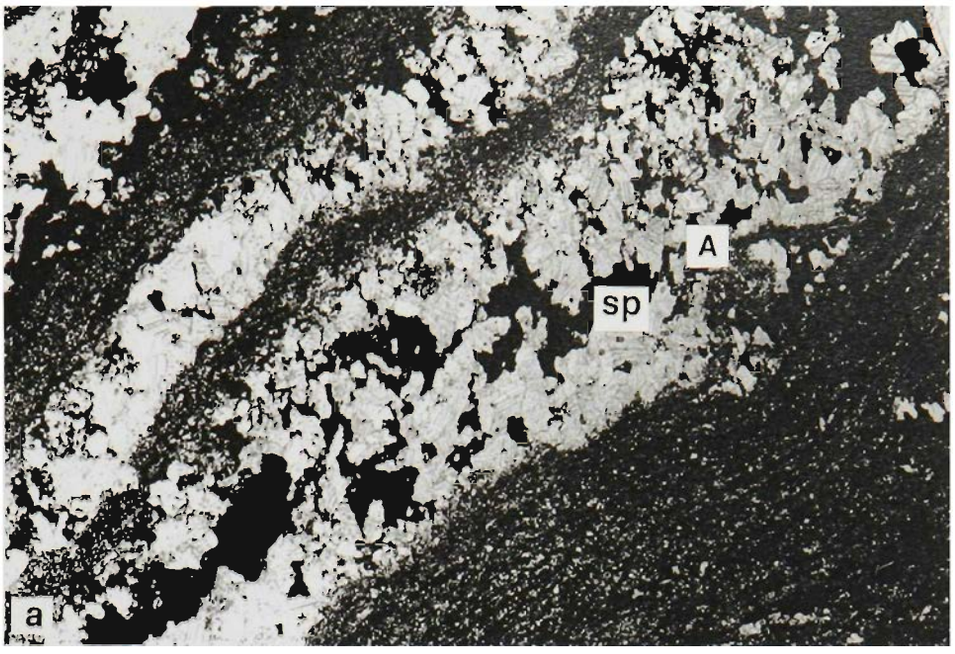
A
sp
a


sp
b

PART C.

Figure 12 c. Fine-grained pyrite overprinting a steep east-dipping spaced carbonaceous cleavage seam which is parallel to the axial plane of the broad fold shown in Fig. 8. Bedding is sub-horizontal (up the page). Field of view, 1.5mm. Plane polarized light.

Figure 12 d. Parasitic D_3 fold with dolomite in a saddle reef location which is partially replaced by sphalerite. Location as for Fig. 8.


c

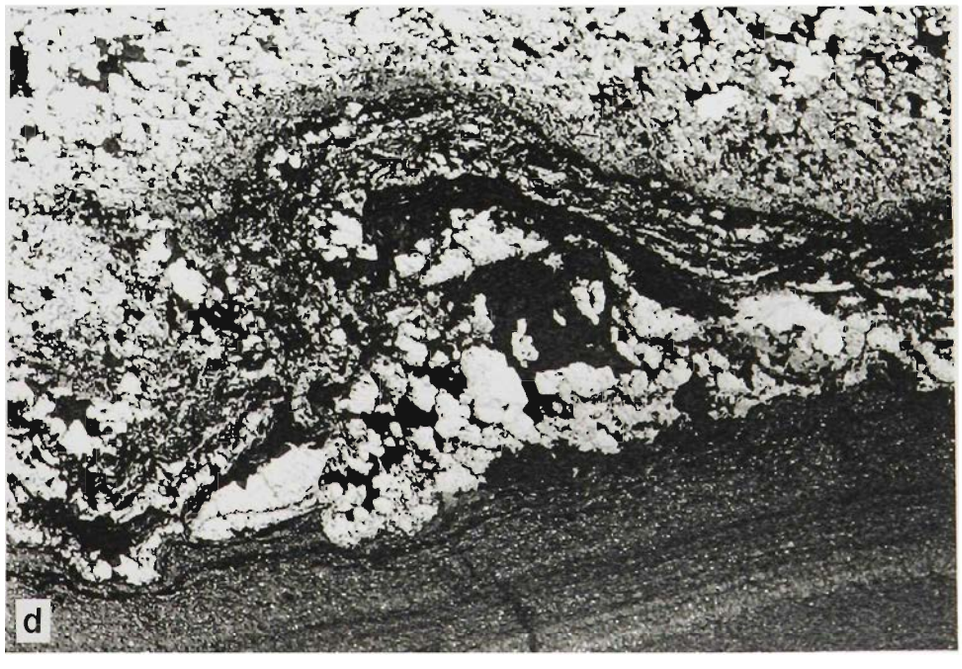
d

PART C.

Figure 12 e. Pyrrhotite (po) aggregates in ovoid quartz structures. Cleavage s_2 is truncated by these shapes, which are parallel to the high angle cleavage (s_4). Location 4 pod footwall LZ 119.

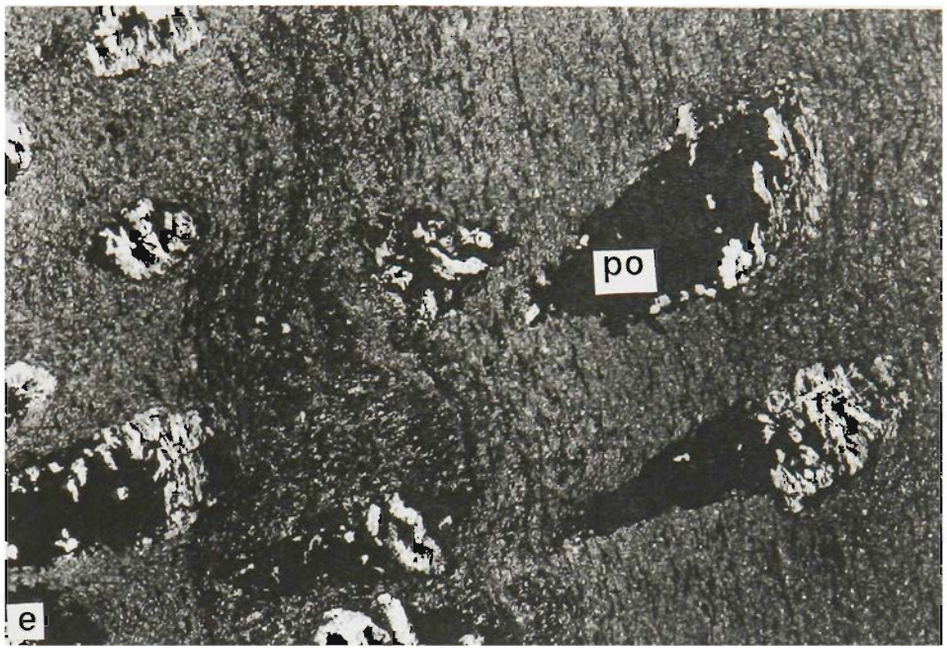
po
e

PART C.

Figure 13 a. Surface plan with location of drill holes used to obtain correlated samples from the hangingwall of 8 orebody. HYC.

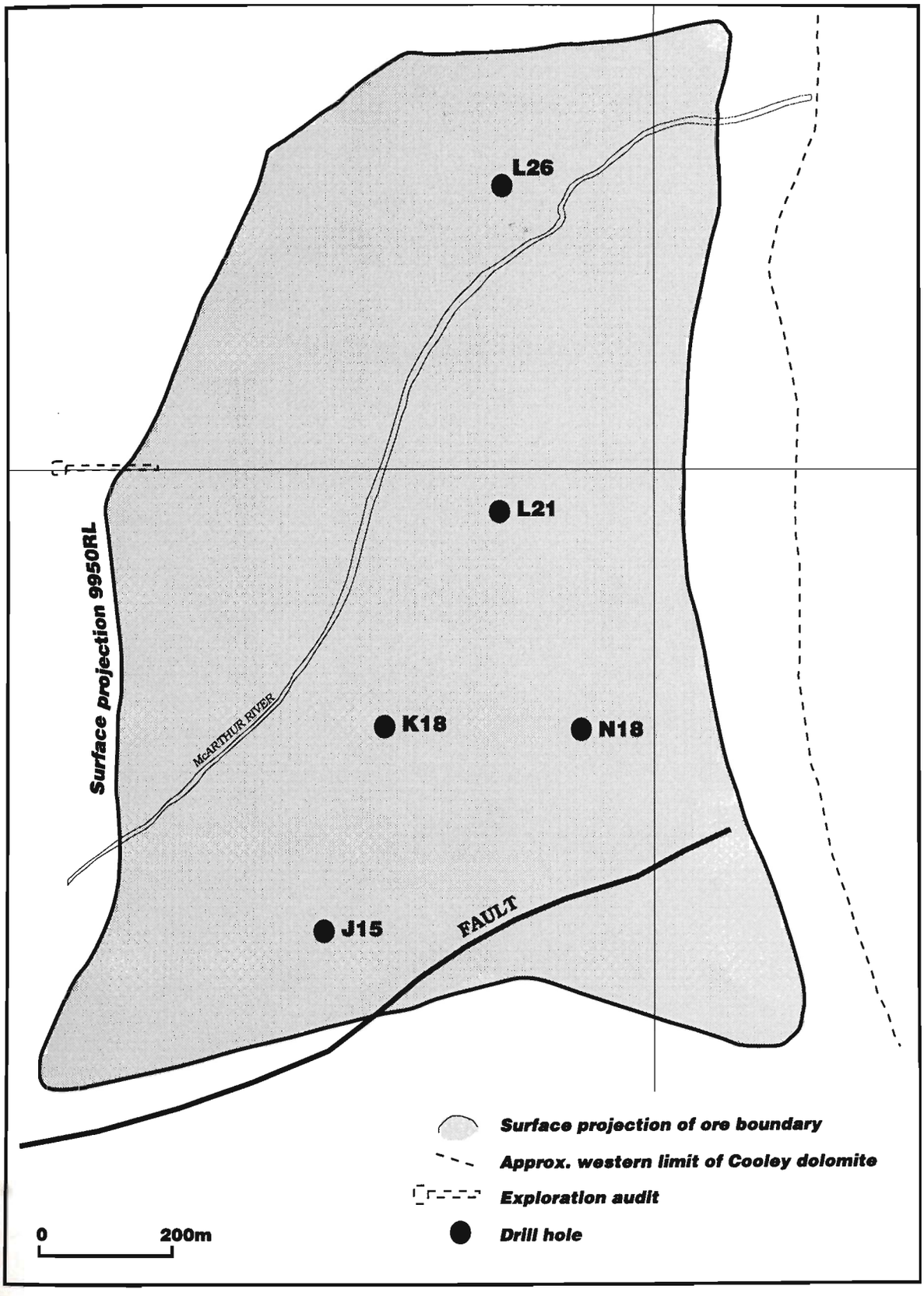
L26
L21
K18
N18
J15
FAULT
McARTHUR RIVER
Surface projection 9950RL
Surface projection of ore boundary
Approx. western limit of Cooley dolomite
Exploration audit
Drill hole
0
200m

Figure 13 b. Correlated mineralised sequence in the upper part of 8 orebody, from J15 in the south to L26 in the north. Direct projection of thin sections. Sulphides are in bituminous layers (black).

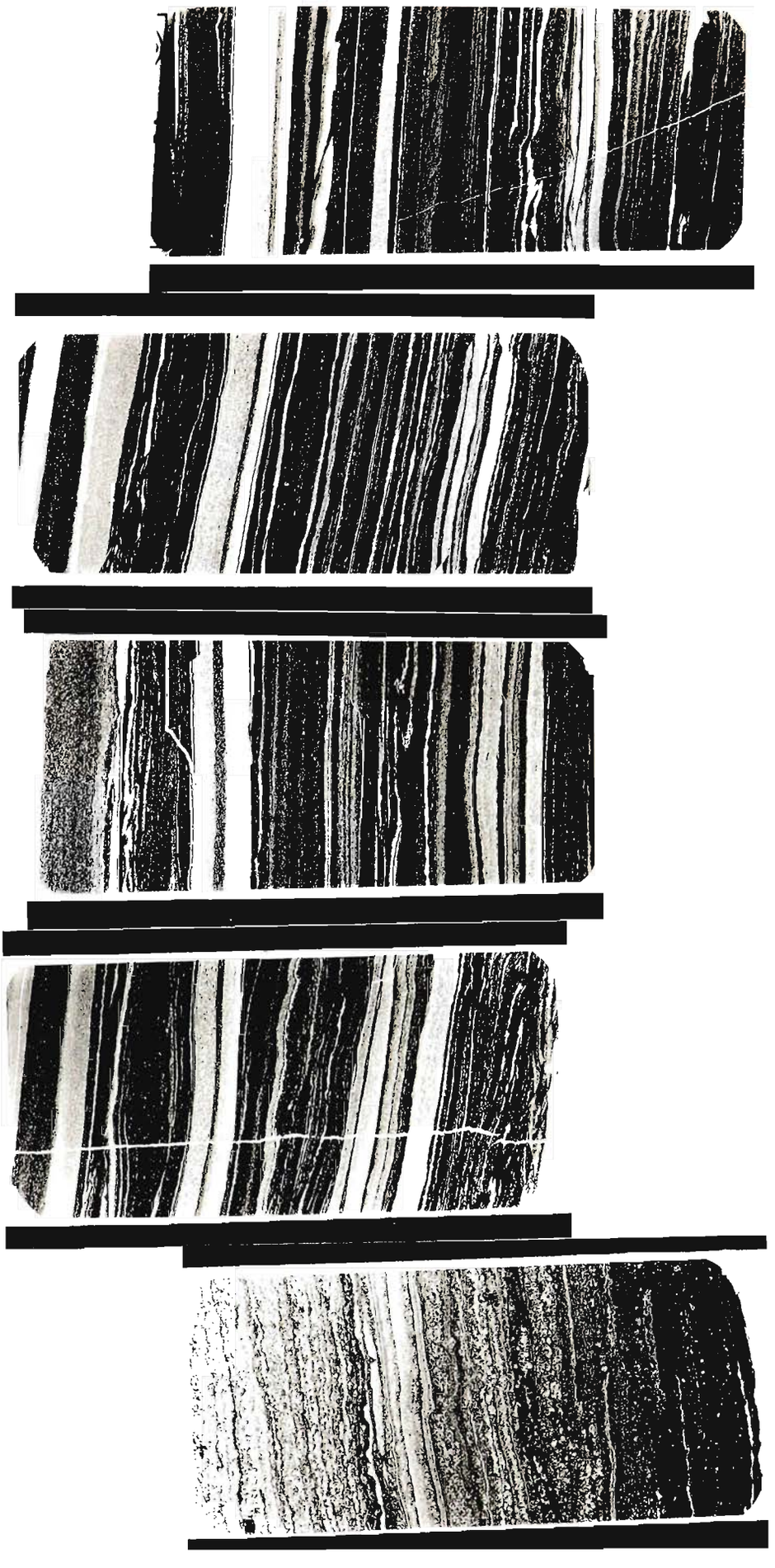

PART C.

Figure 13 c. Individual unmineralised laminae can be matched between cores shown in Fig. 13b (see tie lines). Thickness variations in the mineralised part of the sequence result from thrusting and extensional faulting.

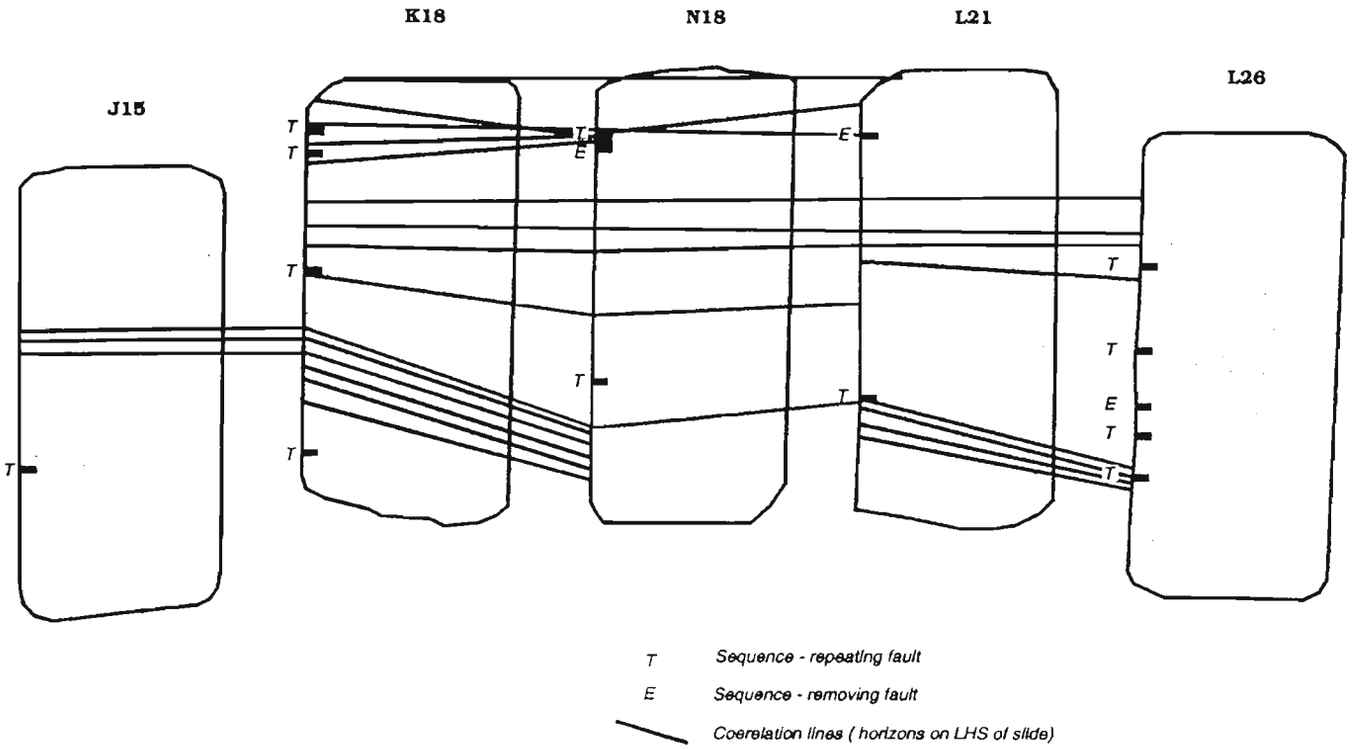
K18
N18
L21
J15
L26
T
E
Sequence - repeating fault
Sequence - removing fault
Coerelation lines (horizons on LHS of slide)

PART C.

Figure 14. Wall section of development in H.Y.C. 2-3 orebody zone. Larger second phase thrusts and folds are shown (in 3o/b lower, and at D), as are folds with a subhorizontal axial plane. From mapping by S. de Kruijff (1990). Looking south..

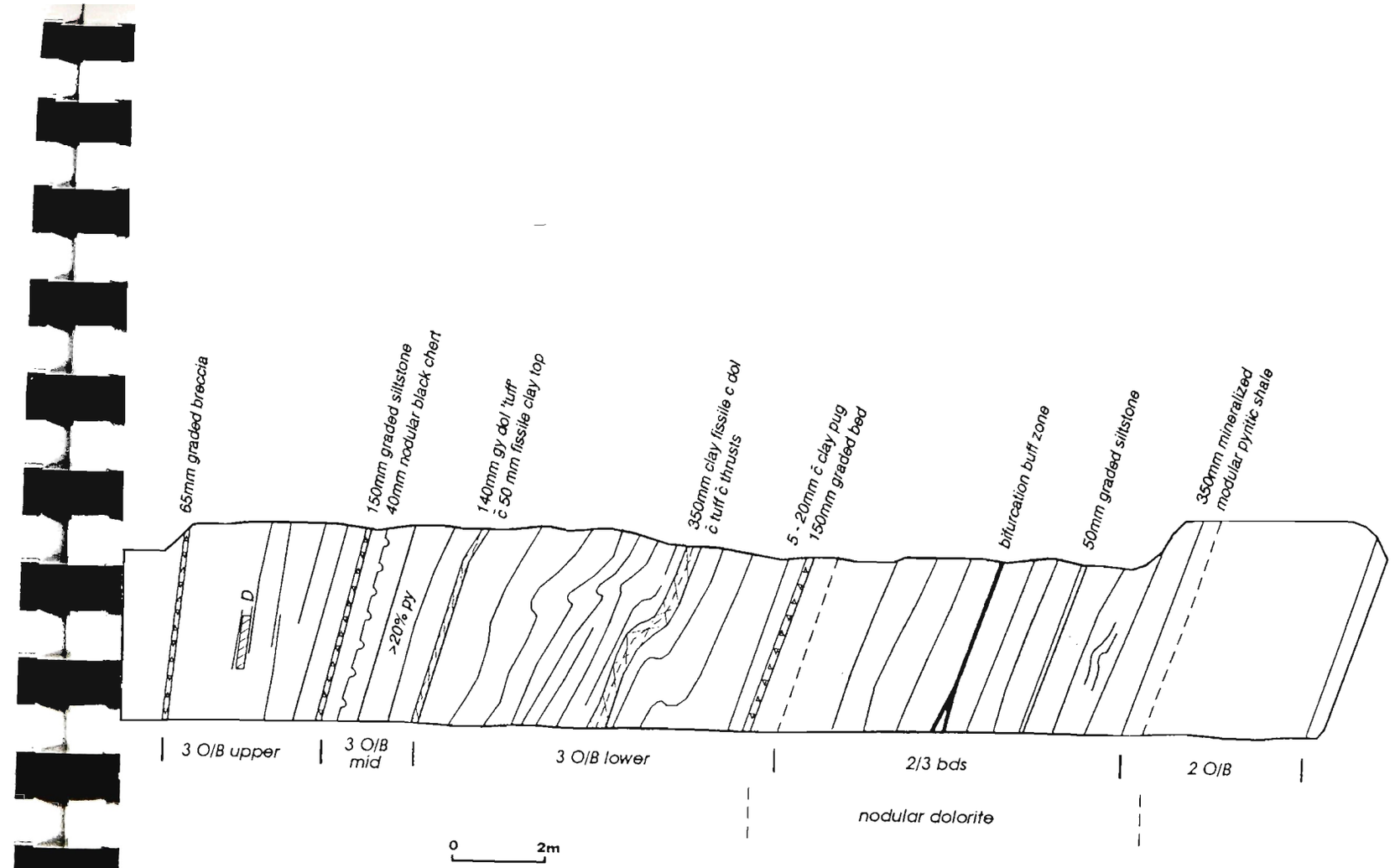
65mm graded breccia
150mm graded siltstone
40mm nodular black chert
140mm gy dol 'tuff'
c 50 mm fissile clay top
350mm clay fissile c dol
c tuff c thrusts
5 - 20mm c clay pug
150mm graded bed
bifurcation buff zone
50mm graded siltstone
350mm mineralized
nodular pyritic shale
D
>20% py
3 O/B upper
3 O/B
mid
3 O/B lower
2/3 bds
2 O/B
nodular dolorite
0
2m

Fig 14

PART C.

Figure 15 a. High grade H.Y.C. ore with good development of coarse-grained Pyrite II. Structures include early extension faults, phase 1 thrusts and phase 2 folds and Location: 3 orebody D in 13a, looking south.


a

PART C.

Figure 15 b. Illustrative sketch of Fig 15a showing the scale and distribution of both phases of low-angle thrusts, associated folds, and extensional structures. Looking north.

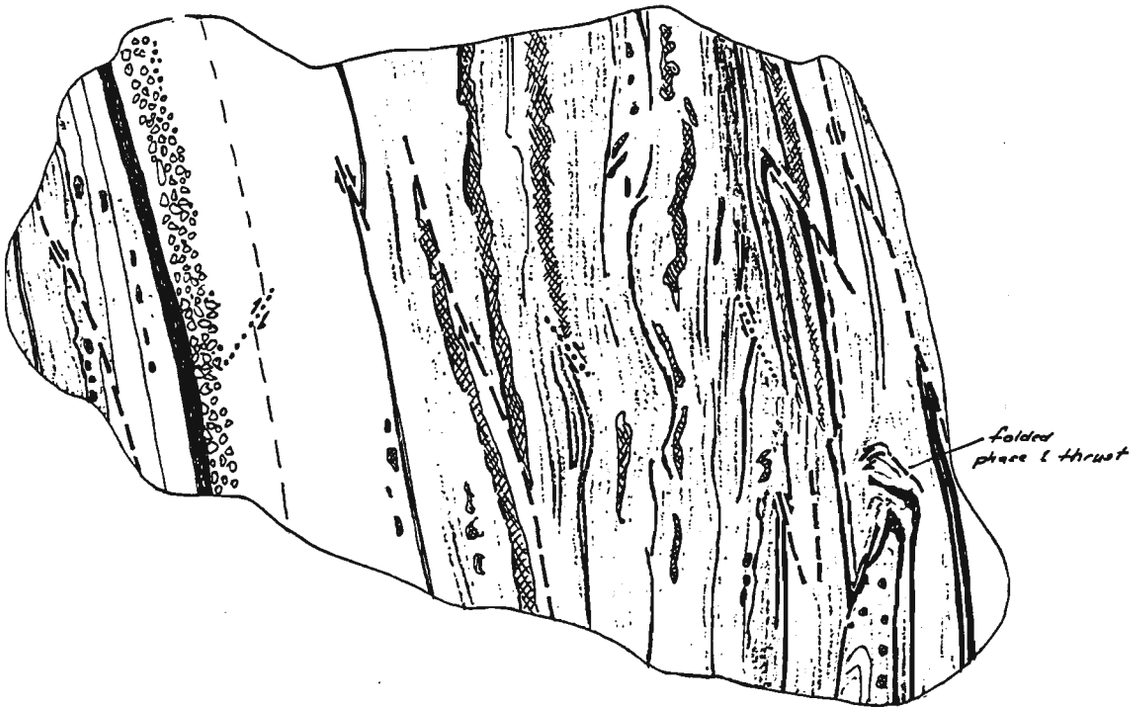

LEGEND.

- Graded polymict breccia horizon ~ 300mm.
- Carbonaceous non-mineralised siltstone.
- Fine-grained sphalerite and pyrite layers.
- Aggregates and layers of coarser-grained pyrite.
- Phase I thrust faults.
- Phase II thrust faults.
- Extensional faults.

Figure 16. Margin of Cooley Dolomite breccia. Three distinct lithologies are illustrated. 1. Highly carbonaceous laminite with pyritic bands. 2. Non-laminated grey dolomite with some microbreccia fragments. 3 Non-carbonaceus dolomite occurring as veins and irregular masses. Textures indicate that 1 has been overprinted by 2 and 3 in turn. Location S32/05.

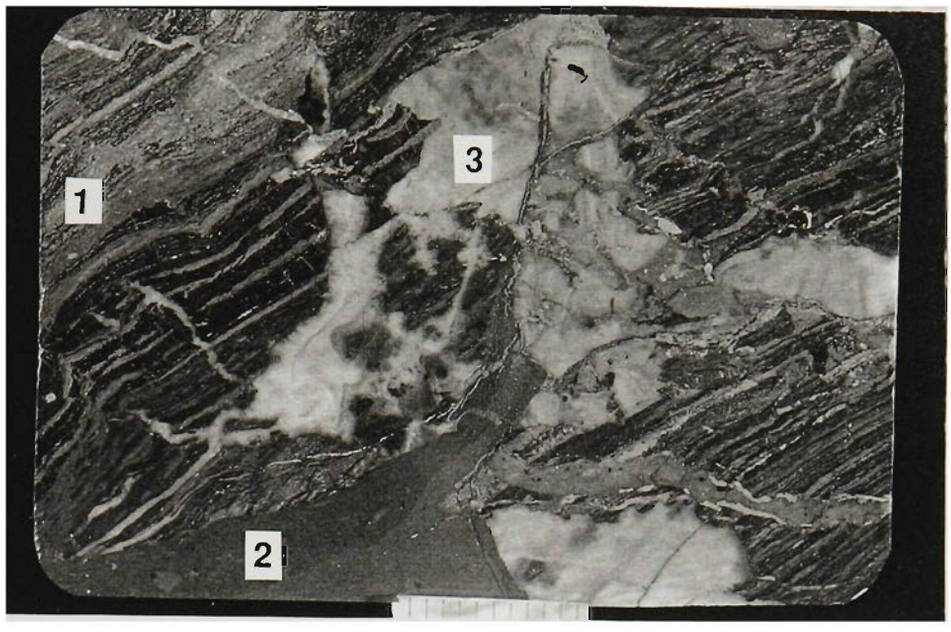
1
2
3

Figure 17. Range of polymict breccias showing varying degrees of incorporation of laminated carbonaceous siltstone.

a. Clast-supported graded breccia with mineralised laminated siltstone at the base, on the left of the calcite-marcasite vein at A. There is only one small pyritic clast inside the breccia. Location, 3 orebody footwall.

Figure 17 b. Breccia with fragments which fit together within a largely non-laminated carbonaceous pyritic matrix with smaller clasts. The central whitish part of the composite fragment has the same fractured texture as the Cooley Dolomite. Location, K18, 208.2m.

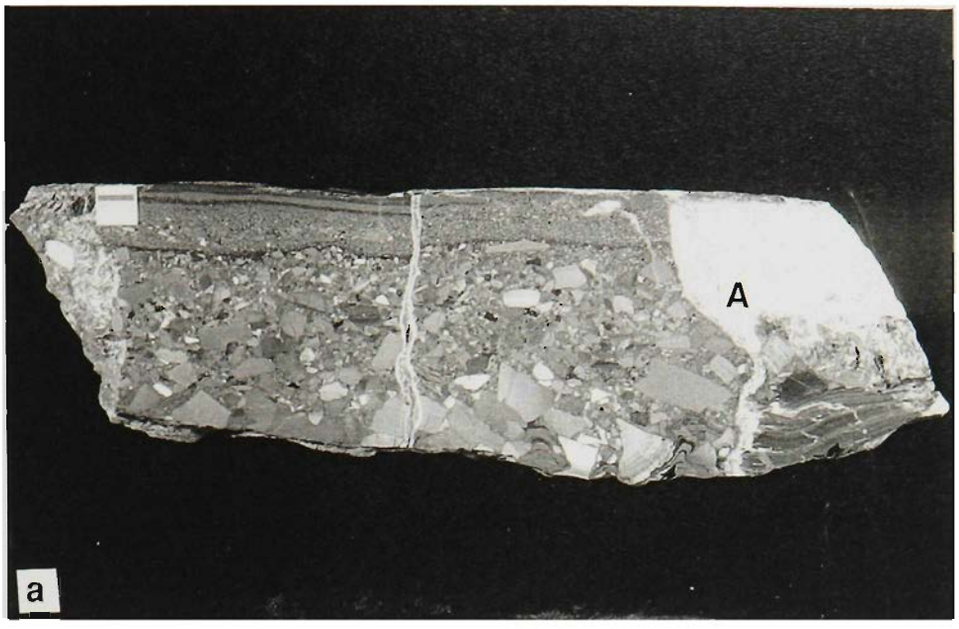
A
a

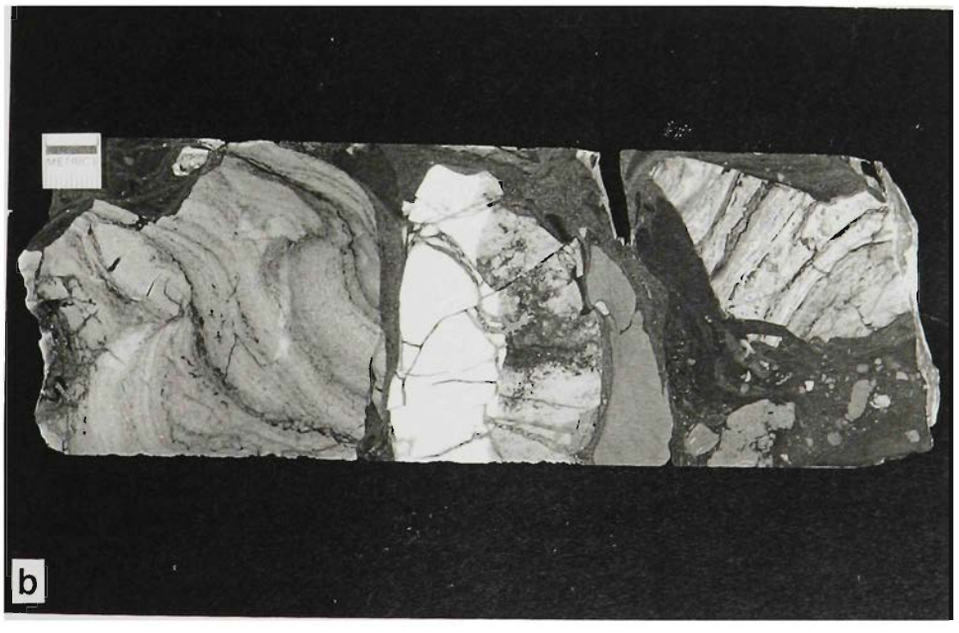
b

PART C.

Figure 17 c. Non-graded breccia with pyritic laminite at the base and irregularly shaped almost continuous blocks and wisps of pyritic laminite within it. The pyritic laminite appears to have been digested by the breccia. Location, N40, 336.0m.

Figure 17d. Irregular clast sizes within a breccia which contains distinct bands of sulphidic laminite, including a zone with an isoclinal fold A. The matrix is non-laminated but highly pyritic. The clast at B has differential shortening of the carbonaceous mudstone around it. Location, L21/50, 269.46m.

Figure 17 e. Breccia which is 80mm thick on one side of the drill core and non-existent on the other. It is cross-cutting to bedding at a high angle both above and below. Base of sequence is to the right.. Location: CPD-2, 112.9m. 11km north of H.Y.C. deposit.

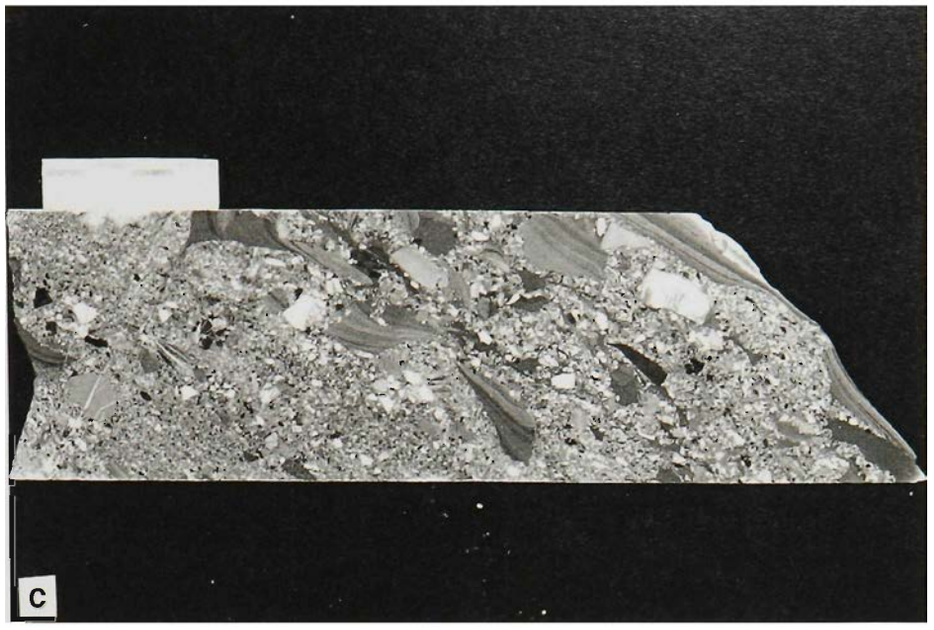
c

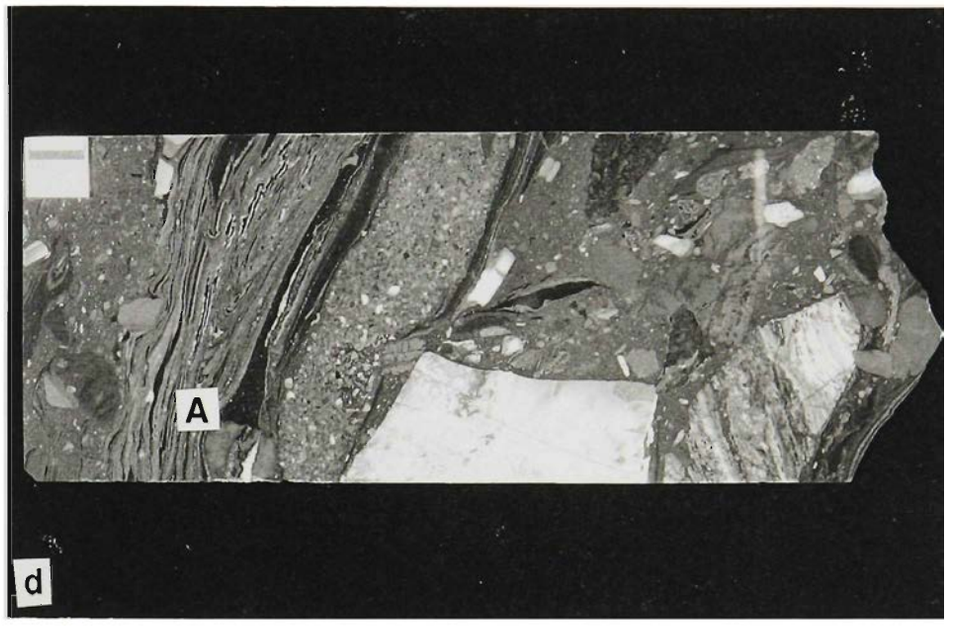
A
d

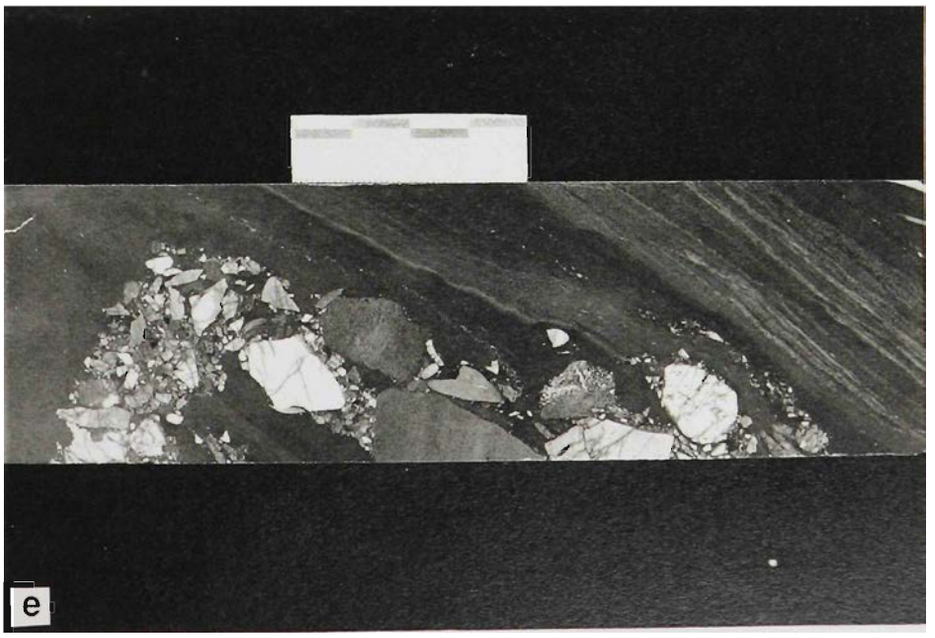
e

PART C.

Figure 18 a. Mineralised "clasts" from the top of a polymict breccia horizon. In the "clast" at the top, microfaults parallel to the second cleavage do not displace the "clast" boundary and therefore it must have been incorporated after the faults formed. Location, N18, 319.0.


a

PART C.

Figure 18 b. Detail of a. Clasts can be related using the late dolomite vein.

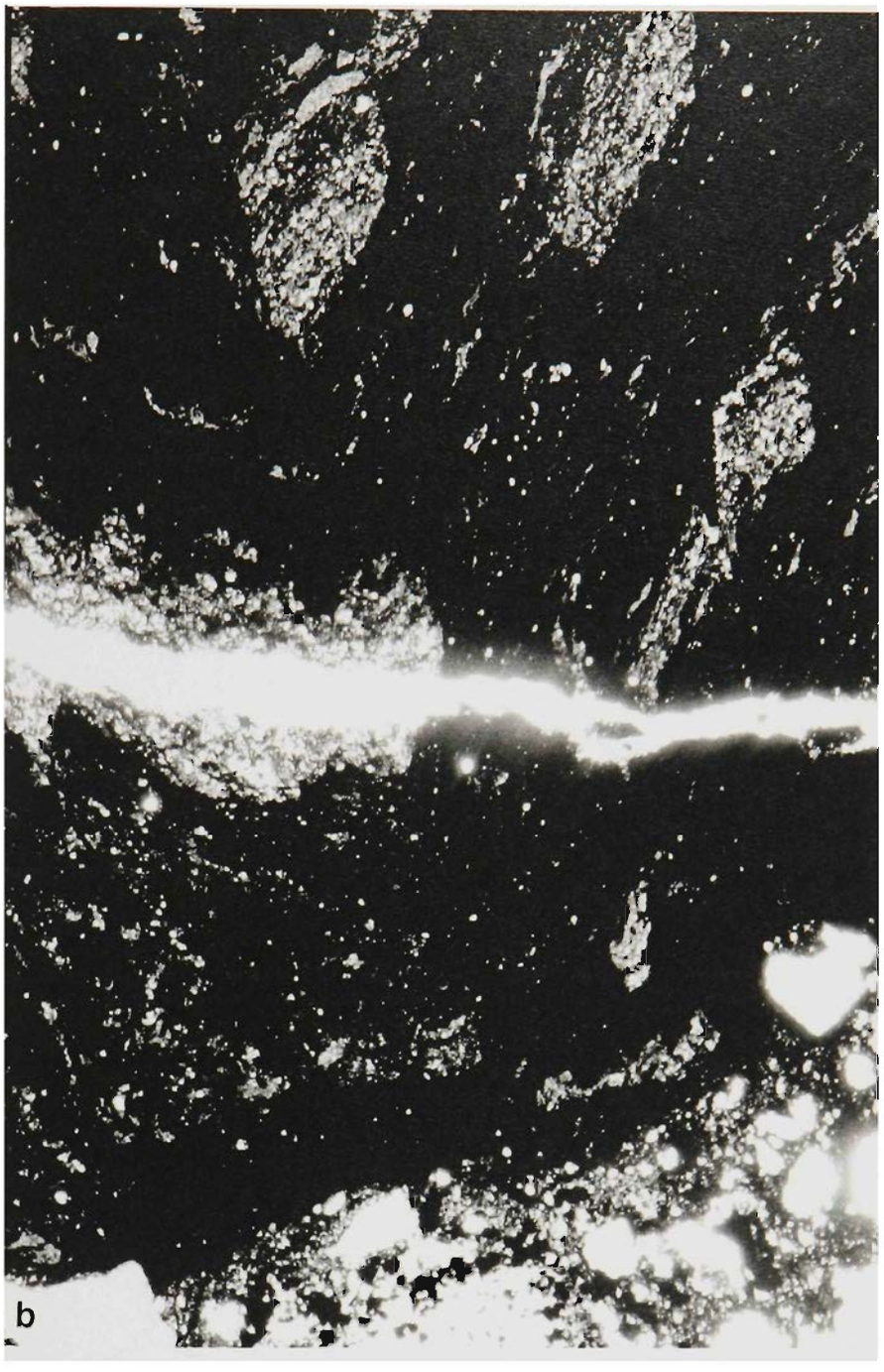
b

PART C.

Figure 18 c. Dolomitic clasts showing angularity, and a rind of a more carbonaceous lithology enclosing the clast in the centre. Beneath it is a jigsaw fitting of similar clasts. Location, N18, 319.5m.

Figure 18 c. Very irregular shape of breccia clast with protrusions in a pyritic carbonaceous matrix which shows transitional boundaries to tightly folded mineralised laminite. both above and below. Location, L21, 269.46m.

c

d

PART C.

Figure 19. Polymict breccia from within the Teena dolomite. Angular clasts similar to stratabound breccias from the H.Y.C. sequence. This breccia cuts across bedding. Location. Access decline, 1994.


CENTIMETRES
INCHES
MIM
EXPLORATION

PART C.

Figure 20 a. Cross section on 183900N showing the onlap interpretation. In this interpretation, the Cooley Dolomite is a fault breccia in Mara dolomite, related to the Mount Stubbs Fault, and the uplifted block is onlapped unconformably by the upper part of the Barney Creek Formation.

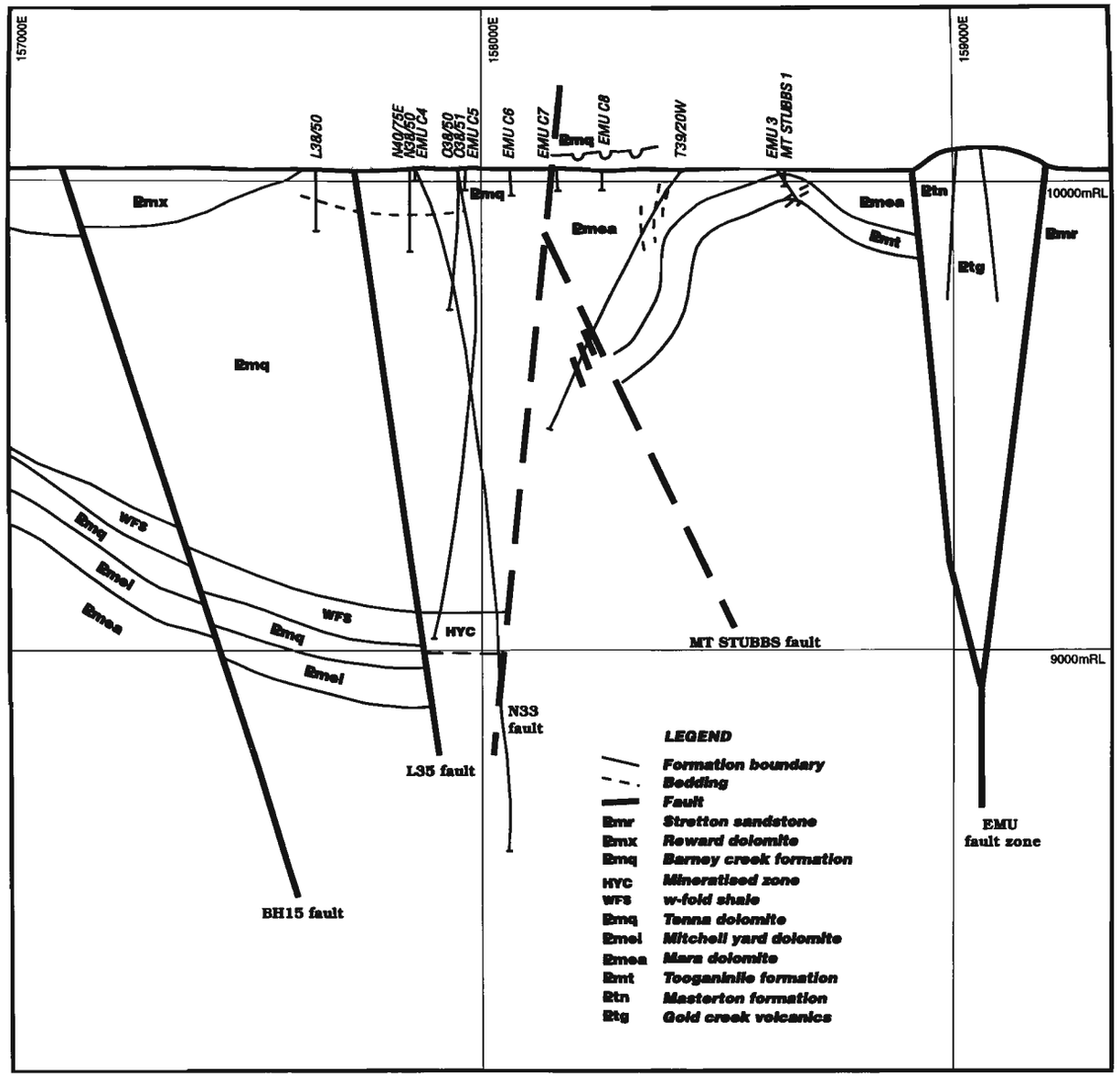
157000E
158000E
159000E
L38/50
N40/75E
N38/50
EMU C4
C38/50
C38/51
EMU C5
EMU C6
EMU C7
Emq
EMU C8
739/20W
EMU 3
MT STUBBS 1
10000mRL
9000mRL
Emx
Emq
Emea
Emt
Etn
Etg
Emr
WFS
Emel
HYC
MT STUBBS fault
N33
fault
L35 fault
BH15 fault
EMU
fault zone
LEGEND
Formation boundary
Bedding
Fault
Emr Stretton sandstone
Emx Reward dolomite
Emq Barney creek formation
HYC Mineratised zone
WFS w-fold shale
Emq Tanna dolomite
Emel Mitchell yard dolomite
Emea Mara dolomite
Emt Tooganinnie formation
Etn Masterton formation
Etg Gold creek volcanics

PART C.

Figure 20 b. Same section as (a) with the alternative interpretation of the Cooley dolomite as a fracture-controlled alteration body with relatively abrupt boundaries. The degree of Cooley alteration refers to the amount of bedding preserved, the uniformity of colouration and the proportion and vagueness of the areas of darker dolomite.

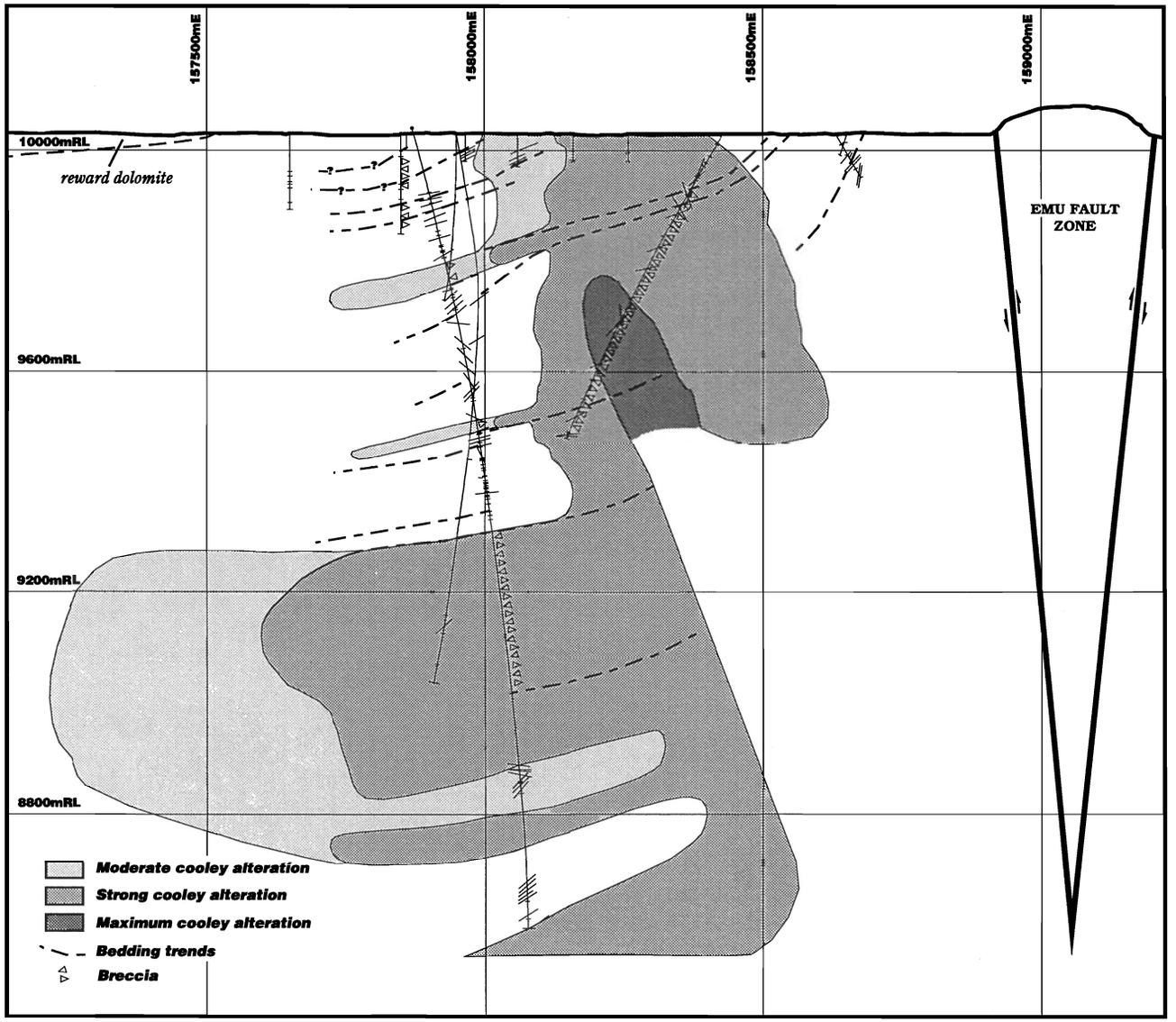
157500mE
158000mE
158500mE
159000mE
10000mRL
9600mRL
9200mRL
8800mRL
reward dolomite
EMU FAULT ZONE
Moderate cooley alteration
Strong cooley alteration
Maximum cooley alteration
Bedding trends
Breccia

Figure 21. Concretionary structure in pyritic sequence. Note the thicker continuation of the dark pyritic layer into the concretion where the concentration of pyrite is much reduced, and the thinning of layers around the concretion. Location, N18, 349.9m.

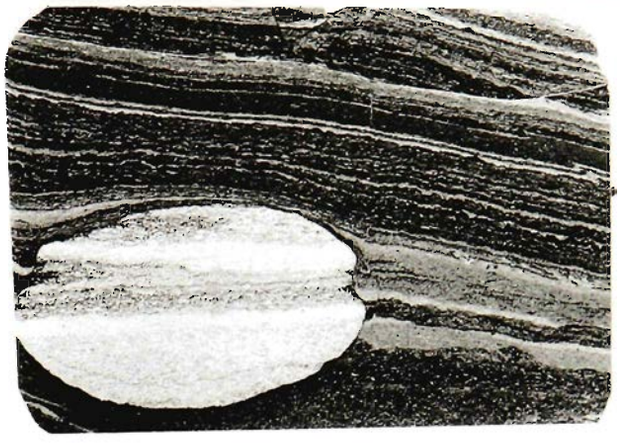

Figure 22 a. Nodular dolomite in highly pyritic sequence. 2-3 orebody interval, underground development.

Figure 22 b. Detail of nodular dolomite, showing that nodular layers have a corresponding relationship to the siltstone layers as the bituminous mineralised layers. Location.. J15, same sample as Fig. 13b.

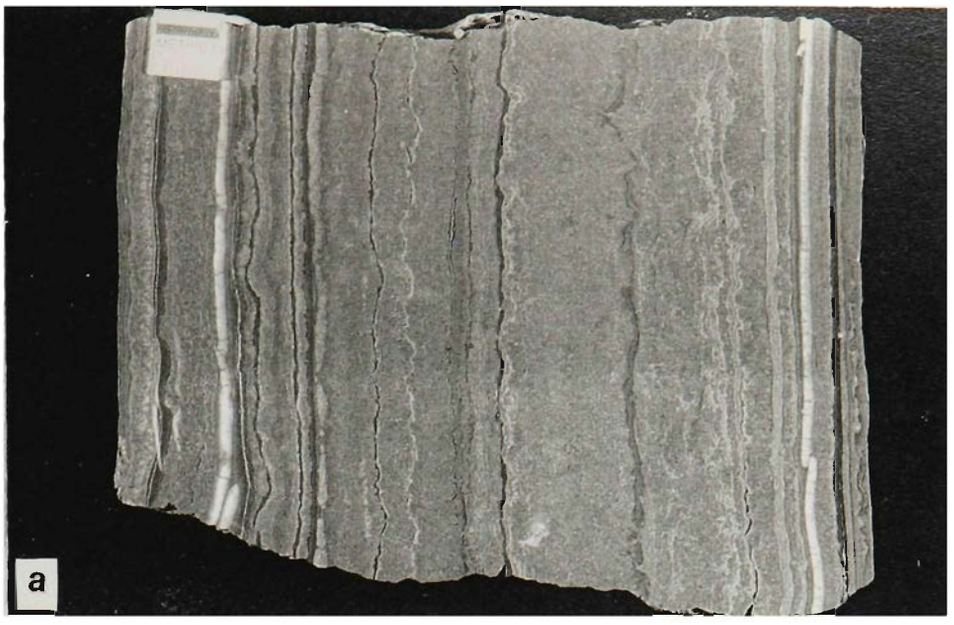
a


b

Figure 23. Microstructural relationships of sulphides. a. Refolded folds and two generations of shortening. A phase 1 thrust is refolded around the fold in centre (siltstone layer is repeated). Phase 1 thrusts repeat the layers on the bottom right. Location development D in Fig. 14. Looking north.

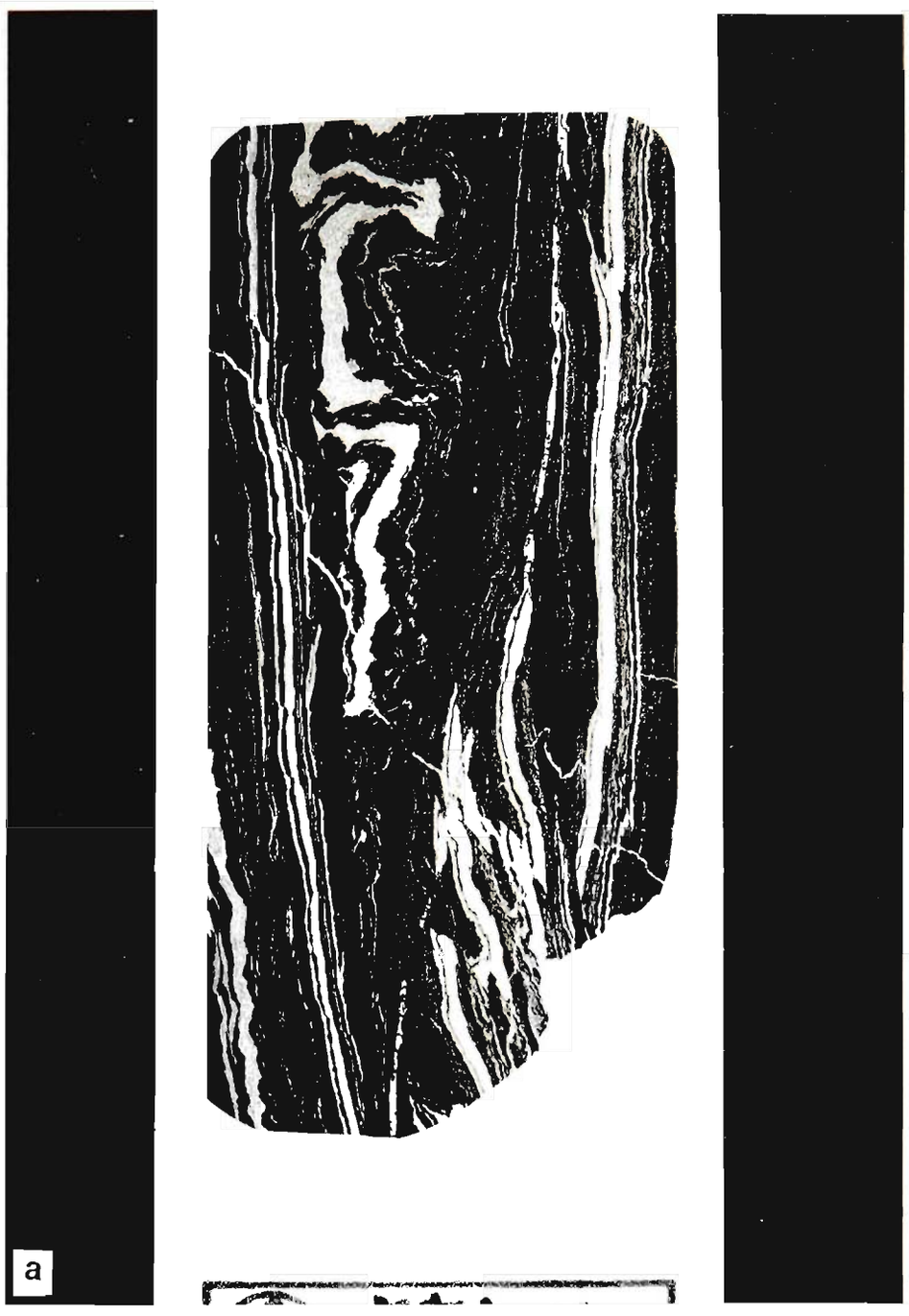
a

Figure 23 b. Phase I thrust (NE to SW on photo) with at least 15mm of displacement, apparently overgrown by a 100mm sphalerite mass (centre) with fine inclusions of pyrite, which has the same characteristics as sphalerite further along the bedding. Location LZ 142. 3 orebody development.

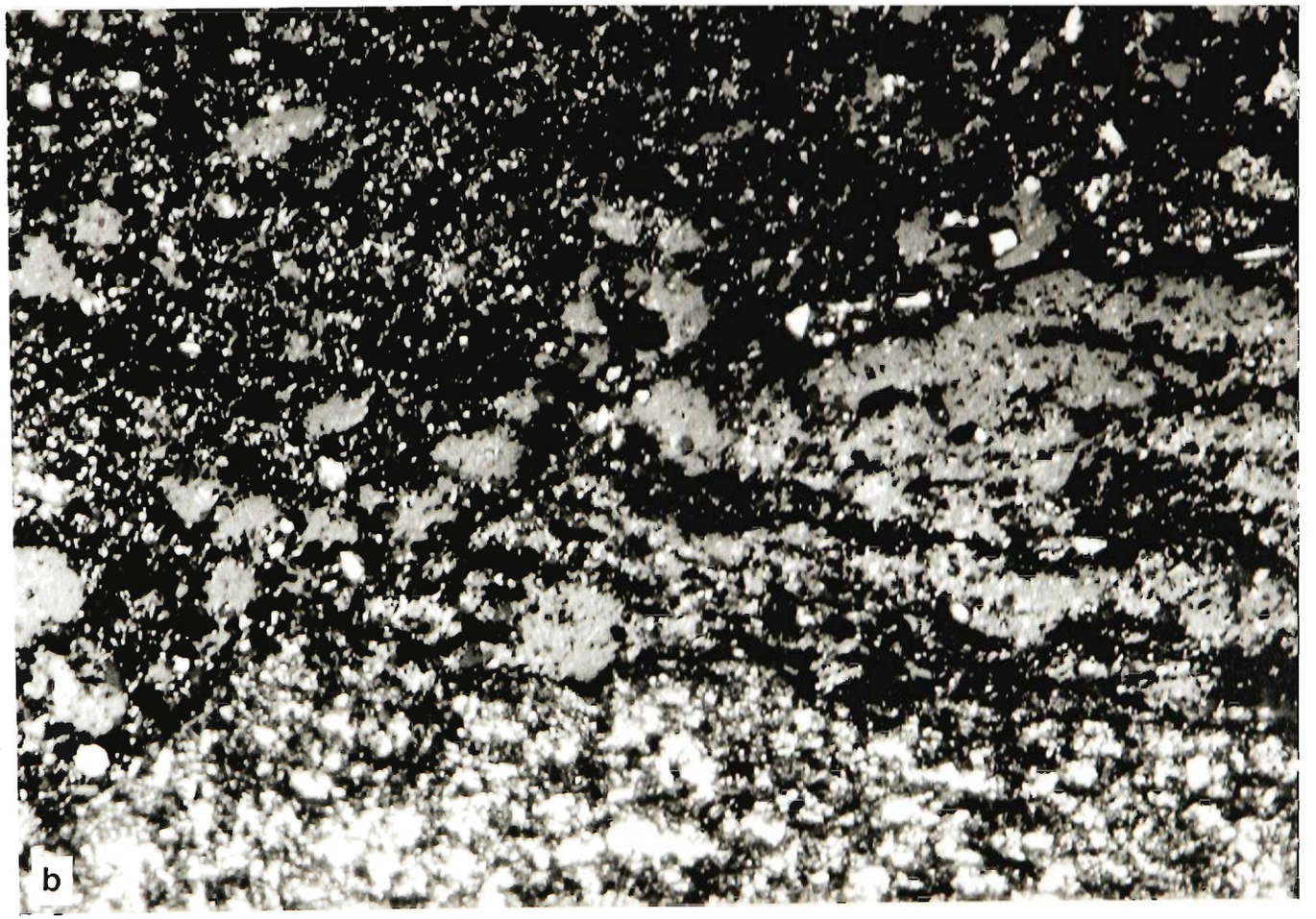
b

PART C.

Figure 23 c. Change in density of sphalerite aggregates (in black zones) across extensional microfaults, indicating the sphalerite to be deposited later than the microfaults.. Field of view (long) 2mm. Location, LZ71. N18, 315.2m.

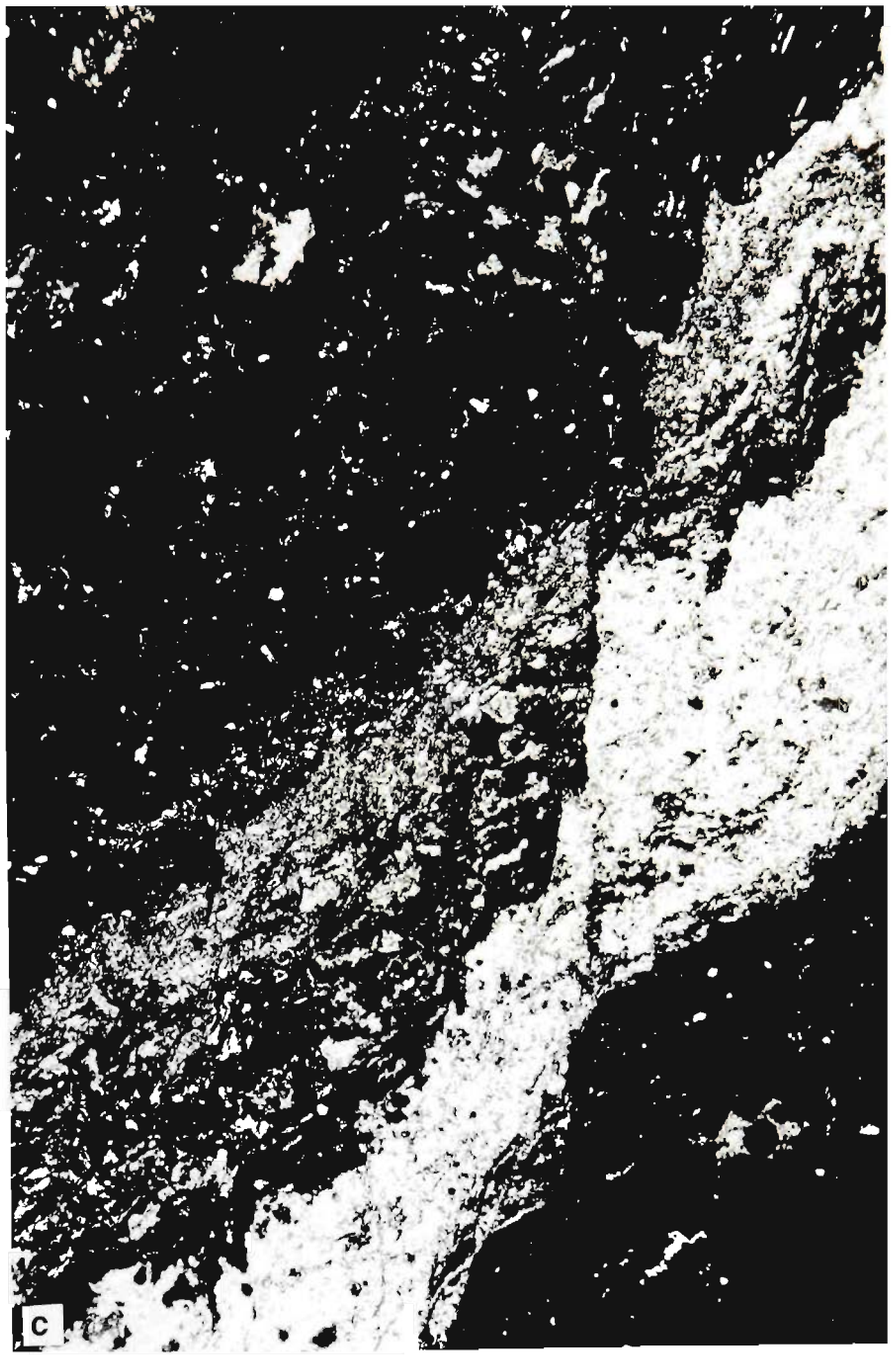
C

Figure 23 d. Different distribution of sphalerite (in black zones) along bedding either side of a dolomite vein (vertical). Veins similar to these cut across the Phase II thrusts. Scale 2mm vertical. Location LZ71, N18, 315.2m.


d

Figure 23 e Sulphides (in black zones) cutting across bedding-parallel cleavage in the hinge zone of a composite fold. Field of view (long) 5mm. Location, upper fold from Fig.23a.

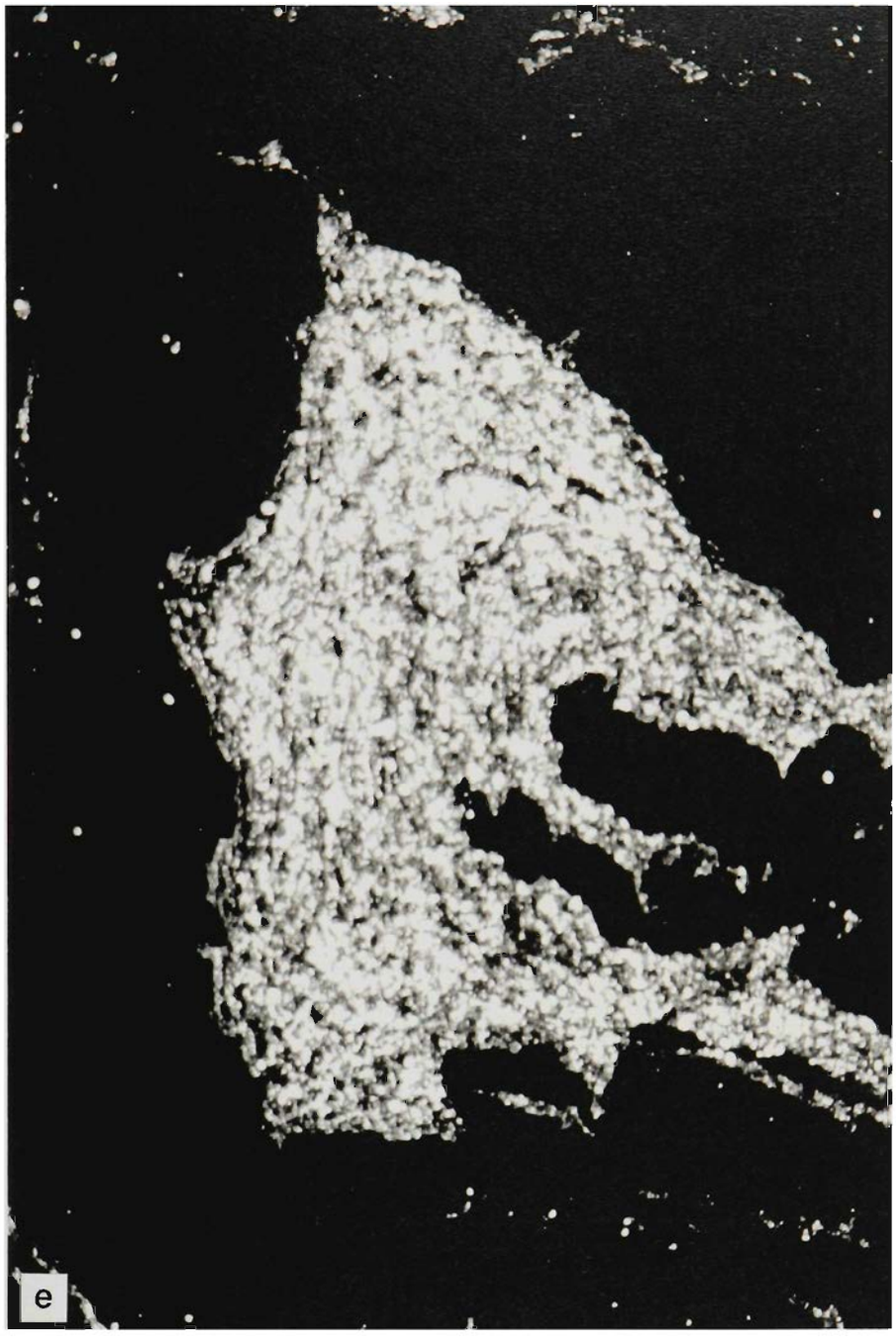
e

PART C.

Figure 24 a. Extensional replacive microveinlets in the mineralised zone at Mount Novit. Location: surface exposure, 18,700mN, 11650mE.

Figure 24 b. Silicified laminated siltstone with replacive ferroan dolomite veinlets giving a blotchy pseudobreccia appearance, but with minimal disruption of bedding. The sulphide (white) is mostly pyrrhotite with minor pyrite and is exclusively associated with the dolomite zones. Location: Kw579S 894.0m. c. Dolomitic replacive microveinlets, Location H830, 288.0m.


a

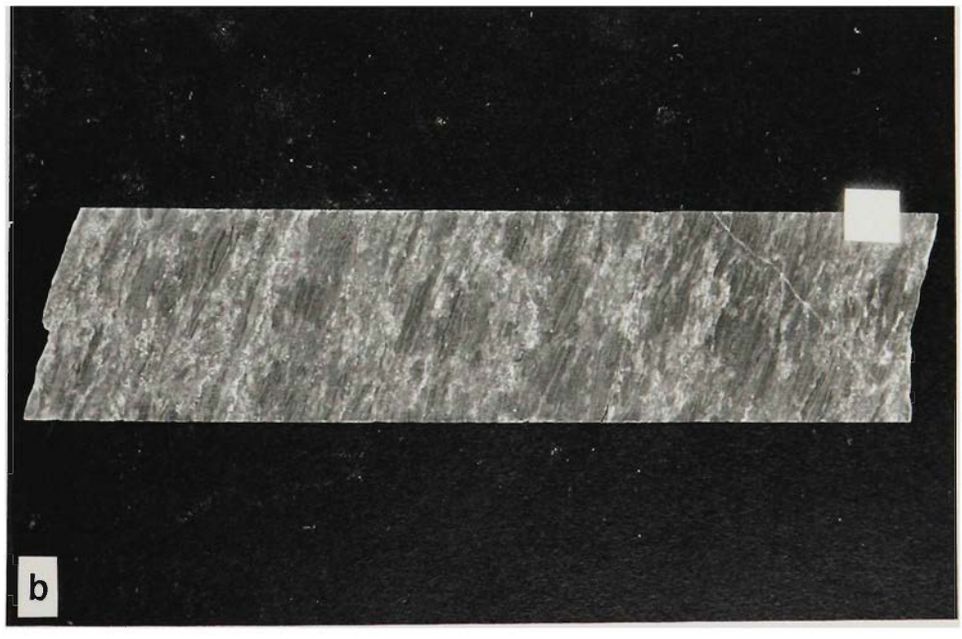
b

PART C.

Figure 24 c. Dolomitic replacive microveinlets, Location H830, 288.0m.

c

PART C.

Figure 25 a. Fold zone at Mount Novit. The folds are perfectly cylindrical and have a very well developed rodding lineation parallel to the fold hinge.

Figure 25 b. Strong lineation on s_2 parallel to bedding, with "birdswing" veins folded about the lineation. Location: 18,4700mN, 11,670mE.

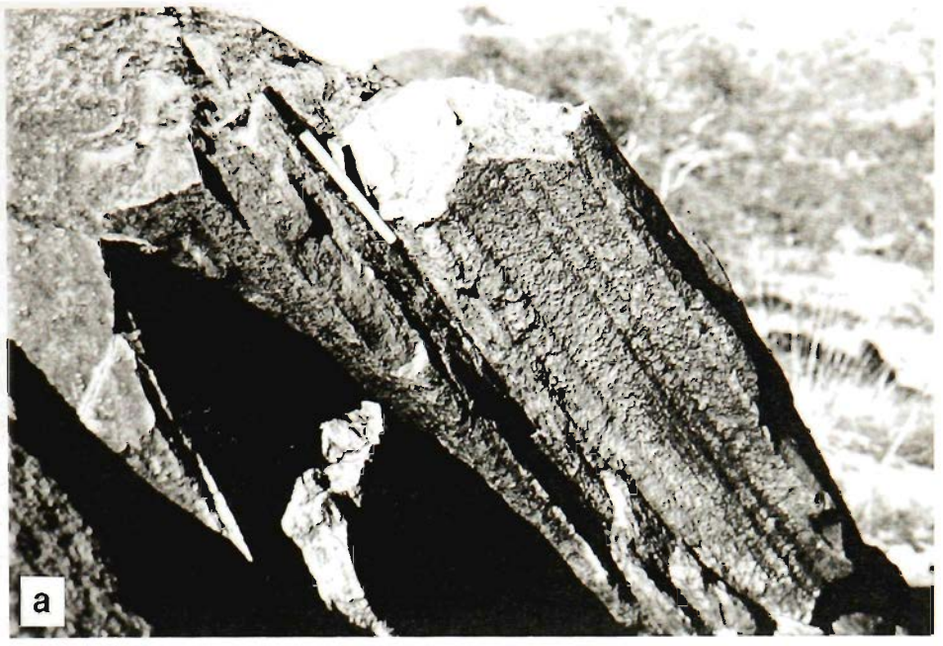
a


b

Figure 26. Series of mineralised samples from the Mount Novit zone. a. Carbonaceous schist breccia. Copalot shaft. b. Fine-grained breccia with rounded fragments. Location H830 328.4m.

Figure 26 c. Highly sericitic slate with crenulations overprinted by dolomite and containing sphalerite. Location H830 320.4m.


a
b

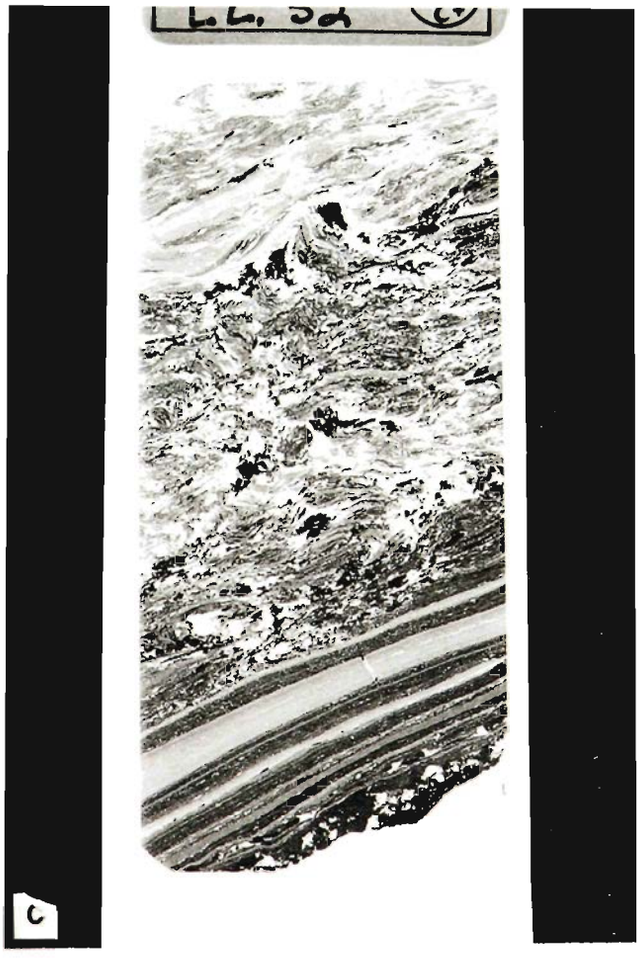
c

PART C.

Figure 27 a. Calcitic alteration in a fold zone east of the Mount Isa fault. Strain partitioning is evident between the laminated siltstone and the zones of calcite. The left half of the slide has been stained for calcite. The folding and alteration pattern is strongly similar to folded siltstones in lead-zinc rich zones elsewhere.

a

PART C.

Figure 27 b. Detail of A. Calcite is locally transgressive to the folds, e.g.at A. Location: H830, 444.1m.

Figure 27 c. Detail of a. Cleavage-parallel extensional microfaults rotate into the calcitic alteration. Location: H830, 444.1m.

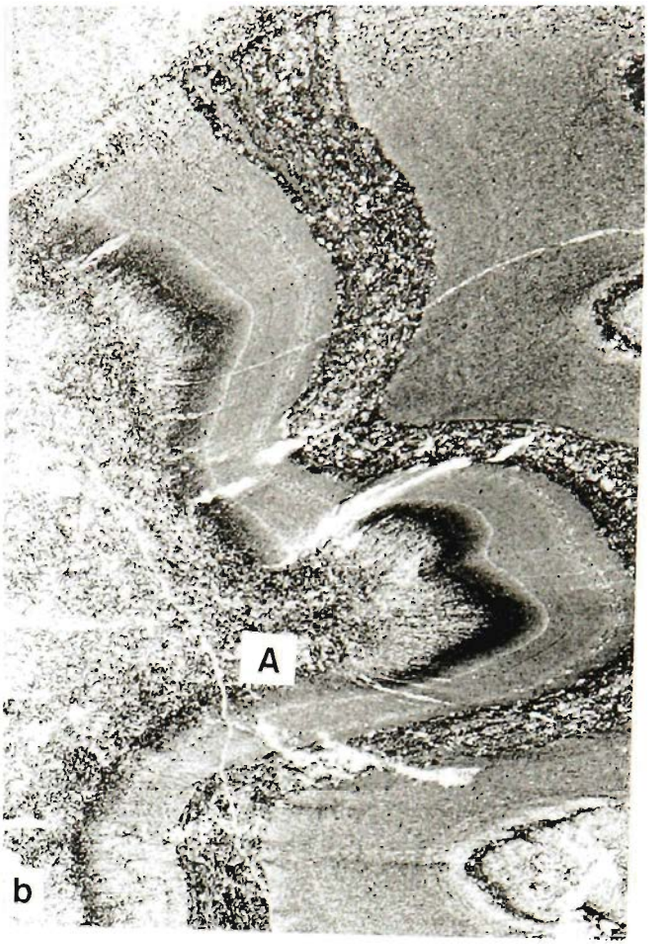
A
b


c

Figure 28. Microstructural relationships of sulphides. a Crenulation of strong bedding-parallel schistosity with overgrowing of dolomite and quartz. Dolomite grains have a strong foliation parallel to the crenulation hinges and are overgrown by strain-free dolomites. Quartz has been strained and recrystallised. Moderate biotite is aligned parallel to the strong schistosity. Sphalerite (sph) and galena (gal) apparently overgrow the dolomite and the quartz.

Figure 28 b. Strongly cross-cutting pyrrhotite (left) and sphalerite (right) developed stratigraphically above and below a fine-grained sericitic layer (vertical). The sulphides form a regular pattern of microveins replacing quartz, dolomite K-feldspar and biotite, which are approximately parallel to the second schistosity A. Some of the veins containing more biotite are sub-parallel to crenulation hinges in direction B.

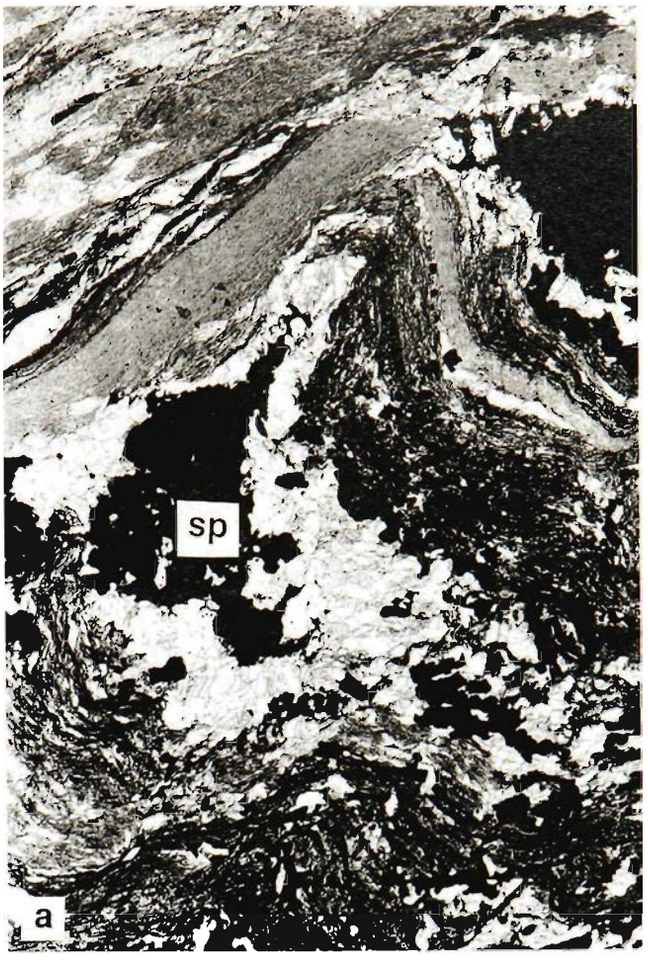
sp
a


B
A
b

Appendix 1.

FILE NOTE

From: W. Perkins 27 April, 1994.

To: D. Wilson.

Notes on Emu Plains Review, 10-24 Nov. 1993.

Summary.

The bulk of the time was spent in preparation of a series of 1:10,000 scale cross-sections, covering the zone from east of the Emu Fault and extending across the Western Fault Block to encompass the trough containing the major thickness changes in the Barney Creek Formation. These sections were used in the review presentation on 25, 26 November.

Preparation of the sections involved inspection of the standard logs, and the photographs and graphic logs by Martin Neudert where available. The 1:10,000 sections were drawn using the standard interpretation of the Cooley Zone being bounded to the west by the Mount Stubbs Fault, and on the top by an unconformity "onlap" of upper Barney Creek Formation.

An alternative interpretation of this zone is that it mostly represents in situ alteration of the steep limb of a post-McArthur Group fold in Barney Creek Formation. This interpretation removes the necessity of a major fault (Mount Stubbs Fault) and the unconformity "onlap". These boundaries, although probably controlled by local fractures and faults, may be largely alteration fronts.

The implication for copper ore search is that much of the presently known Cooley-zone copper mineralisation eg. in DDH R27, is contained within altered Barney Creek Formation, and not in older formations. Rather than concentrating exploration on the edge of the Cooley zone, it is likely that a target may exist further within the alteration system. Using the concept derived from work on Isa copper that precursor fine-grained pyrite is not a necessary precondition for high-grade copper ore, dolomitic sequences to the east and below the Barney Creek Formation are potential targets.

W. Perkins

cc. P. Stoker.

S. Robinson - Target Generation Group.

Discussion.

Existing Interpretation.

From work mainly done by Matt Williams and Mark Hinman, the interpretation of stratigraphic and structural relationships around the Cooley Zone has been extended to the northernmost drill section containing Emu 17 and Emu18 and L1 DDHs. The most detailed work has been done using oriented core by Mark Hinman on the 182900N and 183200N sections. On those sections, the Mount Stubbs Fault is interpreted to be a moderately east-dipping zone with a series of fault slices to the east of it, which contain overturned blocks of correlated footwall sequence rocks. Although significant thicknesses of Cooley-style alteration are shown west of the Mount Stubbs Fault in R29/05, associated with low angle faults, Hinman believes that Cooley-style alteration only affects the upper parts of the breccia cycles and not the carbonaceous laminites.

The onlap interpretation is derived from shallow fences of holes, such as the I series (approx. 186700N), G series (approx. 185900N), E series (approx. 185100N), and Emu 14, Emu 16 (approx. 184700N). There is debate about the stratigraphic level of "onlap" but now most agree that it is upper Barney Creek Formation, with Mara Dolomite beneath it adjacent to the Mount Stubbs Fault. The apparent displacement on the Mount Stubbs Fault in section ranges from almost nil on 181900N to greater than 1000m. on 183500N.

Possible alternative interpretation.

DDH's S32/05 ND and R27 both appear to show extensive Cooley-style alteration of HYC carbonaceous laminites. In S32/05, the zone examined was between 28m. and 47m. The interval from 28m. to 32.9m. consists of a breccia with angular to ragged-edged buff-cream fragments in a darker carbonaceous matrix. From 32.9m. to 41m. contains about 50% strongly pyritic carbonaceous HYC shale and 50% irregular Cooley breccia. Samples in particular at 36.1 and 36.5 seem to show a transition from laminated sediment to Cooley alteration, with transgressive darker zones obliterating the bedding, overprinted by sharp-edged but irregular vein-like zones and angular blocks of Cooley dolomite. The sequence from 41m. to 47m. is again Cooley-style breccia, but with angular relics of carbonaceous shale. R27 has a wide zone of very pale breccia with interstices containing carbonaceous matter, fine-grained pyrite, and chalcopyrite. This matrix composition and the fact that the zone lies on dip continuation from the HYC mineralised sequence are indicative of derivation from it.

Wholesale bleaching and diminution of organic carbon are a feature of thick sequences of Urquhart Shale at Isa Mine, particularly in the zone surrounding the 3500 orebody. Correlation in 7 orebody shows that this front of bleaching can occur over 20 metres. I suggest that the front of Cooley dolomite may be even more abrupt in general,

coinciding as it does with monoclinal steepening.

Cross-section on 183900N.

An alternative interpretation for the section produced by Matt Williams for the review is attached (Fig.1). Information comes from the N40 log and core examination, and photos of T39 and the shallow holes. The basis for the interpretation is the apparent continuity of bedding orientation from holes within definite HYC sequence to dolomitic horizons which have been interpreted as belonging to Mara Dolomite. Breccias intersected in T39 W. Dec. are similar to those in N40 except that they have a reduced range of clast colours and textures, which could represent increased Cooley alteration.

Two sets of apparent bedding orientations for T39 are shown. One is based on an assumption of north-south strike and consistency of orientation, and the other is from core orientation as determined by Dugi Wilson. There have been problems with core orientation in some holes, particularly the steeper ones such as N40. If the calculated core orientations in T39 are correct, then it is more difficult to interpret the brecciated sequence as the direct in situ altered equivalent to the sequence in N40.

The degree of Cooley alteration refers to the amount of bedding preserved, the uniformity of colouration and the proportion and vagueness of the areas of darker dolomite.

Copper Targetting.

The implication of the Cooley zone being more of an in situ alteration system, rather than a separate fault block, is that a potential copper orebody could be deeper downwards and towards the east within it. With the steep limb development to the east, adjacent to the HYC deposit, this means that trends would cross downwards into footwall sequences rather than remain in HYC sequence equivalents. Under a model requiring the prior existence of fine-grained pyrite in order to precipitate chalcopyrite, such a scenario would obviously be downgraded. However, while all high grade copper deposits in carbonaceous sequences are associated with stratiform pyrite, there is debate about it being a necessary precursor. Replacement of fine-grained pyrite by chalcopyrite at Mount Isa constitutes a minuscule proportion of the mass of chalcopyrite. Replacement of silicified dolomite seems to constitute the dominant mechanism of deposition of high grade copper ore. Only minimal carbonaceous material seems to be a requirement for this reaction. There is little evidence of association of chalcopyrite with silicification in known HYC mineralisation. However, by analogy with Isa "silica-dolomite", a more silicified core could exist deeper down within the Cooley zone.

I recommend persisting with the concept of a zonal link between the major HYC

lead-zinc deposit and a separate copper-rich target. Much of the exploration to date has been concentrated directly adjacent to the lead-zinc deposit, on the edge of the alteration system. This would be analogous to looking for copper ore on the edge of the "silica-dolomite" system, rather than deeper down in the core of it.

PART D.

Processes in the Formation of Stratiform Lead-Zinc Ore at Mount Isa and Hilton, Queensland.

Figures 1-4

APPENDIX 2

APPENDIX 3

APPENDIX 4

PART D.

Figure 1 a. Longitudinal projection of six locations in the 7 orebody stratigraphic interval sampled for geochemical profiles.

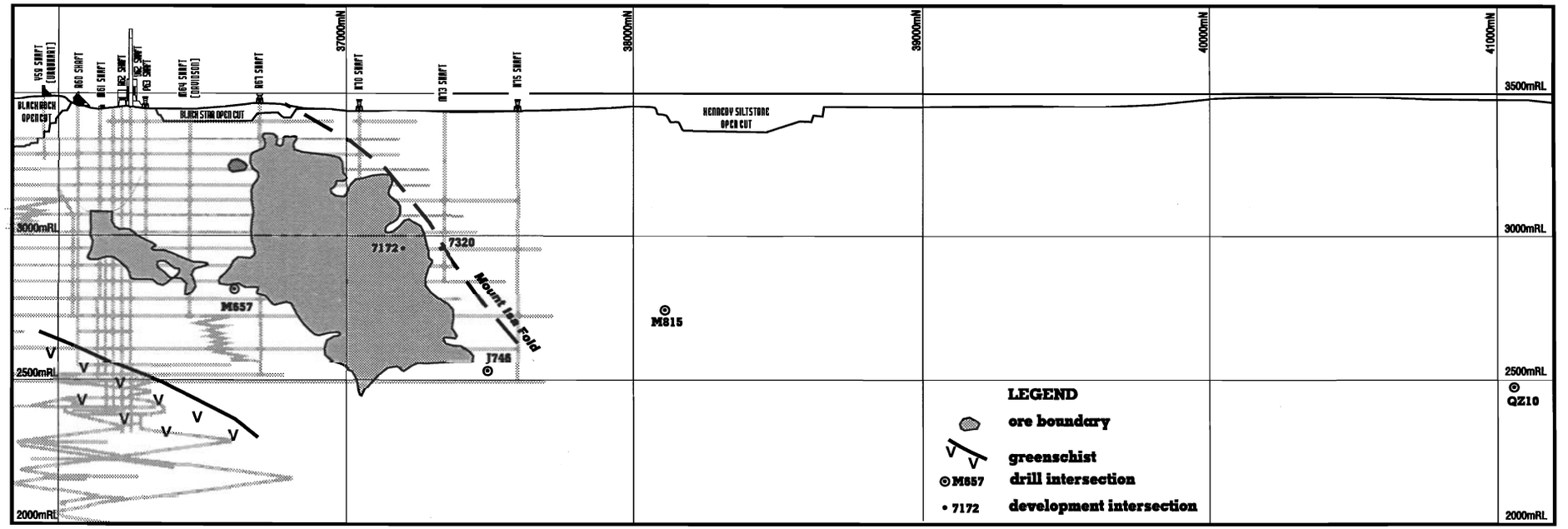
VSS SHAFT (UNWATERED)
NSS SHAFT
NS1 SHAFT
NS2 SHAFT
NS3 SHAFT
NS4 SHAFT
NSN SHAFT (DEVELOPED)
NS5 SHAFT
NT10 SHAFT
NT13 SHAFT
NT15 SHAFT
97000mN
38000mN
39000mN
40000mN
41000mN
3500mRL
3000mRL
2500mRL
2000mRL
BLACKROCK OPENCUT
BLACK STAR OPEN CUT
KENDOW SILTSTONE OPEN CUT
7172
7320
M657
M815
J746
Mount Ida Fold
LEGEND
ore boundary
greenschist
M657 drill intersection
7172 development intersection
QZ10

Figure 1 b. Plan of part of the northern end of 11 Level with 7 orebody development intersections sampled in the hinge of the Mount Isa Fold, and south of it. Ore grade intersections are shown where measured relative to the orebody markers. Note the abrupt termination of the orebody close to the fold hinge.

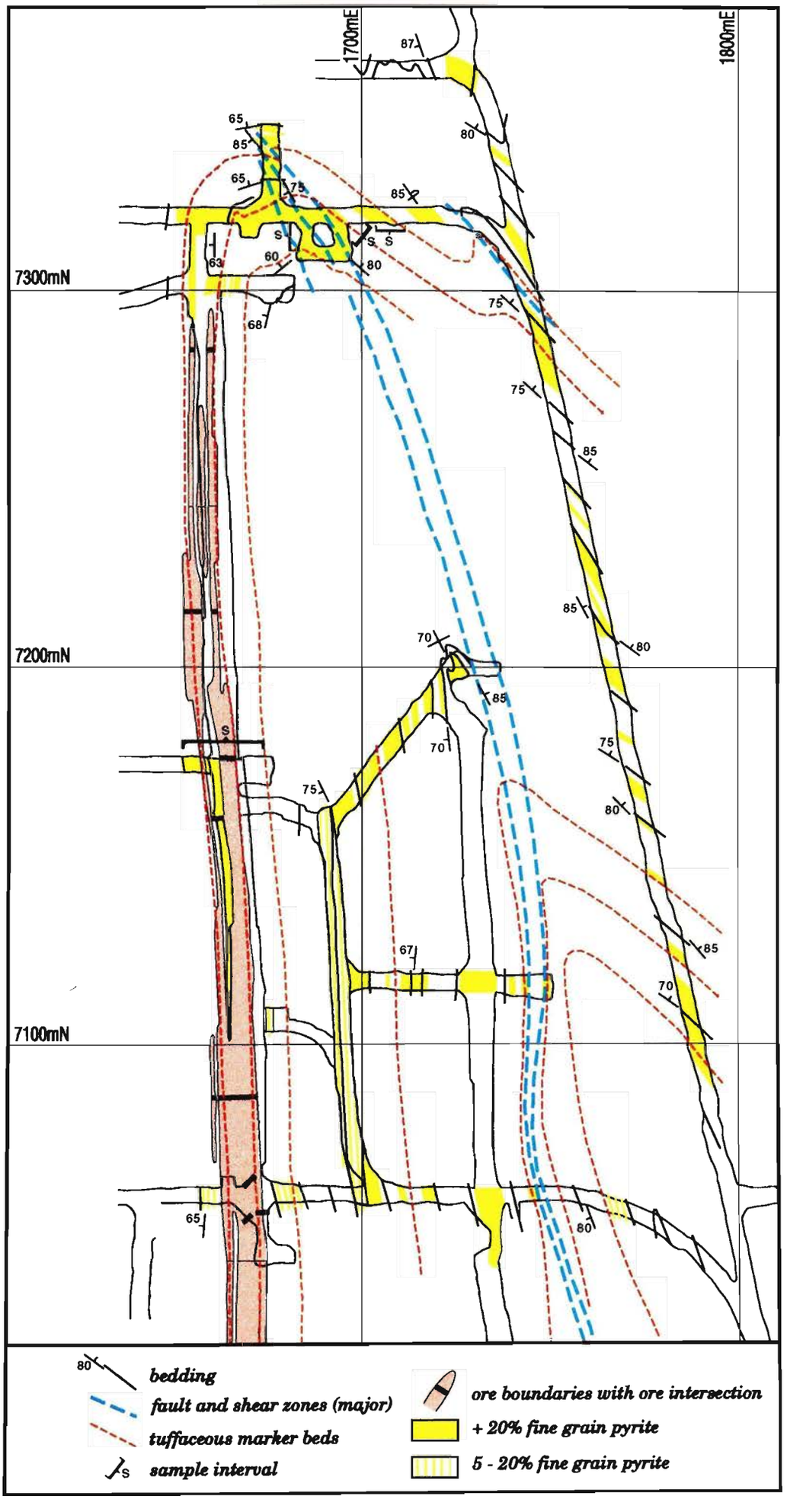
1700mE
1800mE
7300mN
7200mN
7100mN
bedding
fault and shear zones (major)
tuffaceous marker beds
sample interval
ore boundaries with ore intersection
+ 20% fine grain pyrite
5 - 20% fine grain pyrite

PART D.

Figure 1 c. Sample intervals for measured splits in 7 orebody. Plotted relative to 7 orebody footwall marker shown as C. B sequence location shown as B. Series of bar plots of 7 orebody intersections showing the distribution of major and minor elements for correlated zones within the orebody sequence. The marks on the left of each profile correspond with B and C in the sample locations diagram. The majors, sulfur (S), and elemental and organic carbon (C) are shown as %, and the metals Ba, Pb, Ag, Zn, Cu as ppm.

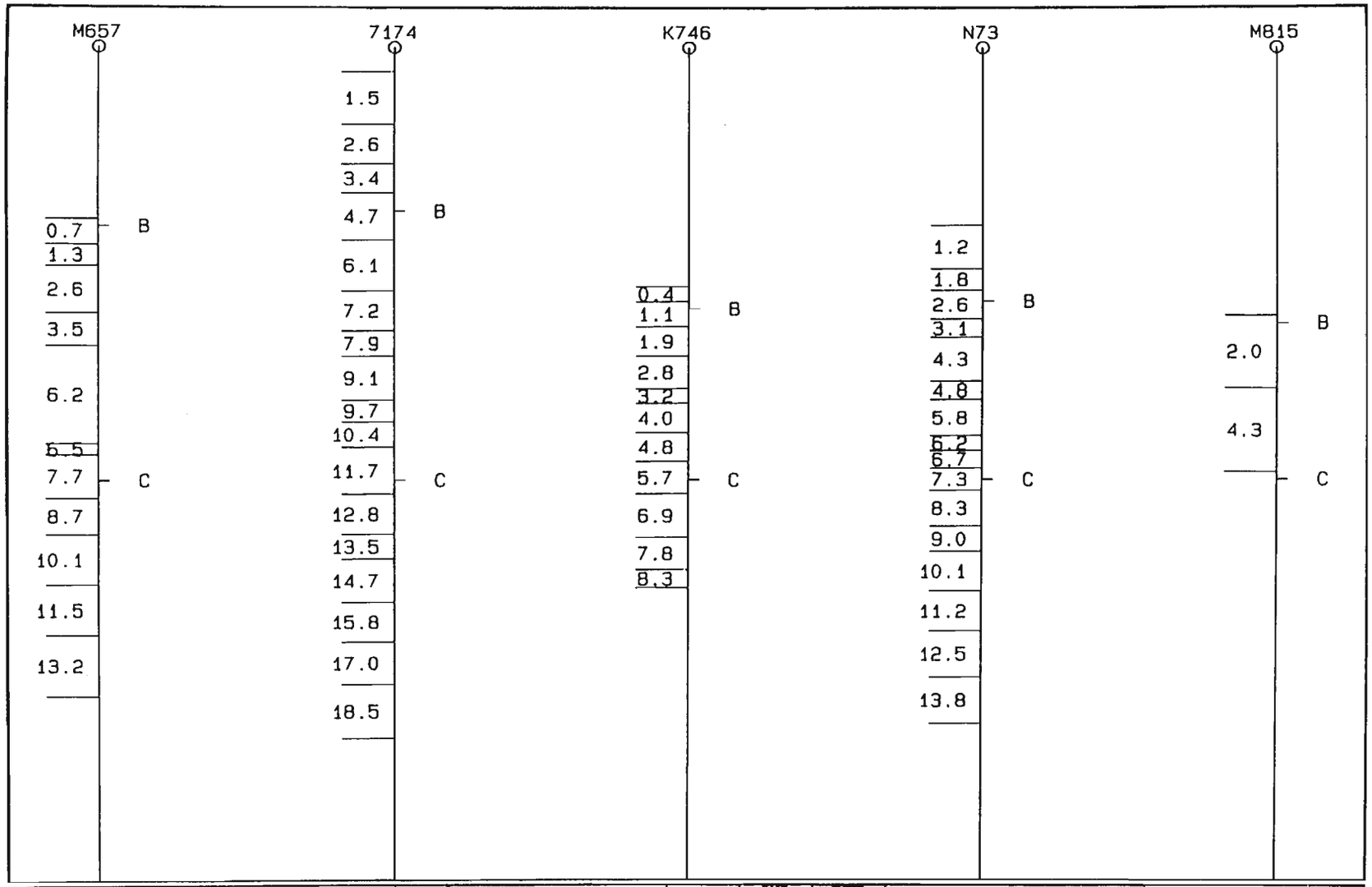

			XSCALE 1: 220	DATE 27/06/96	SHEET 1 of 1	W.G. PERKINS	7 ONEBODY SAMPLE LOCATIONS
			YSCALE 1: 180	REF No. 1	FILE ALLTOB.PLT		

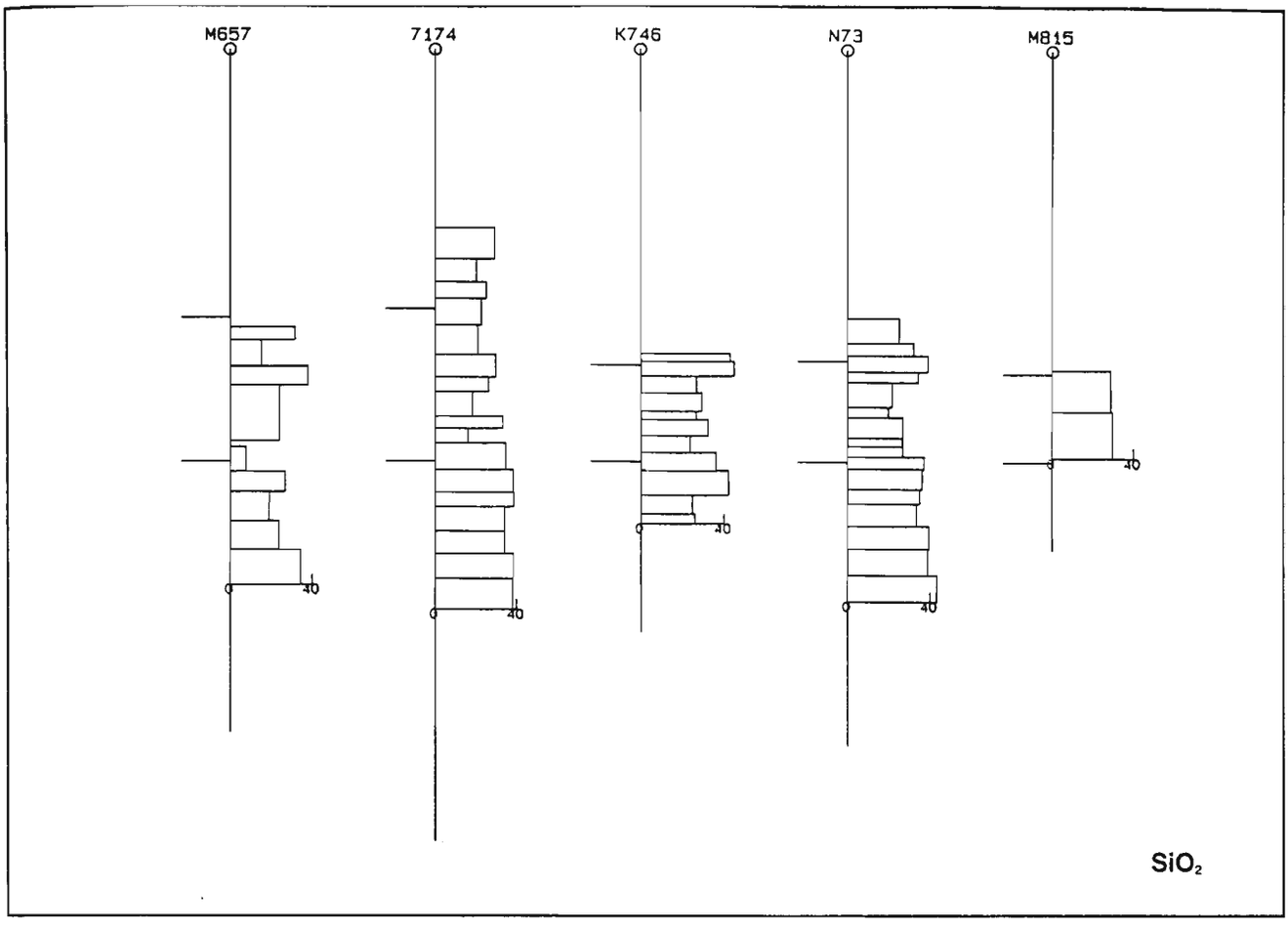
M657
7174
K746
N73
M815
40
SiO2

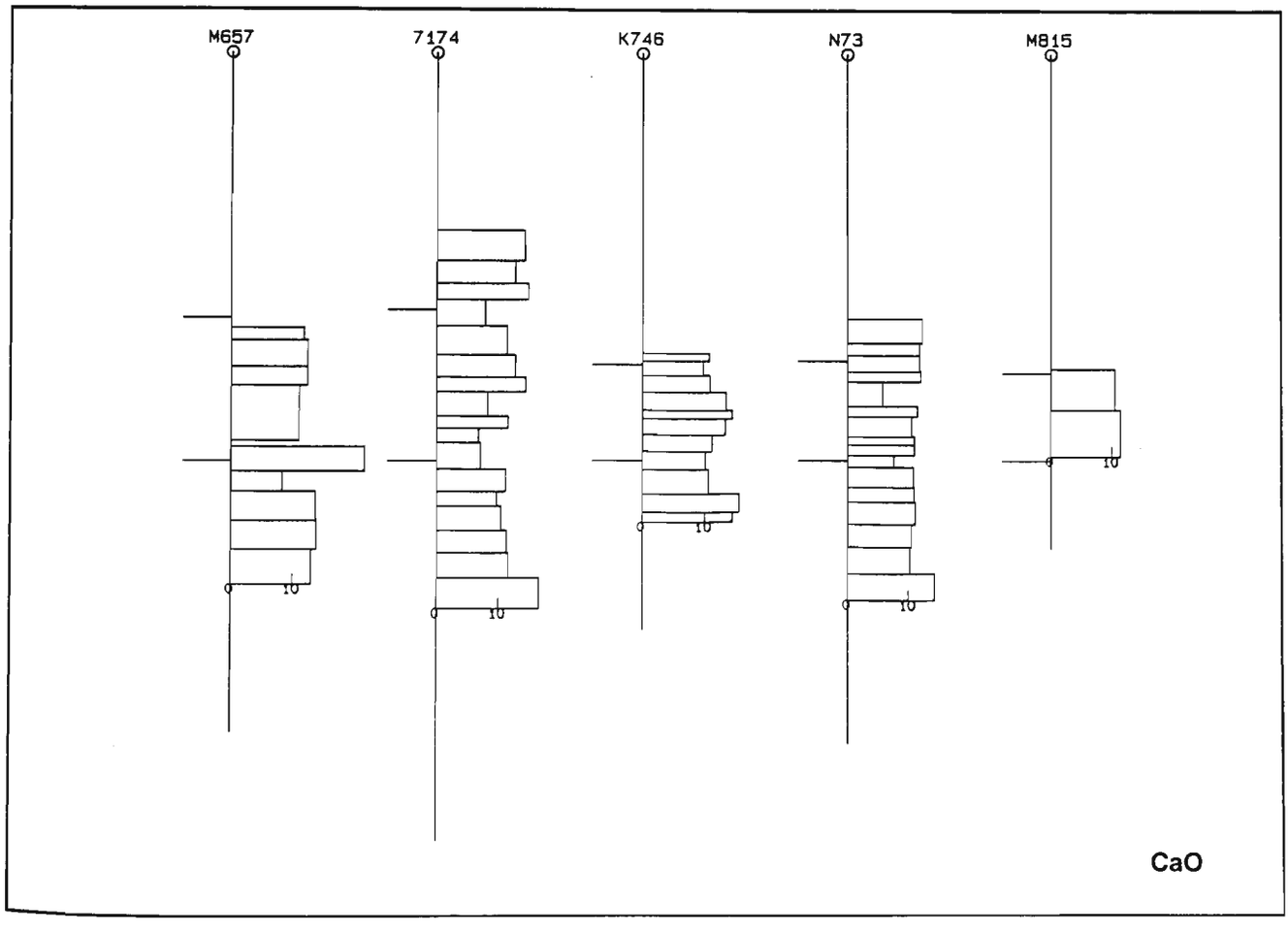
M657
7174
K746
N73
M815
10
CaO

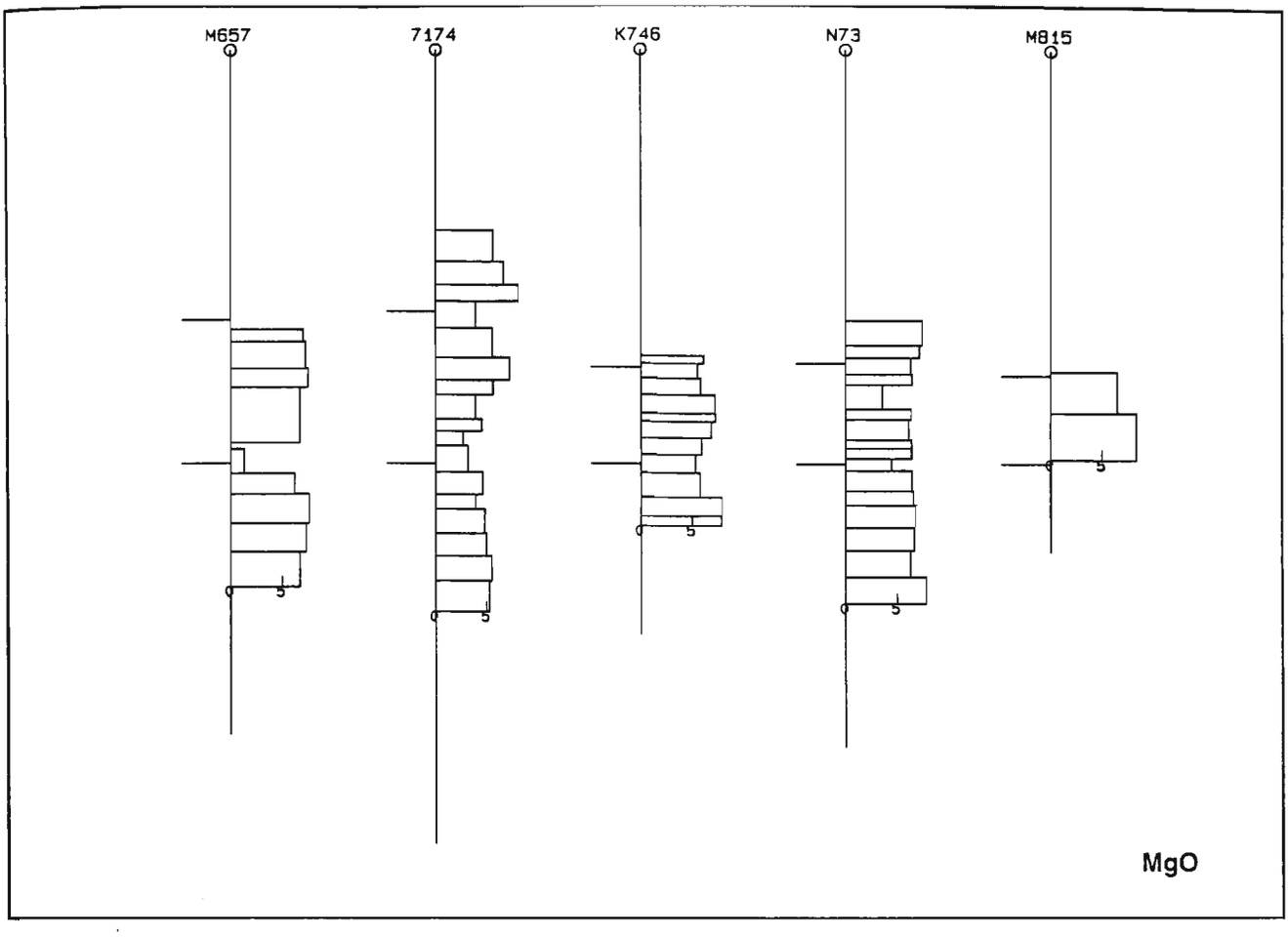
M657
7174
K746
N73
M815
MgO

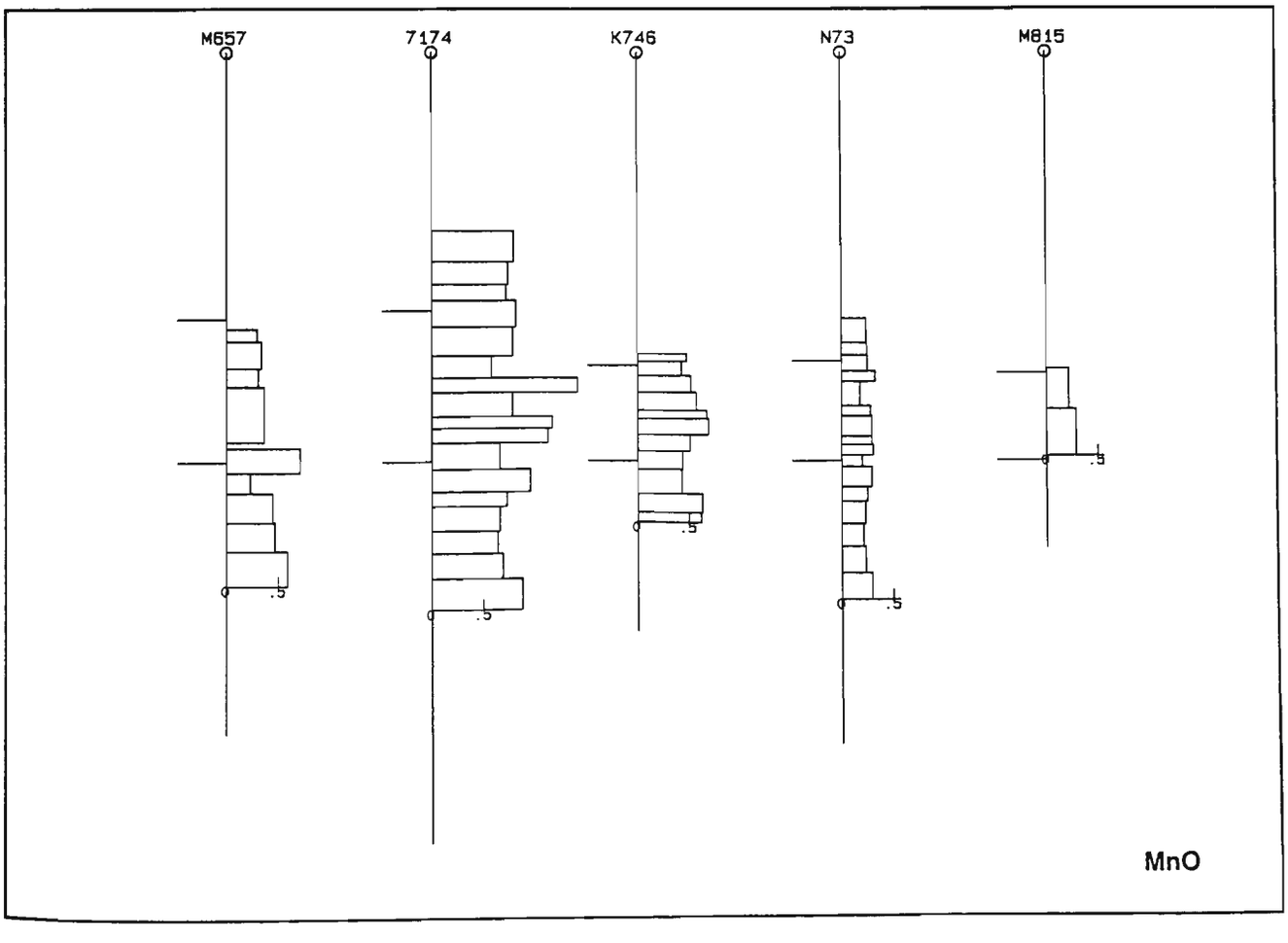
M657
7174
K746
N73
M815
MnO

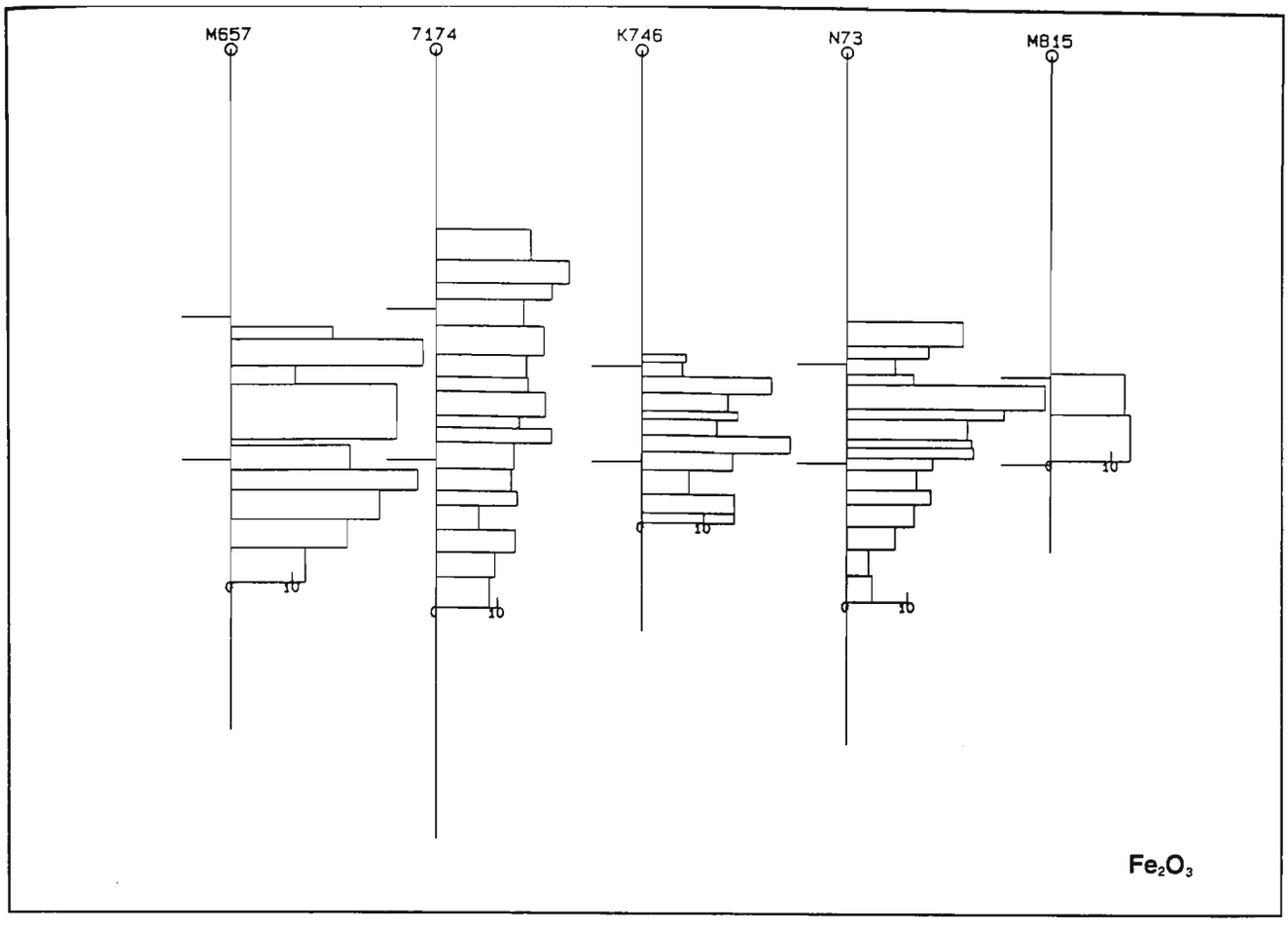
M657
7174
K746
N73
M815
0
10
Fe_2O_3

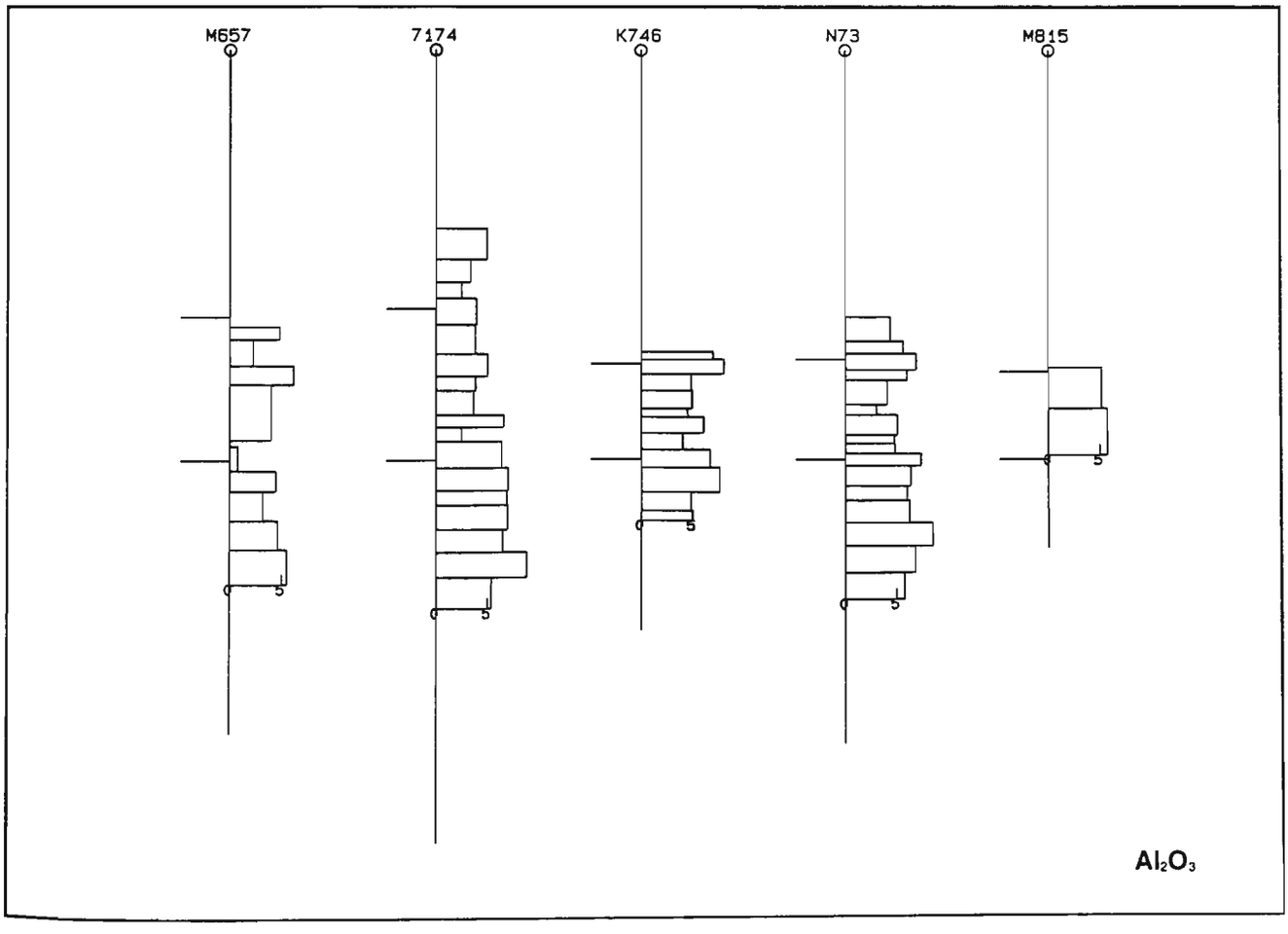
M657
7174
K746
N73
M815
0
5
Al_2O_3

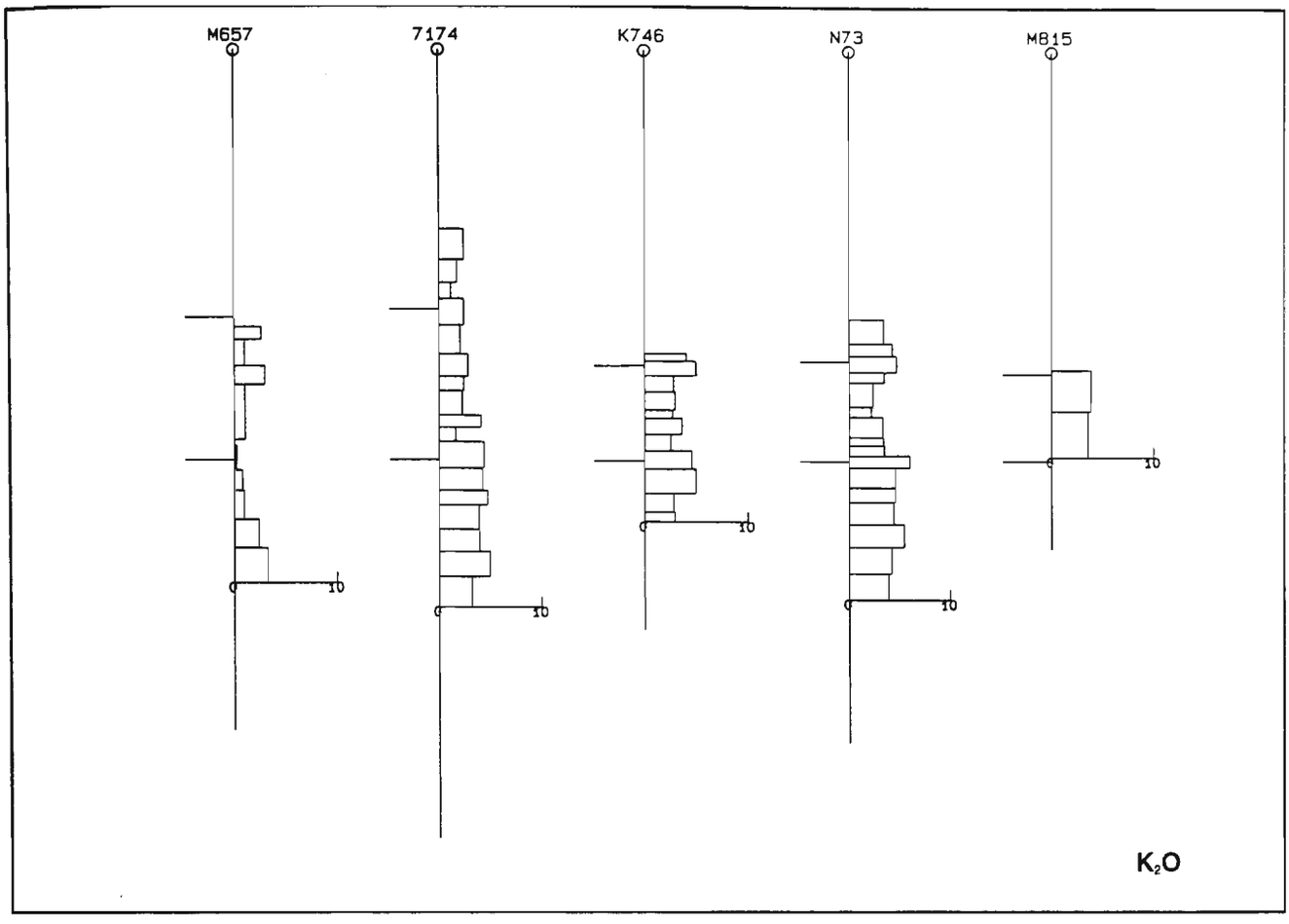
M657
7174
K746
N73
M815
10
10
10
10
10
K_2O

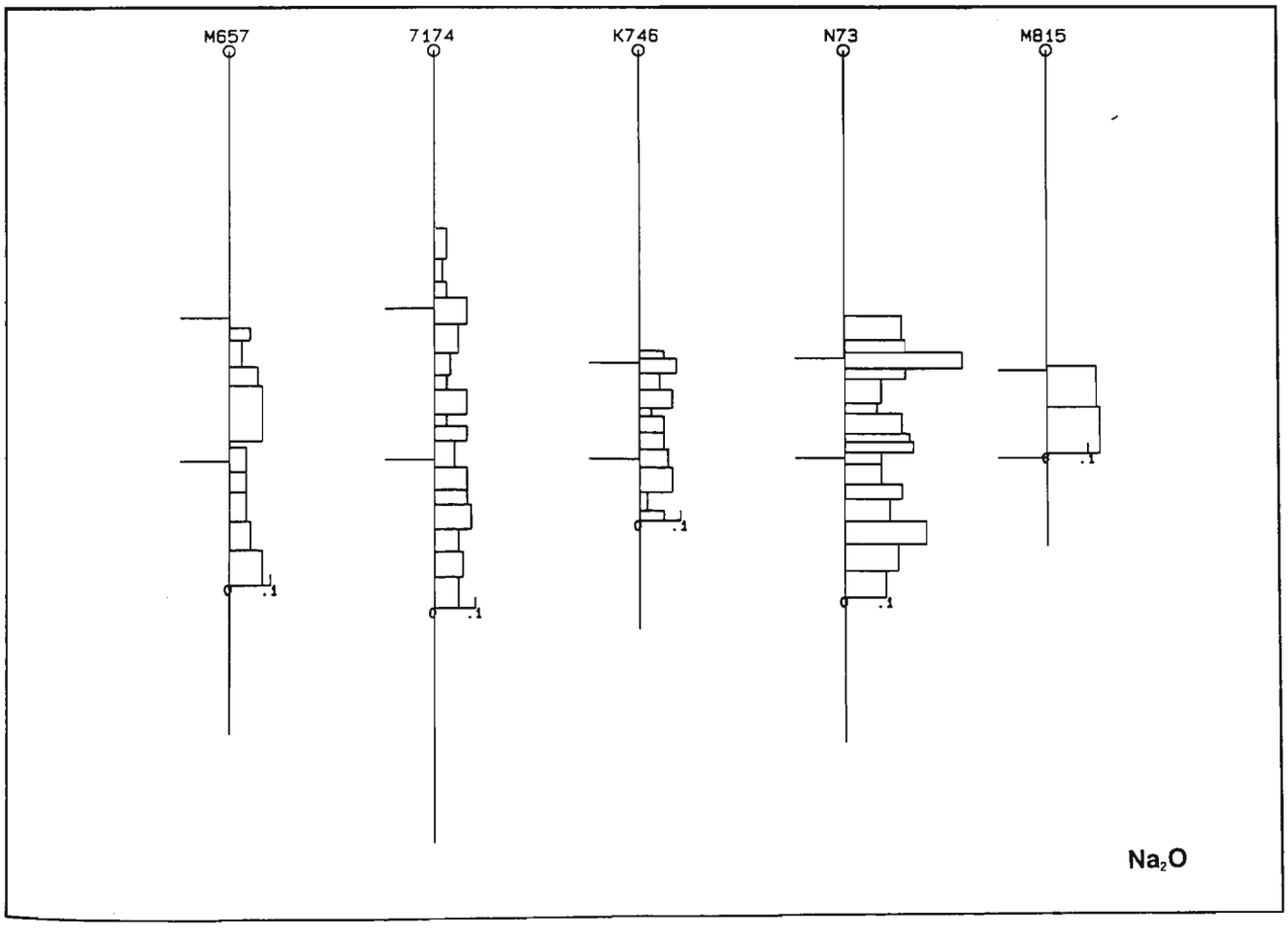
M657
7174
K746
N73
M815
.1
.1
.1
.1
.1
Na_2O

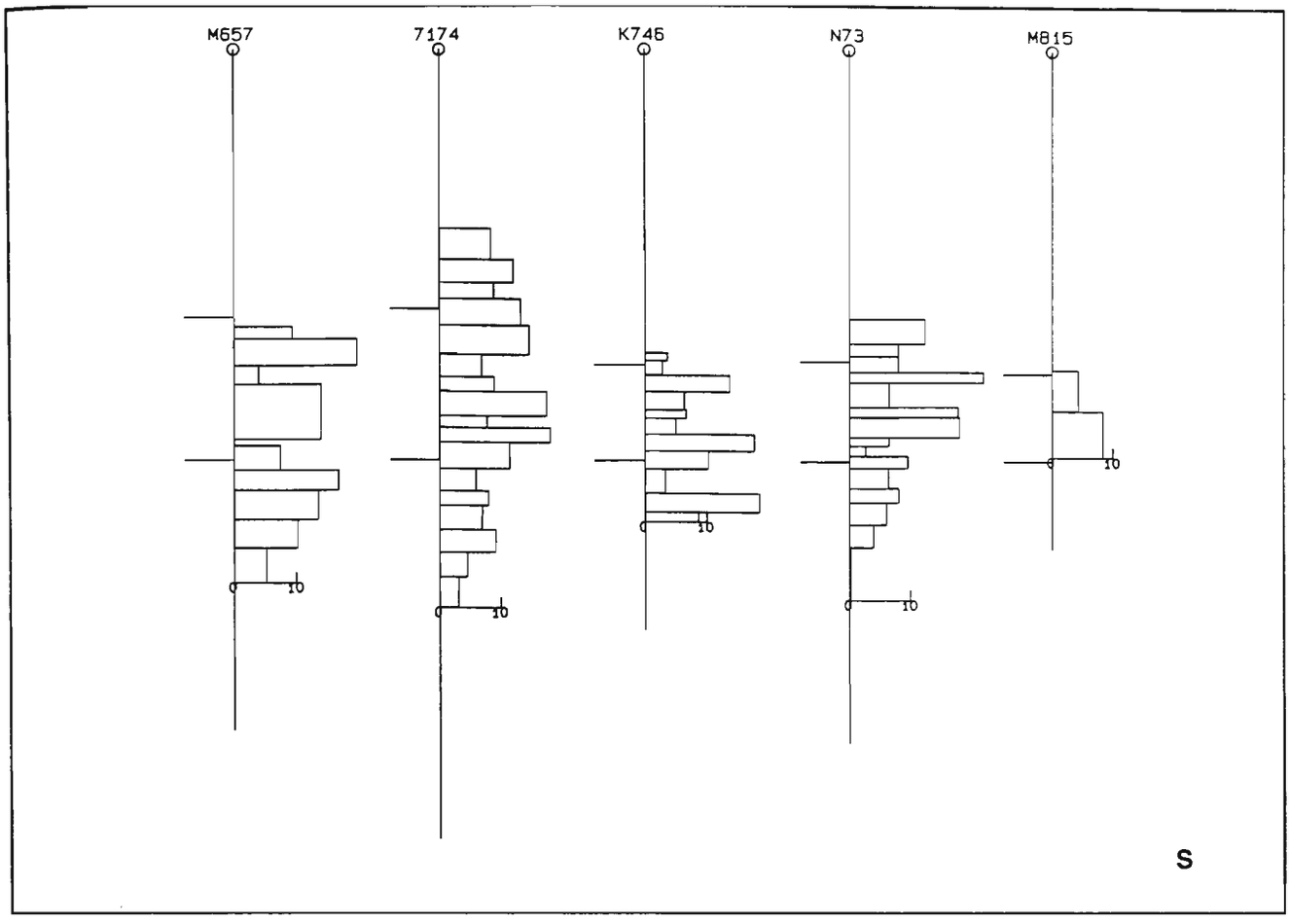
M657
7174
K746
N73
M815
10
10
10
10
10
S

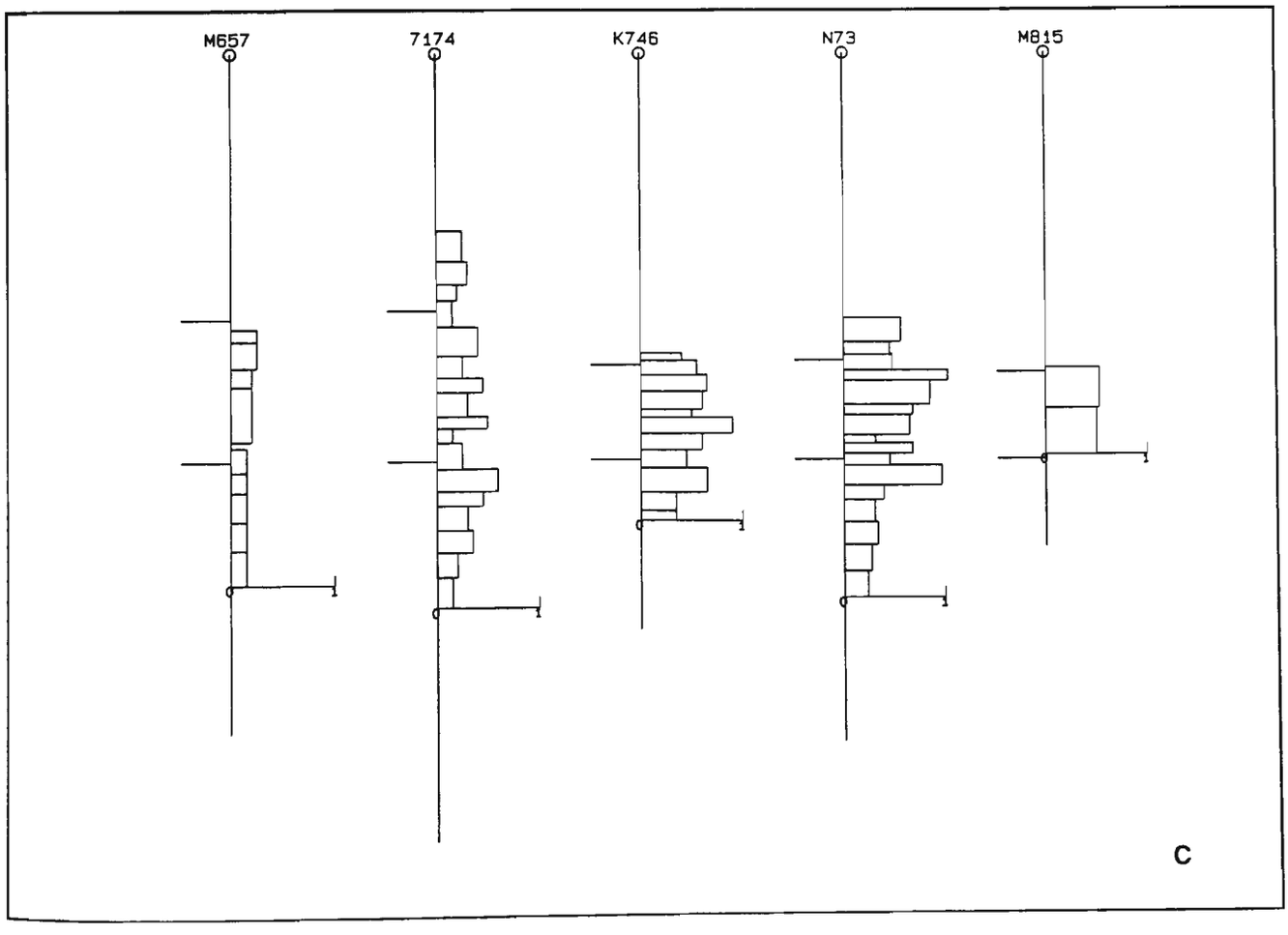
M657
7174
K746
N73
M815
1
1
1
1
1
C

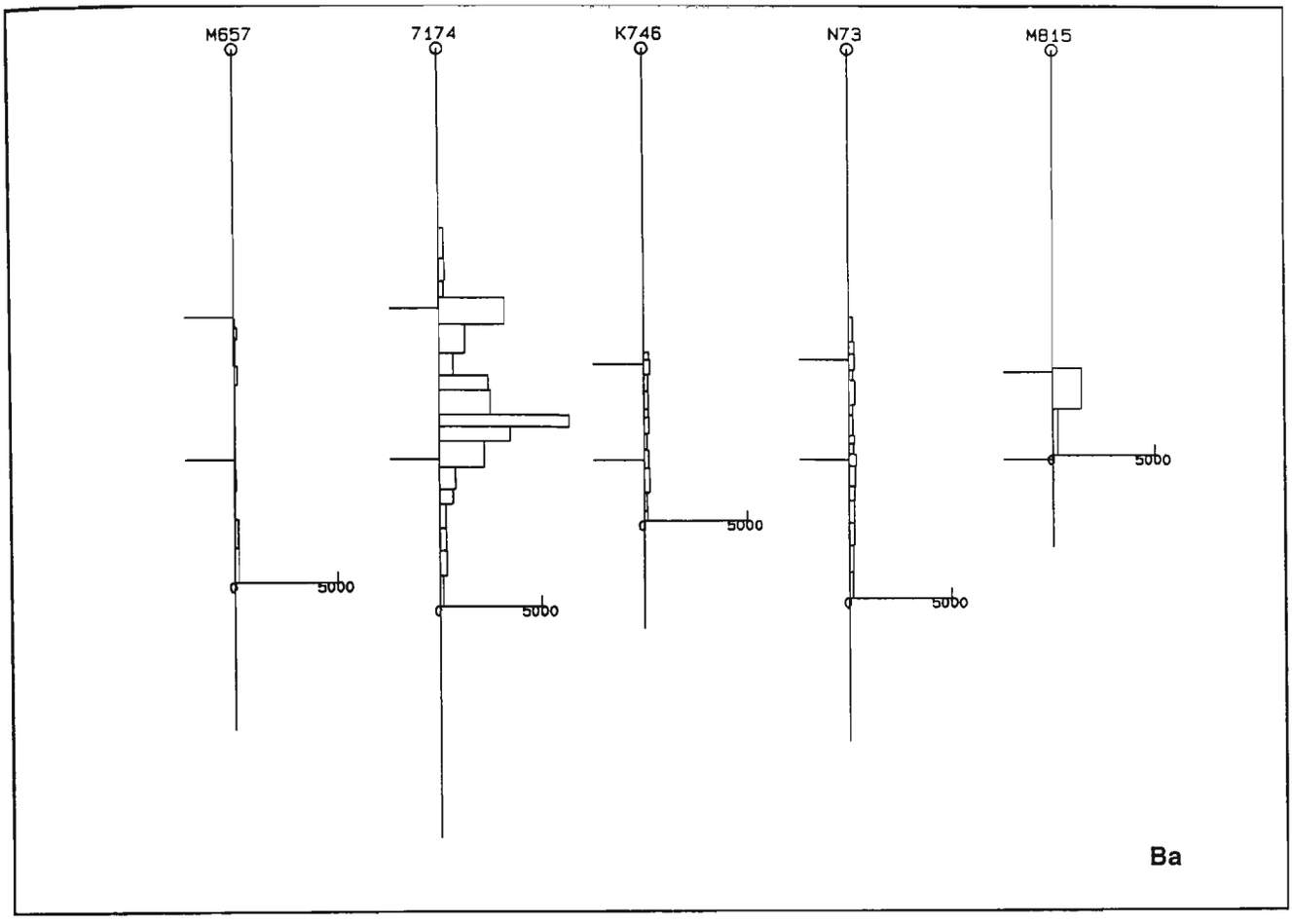
M657
7174
K746
N73
M815
5000
5000
5000
5000
5000
Ba

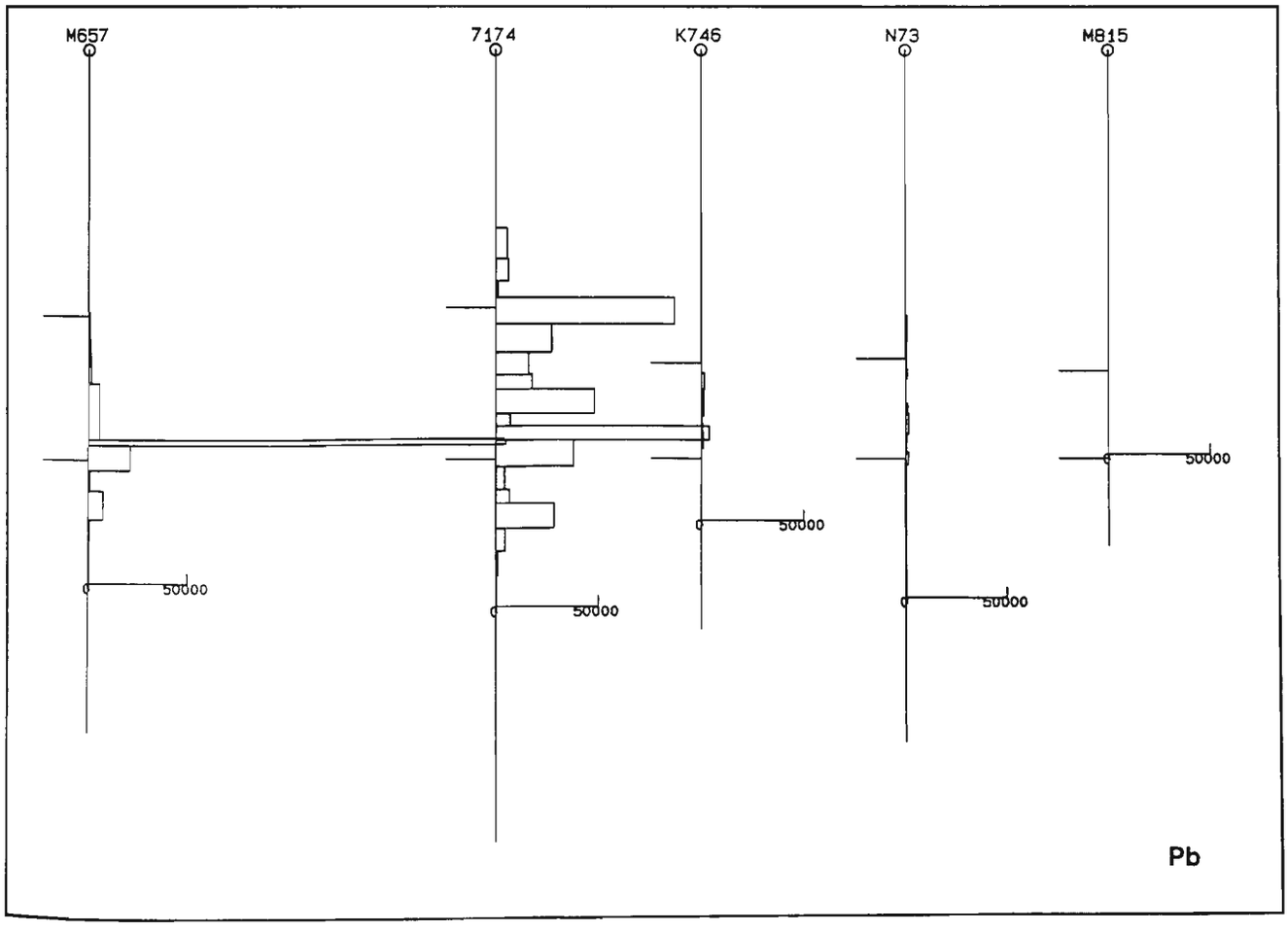
M657
7174
K746
N73
M815
50000
50000
50000
50000
50000
Pb

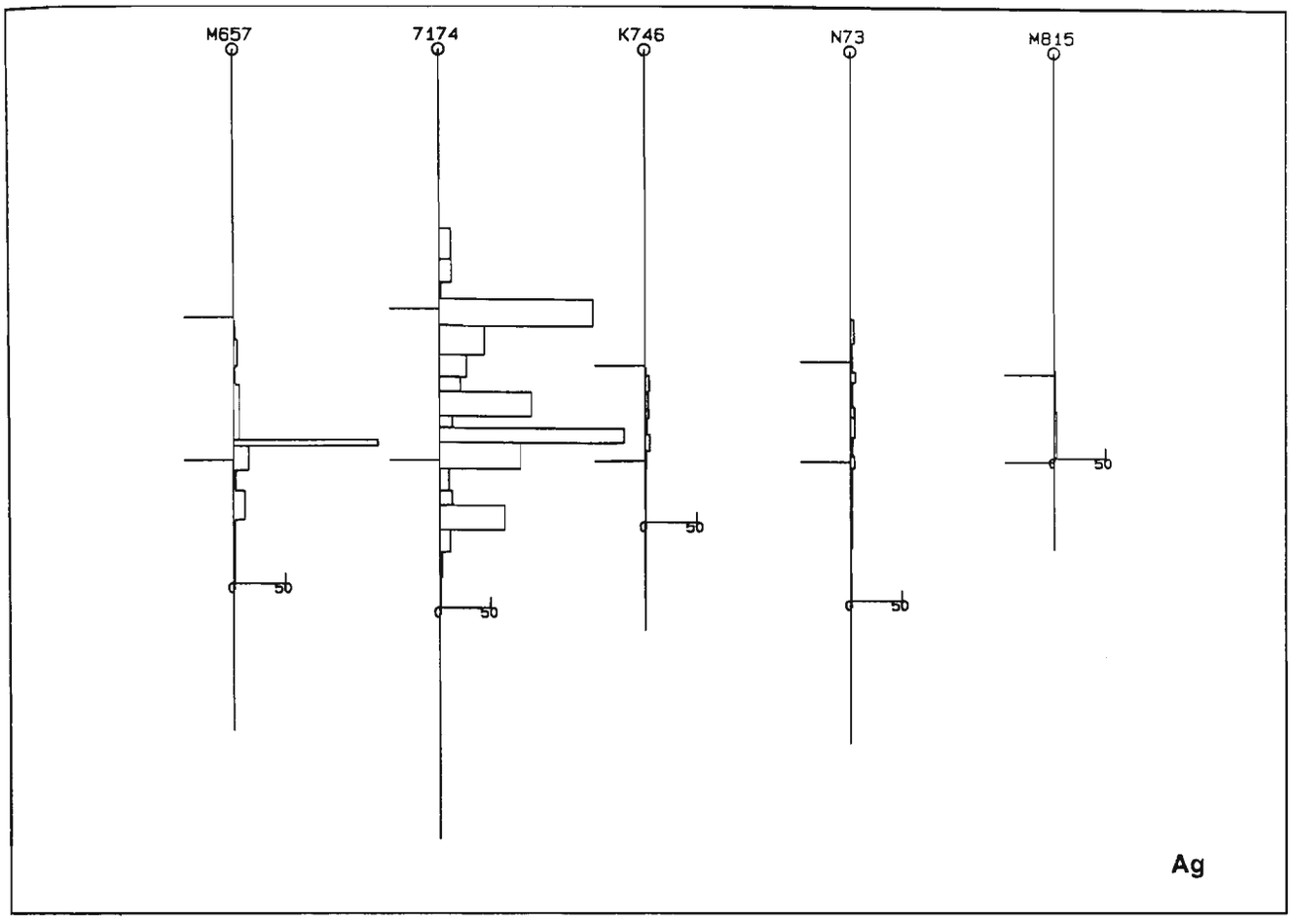
M657
7174
K746
N73
M815
50
50
50
50
50
Ag

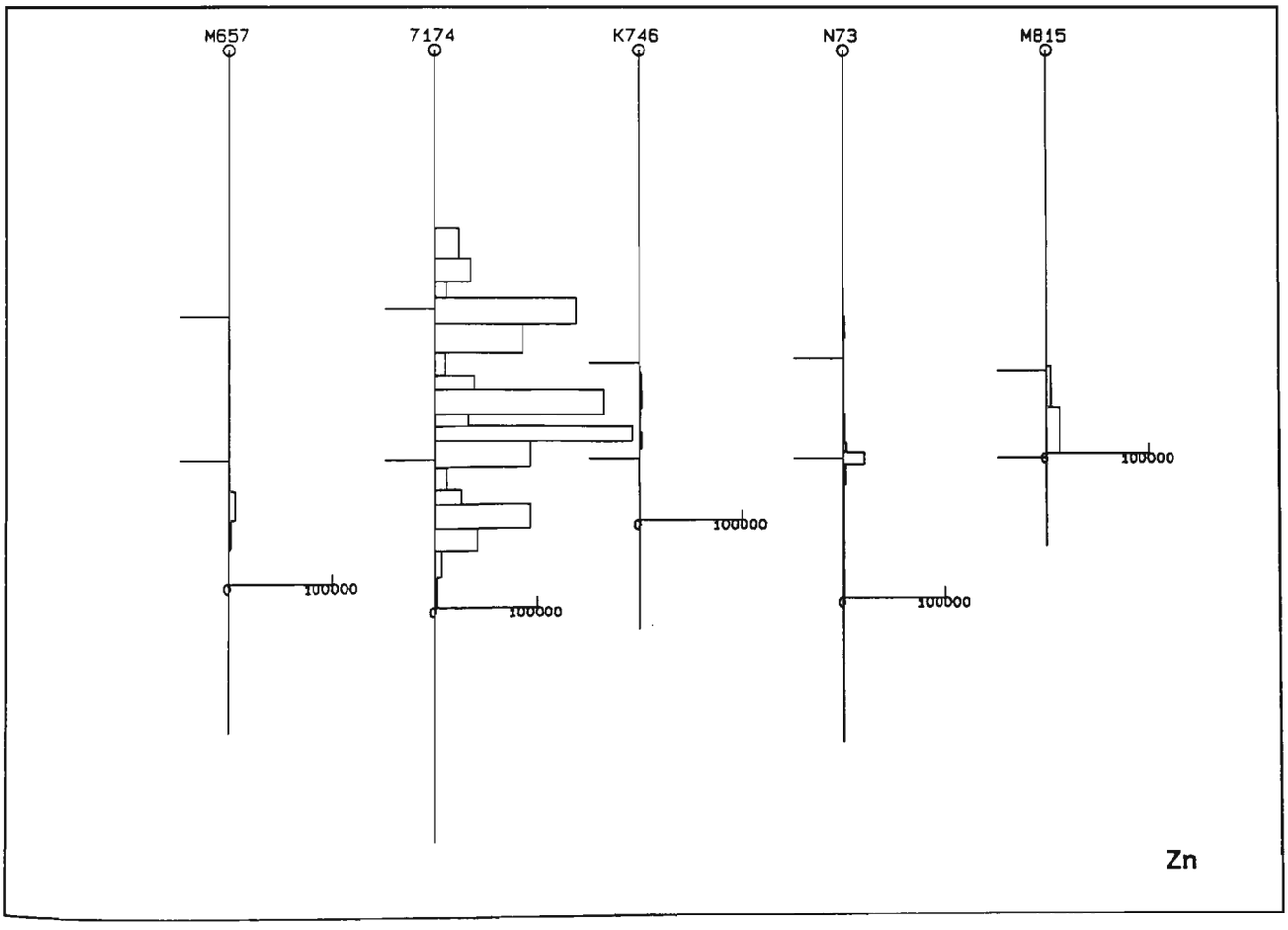
M657
7174
K746
N73
M815
100000
100000
100000
100000
100000
Zn

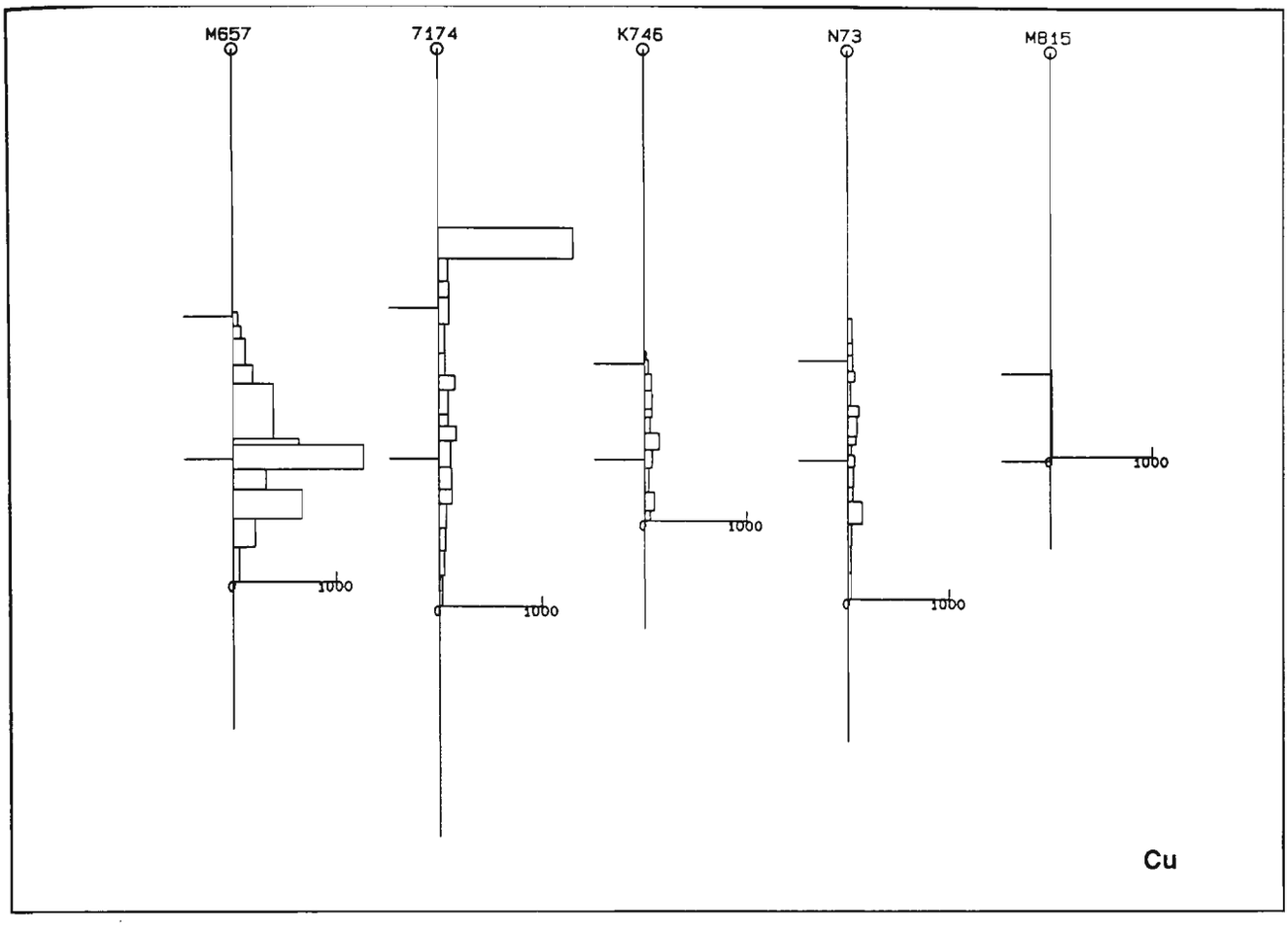
M657
7174
K746
N73
M815
1000
1000
1000
1000
1000
Cu

PART D.

Figure 2 a. Longitudinal projection of a selection of samples used to obtain chemical distribution in the B sequence.

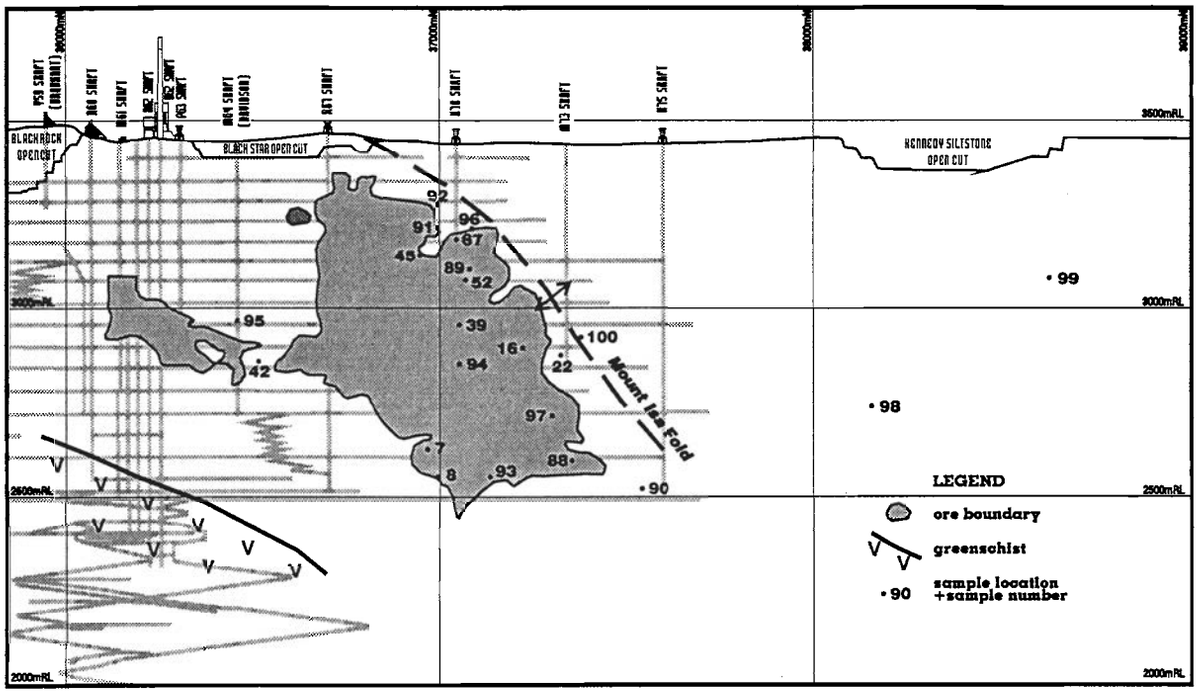
BLACKROCK OPENCUT
BLACK STAR OPEN CUT
HERMCOM SILESTONE OPEN CUT
3500mRL
3000mRL
2500mRL
2000mRL
92
91
96
67
45
89
52
95
39
16
100
42
94
22
Mount Isa Fold
98
99
97
7
88
8
93
90
LEGEND
ore boundary
greenschist
sample location
+sample number
90

Figure 2 b. Series of longitudinal projections on the B sequence at the top of 7 orebody with distribution of major and minor elements.

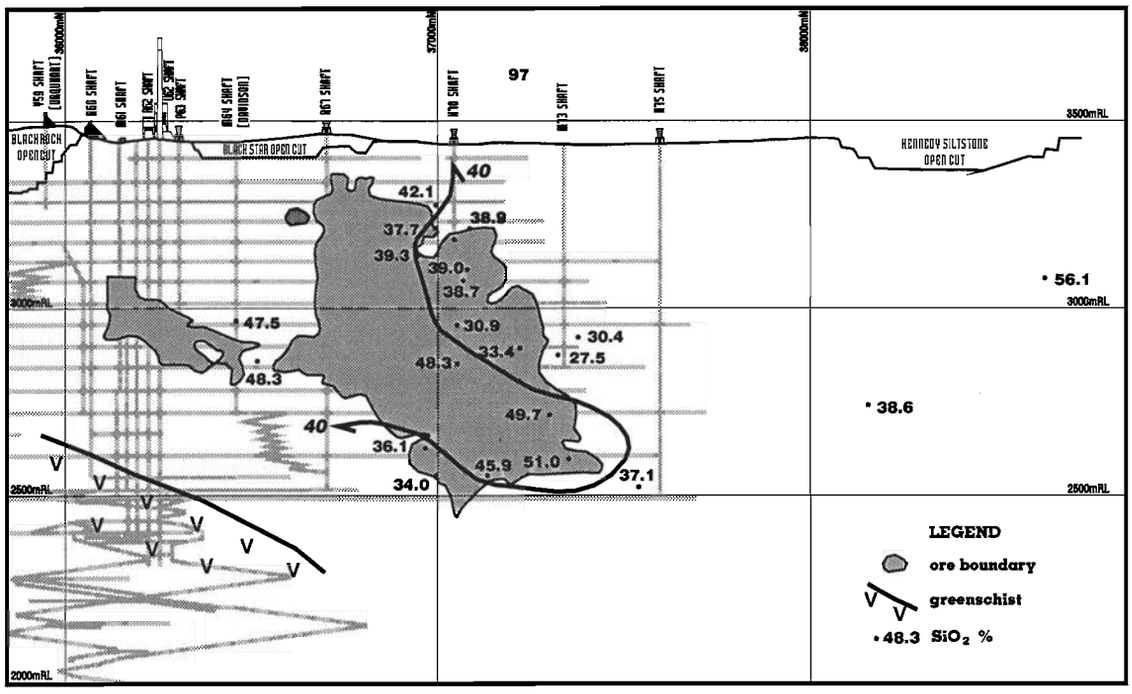
97
BLACKROCK OPENCUT
BLACK STAR OPEN CUT
KENNEDY SILTSTONE OPEN CUT
3500mRL
3000mRL
2500mRL
2000mRL
40
42.1
37.7
38.9
39.3
39.0
38.7
47.5
48.3
30.9
33.4
30.4
27.5
48.3
49.7
40
36.1
45.9
51.0
37.1
34.0
56.1
38.6
LEGEND
ore boundary
greenschist
48.3 SiO2 %

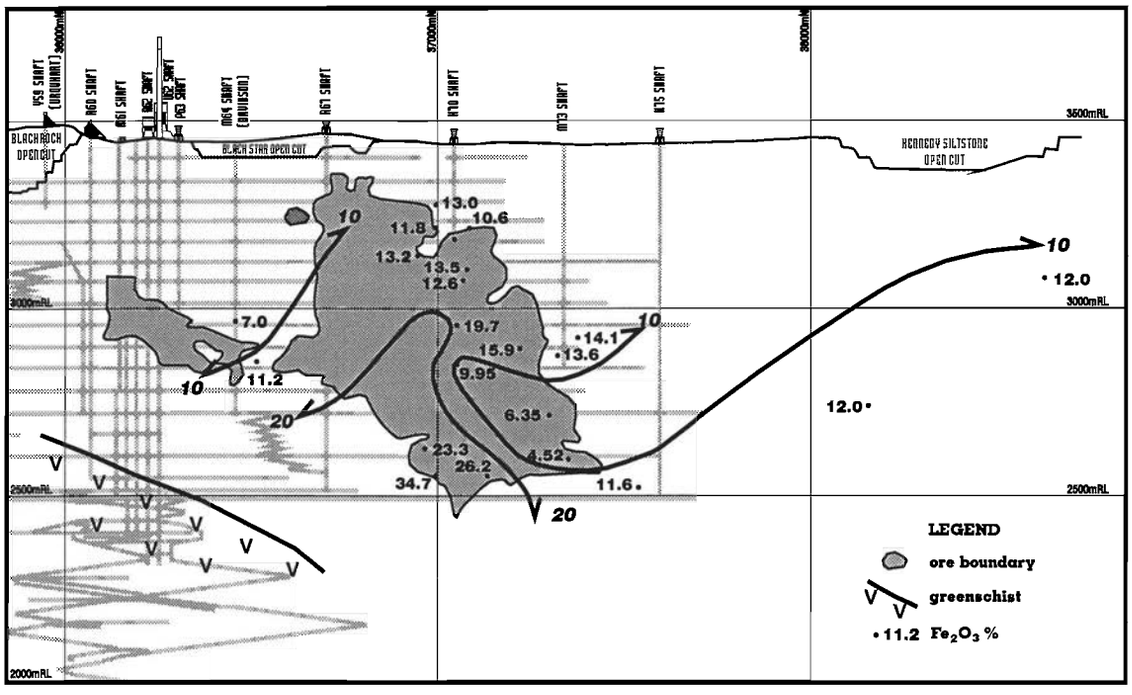
BLACKROCK OPENCUT
BLACK STAR OPEN CUT
KENNEDY SILTSTONE OPEN CUT
3500mRL
3000mRL
2500mRL
2000mRL
13.0
10
11.8
10.6
13.2
13.5
12.6
10
12.0
7.0
19.7
14.1
10
15.9
13.6
10
11.2
9.95
20
6.35
12.0
23.3
26.2
4.52
34.7
11.6
20
LEGEND
ore boundary
greenschist
11.2 Fe2O3 %

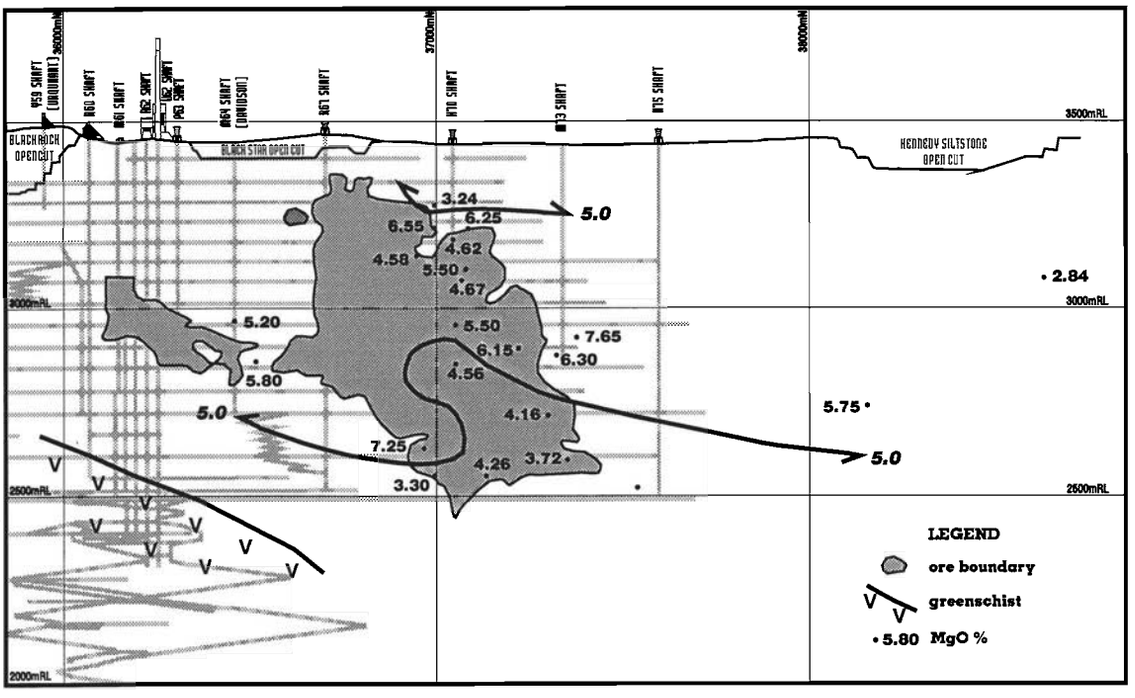
BLACKROCK OPENCUT
BLACK STAR OPEN CUT
KENNEDY SILTSTONE OPEN CUT
3500mRL
3000mRL
2500mRL
2000mRL
3.24
6.25
5.0
6.55
4.62
4.58
5.50
4.67
2.84
5.20
5.50
7.65
6.15
6.30
5.80
4.56
4.16
5.75
5.0
7.25
4.26
3.72
3.30
5.0
LEGEND
ore boundary
greenschist
5.80 MgO %

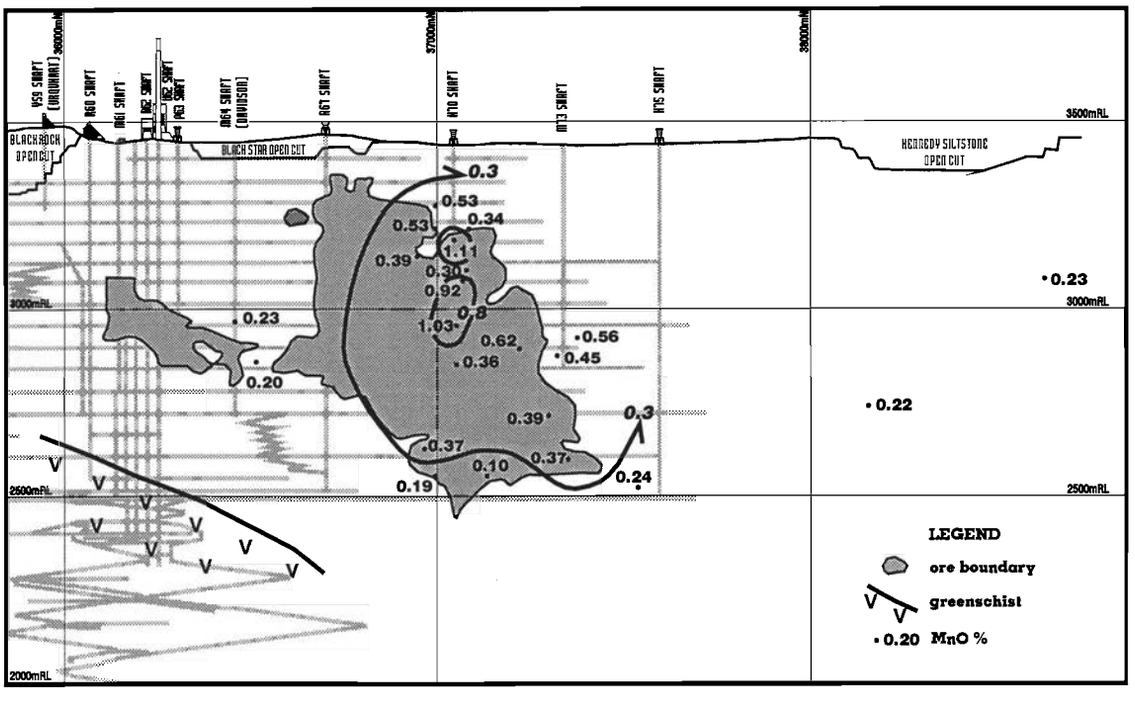
BLACKROCK OPENCUT
BLACK STAR OPEN CUT
KENNEDY SILTSTONE OPEN CUT
3500mRL
3000mRL
2500mRL
2000mRL
0.3
0.53
0.53
0.34
0.39
1.11
0.30
0.92
0.23
0.8
1.03
0.62
0.56
0.36
0.45
0.20
0.39
0.3
0.37
0.10
0.37
0.19
0.24
0.23
0.22
LEGEND
ore boundary
greenschist
0.20 MnO %

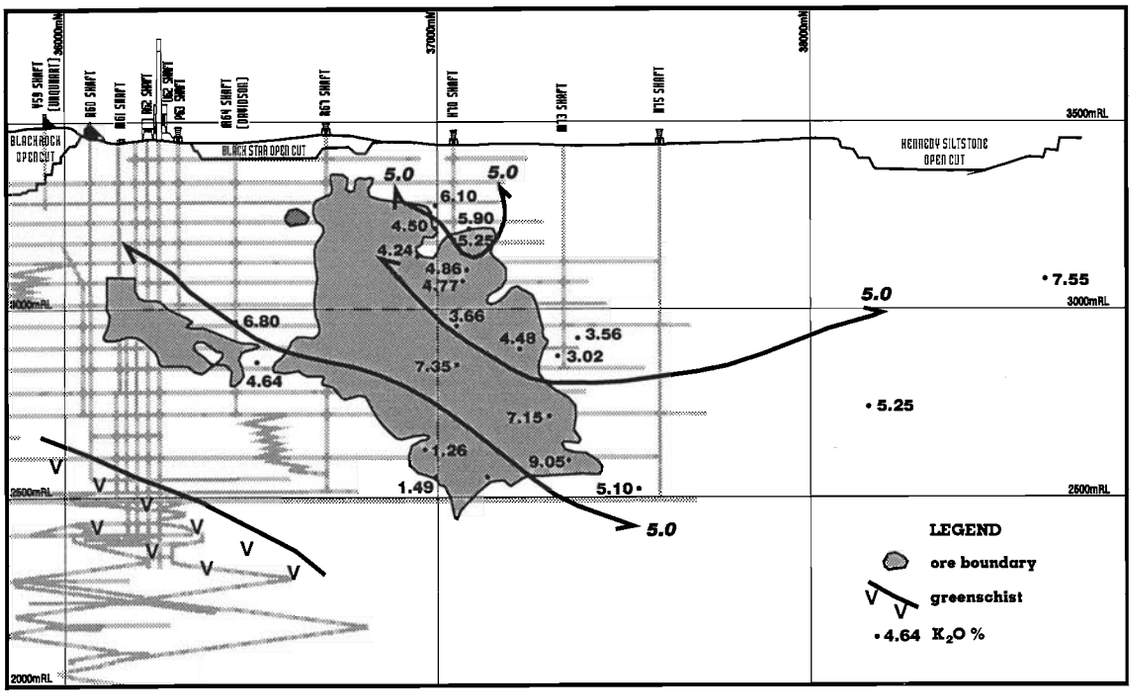
BLACKROCK OPENCUT
BLACK STAR OPEN CUT
HERRADY SILTSTONE OPEN CUT
3500mRL
3000mRL
2500mRL
2000mRL
5.0
6.10
5.90
5.25
4.50
4.24
4.86
4.77
6.80
4.64
3.66
4.48
3.56
3.02
7.35
7.55
5.25
7.15
1.26
9.05
1.49
5.10
LEGEND
ore boundary
greenschist
4.64 K2O %

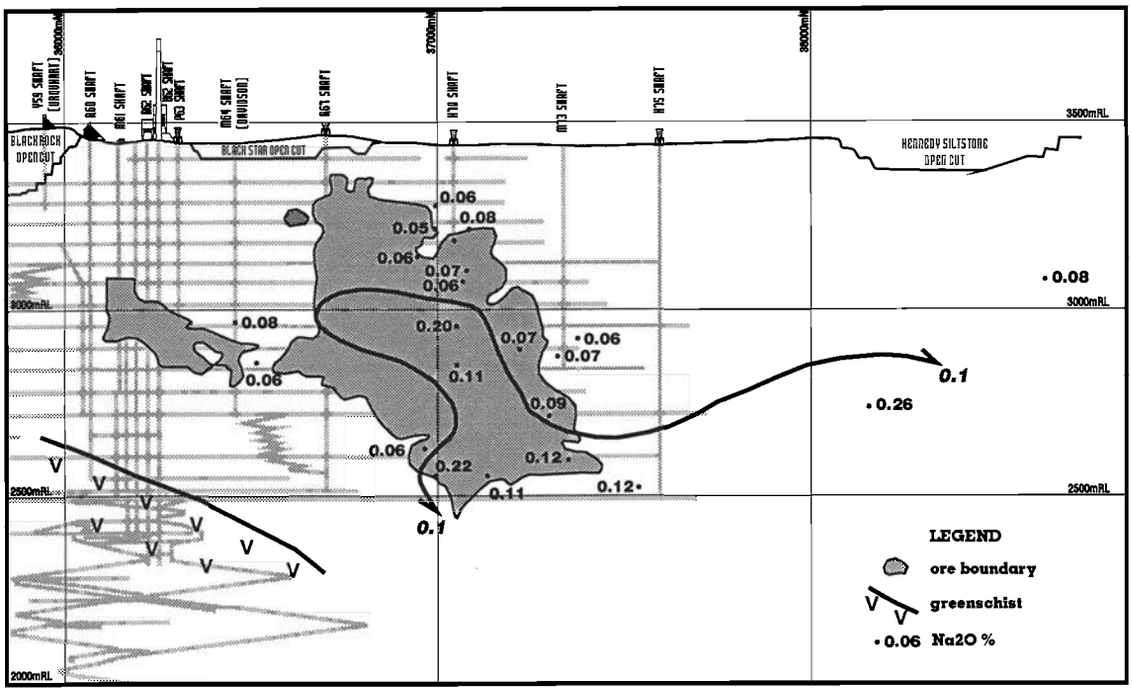
BLACKROCK OPENCUT
BLACK STAR OPEN CUT
HERRADY SILTSTONE OPEN CUT
3500mRL
3000mRL
2500mRL
2000mRL
0.06
0.08
0.05
0.06
0.07
0.06
0.08
0.20
0.07
0.06
0.07
0.06
0.11
0.09
0.08
0.1
0.26
0.06
0.22
0.12
0.11
0.12
0.1
LEGEND
ore boundary
greenschist
0.06 Na2O %

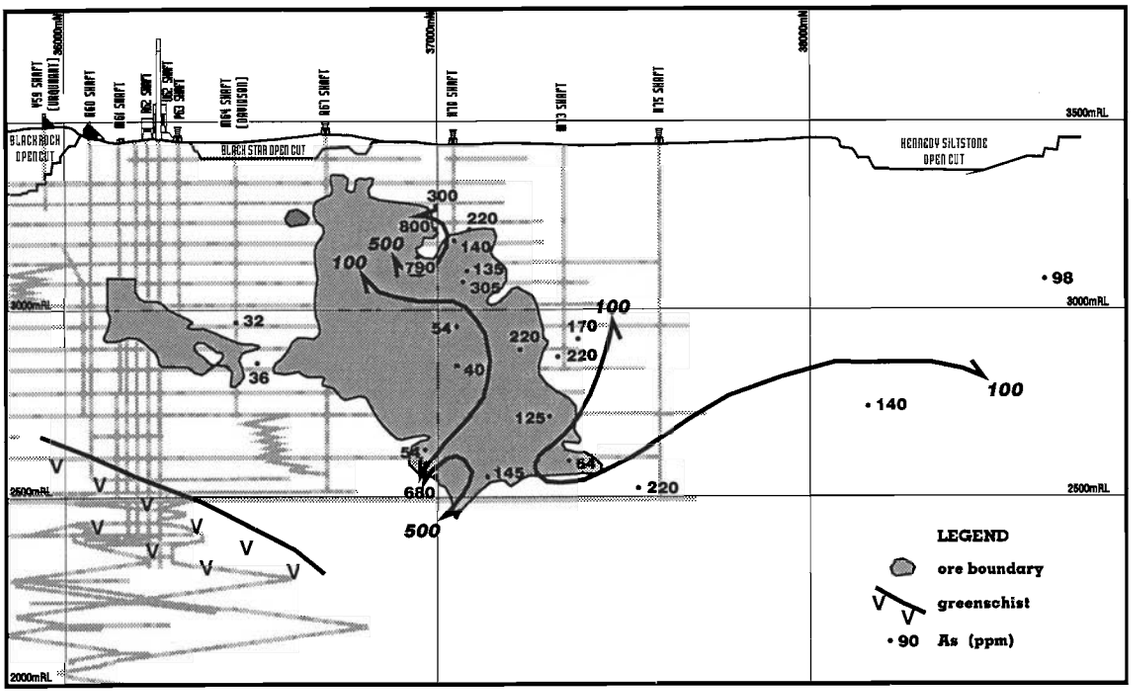
V53 SHAFT (URANIUM)
R60 SHAFT
R61 SHAFT
R62 SHAFT
R63 SHAFT
R64 SHAFT (DAVIDSON)
R67 SHAFT
N10 SHAFT
N13 SHAFT
N15 SHAFT
36000mN
37000mN
38000mN
3500mRL
3000mRL
2500mRL
2000mRL
BLACK ROCK OPEN CUT
BLACK STAR OPEN CUT
KENNEDY SILTSTONE OPEN CUT
300
800
220
500
140
100
790
139
305
98
32
54
100
170
220
220
36
40
100
140
125
54
54
145
220
680
500
LEGEND
ore boundary
greenschist
90 As (ppm)

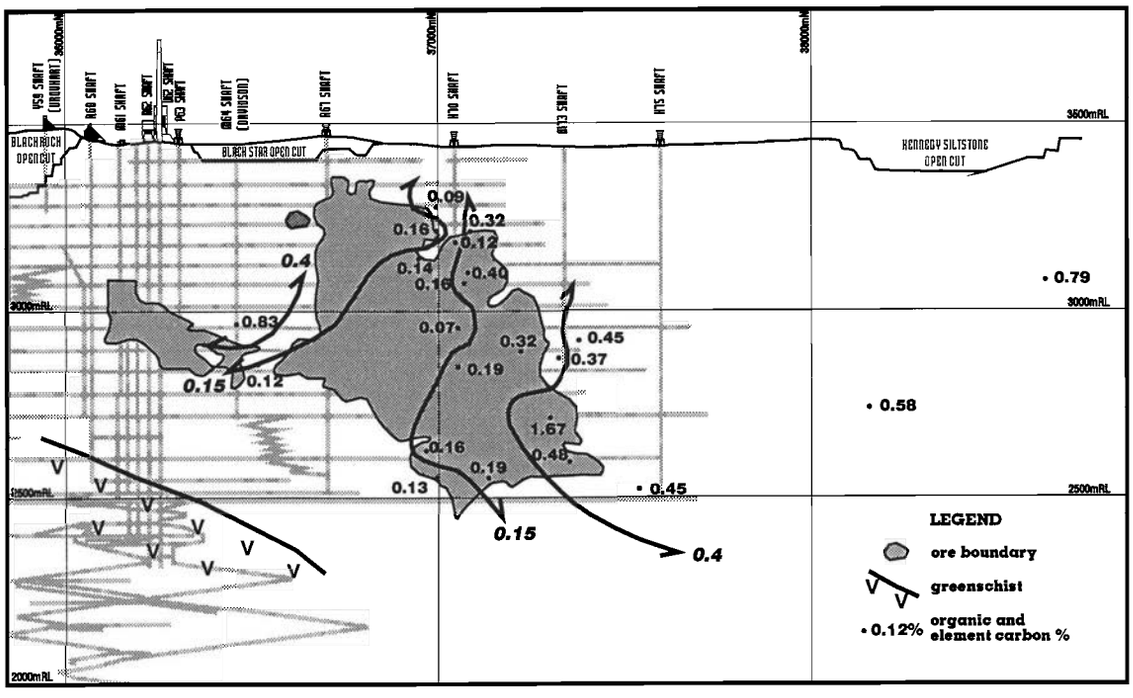
V53 SHAFT (URANIUM)
R60 SHAFT
R61 SHAFT
R62 SHAFT
R63 SHAFT
R64 SHAFT (DAVIDSON)
R67 SHAFT
N10 SHAFT
N13 SHAFT
N15 SHAFT
36000mN
37000mN
38000mN
3500mRL
3000mRL
2500mRL
2000mRL
BLACK ROCK OPEN CUT
BLACK STAR OPEN CUT
KENNEDY SILTSTONE OPEN CUT
0.09
0.32
0.16
0.12
0.4
0.14
0.40
0.79
0.16
0.83
0.07
0.32
0.45
0.37
0.15
0.12
0.19
0.58
1.67
0.16
0.48
0.19
0.13
0.45
0.15
0.4
LEGEND
ore boundary
greenschist
0.12% organic and element carbon %

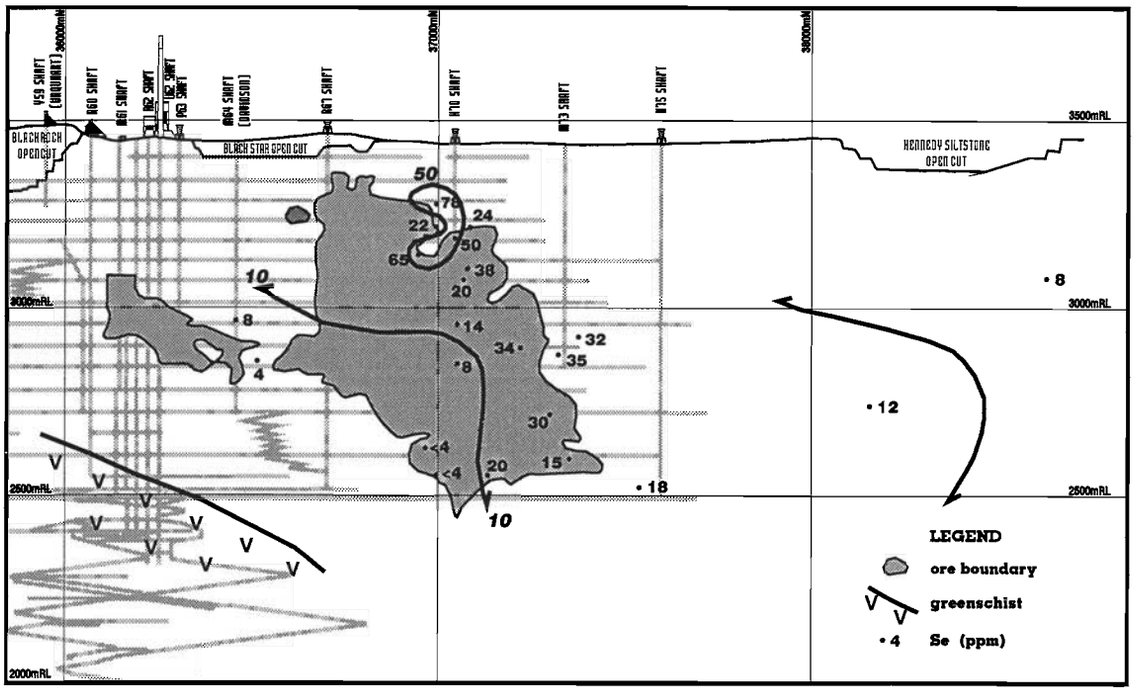
BLACKROCK OPENCUT
BLACK STAR OPEN CUT
KENNEDY SILTSTONE OPEN CUT
3500mRL
3000mRL
2500mRL
2000mRL
LEGEND
ore boundary
greenschist
• 4 Se (ppm)

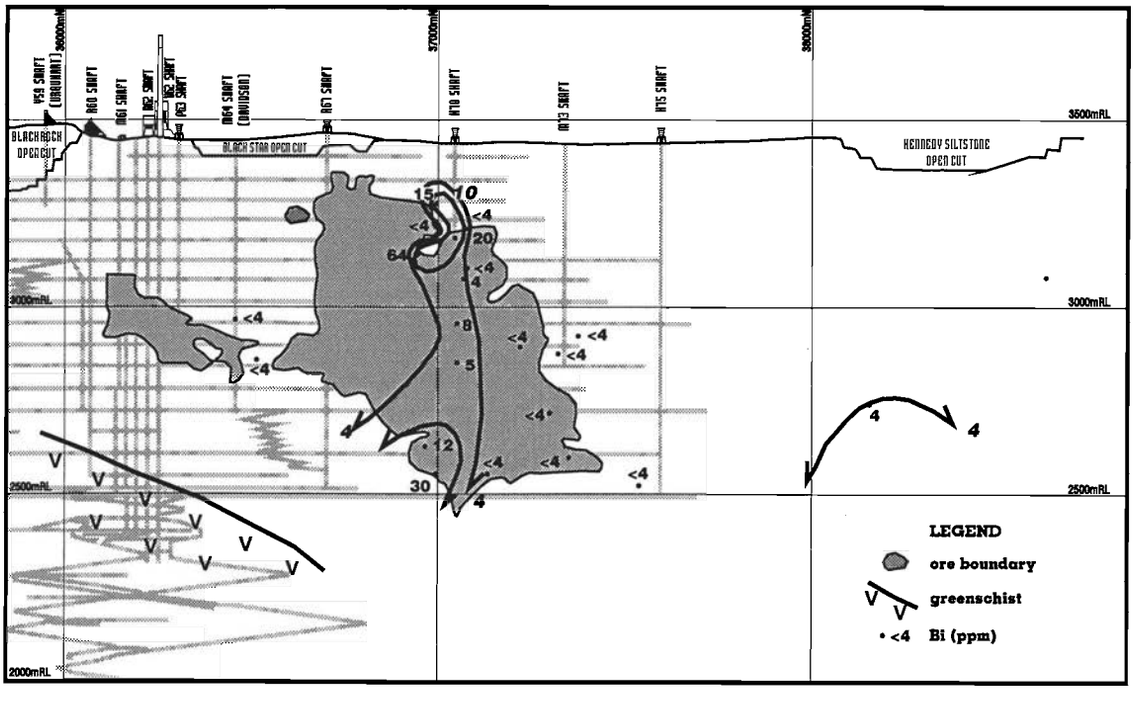
BLACKROCK OPENCUT
BLACK STAR OPEN CUT
KENNEDY SILTSTONE OPEN CUT
3500mRL
3000mRL
2500mRL
2000mRL
LEGEND
ore boundary
greenschist
• <4 Bi (ppm)

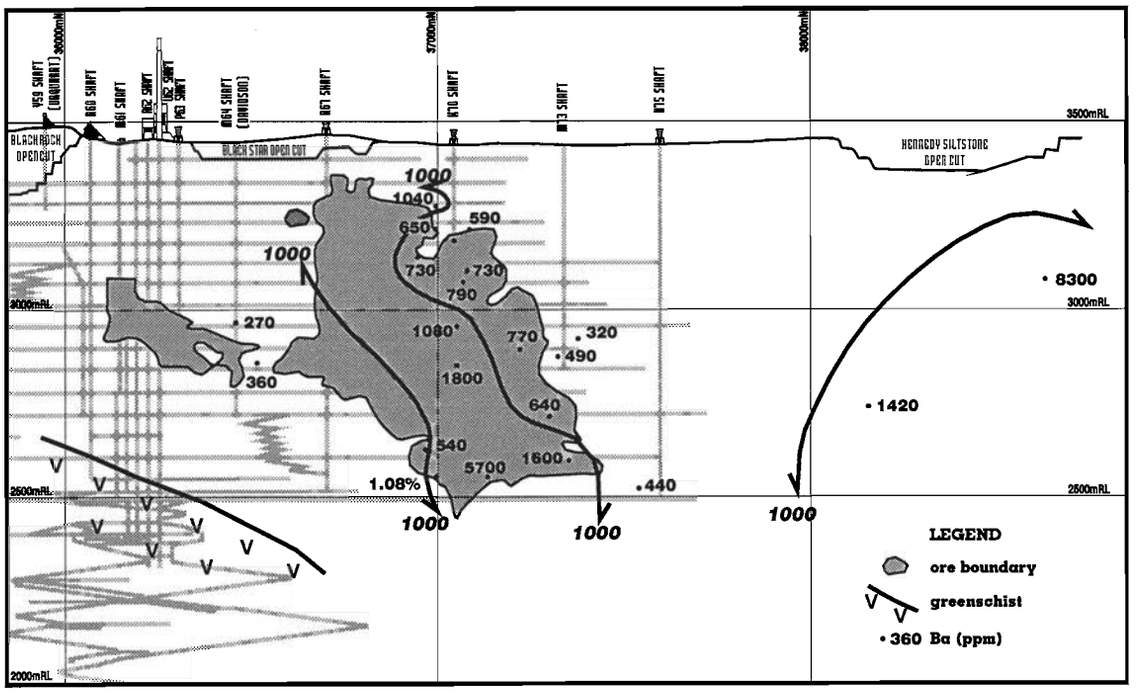
V59 SHAFT (UNDERMINT)
A60 SHAFT
A61 SHAFT
A62 SHAFT
A63 SHAFT
A64 SHAFT (DAVIDSON)
A67 SHAFT
A70 SHAFT
A73 SHAFT
A75 SHAFT
BLACKROCK OPENCUT
BLACK STAR OPEN CUT
HENNEBY SILTSTONE OPEN CUT
3500mRL
3000mRL
2500mRL
2000mRL
1000
1040
650
590
730
790
270
360
1080
770
320
490
1800
640
540
5700
1600
440
1.08%
8300
1420
LEGEND
ore boundary
greenschist
360 Ba (ppm)

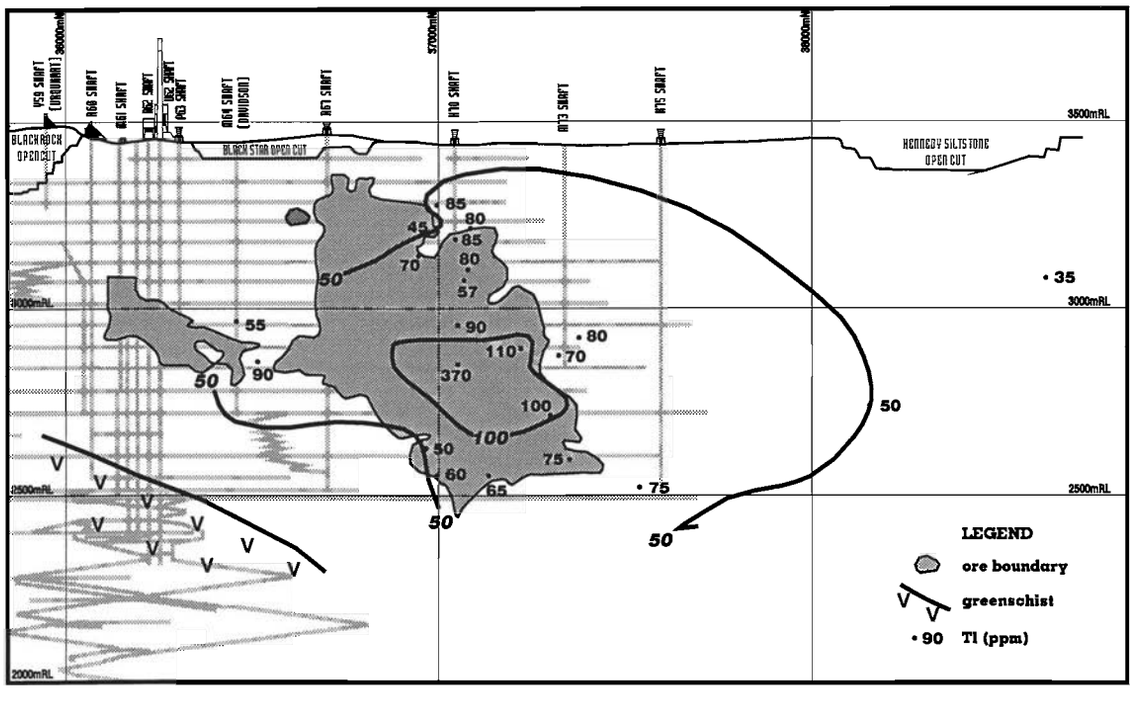
V59 SHAFT (UNDERMINT)
A60 SHAFT
A61 SHAFT
A62 SHAFT
A63 SHAFT
A64 SHAFT (DAVIDSON)
A67 SHAFT
A70 SHAFT
A73 SHAFT
A75 SHAFT
BLACKROCK OPENCUT
BLACK STAR OPEN CUT
HENNEBY SILTSTONE OPEN CUT
3500mRL
3000mRL
2500mRL
2000mRL
85
80
45
85
70
80
50
57
55
90
80
110
70
90
370
100
100
50
75
60
65
75
35
50
50
50
LEGEND
ore boundary
greenschist
90 Tl (ppm)

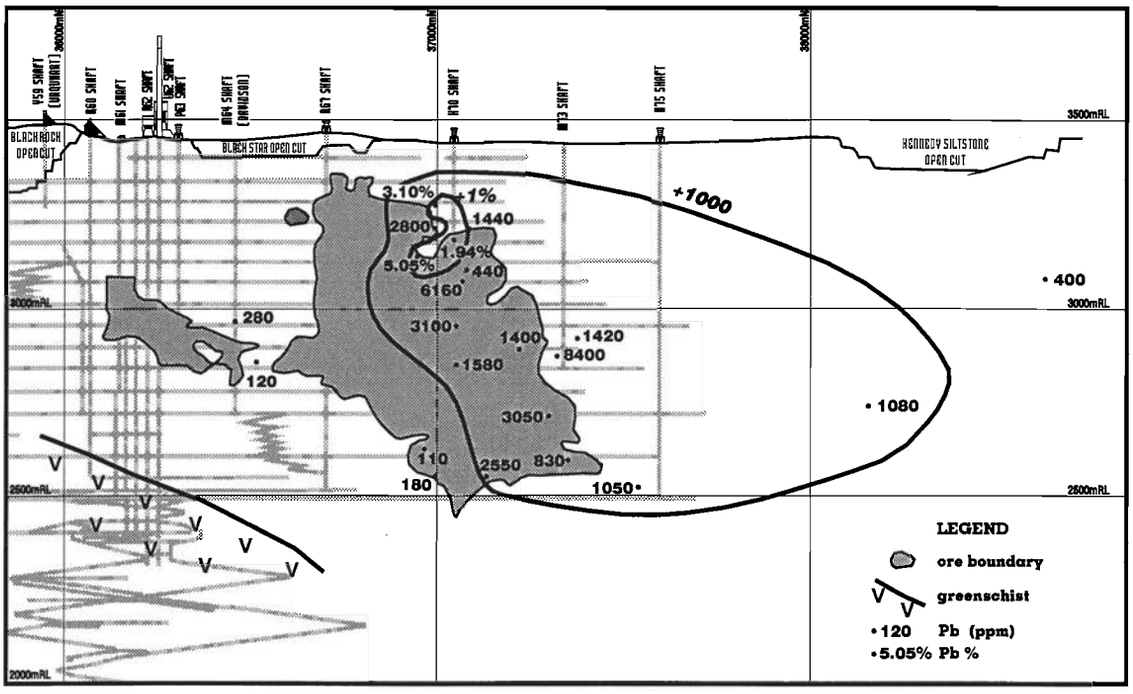
BLACKROCK OPENCUT
BLACK STAR OPEN CUT
KENNEDY SILTSTONE OPEN CUT
3500mRL
3000mRL
2500mRL
2000mRL
3.10%
1%
1440
2800
1.94%
5.05%
440
6160
280
3100
1400
1420
8400
1580
120
3050
110
2550
830
180
1050
1000
400
1080
LEGEND
ore boundary
greenschist
120 Pb (ppm)
5.05% Pb %

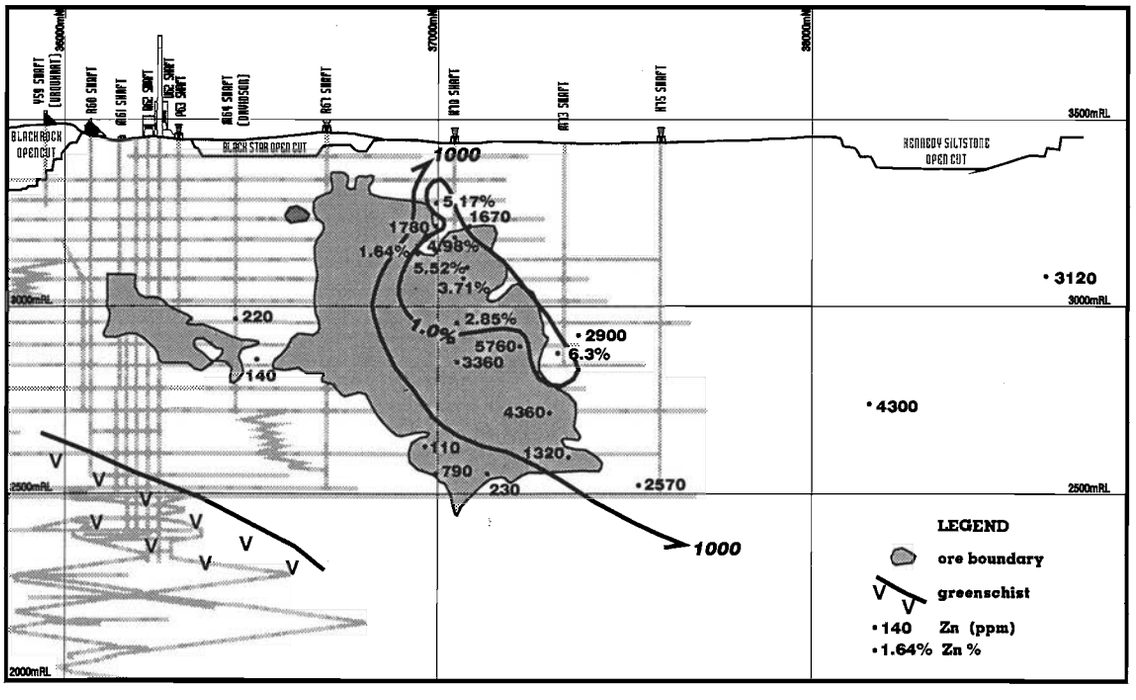
BLACKROCK OPENCUT
BLACK STAR OPEN CUT
KENNEDY SILTSTONE OPEN CUT
3500mRL
3000mRL
2500mRL
2000mRL
1000
5.17%
1670
1780
1.64%
4.98%
5.52%
3.71%
2.85%
1.0%
2900
5760
6.3%
3360
220
140
4360
110
1320
790
230
2570
3120
4300
1000
LEGEND
ore boundary
greenschist
140 Zn (ppm)
1.64% Zn %

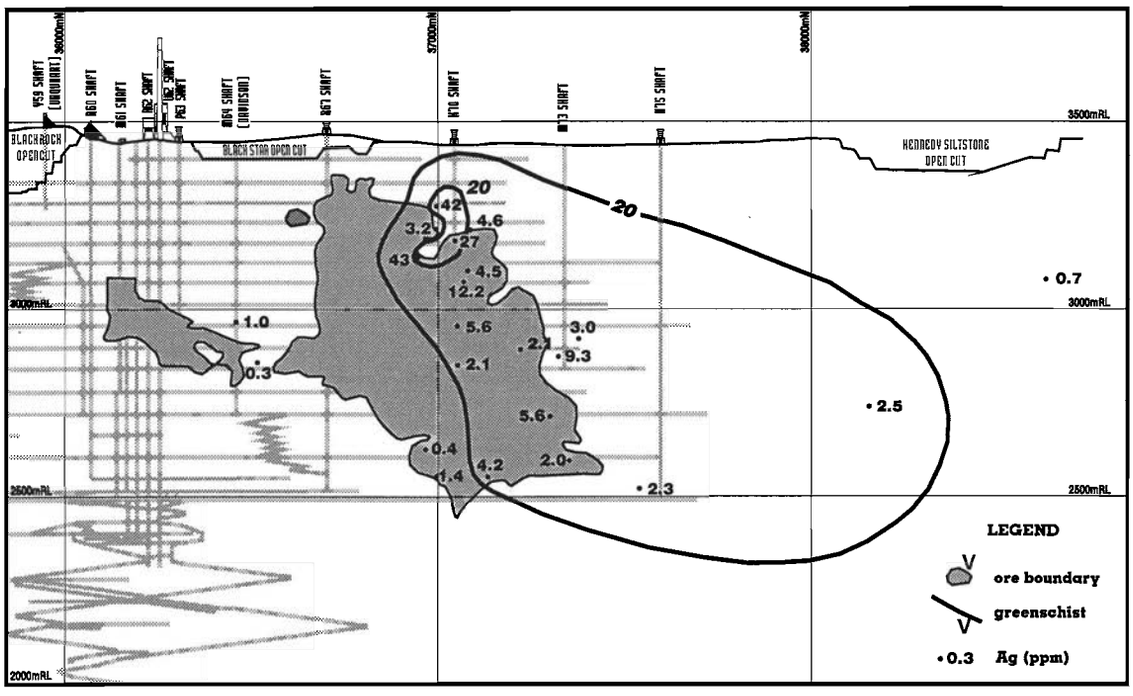
BLACKROCK OPENCUT
BLACK STAR OPEN CUT
KENNEDY SILTSTONE OPEN CUT
3500mRL
3000mRL
2500mRL
2000mRL
20
42
4.6
3.2
27
43
4.5
12.2
1.0
0.3
5.6
3.0
2.1
9.3
2.1
5.6
0.4
4.2
2.0
1.4
2.3
2.5
0.7
LEGEND
ore boundary
greenschist
0.3 Ag (ppm)

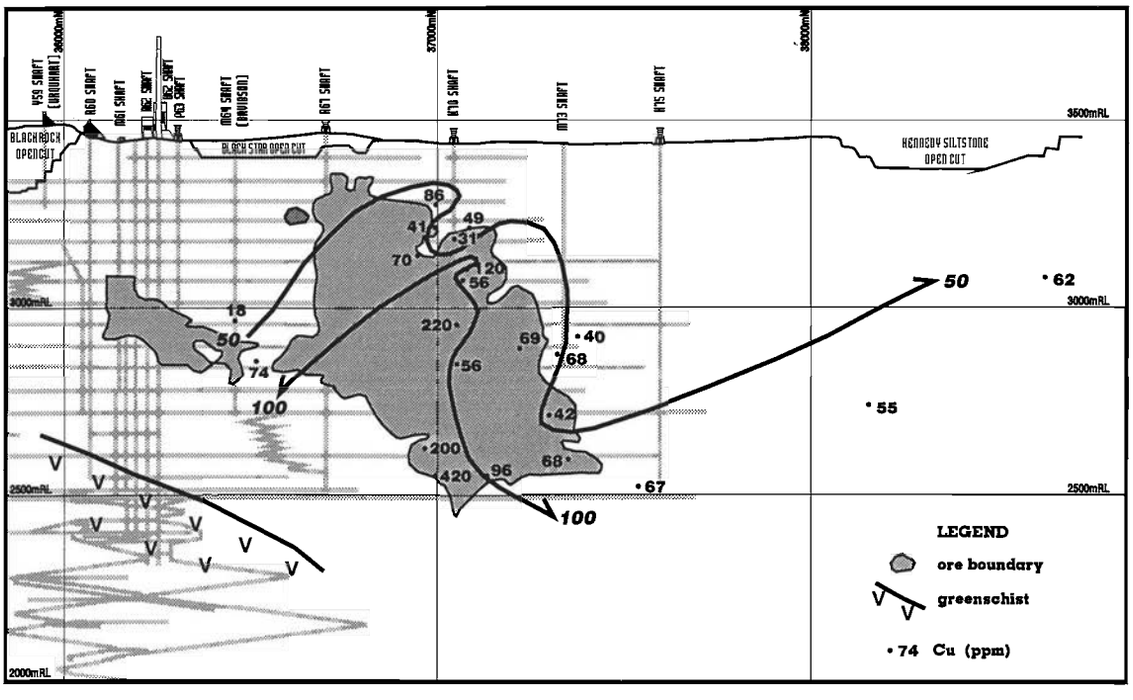
BLACKROCK OPENCUT
BLACK STAR OPEN CUT
KENNEDY SILTSTONE OPEN CUT
3500mRL
3000mRL
2500mRL
2000mRL
86
49
41
31
70
20
56
18
50
74
100
220
69
40
68
56
42
200
420
96
68
67
100
50
62
55
LEGEND
ore boundary
greenschist
74 Cu (ppm)

Figure 3. Graph of changes in chemical composition of a correlated zone across a sphalerite front illustrated in Part A, Figure 23. The mineralised side has 10.1% Zn compared with only 2550 ppm on the relatively unmineralised side. The relative depletion in CaO, MgO, and CO_2, indicate that dolomite is the major replaced component.

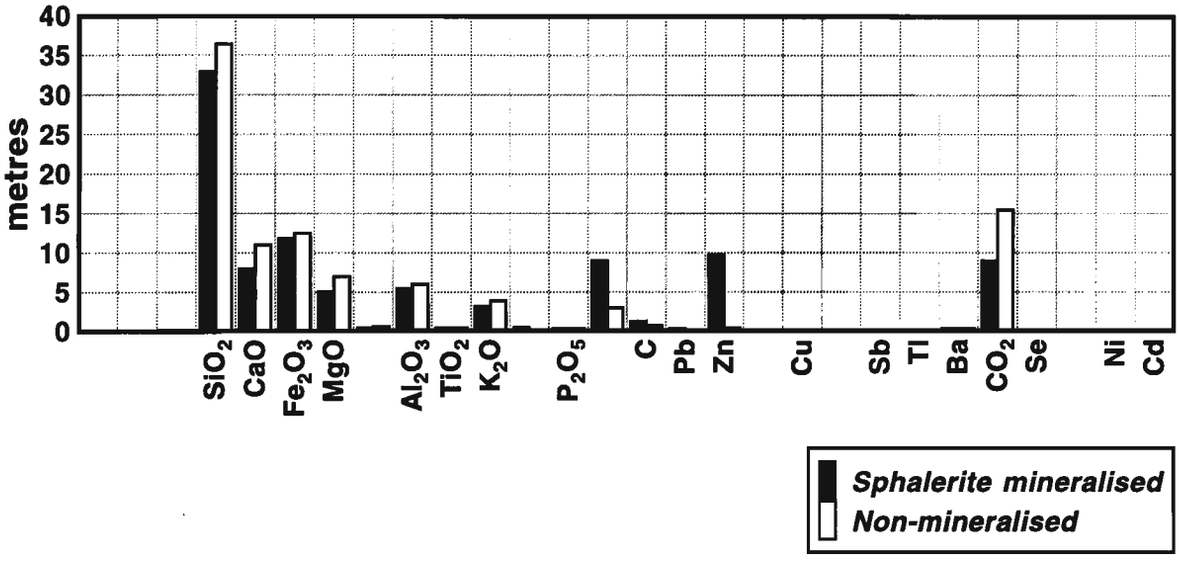
metres
40
35
30
25
20
15
10
5
0
SiO2
CaO
Fe2O3
MgO
Al2O3
TiO2
K2O
P2O5
C
Pb
Zn
Cu
Sb
Tl
Ba
CO2
Se
Ni
Cd
Sphalerite mineralised
Non-mineralised

Figure 4. Distribution of sulphur isotopes, mostly within the copper orebodies, projected onto a north-south longitudinal projection. In conjunction with Andrew et. al. 1989, Fig. 2, it shows the zonal pattern from lower values within the orebodies to higher values in the low-grade outer periphery.

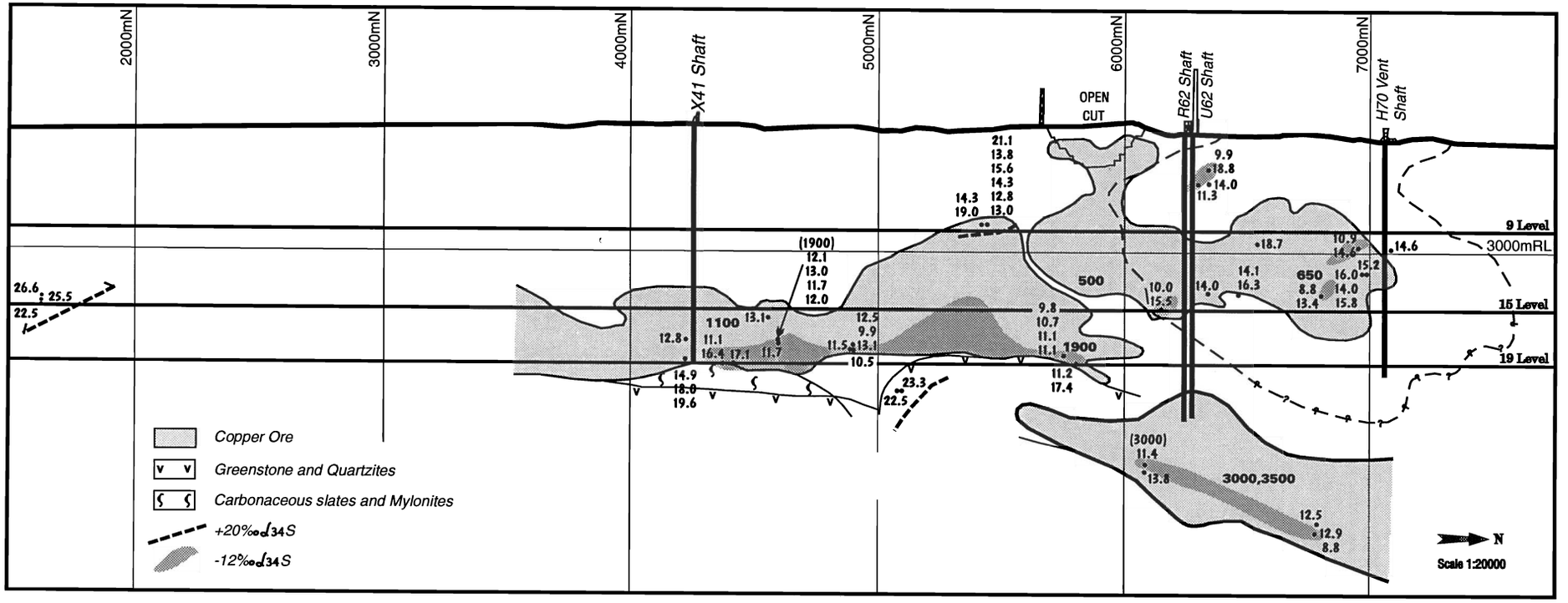
2000mN
3000mN
4000mN
5000mN
6000mN
7000mN
X41 Shaft
R62 Shaft
U62 Shaft
H70 Vent Shaft
OPEN CUT
9 Level
15 Level
19 Level
3000mRL
(1900)
1100
1900
500
650
(3000)
3000,3500
Copper Ore
Greenstone and Quartzites
Carbonaceous slates and Mylonites
+20‰ δ34S
-12‰ δ34S
N
Scale 1:20000

PART D.

APPENDIX 2.

Geochemical data for -

7 Orebody B sequence

7 Orebody Zones

Hilton 4 Pod

11 Level sphalerite front

sample number	metres	from	to	SiO2	CaO	Fe2O3	MgO	MnO
M657 W I No 1								
QQ10672	21.5-23.2	11.5	13.2	34.2	13	12.1	6.75	0.59
QQ10673	23.2-24.6	10.1	11.5	23.8	13.9	18.9	7.35	0.47
QQ10674	24.6-26.0	8.7	10.1	19.1	13.8	24.1	7.65	0.45
QQ10675	26.0-27.0	7.7	8.7	27	8.35	30.4	6.25	0.23
QQ10676	27.0-28.2	6.5	7.7	7.6	21.7	19.3	1.3	0.72
QQ65595	28.2-28.5	6.2	6.5					
QQ10677	28.5-31.2	3.5	6.2	24	11.2	26.9	6.75	0.37
QQ10678	31.2-32.1	2.6	3.5	38.1	12.4	10.5	7.55	0.31
QQ10679	32.1-33.4	1.3	2.6	15.2	12.5	31.2	7.3	0.34
QQ10680	33.4-34.0	0.7	1.3	31.6	11.8	16.5	7.05	0.3
QQ65596	34.0-34.7	0	0.7					
K 746 W I No 1								
QQ65582	49.9-50.4	7.8	8.3	26	14.5	15	7.9	0.62
QQ65583	50.4-51.3	6.9	7.8	24.8	15.6	15	7.95	0.63
QQ65584	51.3-52.5	5.7	6.9	42.3	10.6	7.65	5.75	0.43
QQ65585	52.5-53.5	4.8	5.7	36.2	10.1	14.8	5.3	0.44
QQ65586	53.5-54.3	4	4.8	23.7	11.2	24.1	5.9	0.51
QQ65587	54.3-55.1	3.2	4	32.3	13.4	12.1	6.85	0.69
QQ65588	55.1-55.5	2.8	3.2	26.4	14.5	15.6	7.3	0.68
QQ65589	55.5-56.4	1.9	2.8	29.4	13.5	13.9	7.25	0.57
QQ65590	56.4-57.3	1.1	1.9	26.7	10.9	21	5.8	0.52
QQ65591	57.3-58.0	0.4	1.1	45	9.75	6.55	5.5	0.43
QQ65592	58.0-58.4	0	0.4	43.1	10.8	7.1	6.1	0.48
7174 X/C 11/L								
27774	0-1.6	0	1.5	29.3	14.3	15.4	5.65	0.8
27775	1.6-2.8	1.5	2.6	20.4	12.8	21.6	6.65	0.74
27776	2.8-3.6	2.6	3.4	25.2	14.9	18.8	8.1	0.72
27777	3.6-5.0	3.4	4.7	22.6	7.85	14.2	3.9	0.82
27778	5.0-6.5	4.7	6.1	20.7	11.4	17.5	5.55	0.79
27779	6.5-7.7	6.1	7.2	29.8	12.8	14.7	7.25	0.58
27780	7.7-8.4	7.2	7.9	26.3	14.5	15	5.65	1.42
27781	8.4-9.7	7.9	9.1	18.4	8.3	17.8	3.94	0.79
27782	9.7-10.3	9.1	9.7	33.4	11.6	13.5	4.54	1.17
27783	10.3-11.1	9.7	10.4	15.9	6.75	18.8	2.7	1.13
27784	11.1-12.5	10.4	11.7	34.6	7.1	12.7	3.16	0.66
27785	12.5-13.6	11.7	12.8	38.4	11.2	12.3	4.62	0.96
27786	13.6-14.4	12.8	13.5	38.6	9.7	13.2	3.9	0.73
27787	14.4-15.6	13.5	14.7	33.9	10.4	6.9	4.8	0.66
27788	15.6-16.8	14.7	15.8	34.1	11.3	12.9	5	0.64
27789	16.8-18.1	15.8	17	38.7	11.7	9.55	5.5	0.69
27790	18.1-19.7	17	18.5	38	16.6	8.65	5.3	0.88
N73 X/C 11/L								
QQ27738		12.5	13.8	43.3	14.2	4.24	7.85	0.29
QQ27739		11.2	12.5	38.7	10.2	3.48	6.35	0.23
QQ27740		10.1	11.2	39.6	10.5	7.9	6.7	0.21
QQ27741		9	10.1	33.4	11.1	11.1	6.85	0.23
QQ27742		8.3	9	34.9	10.9	13.8	6.6	0.25
QQ27743		7.3	8.3	36.2	10.8	11.5	6.45	0.29
QQ27744		6.7	7.3	37.2	7.6	14.1	4.46	0.2
QQ27745		0	1.2	25.1	12.3	19.1	7.45	0.24
QQ27746		1.2	1.8	32.2	11.8	13.4	7.2	0.25
QQ27747		1.8	2.6	39.1	11.8	7.9	6.35	0.25
QQ27748		2.6	3.1	34.5	12.1	11.1	6.5	0.33
QQ27749		3.1	4.3	21.4	5.75	32.5	3.52	0.18
QQ27750		4.3	4.8	19.7	11.5	25.8	6.45	0.28
QQ27751		4.8	5.8	26.9	10.5	19.8	6.15	0.3
QQ27752		5.8	6.2	26.6	11	20.5	6.45	0.3
QQ27753		6.2	6.7	26.8	11	20.8	6.45	0.31
M815 Surf								
902391		0	2	28.8	10.5	12.2	6.5	0.22
902392		2	4.3	29.6	11.4	13.1	8.4	0.29
F968 Surf				38	11.55		5.99	
J712 E. Dec				27.46	3.83		3.27	
QZ 10								
	1030			9.38	5.6	5.6	8.71	0.07
	1030.7			13.01	4.12	4.12	8.95	0.08
	1035.5			12.45	3.72	3.72	6.93	0.06
	1038.6			10.14	3.86	3.86	8.03	0.06

sample number	Al2O3	TiO2	K2O	Na2O	P2O5	S	C	Pb
M657 W I No 1								
QQ10672	5.55	0.18	3.22	0.08	0.07	5.15	0.15	320
QQ10673	4.62	0.16	2.38	0.05	0.1	10.2	0.15	580
QQ10674	3.18	0.12	0.93	0.04	0.08	13.5	0.15	7600
QQ10675	4.44	0.15	0.79	0.04	0.08	16.8	0.15	900
QQ10676	0.8	0.04	0.22	0.04	0.05	7.4	0.15	21600
QQ65595								205000
QQ10677	3.98	0.14	1.06	0.08	0.09	14	0.2	6100
QQ10678	6.2	0.23	3	0.07	0.08	3.98	0.2	1350
QQ10679	2.26	0.09	0.99	0.03	0.07	19.9	0.25	1150
QQ10680	4.82	0.18	2.6	0.05	0.08	9.4	0.25	580
QQ65596								660
K 746 W I No 1								
QQ65582	5.05	0.24	2.98	0.06	0.09	8.7	0.35	240
QQ65583	4.84	0.17	2.84	0.02	0.08	18.6	0.35	450
QQ65584	7.7	0.25	4.96	0.08	0.08	3.32	0.65	170
QQ65585	6.7	0.21	4.52	0.07	0.07	10.3	0.45	370
QQ65586	4.1	0.14	2.54	0.06	0.08	17.7	0.6	1200
QQ65587	6.1	0.21	3.6	0.06	0.09	5.05	0.9	660
QQ65588	4.52	0.16	2.72	0.03	0.09	6.75	0.5	1400
QQ65589	5	0.18	2.94	0.08	0.09	6.4	0.6	1450
QQ65590	4.9	0.18	2.84	0.05	0.07	13.8	0.65	1650
QQ65591	8.1	0.29	4.7	0.09	0.07	2.88	0.55	210
QQ65592	7.05	0.27	4.04	0.06	0.08	3.66	0.4	150
7174 X/C 11/L								
27774	4.96	0.18	2.44	0.03	0.06	8.5	0.25	5700
27775	3.38	0.12	1.76	0.02	0.07	12.1	0.3	6300
27776	2.5	0.09	1.17	0.03	0.07	8.85	0.2	1200
27777	3.98	0.14	2.42	0.08	0.07	13.3	0.15	87300
27778	3.82	0.14	2.1	0.06	0.05	14.6	0.4	27500
27779	5.05	0.18	2.84	0.04	0.08	6.85	0.25	16100
27780	3.88	0.15	2.42	0.03	0.07	9	0.45	18100
27781	3.68	0.13	2.28	0.08	0.1	17.4	0.3	48200
27782	6.6	0.22	4.12	0.03	0.09	7.8	0.5	7200
27783	2.46	0.11	1.64	0.08	0.09	18	0.15	104000
27784	6.4	0.2	4.36	0.05	0.07	11.4	0.25	38200
27785	7.05	0.23	4.22	0.08	0.09	5.95	0.6	4300
27786	6.9	0.21	4.7	0.08	0.08	7.95	0.45	6800
27787	7	0.25	3.9	0.09	0.08	6.95	0.3	28400
27788	6.5	0.22	3.98	0.06	0.1	9.1	0.35	4700
27789	8.85	0.29	4.98	0.07	0.1	4.5	0.2	1100
27790	5.4	0.17	3.2	0.06	0.07	3.02	0.15	520
N73 X/C 11/L								
QQ27738	5.85	0.18	3.86	0.1	0.06	0.32	0.23	940
QQ27739	6.9	0.22	4.14	0.13	0.06	0.24	0.27	70
QQ27740	8.6	0.29	5.4	0.2	0.09	3.84	0.33	110
QQ27741	6.35	0.23	4.34	0.11	0.09	6	0.3	270
QQ27742	6.1	0.19	4.56	0.14	0.08	8.05	0.39	220
QQ27743	6.45	0.22	4.54	0.09	0.08	6.3	0.97	210
QQ27744	7.45	0.35	5.95	0.09	0.09	9.55	0.45	1550
QQ27745	4.38	0.17	3.38	0.14	0.1	12.5	0.56	900
QQ27746	5.65	0.2	4.26	0.15	0.09	8.05	0.45	390
QQ27747	7	0.24	4.68	0.29	0.08	8	0.48	400
QQ27748	6.1	0.21	3.46	0.15	0.07	22.1	1.03	860
QQ27749	4.1	0.14	2.32	0.09	0.06	6.4	0.85	260
QQ27750	3.04	0.11	2.18	0.08	0.08	17.8	0.68	1200
QQ27751	5.1	0.18	3.28	0.14	0.08	18.1	0.65	1400
QQ27752	4.8	0.17	3.4	0.16	0.08	6.4	0.31	600
QQ27753	4.86	0.17	3.42	0.17	0.08	2.6	0.68	490
M815 Surf								
902391	5.2	0.18	3.86	0.12	0.08	4.3	0.53	360
902392	5.8	0.21	3.54	0.13	0.09	8.25	0.5	220
F968 Surf	7.7		3.81	0.39		6.05	0.56	1400
J712 E. Dec	4.54		2.92	0.16		11.15	0.15	59200
QZ 10								
		0.33	2.36	0.33				90
		0.24	2.46	0.38				175
		0.24	2.24	0.35				260
		0.26	2.36	0.45				220

sample number	Zn	Ag	Cu	Bi	Sb	Tl	Ba	CO2
M657 W I No 1								
QQ10672	90	1.6	60	4	24	60	220	19.7
QQ10673	2000	2	210	4	28	80	160	21
QQ10674	5740	11	670	4	38	70	30	21.2
QQ10675	560	2.2	320	4	48	110	60	12.7
QQ10676	260	15	1270	12	32	10	10	32.9
QQ65595	44	140	640	3	150	17	10	
QQ10677	330	6.3	390	10	34	60	50	17.2
QQ10678	40	1.4	190	4	6	60	180	18.9
QQ10679	330	3.9	120	4	60	150	50	19.2
QQ10680	110	1.8	80	4	28	110	140	18
QQ65596	48	0.7	48	0.1	1.7	8	15	
K 746 W I No 1								
QQ65582	1050	1	60	6	22	60	190	41.2
QQ65583	1160	1.6	100	4	20	80	170	42.8
QQ65584	110	0.6	40	4	4	50	280	15.6
QQ65585	360	1.5	80	4	28	80	240	14.8
QQ65586	2230	4.8	150	4	48	110	170	16.6
QQ65587	470	1.9	60	4	32	60	260	19.6
QQ65588	890	3.7	80	4	30	70	240	21
QQ65589	2360	3.2	80	4	26	70	240	20.1
QQ65590	1460	4.1	70	4	48	110	220	16
QQ65591	260	0.9	40	4	16	50	320	14.7
QQ65592	80	0.8	20	4	12	40	270	16.3
7174 X/C 11/L								
27774	24000	11	1310	4	42	50	240	18
27775	34800	12	90	4	60	90	300	19.3
27776	11800	2.7	100	4	22	30	240	22.8
27777	138000	150	100	30	180	30	3250	11.6
27778	86900	44	60	12	95	70	1300	16.7
27779	10000	27	60	6	65	60	700	19.2
27780	38400	21	160	4	70	50	2400	19.8
27781	165000	90	90	18	170	90	2550	17.9
27782	33200	13	90	4	44	90	6400	15.6
27783	193000	180	170	60	240	10	3500	9.9
27784	93700	80	110	18	140	70	2200	10.2
27785	11700	9	120	4	40	50	800	15.4
27786	26000	12	130	4	42	60	660	13.2
27787	93700	64	70	10	110	30	320	14
27788	41500	10	60	6	55	60	310	15
27789	6050	2.5	50	4	28	50	360	15.5
27790	2530	1.4	30	4	4	20	190	20
N73 X/C 11/L								
QQ27738	1900	2.1	32	4	4	20	160	
QQ27739	80	0.6	28	4	4	30	190	
QQ27740	70	1.1	34	4	14	40	250	
QQ27741	440	1.5	140	4	32	65	250	
QQ27742	210	2.2	48	4	28	70	270	
QQ27743	2300	1.8	55	4	22	55	280	
QQ27744	20000	3.8	65	4	24	110	350	
QQ27745	1400	3.4	44	6	38	80	200	
QQ27746	1000	2.1	50	4	22	85	260	
QQ27747	1000	2	50	4	28	80	260	
QQ27748	1500	4.7	70	6	60	150	190	
QQ27749	430	1.8	26	4	8	75	280	
QQ27750	240	4	110	4	46	120	200	
QQ27751	1800	3.8	90	4	46	90	200	
QQ27752	1200	2.3	80	4	20	90	260	
QQ27753	3100	2.1	36	4	6	60	210	
M815 Surf								
902391	4700	1.3	16	<4	6	25	1400	
902392	13000	2.9	22	<4	12	65	260	
F968 Surf	14600							13.83
J712 E. Dec	65100							12.6
QZ 10								
	290	1-	24	5-	4-	10	640	
	960	1-	10	5-	4-	10-	740	
	1380	1-	17	5-	4-	10	1140	
	1040	1-	16	5-	4-	10	890	

sample number	Se	Co	Ni	Cd
M657 W I No 1				
QQ10672	1	20	10	7
QQ10673	1	30	10	12
QQ10674	1	50	10	26
QQ10675	1	60	10	8
QQ10676	1	50	10	7
QQ65595		115		6
QQ10677	1	40	10	8
QQ10678	1	20	10	6
QQ10679	1	90	20	8
QQ10680	1	30	10	6
QQ65596		14		1-
K 746 W I No 1				
QQ65582	1	20	10	10
QQ65583	1	40	10	10
QQ65584	1	20	10	6
QQ65585	1	30	10	7
QQ65586	1	30	10	165
QQ65587	1	10	10	8
QQ65588	1	20	10	9
QQ65589	1	20	10	19
QQ65590	1	20	10	12
QQ65591	1	10	10	7
QQ65592	1	10	10	5
7174 X/C 11/L				
27774	1	20	10	92
27775	1	20	10	140
27776	1	10	10	58
27777	1	20	10	440
27778	1	20	10	340
27779	1	10	10	49
27780	1	10	10	180
27781	1	30	10	470
27782	1	20	10	160
27783	1	30	10	520
27784	1	30	10	320
27785	1	10	10	70
27786	1	20	10	110
27787	1	20	10	290
27788	1	30	10	160
27789	1	20	10	31
27790	1	10	10	20
N73 X/C 11/L				
QQ27738	1	5	15	6
QQ27739	1	5	5	1
QQ27740	1	15	20	1
QQ27741	1	20	20	2
QQ27742	1	15	15	2
QQ27743	1	15	10	3
QQ27744	1	30	10	34
QQ27745	1	15	10	5
QQ27746	1	25	10	6
QQ27747	1	15	10	4
QQ27748	1	30	5	6
QQ27749	1	10	5	1
QQ27750	1	40	10	6
QQ27751	1	25	5	6
QQ27752	1	30	5	3
QQ27753	1	15	10	5
M815 Surf				
902391	<1	5	5	5
902392	1	10	5	22
F968 Surf				
J712 E. Dec				
QZ 10				
				1-
				2
				3
				2

B Sequence Chemistry

Appendix 2

Sample No.	SiO2	CaO	Fe2O3	MgO	MnO	Al2O3	TiO2	K2O	Na2O	P2O5	S	C-Org+Elem	Pb	Zn	Ag	Cu
LZ7	36.1	7.9	23.3	7.35	0.37	6.9	0.32	1.26	0.06	0.11	5.8	0.16	110	110	0.4	200
LZ8	34	3.38	34.7	3.3	0.19	8.8	0.39	1.49	0.22	0.1	8.65	0.13	180	790	1.4	420
LZ16	33.4	10.6	15.9	6.15	0.62	7	0.28	4.48	0.07	0.1	7.4	0.32	1400	5760	2.1	69
LZ22	27.5	11.1	13.6	6.3	0.45	4.92	0.19	3.02	0.07	0.08	9.8	0.37	8400	6.30%	9.3	68
LZ39	30.9	9.5	19.7	5.5	1.03	6.85	0.27	3.66	0.2	0.09	8.25	0.07	3100	2.85%	5.6	220
LZ42	48.3	6.4	11.2	5.8	0.2	10	0.38	4.64	0.06	0.1	3.1	0.12	120	140	0.3	74
LZ45	39.3	7.45	13.2	4.58	0.39	7.25	0.29	4.24	0.06	0.1	6.4	0.14	5.05%	1.64%	43	70
LZ52A	32.5	8.8	16.9	4.54	0.86	5.2	0.21	3.1	0.06	0.08	9.7	0.21	1.08%	6.96%	19	83
LZ52B	44.9	9.55	6.3	4.8	0.98	9.8	0.38	6.45	0.07	0.1	0.75	0.11	2250	4590	5.4	30
LZ67	33.7	9.35	13.1	4.62	1.11	6.75	0.26	5.25	0.1	0.09	6.2	0.12	1.94%	4.98%	27	31
LZ88	51	6.65	4.52	3.72	0.37	12.4	0.44	9.05	0.12	0.11	1.65	0.48	830	1320	2	68
LZ89	39	8.4	13.5	5.5	0.3	7.65	0.29	4.86	0.07	0.1	7	0.4	440	2710	4.5	120
LZ90	37.1	10.3	11.6	6.8	0.24	7.55	0.28	5.1	0.12	0.1	6.4	0.45	1050	2570	2.3	67
LZ91	37.7	11.9	11.8	6.55	0.53	5.75	0.22	4.5	0.05	0.07	3.2	0.16	2800	1780	3.2	41
LZ92	42.1	5.55	13	3.42	0.53	7.7	0.3	6.1	0.06	0.08	7.5	0.09	3.10%	5.17%	42	86
LZ93	45.9	0.51	26.2	4.26	0.1	13	0.57	4.22	0.11	0.15	5.05	0.19	2550	230	4.2	96
LZ94	48.3	3.92	9.95	4.56	0.36	12.1	0.44	7.35	0.11	0.11	1.75	0.19	1580	3360	2.1	56
LZ 95	47.5	13	7	5.2	0.23	9.05	0.35	6.8	0.08	0.1	2.05	0.83	280	220	1	18
LZ96	38.9	10.1	10.6		0.34	7.55	0.29	5.9	0.08	0.09	5.8	0.32	1440	1670	4.6	49
LZ97	49.7	6.15	6.35		0.39	11.3	0.49	7.15	0.09	0.11	2.95	1.67	3050	4360	5.6	42
LZ98	38.6	7.6	12		0.22	8	0.3	5.25	0.26	0.09	6.7	0.58	1080	4300	2.5	55
LZ99	56.1	0.77	12		0.23	11.5	0.44	7.55	0.08	0.11	5.65	0.79	400	3120	0.7	62
LZ 100	30.4	13	14.1	7.65	0.56	5.45	0.22	3.56	0.06	0.1	8.25	0.45	1420	2900	3	40

Sample No.	Bi	Sb	Tl	Ba	CO2	Se	Co	Ni	Cd	C-Carbonate	Hg	FeO	As
LZ7	12	<4	50	540	12.1	<.05	7	9	2	3.3	0.05	19.2	54
LZ8	30	<4	60	1.08%	5	<.05	12	11	3	1.36	0.1	30.6	680
LZ16	<4	34	110	770	15.8	<.05	12	8	17	4.32	0.3	7.3	220
LZ22	<4	35	70	490	14.8	<.05	6	12	100	4.05	1.45	6.95	220
LZ39	8	14	90	1080	15.8	<.05	6	10	69	4.32	1.15	17	54
LZ42	<4	4	90	360	10.1	<.05	<4	6	4	2.76	<.05	8.75	36
LZ45	64	65	70	730	12	<.05	14	7	42	3.28	0.7	10.9	790
LZ52A	6	32	55	560	13.5	<.05	12	8	150	3.69	2.6	14	610
LZ52B	<4	8	60	1020	14.8	<.05	<4	<4	45	4.03	0.3	5.45	<2
LZ67	20	50	85	1420	14.4	<.05	6	5	73	3.94	1.4	10.8	140
LZ88	<4	15	75	1600	9.5	<.05	4	<4	8	2.6	0.15	1.96	64
LZ89	<4	38	80	730	13.5	<.05	10	<4	14	3.7	0.25	5.05	135
LZ90	<4	18	75	440	18.5	<.05	12	9	12	4.31	0.15	4.46	220
LZ91	<4	22	45	650	15	<.05	7	<4	12	4.08	0.1	13.2	800
LZ92	15	78	85	1040	8.9	<.05	8	6	130	2.45	1.35	11.1	300
LZ93	<4	20	65	5700	<.02	<.05	5	<4	8	0	0.1	22.4	145
LZ94	5	8	370	2550	5.8	<.05	<4	<4	17	1.58	0.2	8.35	40
LZ 95	<4	8	55	270	10.5	<.05	16	55	4	2.9			
LZ96	<4	24	80	590	16.4	<.05	10	5	15	4.8	0.15	3.5	220
LZ97	<4	30	100	640	5.4	<.05	5	12	20	3.16	0.35	3.06	125
LZ98	4	12	50	1420	11.8	<.05	10	12	18	3.82	0.15	4	140
LZ99	<4	8	35	8300	1.7	<.05	11	17	11	1.25	0.1	4.3	98
LZ 100	<4	32	80	320	19.7	<.05	28	25	11	5.27			

Hilton 4 Pod

Appendix 2

SAMPLE	AS	BA	BI	PB	SB	TL	GRAV43TOEC	GRAV4ACO2	FE0	S	HG	SE	AG	CD	CO	CU
217876	22	1080	-4	120	-4	25	0.49	9.97	-3000	3.55	-0.05	-0.5	4	5	54	68
217877	140	41500	38	23000	-4	45	0.06	14.3	-3000	13.3	0.65	-0.5	165	180	270	94
217878	11	1860	4	320	-4	25	0.21	5.83	-3000	1.6	-0.05	-0.5	4	6	38	22
217879	125	14000	12	22000	10	-10	0.11	12.9	-3000	17.3	1.25	-0.5	26	230	240	170
217880	65	18200	12	2750	5	110	0.13	10.2	-3000	9.55	1.1	-0.5	8	160	160	88
217881	185	85000	-4	23500	-4	20	0.32	12.9	-3000	1.95	1.05	-0.5	62	170	185	70
217882	32	3300	-4	170	4	40	0.26	8.54	-3000	2.2	-0.05	-0.5	2	8	46	25
217883	98	144000	60	1880	-4	30	-0.05	11.8	-3000	16.2	1.6	-0.5	92	165	180	48
217884	35	3750	-4	130	-4	35	0.18	9.04	-3000	19.1	-0.05	-0.5	4	6	46	30
217885	350	7000	-4	40500	-4	45	0.22	7.15	-3000	23	3.7	-0.5	38	610	410	82
217886	140	45000	42	67000	10	-10	-0.05	17.3	-3000	15.7	1.35	-0.5	96	210	260	42
217887	135	1500	8	16500	18	45	1.08	8.91	-3000	21.1	0.7	-0.5	20	155	155	155
217888	16	3200	4	3600	-4	30	0.14	7.3	-3000	3	0.75	-0.5	22	14	56	88
217889	130	6900	-4	27500	12	60	0.27	12	-3000	15.8	0.55	-0.5	36	96	220	125
217890	32	6800	-4	250	-4	55	0.27	10.2	-3000	2.35	-0.05	-0.5	4	5	42	20
217891	180	2350	8	15100	8	45	0.2	10.8	-3000	17.8	0.7	-0.5	28	140	240	135
217892	42	6900	-4	470	-4	45	0.37	9.31	-3000	2.3	0.1	-0.5	5	28	58	24
217893	185	11200	-4	9800	6	50	0.42	13.5	-3000	18.3	0.75	-0.5	24	115	230	100

SAMPLE	NI	AN	SI02	TI02	AL203	FE203	MN0	MG0	CA0	NA20	K20	P205	LO1
217876	32	330	38.4	0.24	6.5	32.5	1.35	4.8	0.64	0.04	0.14	0.13	13.4
217877	30	64000	12.2	0.08	2	40.9	1.61	3.56	2.16	0.04	0.27	0.14	22.1
217878	30	810	48.1	0.31	8.5	22.8	0.71	5.6	1.47	0.05	0.23	0.12	9.35
217879	35	86000	13	0.09	2.26	42.1	1.37	4.32	2.54	0.05	0.34	0.11	19.7
217880	28	58000	29.8	0.19	5.15	32.9	1.21	4.04	0.85	0.09	0.77	0.17	14.8
217881	28	64000	7.45	0.06	1.34	34.7	1.31	4.12	5.25	0.09	0.23	0.12	20
217882	28	810	44.9	0.29	7.75	22.1	0.97	5.45	2.66	0.06	0.55	0.13	11.7
217883	24	61000	9.3	0.07	1.45	28.9	1.36	3	2.66	0.1	0.21	0.14	19.7
217884	30	620	45.3	0.29	7.6	22.5	1.08	5.45	2.52	0.06	0.55	0.12	12
217885	28	255000	11.6	0.09	2.18	32.4	0.91	2.64	1.12	0.12	0.55	0.13	17.2
217886	26	58000	8.6	0.05	1.19	33.9	1.51	3.78	3.62	0.06	0.22	0.09	26.2
217887	34	70000	16.6	0.12	2.86	42.5	0.79	4.86	4.18	0.04	0.52	0.12	18.3
217888	25	2700	45.7	0.28	7.2	25.5	0.98	5.25	1.48	0.04	0.23	0.12	10.9
217889	36	39000	17.9	0.13	3.24	40.7	1.18	5.1	4	0.06	0.61	0.14	18.8
217890	28	540	43.7	0.28	7.5	20.9	0.88	5.65	4.2	0.07	0.77	0.12	12.7
217891	32	64000	19.6	0.13	3.28	41.1	0.92	4.66	3.34	0.06	0.57	0.12	17.7
217892	25	8900	44.8	0.29	7.8	18.2	0.7	5.6	4.8	0.06	0.76	0.13	13
217893	34	52000	14	0.09	2.14	43.5	1.17	4.4	4.88	0.06	0.49	0.1	21.5

LZ 30 ZN Front

Appendix 2

SampleNo.	metres	length	hor. dist.	SiO2	CaO	Fe2O3	MgO	MnO	Al2O3	TiO2	K2O	Na2O	P2O5	S	C	Pb
LZ30A				34.1	8.15	12.3	5.5	0.37	6.2	0.22	3.44	0.07	0.09			1100
LZ30B				38	11.4	12.8	7.1	0.45	6.4	0.22	3.86	0.05	0.08			690

SampleNo.	Zn	Ag	Cu	Bi	Sb	Tl	Ba	CO2	Se	Co	Ni	Cd
LZ30A	10.1	5	58	<4	34	70	970			22	20	240
LZ30B	2550	2	36	<4	16	75	890			24	35	9

PART D.

APPENDIX 3.

Isochrons for North Australian Pb/Zn deposits from Page et. al. 1994 AGSO research newsletter number 20.

Table of model ages for North Australian lead-zinc deposits from Carr et. al. 1994.

Appendix 3.

Isochrons for North Australian Pb/Zn deposits from Page et. al. 1994 AGSO research newsletter number 20.

Table of model ages for North Australian lead-zinc deposits from Carr et. al. 1994.

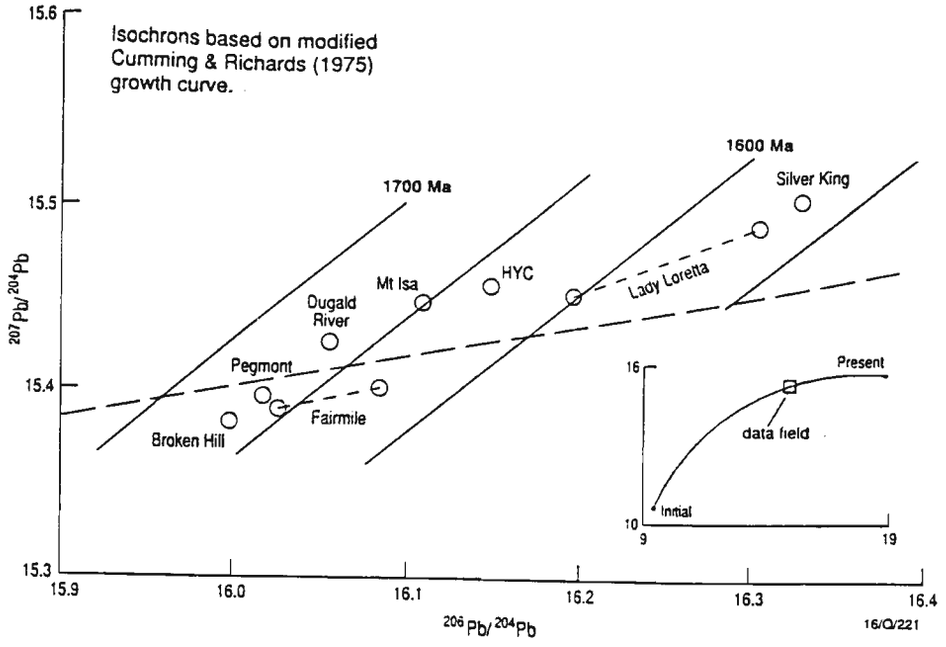

Fig. 2. A $^{207}Pb/^{204}Pb$ *versus* $^{206}Pb/^{204}Pb$ plot for major sediment-hosted Pb–Zn deposits in the Mount Isa Inlier.

The position of these deposits on the Pb-isotope growth curve for stratabound Pb–Zn ores is shown on the inset diagram. Isochrons of 1700, 1650, 1600, and 1550 Ma are shown as straight lines.

Deposit	Age (U–Pb) (see page et al., 1994) (Ma)	Modified Cumming and Richards (1975) model age (Ma)	Cumming and Richards (1975) model age (Ma)	Stacey and Kramers (1975) model age (Ma)
Century	1595 ± 6	1570	1435	1530
HYC	1640 ± 7	1635	1510	1610
Mt Isa	1650 ± 7	1650	1525	1625
Broken Hill	1690 ± 5	1670	1545	1610
Pegmont	< 1677 ± 9	1665	1545	1615
Dugald River	?	1665	1545	1630

PART D.

APPENDIX 4.

Sample details and report by Stewart Eldridge on sulphur isotopes from 7 orebody B sequence fine-grained pyrite.

DETAILS OF SAMPLES - ION MICROPROBE PROJECT

RC 295. LZ18A 11/L 7172N, 1652E

Highly pyritic laminated siltstone from No. 6 orebody zone (2m above 6 orebody footwall tmb) Sample face cut perpendicular to bedding/cleavage intersection lineation. Good example of ~10μm pyrites overgrowing both bedding - parallel and cross-cutting cleavage seams. Series of sample points (7 indicated) covering skeletal-type pyrites through close-packed zoned pyrites. This specimen has also been examined by SEM.

RC 635 19D Sub 7355N 1465E, 6 Orebody

Highly pyrite sample from fold hinge zone showing pyrite aggregate trains along cleavage. Series of sample points along this cleavage trains to look at variation between layering and cleavage 8 sample points indicated cleavage 85 - 240.

RC 299B LZ23 11/L 7175N, 1659E

Pyritic and sphalerite-mineralized sample from correlated sequence between markers (2) and (3) of 7 orebody 4 sample points representing pyrites from specific horizons plus one of adjacent sphalerite

RC298B LZ22 13D Sub-level 7360N 1623E, 2876RL

Sample sequence as above (tmb 2 correlates)
Correlation with LZ39

LZ22 - LZ39
(1) - (1)
(2) - (2)
(3) - (3)

RESEARCH SCHOOL OF EARTH SCIENCES
THE AUSTRALIAN NATIONAL UNIVERSITY
INSTITUTE OF ADVANCED STUDIES · GPO BOX 4 CANBERRA ACT 2601
TELEPHONE 062 49 3406 TELEX 62693 FAX 062 49 0738

Content has been removed
for privacy reasons

SHRIMP $\delta^{34}S$ DATA: Mt. ISA Pb/Zn

Sample No.	Mineral	Comments	$^{34}S/^{32}S$ Sample	std. error (1σ)	$^{34}S/^{32}S$ Standard	std. error (1σ)	$\delta^{34}S$ Sample	error (2σ)
298B #1	pyrite	aggregate below TMB	0.043381	0.000043	0.043693	0.000023	5	2
#2	"	aggregate in wavy zone	0.043221	0.000044	"	"	3	2
#3	"	cluster below dark band	0.043333	0.000039	"	"	4	2
#3*	"	cluster a little further along	0.043444	0.000043	"	"	6	2

The analyses 1 and 2 were obtained from the areas you designated. 3 and 3* were taken where the grain size of the pyrite allowed. 3* was taken in case 3 failed, but it appears in examination of the craters and the data that both were successful and all data fall around 4‰, when taking into acount analytical error, regardless of stratigraphic position.

Sample No.	Mineral	Comments	$^{34}S/^{32}S$ Sample	std. error (1σ)	$^{34}S/^{32}S$ Standard	std. error (1σ)	$\delta^{34}S$ Sample	error (2σ)
299B #1	pyrite	aggregate just below TMB	0.043252	0.000052	0.043763	0.000024	0	3
#2	"	aggregate in cross-cut zone	0.043716	0.000051	"	"	11	3
#2*	"	finer-grained than #2	0.043658	0.000046	"	"	9	2
#3	"	cluster above silty bed	0.044106	0.000051	"	"	20	3
#4	"	in contact with sphalerite	0.043824	0.000045	"	'	13	2
#5	"	"coarse cube" with po	0.043933	0.000043	"	'	16	2

The errors here are a little larger in some cases because a smaller spot was used to access smaller targets. Also, two points were analysed in the number 2 circle to make sure of getting something reliable. Both analyses appear to be good and the numbers are indistinguishable within analytical uncertainty. It appears that there are at least three populations of pyrite in this sample: the pyrite just below the TMB, the "cross-cut pyrite" and the cluster above the silty bed. The pyrite in contact with the sphalerite cannot be separated from that in the "cross-cut" It is interesting to note that the pyrite below the TMB is very light isotopically and, at 0‰±3, it just overlaps in composition with the 5‰±2 from 298B. The #5 analysis was agreed to verbally when we spoke during SGEG and is from relatively coarse material near to the pyrite bands which yielded the #2 analyses (po=pyrrhotite). It is within error of the "crosscut" and "with sphalerite" pyrites of #s 2 and 4.

Sample No.	Mineral	Comments	$^{34}S/^{32}S$ Sample	std. error (1σ)	$^{34}S/^{32}S$ Standard	std. error (1σ)	$\delta^{34}S$ Sample	error (2σ)
295 #1	pyrite	coarse cube with sphalerite	0.044128	0.000031	0.043955	0.000038	16	2
#2	"	isolated skeletal shape	too small to hit well					
#3	"	" " "	0.043881	0.000039	0.043700	0.000023	16	2
#4	"	cluster of rounded grains	0.044030	0.000029	0.043955	0.000038	14	2
#4*	"	as above; adjacent band	0.044273	0.000032	'	"	19	2
#5	"	aggregate of grains	0.044246	0.000036		"	19	2
#6	"	aggregate of grains near 5	0.044199	0.000029	'	"	17	2
#7	"	zoned gains in a cluster	0.044382	0.000033	"	"	22	2

Most of the pyrites (1-7) may well fall into one group of roughly 16.5‰±~2.5 and I wouldn't really try much harder to break any out of the group, especially if 4 and 4* are averaged to give16.5‰. The total spread of 5‰ in this group is not that much greater than the allowed ±4‰ so I wouldn't lose any sleep over the spread. The sample #7 may actually fall outside of this group though it would be difficult for me to assign this to any specific cause other than stratigraphically-related variation as seen in other samples I've examined from the Isa.

Sample No.	Mineral	Comments	$^{34}S / ^{32}S$ Sample	std. error (1σ)	$^{34}S / ^{32}S$ Standard	std. error (1σ)	$\delta^{34}S$ Sample	error (2σ)
635 #1	pyrite	cluster of three grains	too small to hit well					
#2	"	small aggregate of crystals	too small to hit well					
#3	"	aggregate along cleavage	0.044306	0.000057	0.043700	0.000023	26	3
#4	"	AA; near to #3	0.044263	0.000031	0.043899	0.000019	20	2
#4*	"	cluster near #4	0.044379	0.000033	"	"	23	2
#5	"	aggregate in cleavage band	0.043831	0.000035	"	"	10	2
#6	"	cluster, same band as #5	0.043953	0.000032	"	"	13	2
#7	"	zoned gains in a cluster	0.044562	0.000039	"	"	32	2
#8	"	group ~ along same zone	0.044258	0.000033	"	"	20	2
#9	pyrrhotite	"coarse patch" near #8	0.044070	0.000033	0.043531	0.000020	14	2
#10	"	"coarse patch" near #11	0.044077	0.000034	"	"	14	2
#11	pyrite	cluster in separate band from 3+4 and 8 or 5-7	0.044258	0.000033	0.043899	0.000019	20	2

This is the most complicated sample of the four investigated. Analyses 3, 4, 4*, 8 and 11 give results which fall into one group while 5 and 6 clearly belong to some other population even though they are nearby. 7 stands alone in composition, being the isotopically heaviest. The pyrrhotite, which was verbally agreed to be analysed, is not in isotopic equilibrium with the pyrite of the 3, 4, 8 and 11 group, but may be related to the 5 and 6 pair. The crater for the #7 analysis appears normal, but may well be worth re-analysing anyway as it really stands out. Should it remain an outlier after checking, the sample would have three populations of pyrite in a fairly small area.